

STATUS OF THESIS

Title of thesis

SYNTHESIS, CHARACTERIZATION AND EVALUATION OF
MIXED MATRIX MEMBRANES FOR CO₂ SEPARATION

I, SIKANDER RAFIQ

hereby allow my thesis to be placed at the Information Resource Center (IRC) of Universiti Teknologi PETRONAS (UTP) with the following conditions:

1. The thesis becomes the properties of UTP.
2. The IRC of UTP may make copies of the thesis for academic purposes only.
3. This thesis is classified as

Confidential

Non-confidential

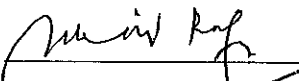
If this thesis is confidential, please state the reason:

A patent has been filed from a part of this research work.

The contents of the thesis will remain confidential for _____ - _____ years.

Remarks on disclosure:

Endorsed by


Signature of Author


Assoc. Prof. Dr. Zakaria Man
Chemical Engineering Department
Universiti Teknologi PETRONAS

Signature of Supervisor
Assoc. Prof. Dr. Zakaria Man

Permanent Address:
182-EII, Johar Town
Lahore-Pakistan


Date: 21-03-2013

Date: 21/3/2013

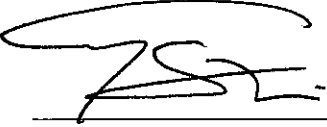
UNIVERSITI TEKNOLOGI PETRONAS
SYNTHESIS, CHARACTERIZATION AND EVALUATION OF MIXED MATRIX
MEMBRANES FOR CO₂ SEPARATION

by
SIKANDER RAFIQ

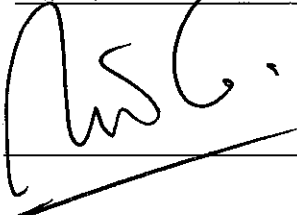
The undersigned certify that they have read, and recommend to the Postgraduate Studies Programme for acceptance, this thesis for the fulfilment of the requirements for the degree of Doctor of Philosophy in Chemical Engineering.

Signature :  - **Assoc. Prof. Dr. Zakaria Man**
Chemical Engineering Department
Universiti Teknologi PETRONAS

Main Supervisor : Assoc. Prof. Dr. Zakaria B Man

Signature :  **Ir. Dr. Abdul Halim Shah Maulud**
Senior Lecturer
Chemical Engineering Department
Universiti Teknologi PETRONAS
Bandar Seri Iskandar, 31750 Tronoh
Perak Darul Ridzuan, MALAYSIA
Email: halims@petronas.com.my

Co- Supervisor : Dr. Abdul Halim. Shah B Maulud

Signature :  **Assoc. Prof. Dr. Mohamad Azmi Bustam @ Khalil**
Head, Chemical Engineering Department
Universiti Teknologi PETRONAS

Head of Department : Assoc. Prof. Dr. Mohd Azmi B Bustam @ Khalil

Date : 27/3/2013

SYNTHESIS, CHARACTERIZATION AND EVALUATION OF MIXED MATRIX
MEMBRANES FOR CO₂ SEPARATION

by

SIKANDER RAFIQ

A Thesis

Submitted to the Postgraduate Studies Programme

as a Requirement for the Degree of

DOCTOR OF PHILOSOPHY

CHEMICAL ENGINEERING

UNIVERSITI TEKNOLOGI PETRONAS

BANDAR SERI ISKANDAR,

PERAK

MARCH 2013

DECLARATION OF THESIS

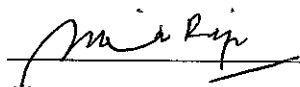
Title of thesis

SYNTHESIS, CHARACTERIZATION AND EVALUATION
OF MIXED MATRIX MEMBRANES FOR CO₂ SEPARATION

I, SIKANDER RAFIQ


hereby declare that the thesis is based on my original work except for quotations and citations which have been duly acknowledged. I also declare that it has not been previously or concurrently submitted for any other degree at UTP or other institutions.

Witnessed by


Signature of Author

Permanent Address:
182-EII, Johar Town
Lahore-Pakistan

Date: 21-03-2013


Signature of Supervisor
Assoc. Prof. Dr. Zakaria Man

Assoc. Prof. Dr. Zakaria Man
Chemical Engineering Department
Universiti Teknologi PETRONAS

Date: 21 | 3 | 2013

DEDICATION

To My Father Khaleeq, Mother Shahida

To My Sisters Aneela and Eram

Special Thanks to My Uncles, Kalim Laique and Sami

&

Finally to My Late Grandparents, Zubaida Rafiq & Razia Mujeeb

ACKNOWLEDGEMENT

First of all, I am grateful to ALLAH SWT, the almighty God, the source of my life, for enabling me to complete the research.

I thank my family, my beloved father Mohammad Khaleeq, mother Shahida and my sisters Aneela and Eram and brother Ahmad for their endless support and prayers. They are always close to my heart.

I am highly thankful to University Teknologi PETRONAS (UTP) Malaysia for providing me this great opportunity conducive to my academic pursuit.

I would like to pay my sincere gratitude to my supervisor Assoc. Prof. Dr. Zakaria Man for his continuous guidance that has steered me to complete my research work. His kind support during my research activities was a great source of encouragement for me. I am highly thankful to my co-supervisor Sn. Lect. Ir. Dr. Abdul Halim Shah B Maulud for his thoughtful inputs, guidance and facilitation through critical stages of my work.

I am thankful to the respective present and previous HODs of the Chemical Engineering Department, Assoc. Prof. Dr. Mohd Azmi B Bustam@ Khalil and Assoc. Prof. Dr. Shuhaimi B Mahadzir for their continued trust and support during my study period at UTP.

Special thanks to Assoc. Prof. Dr. Mohd Ibrahim B Abd Mutalib, Dr. Farooq Ahmad, King Khalid University Saudi Arabia, Prof. Dr. Saikat Maitra, West Bengal University of Technology, India, and Dr. Nawshad Muhammad, Pakistan for their technical assistance during my research studies.

I would also like to extend my appreciation to all the technologists from UTP Mr. Jailani, Mr. Yusuf, Mr. Idrus, Mr. Rosli, Mr. Fauzi, Mr. Irwan, Mr. Anuar, Mr. Omer,

Mr. Faisal and Mr. Mahfooz for their assistance in carrying out my research work.

Finally, my sincere gratitude to the postgraduate office staff Miss Kamaliah, Mr. Kahar, Mr. Jahadi and Mr. Imran for their assistance during my study period. Special thanks to all of my postgraduate friends for their support and acquaintance.

ABSTRACT

The use of membrane technology for gas separation applications has been successfully employed since the last few decades. For efficient separation of CO₂/CH₄, high performance gas separating membranes is desired. For CO₂ separation, asymmetric flat sheet membranes are preferred because of their high gas permeance as compared to dense films. In this study, various composition of polyimide (PI) ranging from 5 to 20 wt.% were blended with polysulfone (PSF) and used for the formation of asymmetric flat sheet membranes via dry/wet phase inversion technique. Morphological analysis indicated that the surfaces of the fabricated membrane blends possessed homogenous surfaces and their cross-sections showed a non-porous top and a diminutive porous substructure. Differential scanning calorimetry (DSC) analysis showed the existence of single glass transition temperature (T_g) for different membrane blends which indicated miscibility among the polymeric blends. Mechanical analysis showed improvement in young's modulus, tensile strength and elongation at break properties with the increase in PI composition in the membrane blends. Solvents with various compositions of N-methyl-2-pyrrolidone to dichloromethane (NMP/DCM) were used to prepare the membranes and it was found that 80/20v/v% solvent composition offered maximum CO₂/CH₄ gas performance. Heat treatment was carried out on the membranes prepared from the NMP/DCM (80/20) solvent composition which showed improvement in ideal selectivities with a slight decrease in the permeance. Thermogravimetric (TGA) showed improvement in the maximum degradation temperature (T_d) and activation energy (E) with the increase in PI contents in the membrane blends.

The performance of asymmetric membrane was further enhanced by incorporating inorganic silica of tetraethyl orthosilicate (TEOS) at various proportions ranging from 5-20 wt.% in the PSF/PI-20% polymeric blend to form mixed matrix membranes (MMMs). The developed MMMs showed different morphologies of the surfaces and cross-sections of the membrane where agglomeration was observed at 20 wt. % silica

loading. Improvements in T_g , T_d and E were observed with the increase in the silica loadings in the MMMs. XRD analysis showed decrease in the d-spacing with the increase in silica loadings causing restriction in the polymer chain mobility. Mechanical analysis indicated a steady increase in Young's modulus and tensile strength up to 15 wt. % silica loading. The elongation at break property decreased with an increase in the silica contents which indicated the rigidity of the MMMs. The gas permeation results showed that the CO_2 permeance increased from 73.7 ± 0.2 GPU at 5 wt. % silica content to 95.7 ± 0.4 GPU at 20 wt.% silica content. However the maximum ideal selectivity, $\alpha_{\text{CO}_2/\text{CH}_4}$ of 61.0-60.2 at 2-10 bar feed pressure is observed at 15 wt.% silica content. The selectivity using mixed gas analysis at various CO_2/CH_4 compositions of 30/70 v/v%, 50/50 v/v% and 30/70 v/v% showed consistent results with the ideal gas selectivity.

Finally, various theoretical gas permeation models for predicting CO_2 gas permeance in the MMMs were applied. Investigations by SEM indicated the fillers shape to be actually prolate ellipsoids It was observed that Maxwell-Wagner-Sillar (MWS) model showed the least average absolute relative error (AARE%) values in a range of 1.12-2.17 at 2-10 bar.

ABSTRAK

Penggunaan teknologi membran untuk aplikasi pengasingan gas telah diimplementasikan sejak beberapa dekad yang lalu. Bagi menghasilkan keberkesanan dalam pengasingan CO_2/CH_4 , membran pengasingan gas yang berprestasi tinggi amat diperlukan untuk tujuan ini. Bagi pengasingan CO_2 , kepingan membran nipis yang asimetri adalah diperlukan kerana mempunyai ketelapan gas yang tinggi berbanding membran yang tinggi ketumpatannya. Dalam kajian ini, pelbagai komposisi poli-amida (PI) dalam lingkungan 5 ke 20 wt % telah diadun dan dicampur bersama poli-sulfon (PSF) untuk menghasilkan kepingan membran nipis yang asimetri melalui teknik fasa penyongsangan kering/basah. Analisis morfologi menunjukkan bahawa membran yang telah dihasilkan mempunyai permukaan yang rata atau homogenus dan keratan rentas menunjukkan bahagian atas yang langsung tidak berpori disusuli substruktur pori yang sangat kecil. Analisis kalorimeter pengimbasan berbeza atau differential scanning calorimetry (DSC) menunjukkan kewujudan suhu peralihan gelas yang tunggal atau single glass transition temperature (T_g) bagi setiap adunan membran yang berbeza. Hal ini menunjukkan adanya kebolehcampuran bagi setiap adunan. Analisis mekanikal menunjukkan pembaharuan dalam modulus young, kekuatan tegangan dan pemanjangan pada sifat patah atau break property dengan penambahan dalam komposisi PI dalam adunan membran. Pelarut dengan pelbagai gabungan komposisi N-metil-2-pyrrolidon dan diklorometana (NMP/DCM) telah digunakan untuk menyediakan membrane-membran dan didapati bahawa 80/20 v/v% komposisi pelarut memberi prestasi gas CO_2/CH_4 yang maksimum. Rawatan haba telah dijalankan pada membran dengan menggunakan komposisi pelarut NMP / DCM (80/20) sekaligus menunjukkan peningkatan dalam pemilihan yang sangat ideal dengan sedikit penurunan dalam kebolehaliran. Termogravimetri (TGA) menunjukkan terdapatnya peningkatan dalam suhu degradasi maksimum (T_d) dan tenaga pengaktifan (E) apabila kandungan PI semakin dalam adunan membrane semakin tinggi. Prestasi membran asimetri telah dipertingkatkan dengan menggabungkan silika organik tetraethyl orthosilicate (TEOS) antara 5-20 wt.% campuran PSF/PI-20%

polimer untuk membentuk membran matriks campuran atau mixed matrix membranes (MMMs). MMMs yang dihasilkan menunjukkan morfologi permukaan yang berbeza dan keratan rentas membran yang mempunyai aglomerasi pada penambahan silika sebanyak 20 wt.%. Penambahbaikan di T_g , T_d dan E berlaku dengan adanya penambahan silika dalam MMMs. Analisis XRD menunjukkan penurunan pada jarak- d melalui penambahan silika yang menyebabkan berlakunya sekatan dalam pergerakan rantai polimer. Analisis mekanikal pula menunjukkan peningkatan yang bagus pada modulus Young beserta kekuatan tegangan dengan penambahan silika sebanyak 15 wt. Pemanjangan pada sifat patah atau break property adalah menurun dengan adanya peningkatan dalam kandungan silika yang menunjukkan sifat kekerasan yang ada pada MMMs. Keputusan penyerapan gas menunjukkan bahawa kebolehaliran CO_2 meningkat dari 73.7 ± 0.2 GPU pada kandungan silika sebanyak 5 wt.% kepada 95.7 ± 0.4 GPU pada kandungan silika sebanyak 20 wt%. Walau bagaimanapun pemilihan terbaik yang maksimum iaitu α_{CO_2/CH_4} sama dengan 61.0-60.2 pada tekanan yang ditingkatkan sebanyak 2-10 bar hanya akan dihasilkan pada kandungan silika sebanyak 15wt.%. Pemilihan untuk menggunakan analisis gas campuran pada pelbagai komposisi CO_2/CH_4 seperti 30/70v/v%, 50/50v/v% dan 30/70v/v% menunjukkan hasil yang konsisten dengan pemilihan gas ideal. Kesimpulannya, pelbagai model teori penyerapan gas untuk meramalkan kebolehaliran gas CO_2 dalam MMMs telah digunakan. Kajian melalui penggunaan SEM menunjukkan bentuk pengisi atau fillers secara keseluruhannya menjadi ellipsoids. Hal ini telah diperhatikan dengan model Maxwell-Wagner-Sillar (MWS) bahawa terdapatnya purata nilai kesilapan relatif mutlak (AARE%) yang rendah antara 1.12-2.17 pada 2-10 bar.

In compliance with the terms of the Copyright Act 1987 and the IP Policy of the university, the copyright of this thesis has been reassigned by the author to the legal entity of the university,

Institute of Technology PETRONAS Sdn Bhd.

Due acknowledgement shall always be made of the use of any material contained in, or derived from, this thesis.

© SIKANDER RAFIQ, 2013

Institute of Technology PETRONAS Sdn Bhd

All rights reserved.

TABLE OF CONTENTS

STATUS OF THESIS	i
APPROVAL PAGE	ii
TITLE PAGE	iii
DECLARATION OF THESIS	iv
DEDICATION	v
ACKNOWLEDGEMENT	vi
ABSTRACT	viii
ABSTRAK	x
COPYRIGHT PAGE	xii
TABLE OF CONTENTS	xiii
1. INTRODUCTION	1
1.1 Overview	1
1.2 Natural Gas	1
1.3 Gas Separation Techniques	3
1.3.1 Absorption Technique	4
1.3.2 Adsorption Technique	5
1.3.3 Membrane Technique	6
1.4 Problem Statement	8
1.5 Objectives of Research	9
1.6 Scope of Study	10
1.6.1 Preparation and Characterization of Base Asymmetric Polymeric Membranes	10
1.6.2 Development and Characterization of Mixed Matrix Membranes	11
1.6.3 Prediction of CO ₂ /CH ₄ Performance by Modeling Approach	11
1.7 Organization of Thesis	11

2. BACKGROUND AND THEORY	13
2.1 Overview	13
2.2 Membrane Classification	13
2.3 Asymmetric Membrane Fabrication Techniques	16
2.3.1 Solution Cast Composite Membranes	17
2.3.2 Interfacial Composite Membrane	17
2.3.3 Dynamically Formed Membranes	18
2.3.4 Phase Inversion (Solution Precipitation) Membranes	18
2.3.5 Dry/Wet Phase Inversion Technique	20
2.4 Solubility Parameter Estimation	23
2.5 Gas Transport in Membranes	24
2.5.1 Permeation	26
2.6 Selection of Glassy Polymers	30
2.6.1 CO ₂ Plasticization in Glassy Polymers	34
2.7 Membrane Configurations	39
2.8 Mixed Matrix Membranes	41
2.8.1 Interfacial Defects Elimination in MMMs	42
2.8.2 Selection of Sol-gel process and Silica Inorganic Fillers	43
2.8.3 Thermal Stability of MMMs	45
2.9 Modeling in Mixed Matrix Membranes	50
3. MATERIALS AND METHODOLOGY	55
3.1 Overview	55
3.2 Materials	55
3.2.1 Polymers	55
3.2.2 Solvents	56
3.2.3 Solubility Parameter	57
3.2.4 Preparation of Silica Sol	59
3.3 Membrane Development	60
3.3.1 Development of Asymmetric Polysulfone/Polyimide Membranes	61

3.3.2	Development of Mixed Matrix Membranes	63
3.4	Membrane Characterization Techniques	64
3.4.1	Morphological Analysis	65
3.4.2	Thermal Analysis	66
3.4.3	Spectral Analysis	67
3.5	Kinetic analysis	69
3.6	Mechanical analysis	71
3.7	Gas Permeation Evaluation	73
3.8	Modeling in MMMs	76
4.	RESULTS AND DISCUSSION	79
4.1	Overview	79
4.2	Development of Asymmetric Membranes	79
4.2.1	Effect of Blends on Polymer Concentration	79
4.2.2	Glass Transition Temperature	82
4.2.3	Spectral Analysis	84
4.3	Mechanical Analysis	88
4.4	Gas Permeation Analysis	90
4.5	Effect of Solvent Compositions on the Solubility Parameter	93
4.6	Gas Permeation Evaluation at Varying Solvent Compositions	99
4.7	Kinetic Analysis	102
4.8	Development of Mixed Matrix Membranes	105
4.8.1	Spectral Analysis	111
4.8.2	Glass Transition Temperature	114
4.8.3	XRD Analysis	115
4.9	Gas Permeation in the Mixed Matrix Membranes	117
4.10	Kinetic Analysis on the MMMs	121
4.11	Mechanical Analysis on the MMMs	125
4.12	Mixed Gas Analysis	130

4.13 Effect of Particle Geometry on Permeance in MMMs through Modeling Approach	133
5. CONCLUSIONS AND RECOMMENDATIONS	145
5.1 Conclusions	145
5.2 Recommendations	146
REFERENCES	148
PUBLICATION LIST	167
APPENDIX A	171
APPENDIX B	177
APPENDIX C	179
APPENDIX D	197

LIST OF FIGURES

Figure 2.1 Schematic representation of a simple gas separation process through a membrane	14
Figure 2.2 Classification of membranes according to the structural morphology	15
Figure 2.3 Schematic diagram of ternary phase among polymer, solvent and non-solvent [52]	22
Figure 2.4 Schematic diagram for gas permeation involving Knudsen diffusion, Molecular sieving and Solution diffusion mechanism [61]	26
Figure 2.5 A schematic diagram of the glass transition temperature (T_g) between the glassy and rubbery polymer states [65]	30
Figure 2.6 Comparison between the glassy and rubbery polymers in terms of selectivity and permeability of various gases, mentioned as trade-off plots by Robeson [69]	32
Figure 2.7 Separation of gases by (a) Glassy polymers (b) Rubbery polymers [50]	34
Figure 2.8 Robeson's plot related to the CO_2/CH_4 selectivity versus the CO_2 permeability for various polymers showing high performance PI-Matrimid (■), conventional polymers as PEI, PSF, PC, CA (▼) and (○) other polymers [65, 72]	35
Figure 2.9 Graph of various Mixed Matrix Membranes in terms of the CO_2/CH_4 selectivity versus the CO_2 permeability	49
Figure 3.1 Structures of polymers (a) PSF Udel® P-1800 (b) PI Matrimid® 5218	56
Figure 3.2 Flow diagram of asymmetric polymeric membranes and mixed matrix membranes development	61
Figure 3.3 Typical Plot of the Intensity versus the Diffraction Angle	69
Figure 3.4 The dumbbell-shaped specimen for tensile testing	71
Figure 3.5 Schematic Illustration of the Membrane Gas Permeation Testing Unit	73
Figure 3.6 Schematic Illustration of the Membrane Module	74
Figure 3.7 Calibration curves of (a) CO_2 and (b) CH_4 respectively	75
Figure 4.1 SEM images of the membranes surfaces (a) Pure PSF, (b) PSF/PI-10% and (c) PSF/PI-20%, and cross-sections (d) PSF, (e) PSF/PI-10% and (f) PSF/PI-20%	81
Figure 4.2 DSC thermograms of the membrane blends	82

Figure 4.3 Comparison of glass transition temperature of the PSF/PI blended with theoretical models	84
Figure 4.4 Comparative FTIR spectra of the PSF, PI and PSF/PI-20% membranes	85
Figure 4.5 Structures of (a) PSF, Udel® P-1800, (b) PI, Matrimid® 5218 (c) NMP and the possible interactions among the polymer species indicated by arrows and dotted lines	87
Figure 4.6 Representative stress-strain curves of the developed membranes at various polymer concentrations	89
Figure 4.7 Young's modulus, Tensile strength and Strain at break for membrane blends as a function of the PI content	90
Figure 4.8 Permeance of CO ₂ and CH ₄ for the different membranes at various feed pressures	91
Figure 4.9 Effect of the heat treatment at 140°C on the permeance of CO ₂ and CH ₄ for different membranes at various feed pressures	92
Figure 4.10 Comparison of the ideal selectivity of CO ₂ /CH ₄ at various feed pressures: untreated (a),(b) and heat treated (c),(d)	93
Figure 4.11 SEM images of the membranes surfaces (a) PSF, (b) PSF/PI-10% and (c) PSF/PI-20%	94
Figure 4.12 SEM images of the PSF/PI-20% membrane cross-sections with the NMP/DCM solvent mixtures (a) 80/20, (b) 50/50 and (c) 20/80	95
Figure 4.13 Solubility parameter difference of the solvent mixtures with ethanol for the PSF/PI-80/20% blended membrane against (i) Coagulation value and (ii) solubility parameter difference of the solvent mixtures with the PSF/PI-80/20% membrane	98
Figure 4.14 Permeance of CO ₂ and CH ₄ for the PSF/PI-20% blended membranes prepared by different solvent compositions at various feed pressures	99
Figure 4.15 Effect of the PSF/PI membrane blends on the permeance of CO ₂ and CH ₄ at various feed pressures for the NMP/DCM (20/80) composition	100
Figure 4.16 Comparison of the ideal selectivity of CO ₂ /CH ₄ for the NMP/DCM solvent composition of (20/80):(a),(b); (50/50):(c),(d) and (80/20):(e),(f)	101
Figure 4.17 TG curves of (i) PSF, (ii) PSF/PI-10%, and (iii) PSF/PI-20% with heating rates for each at (a) 5, (b) 10, and (c) 15°C/min	102

Figure 4.18 Derivative TG curves of PSF, PSF/PI-10%, and PSF/PI-20% at (i) 5, (ii) 10, and (iii) 15°C heating rates	103
Figure 4.19 Linear Plots of $\ln\beta$ ($d\alpha/dt$) versus $1/T$ (a) PSF/PI-10% and (b) PSF/PI-20% at the same α values (0.01)	105
Figure 4.20 SEM images of the PSF/PI-20% membrane surfaces with silica contents (a) 0% (b) S1 (c) S3 and (d) S4	106
Figure 4.21 SEM images of the PSF/PI-20% membrane cross-sections with silica contents (a) 0% , (b) S1 at low magnification 200X; scale 1 μ m, and (c) S3, (d) S4 at high magnification 1000X; scale 1 μ m	107
Figure 4.22 PSF/PI-20% having silica nanoparticles at the scale 1 μ m (a) S1, (b) S2, (C) S3 and (d) S4	110
Figure 4.23 TEM image of the silica particles in the PSF/PI-20% blends	111
Figure 4.24 FTIR spectra of (a) silica (b) MMMs and (c) PSF/PI-20%	112
Figure 4.25 Structures of (a) PSF,Udel® P-1800, (b) PI,Matrimid® 5218 and (c) silica particles obtained from TEOS (d) APTMOS with their possible interactions	113
Figure 4.26 DSC thermograms of the PSF/PI-20% membranes at various silica loadings	114
Figure 4.27 XRD analysis for the PSF/PI+ silica mixed matrix membranes	116
Figure 4.28 Permeance of the pure CO ₂ and CH ₄ gases for the PSF/PI-20% membrane at different silica compositions against feed pressures	117
Figure 4.29 Effect of the heat treatment at 140°C on the permeance of the pure CO ₂ and CH ₄ gases for the PSF/PI-20% membrane at different silica compositions against feed pressures	118
Figure 4.30 Permeance and selectivity of the pure CO ₂ gas test for the PSF/PI-20% membrane at 2 bar pressure against various silica contents.	119
Figure 4.31 Comparison of the Ideal selectivity of CO ₂ /CH ₄ at various feed pressures without heat treatment: (a), (b) and with heat treated: (c), (d)	121
Figure 4.32 TGA isotherms of the PSF/PI-20% blended membrane with silica contents at (a) 5°C/min, (b) 10°C/min and (c) 15°C/min	122
Figure 4.33 DTG curves of the PSF/PI-20% blended membrane with silica contents at (a) 5°C/min, (b) 10°C/min and (c) 15°C/min	123
Figure 4.34 Linear Plots of $\ln\beta$ ($d\alpha/dt$) versus $1/T$ (a) S1 (b) S4 at same α values (0.004)	124

Figure 4.35 Stress-Strain curve of the mixed matrix membranes at different silica loadings	126
Figure 4.36 Young's Modulus and the Tensile Strength of the MMMs at various silica loadings	127
Figure 4.37 Strain at the Break property of the MMMs at various silica loadings	128
Figure 4.38 Spectrums of Standard CO ₂ /CH ₄ mixtures composition (70%/30%) obtained from gas chromatograph	130
Figure 4.39 CO ₂ /CH ₄ gas mixture composition obtained at 30%/70% CO ₂ /CH ₄ feed mixtures for PSF/PI-20% membrane	131
Figure 4.40 CO ₂ /CH ₄ gas mixture the composition obtained at 50%/50% CO ₂ /CH ₄ feed mixtures for the PSF/PI-20%+S3 membrane	132
Figure 4.41 Overall comparison of theoretical models with experimental data for CO ₂ relative permeance plotted against the volume fraction of the silica particles	134
Figure 4.42 Cross-sectional image of the MMMs with a 15% silica loading at a magnification of 15KX; scale 300nm	135
Figure 4.43 Optimization curves for (a) Lewis-Nielson model and (b) MWS model	136
Figure 4.44 Optimized comparative predictions of (a) Lewis-Nielsen model and (b) MWS model against the experimental data for the CO ₂ relative permeance at 2 bar feed pressure	137
Figure 4.45 Comparison of the MWS model prediction versus the experimental data in terms of the relative permeance (Pr) for CO ₂ at pressures: (a) 2 bar (b) 4 bar (c) 6 bar (d) 8 bar and (e) 10 bar for the different values of ϕ and n	140
Figure 4.46 Graphs of the shape factor, n_f at various silica loadings (\square)	142
Figure 4.47 Estimated shape factor (n_e) values at various silica loadings with the maximum values of n_z	142

LIST OF TABLES

Table 1.1 Typical Composition of natural gas [4]	2
Table 1.2 Pipeline specifications of natural gas [5]	3
Table 1.3 Impurity levels found during fossil fuel emission in	4
Table 2.1 Gas Permeability and Permeance Units	27
Table 2.2 Various types of treatments employed in past studies	38
Table 2.3 Previous Studies on Flat Sheet Asymmetric Membranes for Gas Separation	40
Table 2.4 Selected Studies in Mixed Matrix Membranes for gas separation	46
Table 3.1 Physical properties of polymers used in this study	56
Table 3.2 Properties of organic solvents used in this study	57
Table 3.3 Calculation of the overall solubility parameter using molar attraction constants at 25°C for the polymer and solvent functional group components	58
Table 3.4 Composition of the developed PSF/PI blended membranes	63
Table 3.5 PSF/PI-20%/silica mixed matrix membrane properties	64
Table 3.6 Design of experiments	77
Table 4.1 Summary of the FTIR Spectral Assignments	86
Table 4.2 Mechanical properties of the developed PSF/PI membranes	89
Table 4.3 Solubility Parameter Differences among the coagulant, solvents and polymers	97
Table 4.4 Dynamic TG Data and the E Values of Various PSF/PI Blends	104
Table 4.5 Membrane samples at various weight fractions and glass transition temperatures of PSF/PI-20%+Silica MMMs	115
Table 4.6 XRD results of developed membranes	116
Table 4.7 Dynamic TG data and E values of various MMMs	125
Table 4.8 Effect of the silica loading on the mechanical properties of the mixed matrix membranes	126
Table 4.9 Pure and mixed gas selectivity results for PSF/PI-20% and PSF/PI-20% + silica mixed matrix membrane	131

Table 4.10 Experimental CO ₂ Permeation data for the PSF/PI-20%- SiO ₂ membranes at 2 bar feed pressure	133
Table 4.11 Variation of the theoretical models from the experimental data for relative permeability of CO ₂ at 2 bar feed pressure	134
Table 4.12 Comparative Lewis-Nielsen and MWS model deviations along with the fitted shape factor value at the various filler loading in the MMMs at 2 bar feed pressure	139
Table 4.13 MWS model deviations from the experimental permeation values determined from the SEM image and the estimated shape factor values at the various feed pressures	141

ABBREVIATIONS

6FDA	2,2'-Bis(3,4-dicarboxyphenyl)hexafluoropropane dianhydride
6FDA-6FAP	Fluorinated polyimide
AARE%	Percentage average absolute relative error
APMDMOS	3-acryloxypropyl methydimethoxysilane
APT MOS	3-acryloxypropyl trimethoxysilane
APTS	3-aminopropyl triethoxysilane
AS	3-aminopropyltrimethoxysilane
BDA	1,2,3,4-butanetetracarboxylic dianhydride
BPDA	3,3',4,4'-Biphenyltetracarboxylic dianhydride
BPPO	Brominated Polyphenylene oxide
BTU	British Thermal Unit
CA	Cellulose Acetate
DCM	Dichloromethane
DDS	3,3'-Diaminodiphenyl Sulfone
DEA	Diethanolamine
DSC	Differential Scanning Calorimetry
EVA	Ethylene Vinyl Acetate
FTIR	Fourier Transform Infrared Spectroscopy
GPU	Gas Permeation Unit
HCl	Hydrochloric Acid
MDEA	Methyldiethanolamine
MEA	Monoethanolamine
MMMs	Mixed Matrix Membranes
MTMOS	Methyltrimethoxysilane
MWS	Maxwell- Wagner- Sillar
NMP	N-methyl-2-pyrrolidone
ODA	4,4'-Diaminodiphenyl ether
PBI	Polybenzimidazole
PC	Polycarbonate

PEBAX	Poly(amide-6-b-ethylene oxide)
PEEKWC	Poly(ether ether ketone)
PEI	polyetherimide
PEO	Polyethenylene oxide
PES	Polyethersulfone
PGU	Peninsular Gas Utilization project
PI	Polyimide
PPO	Polyphenylene oxide
PSA	Pressure Swing Adsorption
PSF	Polysulfone
PU	Polyurethane
SEM	Scanning Electron Microcopy
S-PEEK	Sulfonated Poly(ether ether ketone)
TEM	Transmission Electron Microscopy
TEOS	Tetraethyl Orthosilicate
TEPOB	1,3,5-tris(4-aminophenoxy)benzene
TGA	Thermogravimetric Analysis
TMBPA	Tatramethyl Bisphenol-A
TMOS	Tetramethoxysilane
TMPDA	Tetramethylporpylenediamine
TMSPSf	Trimethylsilylated polysulfone
TSA	Thermal Swing Adsorption
UTM	Universal Testing Machine
XRD	X-ray Diffraction

NORMANCLATURE

A	Membrane area	(cm ²)
$\alpha_{i/j}$	Ideal selectivity of component <i>i</i> over component <i>j</i>	(cm ² /s)
C _D	Concentration of dissolved gas in Henry's law	(cm ³ (STP)/cm ³)
C _H	Concentration of dissolved gas in Langmuir	(cm ³ (STP)/cm ³)
D	Diffusivity Coefficient	(cm ² /s)
dC_A / dx	Concentration across the membrane	(mol/cm ³)
D _D	Diffusion coefficients of gas in Henry's law	(cm ³ (STP)/cm ³ .atm)
D _H	Diffusion coefficients of gas in Langmuir law	(cm ³ (STP)/cm ³ .atm)
<i>E</i>	Activation energy	(KJ/mol)
F	Molar attraction constant	(J ^{1/2} /cm ^{1/2} .mol)
F _d	Molar attraction constant for dispersive component	(J ^{1/2} .cm ^{3/2} /mol)
F _p	Molar attraction constant for polar component	(J ^{1/2} .cm ^{3/2} /mol)
J _A	Flux of component A	(g/cm ² .s)
l	Membrane thickness	(cm)
L, L _o	Final and original lengths, respectively	(cm)
p	Partial pressure	(bar)
P	Permeability	(cm ³ (STP).cm/cm ² .s.cmHg)
P/l	Permeance	(cm ³ (STP)/cm ² .s.cmHg)
P _f	Filler permeance	(cm ³ (STP)/cm ² .s.cmHg)
P_i^{cal}, P_i^{exp}	Theoretical and experimental values of species <i>i</i> relative permeance, respectively	(cm ³ (STP)/cm ² .s.cmHg)
P _m	Permeance of the species in continuous phase	(cm ³ (STP)/cm ² .s.cmHg)
P _r	Relative permeance	(-)
Q	Volumetric flow rate	(cm ³ /s)
Q _{stp}	Volumetric flow rate at STP	(cm ³ (STP)/s)
R	Gas constant	(L.atm.K ⁻¹ .mol ⁻¹)
S	Solubility Coefficient	(cm ³ (STP)/cm ³ .atm)

t	Time	(s)
T	Temperature	(K)
T_g	Glass transition temperature	(K)
V	Molar volume	(cm^3/mol)
ε	Strain	(%)
α	Fractional conversion of degradation	(-)
β	Heating rate	($^\circ\text{C}/\text{min}$)
σ	Stress	(MPa)
θ	Angle formed between the beams	degree
2θ	Diffraction angle	degree
ϕ	Volume fraction	(-)
ϕ_f	Filler volume fraction	(-)
ϕ_m	Volume fraction of fillers at maximum packing	(-)
ρ	Density	(g/cm^3)
ρ_p	Density of polymer	(g/cm^3)
ρ_s	Density of silica	(g/cm^3)
δ_d	Solubility parameter for dispersive component	($\text{J}^{1/2}/\text{cm}^{3/2}$)
δ_h	Solubility parameter for hydrogen bonding component	($\text{J}^{1/2}/\text{cm}^{3/2}$)
δ_p	Solubility parameter for polar component	($\text{J}^{1/2}/\text{cm}^{3/2}$)
δ_{mix}	Overall solubility parameter of solvent mixtures	($\text{J}^{1/2}/\text{cm}^{3/2}$)
δ	Overall solubility parameter	($\text{J}^{1/2}/\text{cm}^{3/2}$)
$\Delta\delta$	Solubility parameter difference	($\text{J}^{1/2}/\text{cm}^{3/2}$)

CHAPTER 1

1. INTRODUCTION

1.1 Overview

Natural gas is regarded as one of the most useful energy sources. However to ensure its use for clean burning and that it is environmentally acceptable, gas processing of acidic crude natural gas, such as with carbon dioxide (CO₂) and hydrogen sulphide (H₂S) is essential for their separation. This is elaborated in Section 1.2. Various techniques like absorption and adsorption processing can be employed for natural gas purification and more focus has been paid to membrane processing which is discussed in Sections 1.3. This study is based upon the development of different types of membranes for efficient CO₂ separation. Sections 1.4, 1.5 and 1.6 highlight the problem statement, research objectives and the scope of this work.

1.2 Natural Gas

Natural gas is an essential component of the world's energy supply and has been used for more than 150 years. It is as one of the clean energy resources and a substitute for oil. Natural gas burns up more efficiently in comparison to other sources like oil or coal, and its exhausts produce very limited by-products which are harmful to the environment. Thus, it establishes an environmentally friendly relationship as clean fuel. In light of power production, the relative release of CO₂ into the environment is the least for natural gas (~0.5) as compared to coal (~1.0) and oil (~0.7) per unit of electricity generated. Various technologies have been modified for operation with natural gas, such as heating fuel, in petrochemical industries as feedstock and in automobile industries as motor fuel [1].

In Malaysia, the production of natural gas was about 66.5 billion cubic metres as compared to the total world's production of 3193.3 billion cubic meters at the end of 2010. While in the last two decades, their proven gas reserves raised from 1600 billion cubic metres (1990) to 2400 billion cubic meters in (2010) [2]. These massive natural gas reserves are quite useful to meet the increasing demands of people. Prior to that in 1974, the formation of Petroleum Development Act introduced PETRONAS (National Petroleum Corporation) that took control of the oil and gas sector. In 1975, the company exported crude oil while in 1979, the petroleum business was put on the market. In 1981, the Malaysian government made a policy of broadening their horizons from fuel sources to greater usage of natural gas. In 1984, PETRONAS started the Malaysia's prime energy related project of trans-peninsular natural gas processing and transmission network commonly recognized as the Peninsular Gas Utilization project (PGU) that supplied gas to the first gas-fired power plant. During the 1990s, the power sector was privatized to improve and enhance power supply. Due to this rationalized process, the power generation zone was opened for independent power producers which brought about 35% of the total power generation. To-date 70% of the total power generation has been dominated by natural gas rather than oil based energy supply [3].

Table 1.1 Typical Composition of natural gas [4]

Components	Feed Content
CH ₄	70-90%
C ₂ to C ₄	0-20 %
CO ₂	0-8%
O ₂	0-0.2%
N ₂ , H ₂ S	0-5%
Rare gases (A, He, Ne etc.)	traces

Natural gas is a combustible mixture composed of hydrocarbon gases. While methane is the main constituent of natural gas, it may also contain ethane, propane etc. Though the composition of natural gas can fluctuate, Table 1.1 shows the typical

composition of natural gas in its pre-refined state. The presence of undesirable impurities like carbon dioxide (CO₂), hydrogen sulphide (H₂S), nitrogen (N₂) etc. need to be reduced to the minimum concentration in order to achieve pipeline and commercial specifications as shown in Table 1.2.

Table 1.2 Pipeline specifications of natural gas [5]

Components	Range
CO ₂	Less than 2000 ppm
H ₂ O	Less than 120 ppm
H ₂ S	Less than 4 ppm
C3	950-1050 Btu/scf
Total Inert (N ₂ , He etc.)	Less than 4000 ppm

Various types of impurities are released by fossil fuels during combustion which are shown in Table 1.3. CO₂ is one of the most undesirable impurities which is required to be separated from the natural gas and the highest composition is reported to contain 70% in some gas reserves, e.g., the largest Southeast Asia's gas field, Natuna located in Indonesia [6]. In combination with water, CO₂ is highly corrosive and quickly tears down pipelines and equipment. It reduces the heating value of a natural gas stream and wastes pipeline capacity which consequently affects the cost of production. It also freezes at low temperatures. Therefore, CO₂ removal from natural gas is necessary in order to improve the quality of the natural gas produced and to meet the pipeline specifications for natural gas delivery so that it can be made saleable.

1.3 Gas Separation Techniques

Various types of techniques are currently being followed for natural gas purification which include absorption, adsorption, cryogenic separation and membrane technology. Though each process has its own merits for CO₂ removal, in comparison to other separation technologies, the membrane technique is based upon the change in

gas flux through the membrane for a component to be separated rather than involving a phase change.

Table 1.3 Impurity levels found during fossil fuel emission in pounds per billion BTU [7]

Impurities	Natural Gas	Oil	Coal
CO ₂	117,000	164,000	208,000
CO	40	33	208
NO _x	92	448	457
SO ₂	1	1,122	2,591
Particulates	7	84	2,744
Hg	0.000	0.007	0.016

1.3.1 Absorption Technique

Absorption processes have been applied for CO₂ removal for ≥ 50 years. It is carried out by the interaction of the CO₂ with the solvent to form a chemical compound. This process takes place as a result of a chemical reaction from which CO₂ is recovered, eventually. However, absorption may take place without a chemical reaction. These different procedures are termed as chemical and physical processes, respectively [8]. Presently for CO₂ capture, various types of amines that usually involve alkanolamines are used as solvents. These alkanolamines are based upon the level of CO₂ in the feed and treated gas streams. Below are some of the typical alkanolamines used:

- MEA (Monoethanolamine): Typically used for low pressure feed gas systems and in operations that require stringent outlet gas specifications.
- DEA (Diethanolamine): Typically used in medium to high pressure feed gas systems and with a high H₂S/CO₂ ratio.
- MDEA (Methyldiethanolamine): Typically used for low a ratio of H₂S/CO₂ gas stream in order to concentrate H₂S contents in the effluent.

The stoichiometric reaction using MEA and DEA limits the usage of chemical absorption due to the formation of carbamic acid that can restrict the CO₂ absorption to 0.5mol/mol of amine. Though MDEA can overcome this problem, i.e., 1mol/mol of amine, its sluggish CO₂ reactivity can limit its use by giving a more costly and less efficient approach [9]. Moreover, the corrosive nature of amines as a solvent makes it essential to use corrosion inhibitors recurrently in the system. Additionally, these processes involve problems like solvent regeneration, post-treatment steps prior to solvent disposal for environmental safety, involvement of liquid circulation systems and rotating mechanical parts, such as pumps etc. that add difficulty for an economical CO₂ separation process.

1.3.2 Adsorption Technique

In this technique, CO₂ from a gaseous mixture gets concentrated on the surface of the solid adsorbents; the amount depends on their surface area. Typical sorbents for the adsorption process may include zeolites, a carbon molecular sieve, silica gel etc. The desorption step of the adsorbed CO₂ is quite important for regeneration of the adsorbent which may affect its adsorption capacity and can be carried out by the thermal swing adsorption (TSA) and pressure swing adsorption (PSA). Desorption using TSA is carried out by increasing the temperature of the system while PSA lowers the pressure of the system. The typical adsorption process is performed by looping in two beds of adsorbents simultaneously where one bed adsorbs and the second bed desorbs at the same time. TSA is a more time and energy consuming process because of the procedures of heating, desorption, and cooling the system with problems of adequate amount of heat loss. The time factor limits the TSA process and thus is only suitable for the separation of impurities in small amounts from the feed streams. While PSA requires high pressure process due to which make the overall operational cost high [10].

1.3.3 Membrane Technique

The use of the membrane technique has grown at an immense rate over the last three decades [11-12]. In this technique, the separation of impurities is carried out by passing the feed through a thin membrane barrier which preferentially allows the transport of certain species to pass through at a controllable rate. The component of permeated gas is diffused into the membrane from where it is separated from the rest of the non-permeable gas components. This technique is quite advantageous because of its properties that lower the capital investments, energy sectors and environmental effects while easing the operational conditions, such as lowering the temperature and pressure, simplifying the process and decreasing chemical usage [13]. Membrane performance is judged simply by two features, flux and selectivity. Attempts to achieve high permeability and selectivity are main points of interest; however, improvement of one factor is obtained at the expense of the other factor.

The use of polymeric materials for membrane development is of great importance in gas separation applications. These membranes had been applied in several potential applications that include hydrogen recovery from refinery purge streams, enrichment of nitrogen from compressed air and removal of acid gases (CO_2 , H_2S) from natural gas. These glassy polymeric membranes exhibit good mechanical stability and glass transition temperature along with acceptable permeability and selectivity. High performance polymers such as polysulfone (PSF) and polyimide (PI) possess even higher permselectivity in connection with economical use [14-15]. Both dense and porous membranes can be applied for gas separation processes. Membranes that possess both high permeability and selectivity values would be more useful for a cost-effective gas separation process. For this purpose, Loeb and Sourirajan in 1960 successfully prepared integrally-skinned asymmetric membranes [16]. These membranes are made up of a very thin top skin dense layer (0.1-1 μm) on a porous thick sub-layer support (100-200 μm) [17-18]. The top skin layer acts as the actual selective barrier, whereas the bottom sub-layer provides mechanical support to the skin layer, with an insignificant effect on the gas separation. For ultrathin skinned membranes, the effective thickness is about 1000-5000 A° , while less than this thickness will cause the formation of hyperthin-skinned membranes [19]. Both these

types of asymmetric membranes are particularly developed to attain permeance for practical use.

In spite of the advantages that polymeric membranes possess in terms of ease of processing, development and economical manufacturing cost, there is a need to overcome the plasticization effect that causes a tremendous increase in the solubility of gases which raise serious concerns regarding membrane surfaces [20]. Considerable efforts are in progress to improve the separating properties for the polymeric materials in order to overcome plasticization and the upper bound line as indicated by Robeson in 1991 [21].

The progress of inorganic membranes like silica, zeolites, alumina etc, has been of great importance in recent years because they possess the properties with which they can withstand aggressive chemical feed streams as well as high temperature effects. They possess high mechanical strength, thermal stability and stable pore structures. They can achieve high permeability and selectivity; however, problems of processing, brittleness and high cost limit their use for several applications. An example of a zeolite membrane module would cost about USD 3000/m² whereas a polymeric membrane module was around USD 20/m² for a gas separation application [22].

In order to improve the performance of the polymeric membranes and to achieve high permeability and selectivity for gas separation, the combination of organic and inorganic materials have attracted the attention of many researchers. The inorganic materials are incorporated into the polymeric matrix forming mixed matrix membranes (MMMs) which are more versatile in nature. These materials combine the advantages of inorganics (mechanical strength, thermal stability) and organics (high processability, flexibility, reproducibility of properties, dielectric and ductility), and can lead to improved performance, cost-effectiveness and better structural properties of the developed membranes [23].

1.4 Problem Statement

Membrane technology has been actively practiced for many years for the separation of CO₂ from natural gas. It offers numerous advantages over other techniques which make it quite suitable for gas separation. The performance of gas separating membranes is quite important for effective separation of CO₂ from natural gas. So in the fabrication of the membrane, permeance and selectivity parameters are crucial that needs to be addressed for efficient CO₂ separation.

The use of asymmetric membranes, particularly for gas separation applications, is of great interest because of the high gas flux generated by these membranes as compared to dense symmetric membranes. In these asymmetric membranes, high permeance is a consequence of the thin dense top skin supported by a thick porous sub-layer to provide mechanical strength due to which these membranes are favoured for commercial use in gas separation processes [24-25].

Many glassy polymeric materials have been used for membrane fabrication for gas separation based upon industrial or scientific research work. Polysulfone (PSF) is considered because of good thermal, mechanical and chemical stability along with satisfactory gas performance [14-15, 26]. These aspects along with its comparatively low price have demonstrated PSF to be a suitable material used in membrane fabrication. The limitation of achieving high thermal stability has led to the use of high performance glassy polymers such as polyimides. These aromatic polymers exhibit excellent thermal and mechanical stability. They have relatively high glass transition temperature (T_g) as compared to PSF and have attracted many researchers for improved gas performance [27-29]. However, polyimide (PI) is highly susceptible to plasticization in a CO₂ atmosphere resulting in the reduced permselectivity of the membrane for the operating pressure of above 8 bar [30]. In plasticization, the sorbed CO₂ molecules swell the polymer matrix thereby reducing the interaction of adjacent fragments and adjacent chains. This tends to increase the CO₂ diffusion free volume, ultimately resulting in increased permeance with decreased selectivity upon increasing feed pressure [31-32]. Macroscopically, due to plasticization in the membranes, T_g is reduced while softness and ductility is considerably increased [33]. In addition, the high price of PI compared to PSF limits its use for gas separation [34-

35]. It has been observed from the past studies that PSF exhibits high resistance towards plasticization above the operating pressure of 30 bar while maintaining good permselectivity and low cost [20, 29]. Thus, the blending of PSF and PI polymers is likely to reduce plasticization and impart superior properties in the membrane for gas separation [36]. There are reports on PSF/PI blends based upon dense membranes; however, to the best of the author's knowledge, there are no reports on the study related to asymmetric PSF/PI membrane blends [37]. This approach of blending is used to optimize the properties of polymers that belong to glassy families, in terms of gas separation, thermal stability and cost of production.

Moreover, improving the performance of polymeric membranes for gas separation is considered to be a dominant factor in the field of membrane technology. One of the most practical approaches for improving the performance of membranes is by incorporating inorganic material like silica particles into the polymeric matrix to develop MMMs [48-51]. Addition of silica particles in the polymer matrix may disrupt the polymer chain packing, thus, it may lead to enhanced permeability. In the fabrication of the MMMs, proper controls on morphology to obtain homogeneity and to avoid phase separation are quite important aspects. The fabrication of MMMs is then carried out with an asymmetric membrane blend at various silica loadings on the blended PSF/PI asymmetric membrane with a suitable choice of solvents, NMP/DCM. Previous literature on MMMs with inorganic silica particles incorporated in individual PI or PSF is available; however, to the best of the author's knowledge, reports regarding MMMs with inorganic silica in asymmetric polymeric blends of PSF/PI are not available. So the present work is focused on the development of MMMs using inorganic silica nano particles in asymmetric PSF/PI membrane blends.

1.5 Objectives of Research

The main objectives of the research work are as follows:

1. To prepare and characterize base polymeric asymmetric membranes.
2. To study the effect of solvent and solubility parameter between the polymers and solvents followed by gas permeation evaluation.

3. To develop and characterize novel MMMs followed by gas separation performance.
4. To predict CO₂/CH₄ performance for MMMs using modeling approach.

1.6 Scope of Study

The scope of this research work is divided into the subsequent sections:

1.6.1 Preparation and Characterization of Base Asymmetric Polymeric Membranes

The research is focused on the preparation of asymmetric flat sheet PSF/ PI blended polymeric membranes. The composition of PI contents varied between 5-20 wt.% in the PSF matrix. Dichloromethane (DCM) and N-methyl-2-pyrrolidone (NMP) were used as solvents and ethanol was used as a non-solvent. Fabrication of each of the blended membranes was carried out by the dry/wet phase inversion technique at various solvent compositions of 80/20, 50/50, and 20/80 percent. The solubility parameter was determined to predict and understand the miscibility among the polymers and solvents.

Morphological analysis on the membranes was studied by a scanning electron microscopy (SEM) analysis. A spectral analysis of the developed membranes was carried out with Fourier transform infrared spectroscopy (FTIR). The chemical and mechanical properties were measured by an acid-base titration and a universal testing machine respectively. Thermal analysis on the membranes was carried out by a differential scanning calorimetry (DSC) for evaluating T_g's and thermogravimetric analysis (TGA) for thermal stability of the membranes. While kinetic analyses were carried out at multiple heating rates use TGA as a function of the polymer and inorganic compositions following Friedman's model approach. The performance of the developed membranes was evaluated by using CO₂ and CH₄ gas permeance in a

membrane gas permeation testing unit over the range of 2, 4, 6, 8, and 10 bar feed pressures.

1.6.2 Development and Characterization of Mixed Matrix Membranes

Improvement in the blended polymeric membranes was the aim by incorporating inorganic nano silica in the optimized asymmetric PSF/PI membrane blend to form mixed matrix membranes. Silica sol was prepared from TEOS via the sol-gel approach and a coupling agent was used for improving the polymer-filler adhesion. Incorporation was carried out at various filler loadings of 5, 10, 15, and 20 wt. % into the polymeric matrix.

The fabricated MMMs were characterized using the previous techniques that involved SEM, FTIR, DSC, TGA and universal testing machine. In addition, the morphology of the silica particles in the polymer matrix was examined by the transmission electron microscope (TEM). The gas evaluation was for pure and mixed CO₂ and CH₄ gases and was carried out by using the gas permeation testing unit over the range of 2 to 10 bar feed pressures. The samples were further analyzed with various CO₂/CH₄ gas mixtures of 30/70%, 50/50% and 70/30% for evaluating membrane performance.

1.6.3 Prediction of CO₂/CH₄ Performance by Modeling Approach

Various models were applied for the theoretical estimation of the MMMs performance for the CO₂/CH₄ evaluation. It was eventually compared with the experimental performance of pure CO₂ and CH₄ gases.

1.7 Organization of Thesis

This thesis is organized into the following chapters.

Chapter 1 highlights the importance of natural gas which includes its background history and associated acid gas problems particularly for CO₂. Various treatment techniques for natural gas treatment are highlighted in this chapter. This chapter also includes the problem statement, objectives of the research and the scope of the study of this research work.

Chapter 2 includes the background and theory of gas which includes classification of membranes, fabrication of asymmetric membranes that involves various techniques, gas transport through the membranes and a detailed review on MMMs. This chapter also includes the solubility parameter, plasticization in membranes and a discussion on the various types of gas permeation models used for MMMs.

Chapter 3 includes the description of the materials used and the fabrication procedures involved during the experimental work for the development of the asymmetric membrane blends followed by MMMs. The experimental apparatus used and various techniques used during the characterization of the membranes along with the evaluation of the membrane performance are also described.

Chapter 4 includes a discussion on all of the experimental results obtained in this work. It includes the solubility parameter relationship and SEM structures of the developed membrane. It highlights the properties of the formed membranes in terms of thermal and mechanical characteristics, correlation of asymmetric membrane formation and mixed matrix membranes with the membrane performance in terms of the CO₂/CH₄ permeance and CO₂/CH₄ selectivity at different feed pressures. Various gas permeation model predictions were used for a comparative evaluation of the MMM permeation results.

Chapter 5 includes the summary of the performed research work and the concluding remarks along with future work recommendations.

CHAPTER 2

2. BACKGROUND AND THEORY

2.1 Overview

This chapter includes the literature survey of theoretical knowledge and the studies carried out in the past which form the basis for the selection of a suitable type of membranes for gas separation. In this chapter, various types of membranes and membrane fabrication techniques are discussed. Other characteristics, such as the solubility parameter estimation among the components of the casting solution, the gas transport in membranes and the plasticization effects are included. A potential approach of improving the separation properties by incorporating inorganic fillers into the polymer matrix to form a mixed matrix membrane is discussed. It includes the various treatment steps adopted and the problems faced by many researchers in the fabrication of membranes.

2.2 Membrane Classification

Membranes have been considered for more than 150 years and for gas separation processes, they have been used commercially since 1980 [38-39]. A membrane is defined as that selective barrier between the two mediums which has the ability to allow one of the components to pass through to the other [40]. When a mixture of feed gas comes in contact with the upstream side of the membrane, one of the components of the feed gas permeates through the downstream side of the membrane. However, enrichment in one of the components from the feed stream may take place and exists from the upstream side of the membrane as the residue which is commonly known as the retentate. For the permeation to take place, pressure or a concentration gradient must exist across the membrane that acts as a driving force. The separation of

any component from the feed stream is achieved which is based upon the difference in the permeation rates between the components. A schematic representation of a simple gas separation process through a membrane is shown in Figure 2.1.

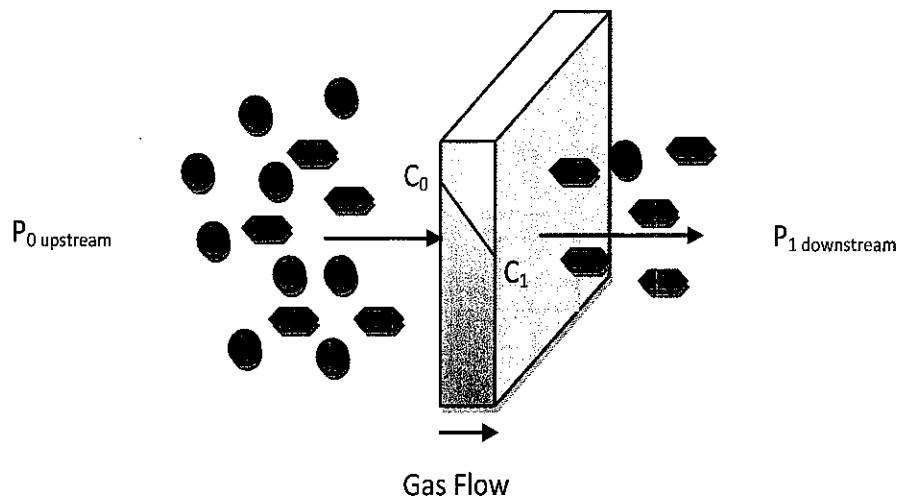


Figure 2.1 Schematic representation of a simple gas separation process through a membrane

Different types of membranes are used over a wide range of applications for treatment purposes and are mostly synthetic. These synthetic membranes vary from organic to inorganic materials and are used in various applications [41]. Depending upon the application, these membranes are used based upon the different strategies for their fabrication to ensure effective separation. Based upon various morphologies, membranes are classified into two main groups which are shown in Figure 2.2

Symmetric membranes are basically homogenous having a consistent structure and the resistance to mass transfer is obtained throughout their entire cross-section. These membranes are further classified into three different categories.

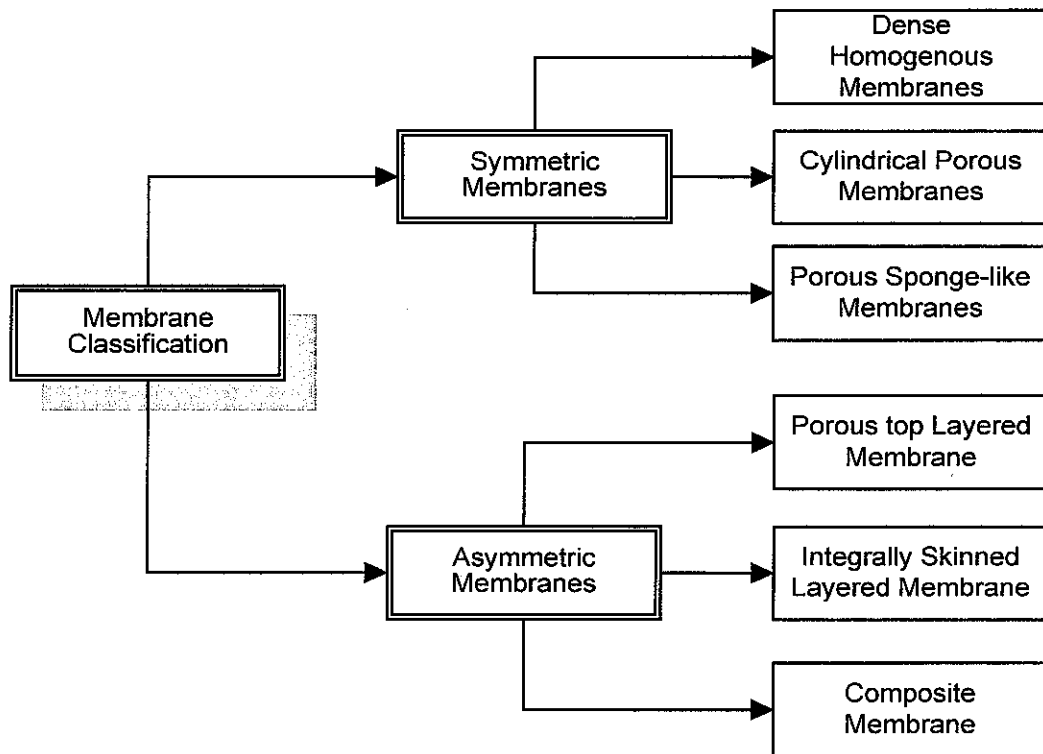


Figure 2.2 Classification of membranes according to the structural morphology

- Dense homogenous membranes are non-porous films which permeate the penetrants with the help of a driving force that may be pressure or a concentration gradient. These types of membranes are used for gas separation and pervaporation (PV) applications. Their membrane thickness varies from 10-200 μm [40].
- Cylindrical porous symmetric membranes have finger like structures and are used for separation of enzymes from dilute solutions.
- Porous sponge-like membranes contain pores or holes in their structures and are normally used for microfiltration (MF) and pertraction applications and have a pore size in a range of 0.2-5 μm [42].

By definition, asymmetric membranes are those which comprise a top thin skin layer (<1 μm) integrated in a series with a thick porous substructure (0.2-0.5mm) [43]. The advantages associated with these membranes is the use of low-cost substrate

which can simultaneously provide membranes with reasonable mechanical properties, and they can lower the cost of materials [44]. Development of asymmetric membranes is considered to be a major breakthrough for various industrial applications as it combines high permeation and selectivity [40]. These types of membranes are further divided into three categories as shown in Figure 2.2. Porous top layered membranes contain pores in the skin layer that increase in size from top to bottom and are used in MF and ultrafiltration (UF) applications [42].

- Integrally skinned layered membranes are made up of a very thin dense skin layer in a range of 0.1-1 μm that is supported by a thick porous sub-layer in a range of 100-200 μm . Moreover, both of the layers are composed of the same material and are developed during a single operation. These types of membranes are used for gas separation applications [39].
- A composite membrane is prepared similarly with a top dense skin layer that is supported by a thick sub-layer support. However, in the preparation of these types of membranes, both the skin layer and the thick sub-layer are made up of different materials. These asymmetric membranes are used in gas separation applications [43].

The development of the membranes is quite important so as to achieve high permeation properties and selectivity. In gas separation applications and other high pressure applications, asymmetric membranes are therefore preferred because they provide enhanced gas fluxes with sufficiently high selectivity and mechanical strength [24, 39, 45].

2.3 Asymmetric Membrane Fabrication Techniques

In most of the industrial application processes, symmetric membranes have been replaced by the asymmetric membranes. In 1960, Loeb and Sourirajan developed high flux asymmetric membranes which are the most flexible, cost-effective and reproducible processes for asymmetric membranes while maintaining high selectivity

[34, 46]. Various methods can be applied for the development of asymmetric membranes. Some of the processes for their development are discussed as follows:

2.3.1 Solution Cast Composite Membranes

This type of composite membrane was first prepared by Ward and Browall. In this technique, a dope polymeric solution prepared in a water-insoluble solvent was spread on the surface of the water present in a trough. A thin polymeric film thus produced on the water surface was then coated onto a microporous support. The thickness formed by this method produced a thin perselective layer having a thickness of 0.5-2 μm . This process was carried out through a semi continuous operation; however, this process was not reliable for large-scale operations [47].

2.3.2 Interfacial Composite Membrane

Cadotte, in the early 1960s, developed a new approach for the preparation of asymmetric membranes that could be used for reverse osmosis operations. In this technique, a pre-polymeric aqueous solution, such as polyamine, was initially coated on the surface of the microporous supported membrane, typically polysulfone. It was followed with immersion in a water-immiscible solvent containing a reactant such as a hexane-acid chloride solution. The amine and acid chloride reacted with the amine at the interface of the two solutions thus forming a thin layer having a dense cross-linked structure.

Membranes thus prepared by this approach are extremely thin in a range of $\leq 0.1\mu\text{m}$. This produces higher fluxes and due to the high cross-linking, its selectivity is high. However, this approach is less applicable for gas separation since water swollen hydrogel fills the pores of the supported membrane. As a result of which the gel becomes rigid glass with low permeability once dried in an oven. The glassy polymer tends to fill up the pores and as a result the composite membrane usually has low flux [47].

2.3.3 Dynamically Formed Membranes

In the early 1970s, dynamically formed membranes were prepared by Johnson and Kraus. In the preparation, an organic or inorganic colloidal layer was formed on the microporous supported membrane by filtering a colloidal solution through it. This colloidal surface dissolved or eroded over a period of time thus decreasing the performance of the membrane. Hence, a new colloidal layer was required to be prepared on the surface of the support. Microporous ceramic or carbon tubes and some typical colloidal materials, such as polyvinyl methyl ether, acrylic acid copolymer or hydrated metal oxides were used. These types of membranes were used for reverse osmosis purposes providing a good water flux and salt rejection. However, these membranes were found to have problems of instability and reproducibility along with reliability and consistency. Therefore, these types of membranes fell short of favour [48].

2.3.4 Phase Inversion (Solution Precipitation) Membranes

Phase inversion is a process in which the casting solution is precipitated into polymer rich and lean phases. The rich phase of a solid polymer forms the matrix of the membrane while the lean phase of the liquid polymer forms the membrane pores [49]. Adjusting the parameters of the two phases can get the desired structure of the developed membrane. Several ways can be adopted to get polymer precipitation that involves cooling, solvent evaporation and precipitation by immersion in water. These methods are discussed below.

2.3.4.1 Thermal precipitation

In this method of thermal precipitation for the development of asymmetric membranes, a film is casted from a hot polymer casting solution, followed by a cooling process to precipitate the polymer. On cooling, the film separates into two phases with one being the polymer-matrix phase with the other being the membrane pore-phase. The initial composition of the polymer casting solution will determine the pore volume of the prepared membrane as this corresponds to the ratio of the polymer

to liquid phase. However, the cooling rate greatly influences the pore size and precipitation of the final membrane [47].

2.3.4.2 Polymer precipitation by solvent evaporation

Polymer precipitation by solvent evaporation is one of the oldest methods of preparing a microporous membrane which started to be used in the 1920s [50]. In this method, a polymer is dissolved into a composition of two solvent mixtures consisting of a more volatile solvent such as acetone and comparatively less volatile non-solvent typically water or alcohol. After casting the solution on the glass plate, the volatile solvents are allowed to evaporate for a certain period of time. The casting solution which is enriched with the less volatile non-solvent will precipitate to form the membrane structure. The continuation of the solvent evaporation-precipitation process depends upon the final formation of the film.

Various factors may affect the porosity and pore size of the membrane formed through this technique. In general, fine pores will be formed for a short evaporation time and larger pores are formed if the evaporation step is prolonged. Similarly, porosity is affected by the non-solvent composition of the casting solution. Hence, increasing the composition of the non-solvent in the casting solution will increase the porosity of the membrane and vice versa [48].

2.3.4.3 Polymer precipitation by absorption of water vapours

In this type of membrane fabrication process, water vapours are required to induce the phase separation during membrane development. The casting solution which consists of the polymer, more volatile solvent mixtures and a less non-volatile solvent is cast on a continuous stainless steel belt. The cast membrane is then passed along a series of chambers with varying environmental effects. During the circulation, the membrane loses more of the volatile solvent by evaporation and, simultaneously, absorbs water vapours from the humid atmosphere. This process takes 10minutes for completion and the membrane formed is quite symmetrical. After precipitation, the

formed membranes were passed into an oven for the complete drying of the remaining solvent. These types of membranes are normally used for microfiltration purposes [48].

2.3.4.4 Polymer precipitation by immersion in a non-solvent bath (Loeb-Sourirajan's technique)

Loeb-Sourirajan's technique is considered to be the most important process for the preparation of asymmetric membranes. In this method, after casting the dope solution on the glass plate, it is immersed into a precipitation bath of water. The surface of the cast solution on the glass plate rapidly precipitates and forms a dense permselective skin layer. This dense surface, formed gradually, slows down the process of the precipitation by restraining the entry of water into the underlying polymer solution thus forming a subporous layer. The top dense skin formed varies in thickness from 0.1-1.0 μm . Loeb-Sourirajan's work is considered to be a critical breakthrough in the field of membrane technology [34, 46].

2.3.5 Dry/Wet Phase Inversion Technique

The dry/wet phase inversion technique is widely employed for the fabrication of these types of asymmetric membranes. It involves drying the casting solution via evaporation under a controlled environment followed by a wet phase in which the casted solution is allowed to precipitate by solvent exchange in a non-solvent precipitation bath [40].

In the formation of asymmetric membranes via the phase inversion technique, the phase diagram for a ternary system is normally used to explain the process among the polymer, solvent(s) and the non-solvent(s).

Figure 2.3 indicates stable, metastable and unstable regions where the stable region indicates that all the components of the casting solution exist in a single phase and are homogeneously miscible indicated by point A. The second, metastable region indicated by point B, shows that the homogeneous casting solution becomes

thermodynamically unstable; however, it will not usually precipitate until well nucleated. The third, unstable region represented by point C, indicates that the casting solution will form two phases spontaneously, i.e., rich and lean polymer phases and form the asymmetric membrane structure through nucleation and a growth mechanism [50]. The figure indicates that the stable and metastable regions are divided by the binodal curve whereas the metastable and the unstable regions are split by the spinodal curve. The point of intersection of the two curves is the critical point.

Two mechanisms involving nucleation and growth or spinodal decomposition are associated with phase separation of a dope casting stable solution [51]. A nucleation and growth decomposition mechanisms takes place in the metastable region when the casting solution become unstable and follows the region as shown by the line ABCD.

Usually, if the concentration of the polymer is low in the dope solution, then the precipitation path crosses the binodal curve, the critical point, and then the phase separation is initiated by the polymer-rich phase. However, if the polymer concentration is high, then the precipitation path passes through the binodal curve above the critical point and then the nucleation of the polymer-lean phase may occur. On the other hand, at high polymer concentrations, the precipitation path bypasses the binodal curve and phenomena, such as vitrification, gelation or crystallization will take place without the growth of the polymer-lean phase.

During the immersing process of the cast polymer solution into the non-solvent precipitation bath, the non-solvent tends to diffuse into the nascent membrane. The spinodal decomposition mechanism occurs if the membranes formed enter the unstable region directly without passing through the metastable region as shown by the line EFGH. The line separates the polymer solution into a polymer-rich phase membrane structure, and the solvent-rich phase that forms interconnectivity between the two phases forms open cell like structures. Moreover, during the immersion precipitation process, instantaneous and delayed demixing can occur [40]. In the case of delayed demixing, the homogenous casting solution requires a longer time, i.e., more than one second to become unstable and eventually to develop into the membrane structure. Whereas, in the case of the instantaneous demixing process, the casting solution becomes unstable as soon as it is immersed into a coagulation bath.

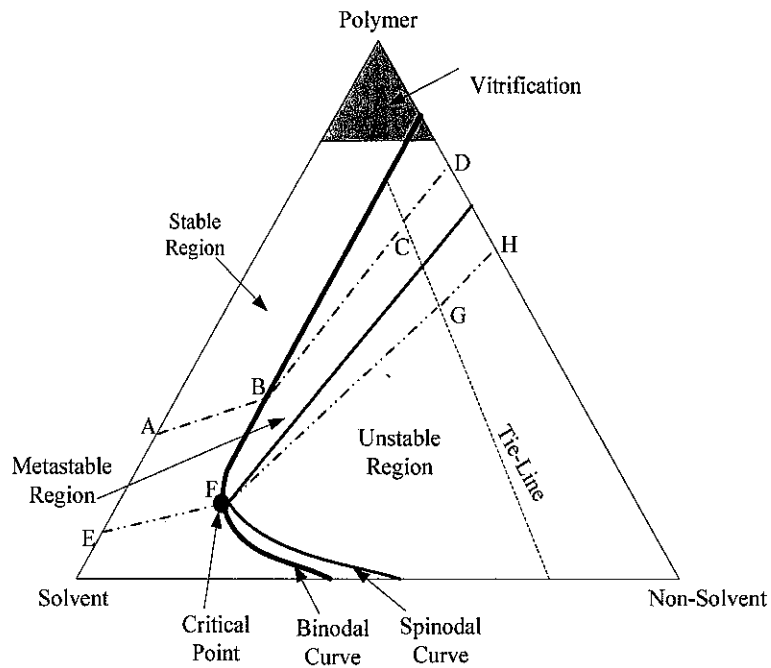


Figure 2.3 Schematic diagram of ternary phase among polymer, solvent and non-solvent [52]

The asymmetric membrane prepared from delayed demixing tends to develop relatively dense skin and a closed, less porous substructure. These types of membranes are favoured for gas separation applications. This is in contrast to instantaneous demixing where the casting solution forms a thin porous top layer with a macrovoid open cell substructure. Delayed demixing occurs due to a relatively large amount of solvent from the membrane that diffuses into the coagulation bath whereas the flow of the coagulant into the membrane is relatively small [51]. This is in contrast to instantaneous demixing where a rapid exchange takes place between the solvent and the coagulant.

On the other hand, the evaporation step prior to the immersion process is quite important in the formation of the final structure of the membrane. During this period of the dry phase inversion, a gas stream passes over the homogenous cast solution that has been appropriately prepared which exists at the boundary of the binodal curve. In such conditions, sufficient volatile solvent will be lost from the nascent membrane during the evaporation step. This relocates the stable nascent membrane to the point

of instantaneous instability and forms a spinodally decomposed structure. This condition will create such a situation in which sufficient volatile solvent on the outermost region of the casting solution will be lost during the evaporation step to drive the homogeneously stable casting solution to become unstable instantaneously to produce a spinodally decomposed structure. The process of the dry phase inversion is essential for producing a very thin and defect free skin layer thus allowing the phase separated membrane surface to seal before being quenched. In general, the pores at the membrane surface where precipitation occurs first and most rapidly are much smaller than those in the interior or the bottom side of the film, and this leads to the asymmetric membrane structure [53-54].

The development of asymmetric membranes is often carried out by the ternary diagram that involves the study on phase separation. However, this requires extensive experimental study to get information for the representative phase diagram about a particular polymer, solvent and non-solvent system. A comparatively easy approach termed as the coagulation value is introduced for obtaining the required information easily on the phase separation of the polymer solution. It corresponds to the rate of demixing between the casting solution and the coagulant to form the membrane. A lower and higher coagulation value indicates faster and delayed demixing rates.

2.4 Solubility Parameter Estimation

The solubility parameter is calculated to express the nature and magnitude of the interactive forces working between the polymers and solvents. It is the measure of the affinity between the components of a mixture. For the purpose of improving the prediction of the solubility parameter, the group contribution method is used to calculate the overall solubility parameter as proposed by Hansen. Hansen's method predicts interaction between the polymers and solvents using three solubility parameters and thus predicts better than any other approach [55]. The overall solubility parameter is shown by the following Eq.(2.1) [56]:

$$\delta = \sqrt{\delta_d^2 + \delta_p^2 + \delta_h^2} \quad (2.1)$$

Where, δ_d , δ_p and δ_h are the dispersive, polar and hydrogen bonding solubility parameters, respectively, calculated by Van-Kravelen and Hoftyzer's method [57].

$$\delta_d = \sum F_{di} / V; \delta_p = \sqrt{\sum F_{pi}^2} / V; \delta_h = \sqrt{\sum E_{hi}} / V \quad (2.2)$$

F_{di} , F_{pi} , E_{hi} are the respective dispersion, dipole force and hydrogen bonding force components of the solubility parameter and V denotes the molar volume. The numerical values assigned to each structural component of the organic compounds can be obtained readily from Table 3.3, mentioned later in Chapter 3. The table indicates the functional groups of the polymers, solvents and the non-solvents used and the number of times any functional group appearing is noted in frequency [58]. The effective Hansen solubility parameter for various mixtures of solvents in the casting solution can be calculated by using Eq.(2.3)[59]:

$$\delta^2 = \left(\sum \delta_d^i \phi^i\right)^2 + \left(\sum \delta_p^i \phi^i\right)^2 + \left(\sum \delta_h^i \phi^i\right)^2 \quad (2.3)$$

Where, δ and ϕ is the volume fraction for i species. The total solubility parameter difference between the casting solution and the non-solvent is then calculated by Eq. (2.4) based upon Hansen's solubility parameter written as [60]:

$$\Delta\delta_{ij} = \sqrt{(\delta_{i,d} - \delta_{j,d})^2 + (\delta_{i,p} - \delta_{j,p})^2 + (\delta_{i,h} - \delta_{j,h})^2} \quad (2.4)$$

Where, i is the solute and j is the solvent. The parameter follows the rule that the smaller the $\Delta\delta_{ij}$ value, the greater the affinity between the solute and the solvent.

2.5 Gas Transport in Membranes

In the gas separation processes, the gas permeation through the membranes is based upon various mechanisms among which solution-diffusion has been widely accepted. The solution-diffusion mechanism is based upon separation through non-porous dense membranes. For the glassy polymers, the gas transport mechanism exists in three steps which includes sorption of the feed gas molecules into the membrane interface, followed by diffusion through the entire membrane thickness and finally desorption of

the absorbed gas on the permeate side (as illustrated in Figure 2.1). In this mechanism, the driving force is based upon the gradient of thermodynamic factors, such as concentration, pressure or temperature between the feed and the permeate sides of the membrane along with the forces of the interaction between the gas molecules and the membrane material.

Different gas transportation mechanisms are followed by the membranes which mainly involve convective, Knudsen diffusion, molecular sieving and solution-diffusion mechanisms (Figure 2.4). With large pore sizes of 0.1-10 μm , gas molecules can pass through the membranes by exclusive collision with each other in a convective flow. At a pore size of 0.1 μm , transportation occurs via the Knudsen flow and the gas molecules pass through by more frequent collisions with the walls than with each other. Here, selectivity for binary gas pairs is obtained by the square root of the ratio of the two gases' molecular weights. With extremely small pores similar to the diameter of the gas molecules, separation is efficiently attained by molecular sieving. With a molecular sieving mechanism, high selectivity is derived from accurate discrimination of size and shape between the different gas penetrates. Here, the transportation occurs with both gas phase diffusion and surface diffusion of the adsorbed gas molecules on the surface of the pores. However, these kinds of membranes are not preferred for large scale operations. With a solution-diffusion mechanism in the dense membranes, gas molecules are transported across the membranes by adsorption on the membrane surface in the feed side followed by the diffusion process and eventually desorption on the permeate side of the membrane. The gas transportation by the solution-diffusion mechanism is relatively sluggish in comparison to the Knudsen diffusion where the flow occurs through non-selective pores in the membranes. Hence, a slight defect in the membrane surface can cause an abrupt decrease in the selectivity values.

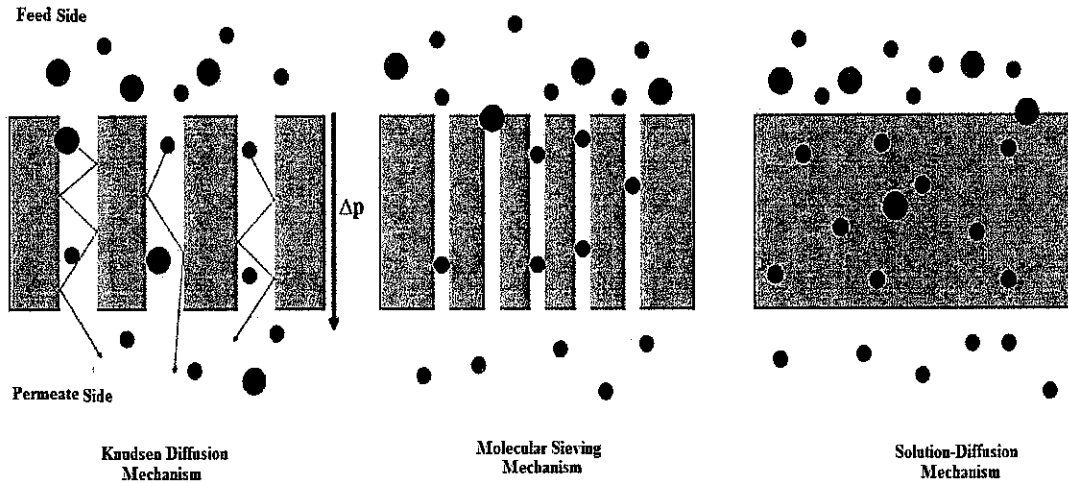


Figure 2.4 Schematic diagram for gas permeation involving Knudsen diffusion, Molecular sieving and Solution diffusion mechanism [61]

2.5.1 Permeation

The performance of the membranes is mainly characterized by two factors which constitutes the flux of a gas component across the membrane thickness while the other is the selectivity of the membrane to achieve the separation of the gas components. Permeability is defined as the measure of the transport flux of a gas component to the difference in partial pressures between the upstream and downstream sides of the membrane Eq.(2.5):

$$P_A = \frac{J_A \times l}{\Delta p_A} \quad (2.5)$$

Where, J is the flux, Δp is the differential partial pressure across the membrane for component A and l denotes the thickness of the membrane.

For asymmetric membranes, since the thickness is difficult to define, it is more suitable to use the term 'permeance' instead of 'permeability'. Hence, permeance, which is also known as the pressure normalized flux, is defined as the permeability per the effective thickness of asymmetric membranes, P/l , and then the Eq.(2.5) takes the form of Eq.(2.6):

$$\frac{P_A}{l} = \frac{J_A}{\Delta p_A} \quad (2.6)$$

The units of permeability and permance are mentioned in Table 2.1. For the solution-diffusion mechanism, permeation of a gas with component A can be obtained by the product of the kinetic factor known as the diffusion coefficient, D_A , and the thermodynamic factor called the solubility coefficient, S_A shown in Eq.(2.7):

$$P_A = D_A \cdot S_A \quad (2.7)$$

Table 2.1 Gas Permeability and Permeance Units

Expression	Unit	Dimension
Permeability, P_A	Barrer	$10^{-10} \frac{\text{cm}^3(\text{STP}) \cdot \text{cm}}{\text{cm}^2 \cdot \text{sec} \cdot \text{cmHg}}$
Permeance, $\frac{P_A}{l}$	Gas Permeation Unit (GPU)	$10^{-6} \frac{\text{cm}^3(\text{STP})}{\text{cm}^2 \cdot \text{sec} \cdot \text{cmHg}}$

The performance of a membrane in a gas mixture can be determined by taking the ratio of a component with a faster permeation rate over the slower permeation rate component in the permeate phase. The ideal selectivity in terms of permeability and permeance for the A and B components in a gas mixture, $\alpha_{A/B}$ is thus written as Eq.(2.8):

$$\alpha_{A/B} = \frac{P_A}{P_B} = \frac{(P/l)_A}{(P/l)_B} = \left(\frac{D_A \cdot S_A}{D_B \cdot S_B} \right) \quad (2.8)$$

So, for the estimation of the membrane separation ability, high permeance and selectivity are the two important parameters for their performance evaluation. Moreover, in terms of solution-diffusion mechanism, ideal selectivity gives the ratio between the product of diffusivity and solubility. Thus, by adjusting the diffusivity and solubility coefficients of the gas penetrants, the performance of the membranes can be further improved.

The diffusivity selectivity (D_A/D_B) can be determined depending upon the difference in the shape and size of the penetrants' gases, segmental chain mobility of polymeric chains and on their average intersegmental distance. While the solubility selectivity (S_A/S_B) depends upon the condensability of the penetrants gases, the interaction between the polymer and the penetrants and on the quantity of the free volume present in the polymer matrix [62].

The solubility of the gases in glassy polymers is usually expressed by the dual-mode sorption which expresses the existence of two types of sites (1) C_D : in which the site is occupied by gas penetrants dissolved in equilibrium free volume; (2) C_H : in which the population of the dissolved penetrants are limited in the excess free volume of material and ceases when all the sites are fully occupied [63].

The first type of site exists for rubbery polymers. Rubbery polymers obey Henry's law which is a linear relationship between the amount of gas sorbed and partial pressure of gas, written as Eq.(2.9)

$$C_D = K_D \cdot p \quad (2.9)$$

Where, K_D is the solubility coefficient that defines Henry's law constant and is valid for sorption of light gases.

The second type of site exists for glassy polymers and fillers, such as carbon molecular sieves, silica, zeolites etc. which follows the Langmuir isotherm for gas sorption. In the Langmuir isotherm, the gas adsorption takes place on a limited number of sorption sites before reaching the saturation point. This adsorption isotherm is considered to be in dynamic equilibrium and the rate of adsorption is equal to the rate of desorption. In it, the sorption rate is proportional to the concentration of the feed gas molecules and the quantity of available sites for sorption. It approaches the state of dynamic equilibrium with the rate of desorption. The Langmuir isotherm is expressed as Eq.(2.10):

$$C_H = \frac{C'_H \cdot b \cdot p}{1 + b \cdot p} \quad (2.10)$$

Where, C'_H is the maximum amount of sorptive capacity and b represents the Langmuir affinity constant.

The total solubility of the gases in glassy materials that describes the dual-mode sorption model is the sum of Henry's law and Langmuir sorption sites and is expressed as Eq.(2.11)-(2.12) [63]:

$$C = C_D + C_H \quad (2.11)$$

$$C = K_D \cdot p + \frac{C'_H \cdot b \cdot p}{1 + b \cdot p} \quad (2.12)$$

Where, C_D is the Henry's law mode concentration and C_H is the Langmuir isotherm.

The diffusion of the gas molecules depends on both Henry's and Langmuir's modes. It was proposed that the Langmuir population is comparatively less mobile than that of Henry's population that forms the basis of the partial immobilization model [64]. For most of the systems, the Langmuir population exhibits some mobility and affects the permeation of the gases. Hence by involving the two diffusion modes, Fick's law of diffusion in Eq.(2.13) can be written as Eq.(2.14)

$$J = -D \frac{dC}{dx} \quad (2.13)$$

$$J = - \left[D_D \frac{dC_D}{dx} + D_H \frac{dC_H}{dx} \right] \quad (2.14)$$

Where, D_D and D_H are the gas diffusion coefficients in the Henry and Langmuir modes, respectively. From the relationship of the solubility and diffusivity coefficients of Eq.(2.7), permeability in the glassy membranes can be expressed by the dual sorption model as shown in Eq. (2.15).

$$P_A = K_{DA} \cdot D_{DA} + \frac{C'_{HA} \cdot b_A \cdot D_{HA}}{1 + b_A \cdot p_A} \quad (2.15)$$

Where, P_A is the permeability of the gas component A. The substitutions in Fick's law were carried out by keeping in view only the diffusion contributions. Lately, it can be further used for multi component systems for the permeation gas evaluation.

2.6 Selection of Glassy Polymers

The use of polymeric membranes for gas separation has been effectively used since 1830s [65]. Among these materials, high performance glassy polymers have now taken over from the rubbery polymers for the last two decades [66]. These engineering polymers possess high gas permeabilities and selectivities along with excellent thermal and mechanical properties. By definition, these polymers are an amorphous polymeric material which exists below their glass transition temperature (T_g) in contrast to the rubbery polymers. T_g is the transition point between the glassy and the rubbery states and defines the characteristics of amorphous polymers as

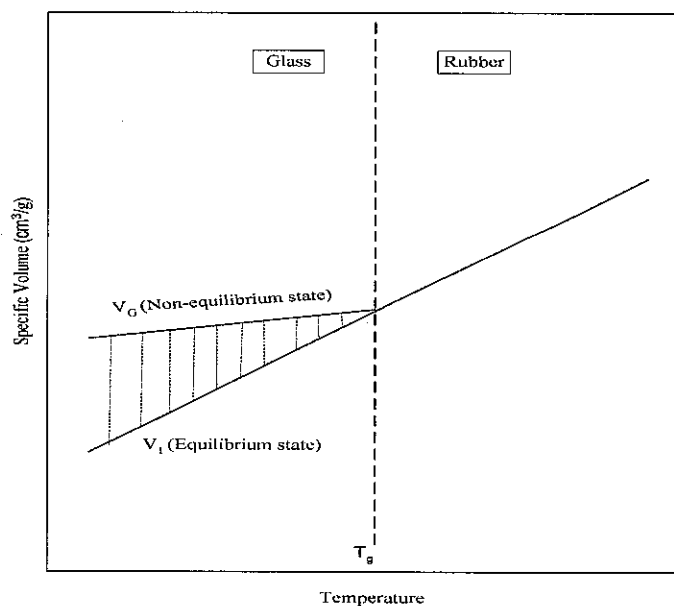


Figure 2.5 A schematic diagram of the glass transition temperature (T_g) between the glassy and rubbery polymer states [65]

shown in the Figure 2.5. These glassy polymers exhibit restricted segmental chain motions and drastically slow down with the decrease in T_g , thus creating packing defects in a non-equilibrium state. Due to this unique characteristic of reduction in the chain mobility, these materials offer more size and shape selective atmospheres for gas diffusion to occur in comparison to rubbery polymers. Moreover, the presence of excess volume allows additional penetrants to be accommodated in comparison to the rubbers. Hence, these glassy polymers are more commonly used in many gas separation processes [67].

Previously, for the purpose of gas separation for commercial use, lots of concerns were aroused regarding the performance of the polymeric membranes. This was due to the large thickness of the membranes which caused the low permeability and selectivity of the membranes. However, later, due to the formation of asymmetric membranes with skin thicknesses as low as 1000\AA by phase inversion technique using the Loeb and Sourirajan method (1964) opened new horizons for gas separation through polymeric membranes [68]. This ultrathin dense skin layer provides the important gas separating function while the porous layer serves as the mechanical support.

With the development of new membrane separation processes, techniques and economic aspects, the need for proper attention towards the permeability and selectivity of the membranes has become a strong subject with worldwide interest for both industrial and academic researchers. For a membrane material to achieve high performance along with thermal and mechanical stability is a requirement for attractive gas separation. Consequently in the last few decades, thousands of articles and patents regarding the structures, synthesis and transportation properties of the gases of polymeric materials have been published to widen the performance horizons in the context of a trade-off relationship. Special attention has been made towards the advancements in high T_g amorphous glassy polymers, such as cellulose acetate, polycarbonates, polysulfones and polyimides. Comparative trade-off plots between the performances of the glassy to the rubbery polymers for various gases (CO_2/CH_4 , O_2/N_2 , H_2/CH_4) as mentioned by Robeson in 1991 are shown in Figure 2.6 [69]. The graphs indicate higher selectivity for glassy polymers that lie near to upper bound

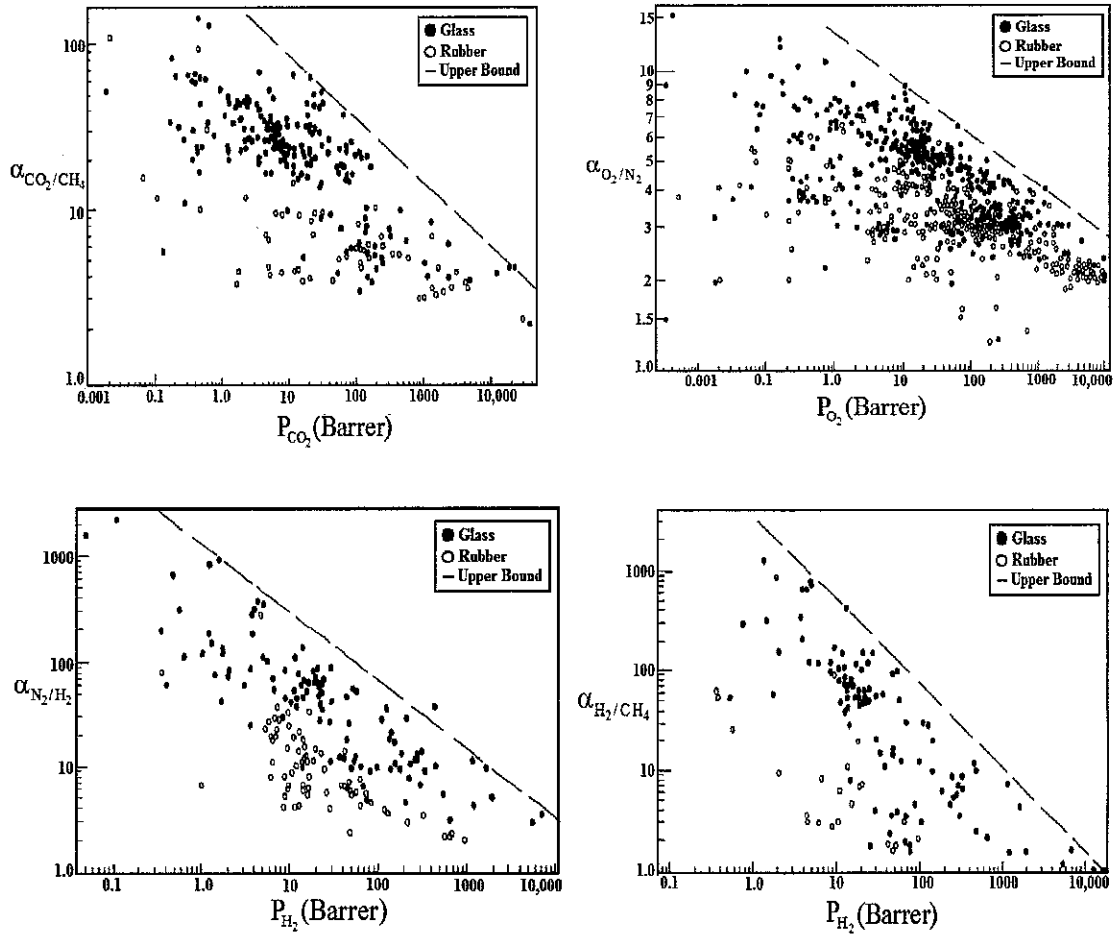


Figure 2.6 Comparison between the glassy and rubbery polymers in terms of selectivity and permeability of various gases, mentioned as trade-off plots by Robeson [69]

lines for various gas pairs in comparison to the rubbery polymers. This is in correlation to the solution-diffusion mechanism coupled with the molecular sizes of the various gases.

With the increase in the molecular size, diffusion coefficients decrease which is due to the fact that larger molecules interact with more polymer chain segments in comparison to small gas molecules. Hence, the diffusion selectivity, D_A/D_B , as in Eq.(2.8) always favors the permeation of molecules having smaller kinetic diameters, such as water (2.65\AA) and CO_2 (3.30\AA) over larger molecules, such as CH_4 (3.80\AA). Moreover, for the sorption coefficient of the gases in polymers, which is the amount of energy required by the gas molecules to get sorbed in the polymer, depends upon

the condensability of the gases. In general, with the increase in condensability of the gases, the sorption coefficient also increases. Hence, the sorption selectivity, S_A/S_B as in Eq.(2.8), favors higher condensable gas components, such as CO_2 (216°K) rather than CH_4 (113°K), in natural gas.

The diffusion selectivity, D_A/D_B , very much depends upon the polymeric material and on the glass transition states of the polymer. In the case of glassy polymers existing below T_g , the polymers are tough and rigid with poor polymeric chain mobility. Thus, the molecular size difference of the penetrating gases largely affects the relative mobility. However, rubbery polymers that exist above T_g possess a large intersegmental polymer chain motion. Moreover, the effect of the molecular size difference among the penetrating gases on relative mobility is low. In some extreme conditions plasticization is caused by gaseous components such as CO_2 . This forms a strong interaction with the membrane material and thus deleteriously changes the characteristics of the membranes. Due to this effect, a decrease in the interactions among the adjacent polymer chain segments occurs that causes enhanced polymer chain mobility [20]. This situation causes the decrease in the mobility selectivity, D_A/D_B , and the ratio even reaches to unity for the permeating molecules of the same sizes. Thus, for desirable optimized mobility selectivity, it is essential to tailor the membrane materials and chemistry for attaining the desired performance.

Separation of the permeating gases in glassy and rubbery polymers is carried out on the basis of relative size and relative condensability, respectively. A comparison between the various gases in terms of their relative size and condensability are shown in Figure 2.7 [50]. It is observed that glassy and rubbery polymers can separate CO_2 and H_2S from CH_4 because of the smaller size and more condensability. However, the best and high performances can only be achieved by glassy polymers. H_2S can be easily separated from natural gas by rubbery polymeric membranes due to its larger size and more condensable properties as compared to CO_2 . Similarly, N_2 is smaller in size than CH_4 and is separated by glassy polymers. However, the comparative size is much smaller between the two gases, so a smaller selective separation is obtained. On the other hand, separation of CH_4 from N_2 can be achieved

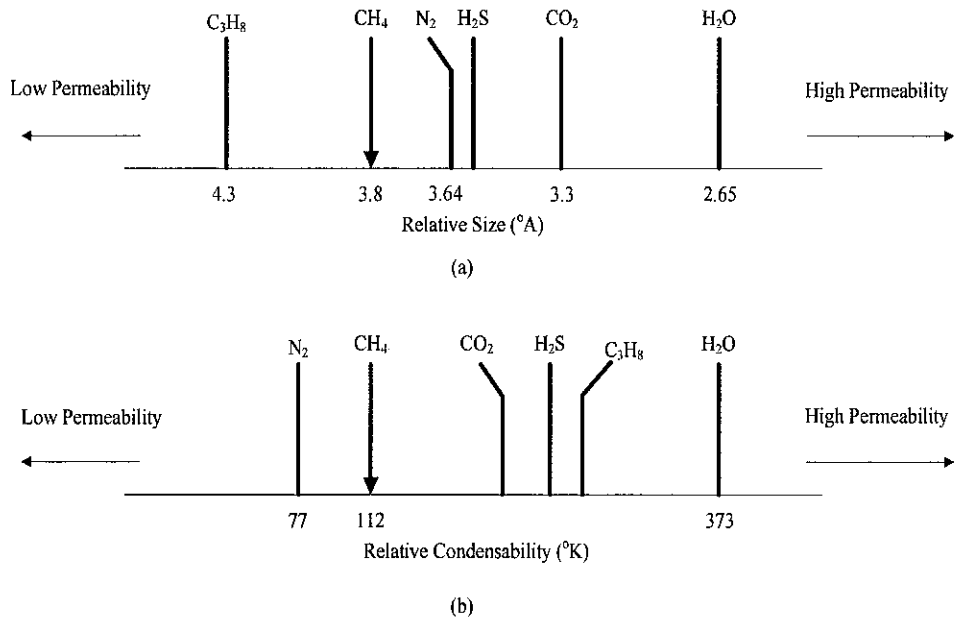


Figure 2.7 Separation of gases by (a) Glassy polymers (b) Rubbery polymers [50]

by rubbery polymers due to the higher condensability where it can maximize sorption selectivity with minimizing size selectivity. Similarly, hydrocarbons such as C₃H₈ possess high condensability as compared to CH₄ and are suitably separated by rubbery membranes.

2.6.1 CO₂ Plasticization in Glassy Polymers

Many glassy polymeric materials have been used for fabricating membranes for gas separation based upon industrial or scientific work due to high permeability and selectivity characteristics. Figure 2.8 shows the transport properties of some of the potential polymers which exist closer to the upper bound as mentioned by Robeson in 1991 [23, 65, 69].

CO₂ is one of the major impurities in natural gas containing CH₄ (~75%) and needs to be separated because of its energy concerning issues and corrosive nature. It falls into the category of acidic gases and its presence in extreme environments may aggravate membrane damage by swelling and thus inducing plasticizing effects in

membranes [70]. In plasticization, the sorbed condensable CO₂ gas molecules swell the polymer matrix, thereby, reducing the interaction among their adjacent chain fragments. This in turn causes an increase in the interstitial space among polymer chains due to which larger free volumes are created with the enhancement in the mobility of side groups by the presence of CO₂ plasticizer. Hence, the diffusivities of the gases are accelerated due to this swelling of the polymeric matrix. Consequently the separation ability of the membrane on the basis of the molecular size is reduced tremendously and hence, caused a decrease in the CO₂/CH₄ selectivity of the membrane [20, 71]. Therefore, lots of efforts are being made in both industrial and academic sectors to tackle the problems being faced by such magnitude associated with membrane performance.

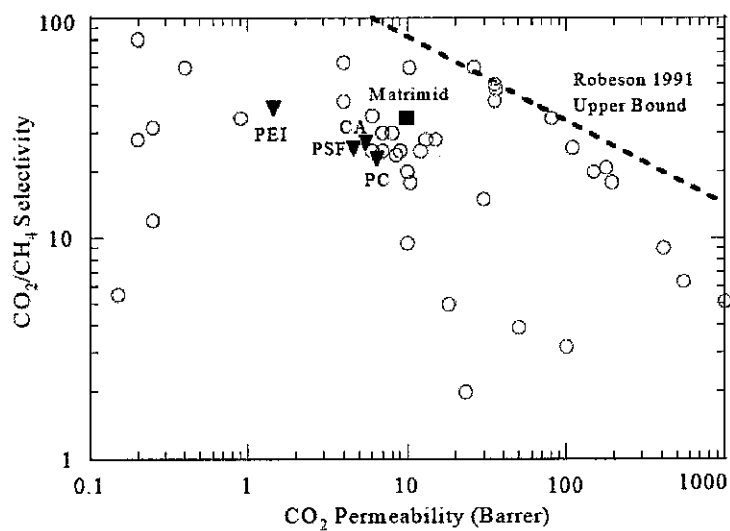


Figure 2.8 Robeson's plot related to the CO₂/CH₄ selectivity versus the CO₂ permeability for various polymers showing high performance PI-Matrimid (■), conventional polymers as PEI, PSF, PC, CA (▼) and (○) other polymers [65, 72]

The effect of plasticization in the glassy polymers causes a significant increase in the permeation behaviour of CO₂ as a function of feed pressure. In the absence of plasticization, permeability of high sorbing gases such as CO₂ decreases with the

increase in the pressure for low pressure feed gas streams which are mainly due to the micro-heterogeneity of the glassy matrix. Macroscopically, due to the plasticization in the membranes, T_g is reduced while softness and ductility is considerably increased [33]. This causes a decrease in the intermolecular forces among the polymeric chains. By definition, the plasticization pressure corresponds to that minimum pressure which is required to induce a permeability increase in the membranes [29-30].

Various studies were carried out with different glassy polymers to investigate the effect of pressure changes on membrane performance. Wonders and Paul [73] found that the PC membrane was plasticized in the sorbing of CO_2 at elevated pressures which altered its permeation behaviour. Zhou et al. [74] noted the predomination of CO_2 plasticization in asymmetric polyimide films and dense films due to the swelling of the matrix caused by sorbing CO_2 molecules that operate on high pressures. It was observed that chemical crosslinking provided the solution for suppressing the plasticization behaviour in the membranes. Similar findings were observed by Bos et al. who indicated that a minimum 8-10 bar is high enough for polyimides to induce CO_2 plasticization [30].

CO_2 acts as a plasticizer that tends to swell the matrix and thus creates accelerated CH_4 permeation which causes a decrease in the selectivity of the membrane. Plasticization can be suppressed by using chemical modifications, such as chemical crosslinking, thermal treatments and by blending with polymers having high plasticization pressure [75-76]. Bos et al. stabilized the developed Matrimid® 5218 film by carrying out a thermal treatment at 350°C [30]. It was observed that permeation in the membranes became constant at elevated temperatures with 30 minutes of heat treatment in single gas operations. The same results were observed for gas mixtures with heat treated and untreated membranes where CH_4 showed higher permeability without heat treated membranes than with treated membranes. Similar studies by Wessling et al. and Barsema et al. on PI membranes showed that the plasticization phenomenon is exaggerated at high feed pressures in thin polyimide membranes [66, 71]. Previous studies were carried out on the regression of the plasticization by CO_2 for PI developed membranes [32, 70, 77]. Bos et al. mentioned that stabilizing a membrane against plasticization depends upon the polymer

orientation on a molecular basis rather than on the treatment methods. It was observed that the PSF membrane showed the highest plasticization pressure of 34 bar than the other polymers used in his study [29].

Concerning the plasticization of membranes at low CO₂ feed pressures for the PI Matrimid, PSF exhibits a high plasticization pressure above 30 bar and maintains good selectivity at low cost [29]. Ismail and Lorna [20], categorised the glassy polymers on the basis of gas permeability and placed PSF in type-1 owing to the ability of high resistivity towards plasticization with pressure. Sanders [78], mentioned the site-saturation mechanism for type-1 that explained the decreasing permeability. By this mechanism, the gas molecules of the penetrants can pass through easily at low concentrations. Thus the microvoids become saturated which do not allow the penetrants to pass through at higher concentrations and so permeability decreases. In comparison to PSF, Bos observed the existence of PI under the type-2 regime which showed plasticizing effects at low pressures [79].

Earlier studies on blending techniques out were carried out successfully. Khan et al. [76] suppressed the plasticization properties of the PI by blending it with S-PEEK in flat sheet membranes by using the solution casting approach. Kapantaidakis et al. [35] studied the blending properties of the polyethersulfone/polyimide blend hollow fibre membranes for gas separation at different compositions showing high permeation properties for CO₂ from 31 to 60 GPU. In another study Kapantaidakis et al. [37] formed dense films of PSF/PI blends at varying polymer compositions. It was found that that plasticization was greatly reduced with PSF/PI-80/20 polymer composition as compared to the other dense membrane blends. Besides that the improvement in permeability was also observed with 80/20 composition as compared to the other membrane blends. It was noticed that plasticization in blended membrane was analogous to PI weight content and the plasticization pressure increased significantly above 35 atm. This finding shows that by blending PI with PSF, the membrane can perform efficiently for high pressure operations or high CO₂ content gas mixtures. Hosseini and Chung [80] studied the effectiveness of membranes from blends of (PBI)/Matrimid 5218 and compared this blend with another blend of Torlon (a polyamide imide)/P84 (polyimide). They observed that PBI/Matrimid blends

exhibited good performance as compared to the other blends. Similar blending work has also been reported by Ismail et al. [81] using flat sheet based polyetherimide /polyimide blends even with inorganic zeolite particles. Their results indicated that the structure and properties of the membranes were improved. A list of a few previous works on various treatment methods is summarised in Table 2.2.

The blending technique is favoured due to the simplified operation associated with reproducibility and commercial viability. It provides the option of reducing the cost price of the membranes [35].

Table 2.2 Various types of treatments employed in past studies

Polymer	Membrane Type	Gas Type	Findings	Ref.
PI (Matrimid5218)	Dense flat sheet	CO ₂ , CH ₄	Heat treatment stabilized membrane plasticization at 350°C	[30]
PI (6FDA based)	Dense flat sheet	CO ₂ ,CH ₄	Crosslinking	[70]
PI (6FDA- DABA)	Dense flat sheet	CO ₂ , CH ₄ ,CO ₂ /CH ₄	Crosslinking	[32]
PSF,PES,PEI,BPA-PC, BPZ-PC, TMBPA-PC, PPO,P84, Matrimid5218, CTA, CA	Dense flat sheet	CO ₂ ,CH ₄	PSF exhibited the highest plasticization pressure of 34 bar	[29]

Table 2.2 Various types of treatments employed in past studies (contd.)

Polymer	Membrane Type	Gas Type	Findings	Ref.
PI (6FDA-durene)	Dense flat sheet	O ₂ / N ₂	Chemical Cross-linking	[74]
PI (P84)	Dense flat sheet, Hollow fibre	He/ N ₂ , CO ₂ /N ₂ , O ₂ / N ₂	Low permeability resisted plasticization	[66]
PI(Matrimid), PES	* Hollow fibre	CO ₂ ,N ₂	Polymer blending technique	[35]
PSF	Asymmetric flat sheet	CO ₂ ,CH ₄	Heat treatment at 140°C	[24]
PI (6FDA-TMPDA)	Dense flat sheet	CO ₂ ,N ₂ , O ₂	Modeling approach on diffusion coefficients	[77]
PI(Matrimid 9725), S-PEEK	Dense flat sheet	CO ₂ ,CH ₄ ,N ₂ , O ₂ ,CO ₂ /CH ₄ CO ₂ /N ₂	Polymer blending and cross-linking	[76]

2.7 Membrane Configurations

Three different configurations are mainly employed in membrane formation which includes flat sheets, hollow fibers or capillaries and tubular devices. For gas

separation applications, polymeric membranes can be formed by hollow fibres or flat sheets. Flat sheet membranes are installed in various types of modules, such as plate and frame or spiral wound modules and are used in large scale separation applications [16]. These flat sheet membranes were initially used for reverse osmosis and were installed in spiral-wound modules. Many of the previous studies have been carried out on flat sheets for gas separation which have been listed in Table 2.3. Flat sheets are comparatively the most convenient technique in which the membranes are developed easily for performing laboratory permeation tests [82].

Table 2.3 Previous Studies on Flat Sheet Asymmetric Membranes for Gas Separation

Polymer	Gas Type	Phase Inversion Process	Ref.
PSF	O ₂ /N ₂	Wet	[83]
TMSPSF	CO ₂ /CH ₄	Wet	[84]
DMPSF	CO ₂ /CH ₄	Wet	[85]
6FDA-6FAP	O ₂ /N ₂ CO ₂ /CH ₄	Dry/Wet	[86]
PPO	O ₂ /N ₂ CO ₂ /CH ₄	Dry	[87]
BPDA-ODA BDA- ODA	CO ₂ /CH ₄	Dry/Wet	[88]
PSF	O ₂ /N ₂	Wet	[89]
PSF	H ₂ /N ₂	Dry/Wet	[46]
PEEKWC	CO ₂ /N ₂ , O ₂ /N ₂	Dry	[90]

Table 2.3 Previous Studies on Flat Sheet Asymmetric Membranes for Gas Separation
(contd.)

Polymer	Gas Type	Phase Inversion Process	Ref.
6FDA-DDS	O ₂ /N ₂	Dry/Wet	[91]
PSF	O ₂ /N ₂	Dry	[92]
PC	CO ₂ /CH ₄	Dry/Wet	[93]
PI	O ₂ /N ₂ CO ₂ /CH ₄	Dry/Wet	[94]
PSF	CO ₂ /CH ₄	Dry/Wet	[45]
PES	O ₂ /N ₂	Dry/Wet	[39]

2.8 Mixed Matrix Membranes

MMMs are becoming quite an attractive for efficient gas separation [95]. For the last thirty years, sufficient work has been carried out but only on polymeric membranes [96]. Despite their low cost with adherent flexibility, they are still subjected to a lot of improvements. In order to improve the performance of these polymeric membranes, changes in their structure and orientation is important but it reduces the permeability and selectivity. To achieve high permeability and selectivity in separation, the combination of organic and inorganic materials have attracted the attention of many researchers. These organic/inorganic mixed matrixes are more versatile in nature. These materials combine the advantages of inorganics (mechanical strength, thermal stability) and organics (high processability, flexibility and reproducibility of properties), and can lead to improved properties [23]. These materials can be successfully utilised for separation of gases. They can be obtained either by sol-gel

processes [97-98] or by the adding of fillers, such as zeolites, silica, carbon molecular sieves, to a polymer matrix [65, 99]. The main concern for the fabrication of mixed matrix membranes is the selection of suitable components and the elimination of the interfacial defects between the two phases for attaining homogeneity in order to avoid phase separation [100].

2.8.1 Interfacial Defects Elimination in MMMs

Various other nano-inorganics have also been tried in the past to improve the properties of the MMMs, but serious dispersion problems have been observed with those nano fillers. They tend to aggregate in the polymeric matrix and form non-selective voids at the interface. The interaction between inorganic and organic components plays a pivotal role in the development of homogeneity in the material and many works have been carried out in this regard. Gur [101] observed that the incorporation of zeolite 13X particles in a PSF membrane had unsuccessful adhesion and no significant improvement in gas permeability was found. Similarly, Mahajan et al. [102] reported the same problem of poor adhesion in the development of mixed matrix membranes using Matrimid with inorganic zeolite 4A fillers. The O₂/N₂ selectivity showed the same intrinsic results with PI having higher O₂ permeation. Similarly, Vankelecom et al. [103] found that by using various types of zeolites in different types of polyimides, such as PI-2540, PMDA-ODA and Kapton formed poor adhesion problems due to the high chain stiffness of PI. It caused disturbance in their closely packed polymeric chains that resulted in void formation. Thus, the formed MMMs showed no significant improvement in selectivity due to the bypassing of the gas around the fillers. However, subsequent works showed that the silane coupling agent, APTS, improved the adhesion properties between the polymer and fillers leading to improved properties [104]. Vu et al. [105] also found initially that by using CMS at various loadings in Ultem® and Matrimid® 5218, poor polymer-sieve contact and aggregation were observed. However, modifications were carried out using casting protocols, and thermal treatment brought improvement in the adhesion and permeation properties of the membranes. The main disadvantages of the incorporation of the inorganic fillers in the polymeric matrix are the agglomeration

and the formation of non-selective voids at their interface [106]. Thus, the success in the development of MMM's largely depends upon the quality of interface between the organic and inorganic species. So, homogeneity of the membranes is most desirable for improving the performance of the membranes.

2.8.2 Selection of Sol-gel process and Silica Inorganic Fillers

For the development of different functional inorganic materials, sol-gel technology has received a lot of attention in the last few years [107-110]. By using the sol-gel process, it is probable to develop the inorganic phase with a very fine and homogenous dispersion into the organic polymeric matrix at the molecular level. An ultra thin microporous structure of silica membranes was developed in the past, which provided improved gas permeation properties [111-112]. The most noticeable advantages of the sol-gel process are the ambient reaction conditions and ease of operation for the synthesis of the silica of the various structures. Besides this, the nano silica/polymer membranes can give improved properties like mechanical, thermal, gas permeability, electrical, fire retardance, and the resistance to external effects like abrasions, and wear and tear. Improvement of these properties can be related to the homogenous dispersion of silica particles at a nano scale in comparison to heterogeneous materials [100, 113]. In sol-gel processes, nano particles can be formed via in situ approach, and the interaction between the fillers and the polymers can be improvised through controlling the reaction conditions for avoiding the formation of voids between the two mediums. For glassy polymers with inorganic fillers prepared by the sol-gel process, improvements in the permeation and selectivity have been observed [98, 114]. Sadeghi et al. [115] noticed that with the addition of silica contents up to 10%, it increased the gas permeation of EVA composite to 200% and permselectivity up to 60–80%. Kusakabe et al. [116] observed that the addition of inorganic silica particles in a polyimide matrix caused a 10 time enhancement in the CO₂ permeability. Similarly, Sadeghi et al.[117] found a significant improvement in the permeation and selectivity of CO₂ by the addition of silica nano particles in PBI membranes via the sol-gel route in the presence of a coupling agent. Permeation and selectivity increased from 0.025 barrer and 3.5 barrer for pure PBI to 0.11 to 71.3 in

MMMs. In another study, Sadeghi et al. [118] used PU with silica nano particles from TEOS and found that with the increase in silica contents up to 20wt.%, selectivities of CO₂/CH₄ and CO₂/N₂ increased considerably. Kim and Lee [119] developed PEBAX/silica nanocomposite membranes through in-situ polymerization of TEOS by using the sol-gel technique. In comparison to pure PEBAX (P_{He} = 18.6, P_{CO₂} = 122, P_{O₂} = 5.84, P_{N₂} = 1.71, $\alpha_{CO_2/He}$ = 6.6, α_{CO_2/N_2} = 71 and α_{O_2/N_2} = 3.4) and other membranes, the 27 wt. % of silica membrane showed the highest permeability and selectivity. The inclusion of silica in the organic membrane decreased the degree of crystallinity and implemented the arrangement of the PEO phase. This enhancement even at elevated temperatures indicated a strong interaction between CO₂ and the residual OH groups on the silica network along with the supplementary sorption sites in the PA block of the polymer. In the sol-gel processes, TEOS and TMOS are commonly used precursors for obtaining silica particles; however, TEOS is favored because of its controllable reaction rate and ease of processing [120-121]. In general, the sol-gel process may be influenced by various factors. These factors include the water/silane ratio, catalyst, temperature, solvent used, environmental effects, reaction time etc. Among these, one of the key factors which may affect the reaction rate is the use of a catalyst [121-122]. Acid or base catalysts may be employed in the sol-gel process which enhances the silicon reactivity. For fast hydrolysis of TEOS, an acid catalyst is required. This gives an open weakly branched structure while a base catalyst leads towards compact colloidal particles as a result of slower hydrolysis and faster polycondensation. In the case of an acid catalyst, linear chain growth results with a particle size of less than 100 nm in diameter. While a base catalyst can result in a large particle size with a spherical diameter of 100nm or above [123]. For gas separation through polymer/silica MMMs, if the membranes are prepared by the sol-gel process then acid catalysts must be used [124-125].

In the fabrication of MMMs, proper control on the morphology for attaining homogeneity avoiding phase separation is quite important. The addition of the silane coupling agent is one of the methods to overcome phase separation as it improves the compatibility between the organic and inorganic and thereby improves the properties of the composite membranes. Yang and Nelson [126] prepared PMMA/silica nanocomposite membranes using 3-acryloxypropyl methydimethoxysilane

(APMDMOS) and 3-acryloxypropyl trimethoxysilane (APT MOS) as coupling agents. Modification of the silica surface by APT MOS gave better results than APMDMOS. Cornelius et al. [127] studied PI/SiO₂ with other various alkoxy silanes to check the permeability of the CO₂, N₂, and CH₄ penetrants. It was observed that the thermal treatment brought about an increment in gas permeation to about 200-500% with a little drop in permselectivity. The increase in permeation was attributed to the change in free volume and the enhancement in segmental chain mobility. Nunes et al. [97] prepared a polyetherimide (PEI) and silica composite membrane using 3-aminopropyltrimethoxysilane (AS) as a coupling agent. It was observed that the uniform dispersion in the nano scale was possible using AS. The developed films showed homogeneity and enhanced thermal stability without silica agglomeration in the matrix as compared to the composites without AS. Suzuki and Yamada [128] developed an improved gas separation membrane from hyper-branched polyimide/silica nanocomposites. The developed hyperbranched polyamic acid as a precursor from the polycondensation of TAPOB and 6FDA along with surface modification with APTrMOS was used for the preparation of the composite membrane via the sol-gel route. It was observed that the permeability coefficients of CO₂, O₂ and N₂ increased with the increase in silica contents due to the increase in gas solubilities [98]. A decreasing trend was observed in the case of CH₄ permeability at the same time which was due to a decrease in the CH₄ diffusivity thus causing enhanced CO₂/CH₄ gas selectivity. A brief overview of the performance of various MMMs involving various combinations of polymers and inorganic fillers has been summarized in Table 2.4 and Figure 2.9.

2.8.3 Thermal Stability of MMMs

Thermal properties related to the temperature of the system are evaluated for their thermal stabilities by degradation behavior of the membrane and are determined by TGA containing silica particles in the membranes. Similarly DSC studies were also conducted for determining the T_g's that showed improvement with the addition in the inorganic fillers.

Table 2.4 Selected Studies in Mixed Matrix Membranes for gas separation

Matrix Materials		Gas Type	Membrane Performance		Refs.
Polymer	Silica-based Fillers		Neat Polymeric Membranes	Mixed Matrix Membranes	
PI	MTMOS Precursor-15wt.%	CO ₂ /CH ₄ CO ₂ /N ₂	$\alpha_{\text{CO}_2/\text{CH}_4} = 31.5$ $\alpha_{\text{CO}_2/\text{N}_2} = 20.18$ $P_{\text{CO}_2} = 77.3$	$\alpha_{\text{CO}_2/\text{CH}_4} = 42$ $\alpha_{\text{CO}_2/\text{N}_2} = 16$ $P_{\text{CO}_2} = 81.1$	[129]
PI	TMOS Precursor-30wt.%	CO ₂ /CH ₄ O ₂ /N ₂	$\alpha_{\text{CO}_2/\text{CH}_4} = 75$ $P_{\text{CO}_2} = 7.4$ $\alpha_{\text{O}_2/\text{N}_2} = 6.9$ $P_{\text{O}_2} = 1.5$	$\alpha_{\text{CO}_2/\text{CH}_4} = 238$ $P_{\text{CO}_2} = 19$ $\alpha_{\text{O}_2/\text{N}_2} = 6.6$ $P_{\text{O}_2} = 3.0$	[128]
BPPO	Silicon dioxide powder	CO ₂ /CH ₄ CO ₂ /N ₂	$\alpha_{\text{CO}_2/\text{CH}_4} = 15.1$ $\alpha_{\text{CO}_2/\text{N}_2} = 22.3$ $P_{\text{CO}_2} = 104$	$\alpha_{\text{CO}_2/\text{CH}_4} = 15$ $\alpha_{\text{CO}_2/\text{N}_2} = 21$ $P_{\text{CO}_2} = 523$	[130]
PEBAX	TEOS Precursor-27 wt.%	CO ₂ /N ₂	$\alpha_{\text{CO}_2/\text{N}_2} = 71$ $P_{\text{CO}_2} = 122$	$\alpha_{\text{CO}_2/\text{N}_2} = 79$ $P_{\text{CO}_2} = 277$	[119]
PSF	Fumed Silica powder	CO ₂ /CH ₄	$\alpha_{\text{CO}_2/\text{CH}_4} = 31.05$ $P_{\text{CO}_2} = 78.11\text{GPU}$	$\alpha_{\text{CO}_2/\text{CH}_4} = 32.74$ $P_{\text{CO}_2} = 90.04\text{GPU}$	[131]
Carbon-based Fillers					
PI	CMS-36wt.%	CO ₂ /CH ₄ O ₂ /N ₂	$\alpha_{\text{CO}_2/\text{CH}_4} = 35.3$ $P_{\text{CO}_2} = 10$ $\alpha_{\text{O}_2/\text{N}_2} = 6.6$ $P_{\text{O}_2} = 2.12$	$\alpha_{\text{CO}_2/\text{CH}_4} = 51.7$ $P_{\text{CO}_2} = 12.6$ $\alpha_{\text{O}_2/\text{N}_2} = 7.9$ $P_{\text{O}_2} = 3.0$	[105]

Note: All Permeability units are in Barrer other than mentioned permeance (GPU)

Table 2.4 Selected Studies in Mixed Matrix Membranes for gas separation
(continued)

Matrix Materials		Gas Type	Membrane Performance		Refs.
Polymer	Carbon-based Fillers		Neat Polymeric Membranes	Mixed Matrix Membranes	
PSF	SWCNT-15wt%	CO ₂ /CH ₄	$\alpha_{\text{CO}_2/\text{CH}_4} = 23.55$ $P_{\text{CO}_2} = 3.9$	$\alpha_{\text{CO}_2/\text{CH}_4} = 16.09$ $P_{\text{CO}_2} = 4.52$	[132]
		O ₂ /N ₂	$\alpha_{\text{O}_2/\text{N}_2} = 5.07$ $P_{\text{O}_2} = 0.84$	$\alpha_{\text{O}_2/\text{N}_2} = 5.1$ $P_{\text{O}_2} = 1.1$	
Ultem® 1000	CMS-35wt.%	CO ₂ /CH ₄	$\alpha_{\text{CO}_2/\text{CH}_4} = 38.8$ $P_{\text{CO}_2} = 1.45$	$\alpha_{\text{CO}_2/\text{CH}_4} = 53.7$ $P_{\text{CO}_2} = 4.48$	[105]
		O ₂ /N ₂	$\alpha_{\text{O}_2/\text{N}_2} = 7.3$ $P_{\text{O}_2} = 0.38$	$\alpha_{\text{O}_2/\text{N}_2} = 8.0$ $P_{\text{O}_2} = 1.09$	
PI Matrimid	Fullerence C ₆₀ -5wt.%	CO ₂ /CH ₄	$\alpha_{\text{CO}_2/\text{CH}_4} = 36$ $P_{\text{CO}_2} = 7.15$	$\alpha_{\text{CO}_2/\text{CH}_4} = 36$ $P_{\text{CO}_2} = 4.54$	[133]
		O ₂ /N ₂	$\alpha_{\text{O}_2/\text{N}_2} = 6.8$ $P_{\text{O}_2} = 1.87$	$\alpha_{\text{O}_2/\text{N}_2} = 6.8$ $P_{\text{O}_2} = 1.25$	
Zeolite-based Fillers					
PES	Zeolite5A-50wt.%	CO ₂ /CH ₄	$\alpha_{\text{CO}_2/\text{CH}_4} = 31.6$ $P_{\text{CO}_2} = 2.6$	$\alpha_{\text{CO}_2/\text{CH}_4} = 36.9$ $P_{\text{CO}_2} = 2.5$	[134]
		O ₂ /N ₂	$\alpha_{\text{O}_2/\text{N}_2} = 5.8$ $P_{\text{O}_2} = 0.47$	$\alpha_{\text{O}_2/\text{N}_2} = 7.4$ $P_{\text{O}_2} = 0.7$	

Table 2.4 Selected Studies in Mixed Matrix Membranes for gas separation
(continued)

Matrix Materials		Gas Type	Membrane Performance		Refs.
Polymer	Zeolite-based Fillers		Neat Polymeric Membranes	Mixed Matrix Membranes	
PI	Zeolite-SSZ-13	CO ₂ /CH ₄	$\alpha_{\text{CO}_2/\text{CH}_4} = 37.1$ $P_{\text{CO}_2} = 57.3$	$\alpha_{\text{CO}_2/\text{CH}_4} = 49.6$ $P_{\text{CO}_2} = 67$	[135]
PI	Zeolite4A-TAP	CO ₂ /CH ₄ CO ₂ /N ₂	$\alpha_{\text{CO}_2/\text{CH}_4} = 1.22$ $P_{\text{CO}_2} = 8.34$ $\alpha_{\text{CO}_2/\text{N}_2} = 3.8$	$\alpha_{\text{CO}_2/\text{CH}_4} = 617$ $P_{\text{CO}_2} = 0.19$ $\alpha_{\text{CO}_2/\text{N}_2} = 102$	[136]
PES	Zeolite-Ag 50wt.%	CO ₂ /CH ₄	$\alpha_{\text{CO}_2/\text{CH}_4} = 35.3$ $P_{\text{CO}_2} = 1.0$	$\alpha_{\text{CO}_2/\text{CH}_4} = 44.0$ $P_{\text{CO}_2} = 1.2$	[137]
Ultem®	Zeolite-HSSZ-13	CO ₂ /CH ₄ O ₂ /N ₂	$\alpha_{\text{CO}_2/\text{CH}_4} = 37.4$ $P_{\text{CO}_2} = 13\text{GPU}$ $\alpha_{\text{O}_2/\text{N}_2} = 7.6$ $P_{\text{O}_2} = 4.0\text{GPU}$	$\alpha_{\text{CO}_2/\text{CH}_4} = 43.9$ $P_{\text{CO}_2} = 6.23\text{GPU}$ $\alpha_{\text{O}_2/\text{N}_2} = 8.2$ $P_{\text{O}_2} = 1.7\text{GPU}$	[138]

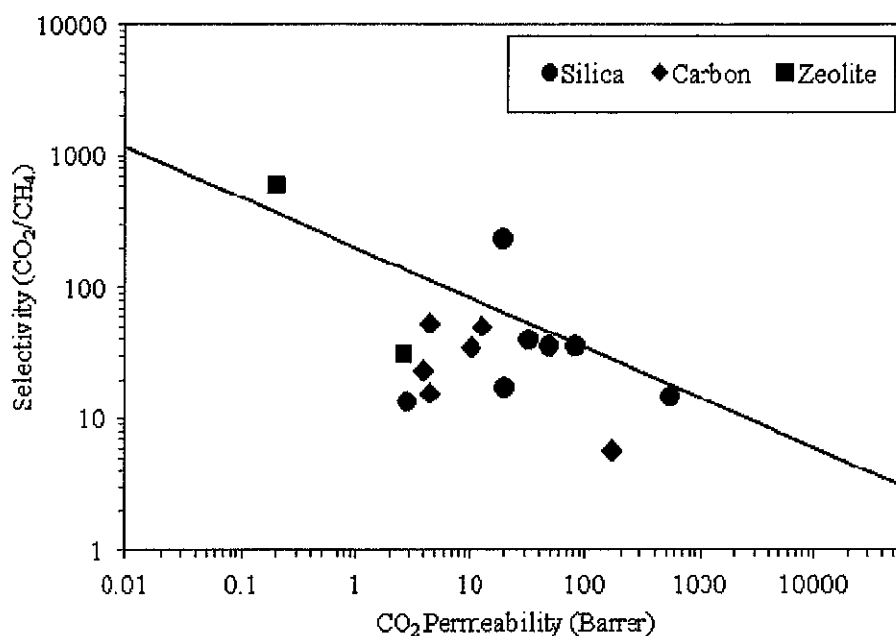


Figure 2.9 Graph of various Mixed Matrix Membranes in terms of the CO₂/CH₄ selectivity versus the CO₂ permeability

The addition of silica nanoparticles to the polymer matrix increases the thermal stability as the inorganic materials behave as insulators and result in the blockage of volatile materials produced during degradation [139]. Shang et al. [140] observed that the thermal properties in PI/silica composites also showed superior results with the increase in silica contents and coupling agents ($T_g = 316^\circ\text{C}$, $T_d = 592^\circ\text{C}$) than those of their corresponding films without silica contents and coupling agents ($T_g = 289^\circ\text{C}$, $T_d = 561^\circ\text{C}$). Nunes et al. [141] observed from DSC study that with the addition of silica contents in the PEI matrix, the T_g value increased from 199°C to 211°C . It can be related to the increase in the rigidity of the composite. Similar observations of increment in thermal stability with the addition of fillers have also been made by other researchers [142-143]. Jadav and coworkers [144] prepared two different types of nanocomposites membranes by introducing Ludox of particle size 16 nm and synthesized silica from TEOS with 3mm particle size. It was observed that nanocomposites membranes exhibited higher thermal stability than pure films. The weight loss was found out to be 17% for pure film which decreased with the SiO₂ loading. At maximum SiO₂ loadings, the weight loss for as-synthesized SiO₂ based

membrane was found out to be 2.9% and for Ludox based membrane it was 5.5%. SiO₂ loadings in the composites were directly related to the residue mass obtained at 550°C. These effects depicted that as-synthesized nano sized silica showed better thermal stability than with the nano sized obtained from Ludox. Improved thermal stability with inorganic fillers into the organic polymer showed higher T_g for the nanocomposite samples measured by DSC. The T_g of the neat polymer was 237°C which increased to 250°C with just 1wt. % SiO₂ loadings, and to a increased T_g value of about 300°C for 10 wt. % SiO₂ contents. Sun et al. [145] prepared epoxy nanocomposites by using various sized fillers in micrometer and nanometer scale. It was observed that T_g values were improved by using nano silica particles in the polymer matrix than with micro silica particles. With nano silica loadings, a significant increase in T_g values was observed. Li and Huang [146] studied the thermal degradation and kinetics of polysulfone (PSF) by thermogravimetry. They observed that the thermal degradation temperature of the PSF increased slightly with an increase in the heating rate. The activation energy of thermal degradation of PSF in air, nitrogen and argon atmospheres was found to be 140, 258 and 293 kJ/mol. It was noticed that the activation energy of thermal degradation calculated by high resolution TG in nitrogen and air were almost the same as measured by traditional isothermal or constant heating rate TG. Zornoza et. al. [147] found that with the increase in silica contents up to 16 wt% in PSF membranes, thermal stability of the MMMs increased gradually indicating superior insulation properties of fillers.

Based on the previous studies performed on the thermal stabilities of membranes, a useful comparison can be made with the current study on the formed MMMs.

2.9 Modeling in Mixed Matrix Membranes

Various existing permeation models have been applied for the prediction of gas permeance through MMMs. These models were based upon the permeation properties of the continuous and dispersed phases [148]. These models were adapted from the thermal/electrical conductivity models where close analogy existed for permeation in the MMMs.

Maxwell's model was developed in 1873 which was based on the electrical conductivity for particulate composite materials. It was adapted for the permeance in the composites, written in the form of Eq. (2.16)[148]:

$$P_r = \frac{P}{P_m} = \left\{ \frac{2(1-\phi) + (1+2\phi)\lambda_{dm}}{(2+\phi) + (1-\phi)\lambda_{dm}} \right\} \quad (2.16)$$

Where, P_r stands for the relative permeance of the species. P and P_m are the effective permeance of the species in the MMMs and in the continuous phase, respectively. The symbol ϕ is the volume fraction of filler particles and λ_{dm} is the ratio between the permeance of the species in the dispersed phase to the continuous phase. The Maxwell equation is valid for the dilute suspension of spheres. It is only applicable for low loadings of filler particles with a volume fraction less than about 20%. In addition, this model cannot predict the permeance in MMMs at the maximum packing volume fraction of fillers. Moreover, it does not account for particle size distribution, particle shape and their aggregation.

The Bruggeman model developed much later in 1935 was based on the dielectric constant for particulate composite materials and can be adapted to permeance, represented in the form of Eq.(2.17) [149].

$$(P_r)^{1/3} \left\{ \frac{\lambda_{dm} - 1}{\lambda_{dm} - P_r} \right\} = [1 - \phi]^{-1} \quad (2.17)$$

This model is an improvement over the Maxwell model through the ability to account for higher filler loadings. Nevertheless, similar to the Maxwell model, it also fails to predict the permeance in MMMs at the maximum packing volume fraction of fillers. Also, it does not account for particle size distribution, particle shape and their aggregation. Moreover, it is an implicit relationship that needs to be solved numerically for estimating the permeance.

The Lewis (1970)-Nielsen (1973) model was originally developed for the elastic modulus of the particulate composite materials. It was adapted for estimating the permeance and is represented according to the following Eq.(2.18) [150-151]:

$$P_r = \frac{P}{P_m} = \left\{ \frac{1 + 2[(\lambda_{dm} - 1/\lambda_{dm} + 2)]\phi}{1 - \psi[(\lambda_{dm} - 1/\lambda_{dm} + 2)]\phi} \right\} \quad (2.18)$$

Where,

$$\psi = 1 + \left\{ \frac{1 - \phi_m}{\phi_m^2} \right\} \phi \quad (2.19)$$

The ϕ_m represents the volume fraction of fillers at the maximum packing with a value of 0.64 for uniform spheres with random closed packing. This model includes the effects of the morphology on the permeance since ϕ_m is a function of particle size distribution, particle shape and their aggregation.

In 2007, Pal developed a model based on the thermal conductivity of a particulate composite material that can be adapted for the permeance in MMMs taken in the form of the following Eq.(2.20) [149]:

$$(P_r)^{1/3} \left\{ \frac{\lambda_{dm} - 1}{\lambda_{dm} - P_r} \right\} = \left\{ 1 - \frac{\phi}{\phi_m} \right\}^{-\phi_m} \quad (2.20)$$

Similar to the Lewis–Nielsen model, the Pal model can calculate the permeance at the maximum packing volume fraction of fillers. It also includes the effects of particle size distribution, particle shape and their aggregation, through the addition of ϕ_m into the equation.

Bouma et al. used the Maxwell-Wagner-Sillar (MWS) (1937) model shown in Eq.(2.21) for the determination of effective permeance in MMMs with the dilute dispersion of ellipsoids [152].

$$P = P_m \left\{ \frac{nP_f + (1-n)P_m + (1-n)\phi_f(P_f - P_m)}{nP_f + (1-n)P_m - n\phi_f(P_f - P_m)} \right\} \quad (2.21)$$

Where, P_f , ϕ_f and n represent the permeance, volume fraction and shape factor of the fillers, respectively. Although the model accounts for the shape factor n , still Bouma assumed the filler shape to be spherical. Gokturk et al. also explored on the effect of

different particle shape and size distributions on the properties of composite polymers [153].

In the case of prolate ellipsoids, the shape factor has a value ranging from $0 \leq n \leq 1/3$ which corresponds to the longest axis, i.e., along the z-direction of the applied pressure gradient across the membrane. While for oblate ellipsoids, the shape factor has a value ranging from $1/3 \leq n \leq 1$ which corresponds to the shortest axis, i.e., also along the z-direction of the applied pressure gradient. For spherical fillers, a shape factor of $n=1/3$ is assigned.

Based on three different cases at varying shape factors as mentioned above, Eq.(2.21) could be rewritten in three different forms for determining the effective permeance and is shown by the Eqs.(2.22)-(2.24).

At,

$$n=0; \quad P_c = P_m(1-\phi_f) + P_f\phi_f \quad (2.22)$$

$$n=1/3; \quad P_c = P_m \left\{ \frac{P_f(1+2\phi_f) + P_m(2-2\phi_f)}{P_f(1-\phi_f) + P_m(2+\phi_f)} \right\} \quad (2.23)$$

and

$$n=1; \quad P_c = P_m \left\{ \frac{P_f}{P_f(1-\phi_f) + P_m\phi_f} \right\} \quad (2.24)$$

Eqs.(2.22) and (2.24) correspond to the effective permeance in the composite membranes representing parallel transport and series transport through the two phases. Eq.(2.23) is the Maxwell equation which was developed for spherical particles ($n=1/3$) in a dilute suspension.

In the determination of the shape of particles n , the z-axis of the particle geometry should be known that corresponds to the major axis of the prolates. So, the shape factor n of the particles in the z-direction denoted by n_z can be calculated as shown by the Eq.(2.26) [153]:

$$e = \sqrt{\left(1 - \frac{b^2}{a^2}\right)} \quad (2.25)$$

$$n_z = \frac{1-e^2}{2e^2} \left(\ln \frac{1+e}{1-e} - 2e \right) \quad (2.26)$$

The variable $\frac{b}{a}$ corresponds to the length ratio between the minor to major axis of the particles.

Various other theoretical models are available in literature; however this thesis is focused on the comparison of the above described models with our experimental data since these models had been used in the past for mixed matrix membrane studies and provides the roots for quantitative estimation so as to achieve qualitative improvement.

CHAPTER 3

3. MATERIALS AND METHODOLOGY

3.1 Overview

This chapter includes the application of various types of materials which are used for membrane development, their experimental procedures and the characterization techniques. Section 3.2 covers the description of the polymers, solvents and silica precursors used in the study. The detailed experimental procedures for the formation of the asymmetric polymeric and mixed matrix membranes are presented in Section 3.3. The characterization techniques and gas permeation procedures on membranes are discussed in Sections 3.4 and 3.5, respectively.

3.2 Materials

The materials which were used in the development of membranes are discussed as follows:

3.2.1 Polymers

Two glassy polymers were used in this study for the fabrication of asymmetric membrane films as a continuous matrix: PSF-Udel® P-1800 and PI-Matrimid® 5218. PSF was selected mainly due to its ease of fabrication, good properties like high strength and good thermal stability associated with low cost and ease of availability. PI was selected because of having a high thermal stability and T_g value. Udel® P-1800 was purchased from Solvay Advanced Polymers, L.L.C, U.S., while Matrimid®

5218 was obtained from Huntsman Advanced Materials Americas Inc. in the powdered form. The chemical structures and physical properties of the polymers are shown in Figure 3.1 and Table 3.1.

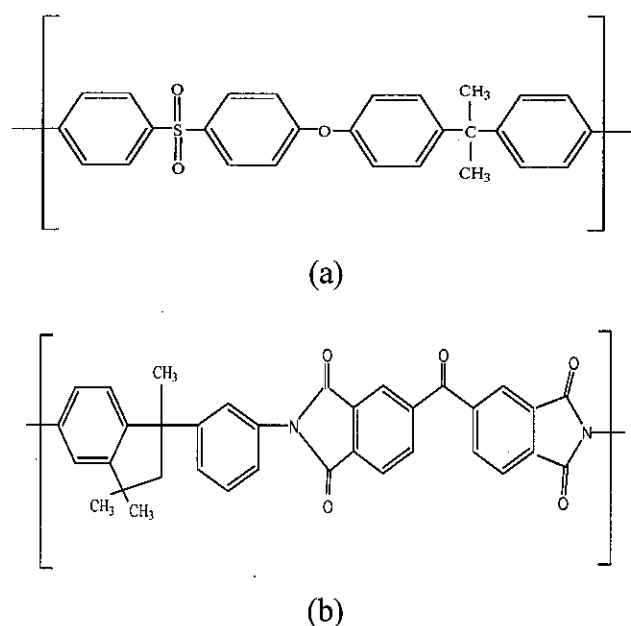


Figure 3.1 Structures of polymers (a) PSF Udel® P-1800 (b) PI Matrimid® 5218

Table 3.1 Physical properties of polymers used in this study

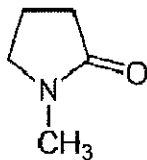
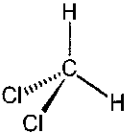
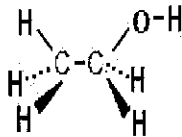
Polymers	Glass Transition T_g , by DSC (°C)	Density, ρ (g/cm ³)	[Ref.]
Udel® P-1800	185.3	1.2	[154]
Matrimid® 5218	302.9	1.2	[155]

3.2.2 Solvents

The gas permeation properties are largely affected by the selection of suitable solvents and structures of the developed membranes. The solvent mixtures of N-methyl-2-pyrrolidone (NMP) having a 99.5% purity with b.p.204.3°C and Dichloromethane

(DCM) with a purity of 99%, b.p.40°C were used in the casting solution to control the rate of evaporation. Ethanol was used as the non-solvent during the phase inversion process to develop the asymmetric membrane in the coagulation medium. Table 3.2 shows the properties of all the solvents used in this work.

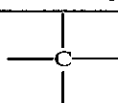
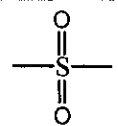
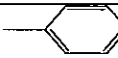
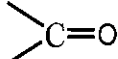
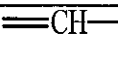
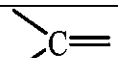

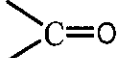
Table 3.2 Properties of organic solvents used in this study

Properties	NMP	DCM	Ethanol
Supplier	Merck	Merck	Merck
Purity	99.5	99	99.8
Structure			
Molecular Weight	99	85	46
Boiling Point (°C)	204	40	78
Melting Point (°C)	-24	-95	-114
Density (g/cm ³)	1.028	1.330	0.789

3.2.3 Solubility Parameter

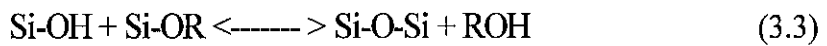
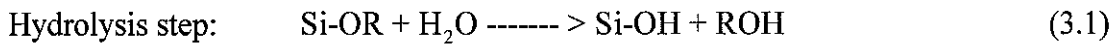
The solubility parameter of the polymers and solvents was calculated from the group contribution for each molecular structural group by using the Hoftzyer and Van-Kravelen method [57]. The group contributions for the structures of each component were well tabulated as shown in Table 3.3. This table was further used to eventually calculate the overall solubility of the individual component and mixtures of the casting solution as will be mentioned in Chapter 4. The solubility parameter was determined to find the miscibility among the polymers and solvents. The calculations regarding the solubility parameter estimation is shown in Appendix A.

Table 3.3 Calculation of the overall solubility parameter using molar attraction constants at 25°C for the polymer and solvent functional group components

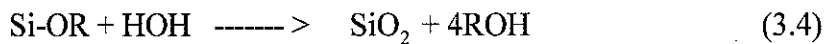
Polymers /Solvents	Functional Groups	Components			Frequency	Overall Solubility (MPa) ^{1/2}
		F _{di} (J ^{1/2} . cm ^{3/2} . mol ⁻¹)	F _{pi} (J ^{1/2} . cm ^{3/2} . mol ⁻¹)	F _{hi} (J. mol ⁻¹)		
PSF	—CH ₃	420	0	0	2	19.47
		-70	0	0	1	
	—O—	100	401	3000	1	
		591	0	13490	1	
		1270	110	0	4	
PI	Tertiary amine	20	800	5000	2	18.98
		290	770	2000	5	
		200	0	0	9	
	—CH ₃	420	0	0	3	
		70	0	0	11	
		1270	110	0	1	
NMP		290	770	2000	1	21.47
	—CH ₂ —	270	0	0	3	
	—CH ₃	420	0	0	1	
	Tertiary amine	20	800	5000	1	
DCM	—CH ₂ —	270	0	0	1	25.30
	—Cl	450	550	400	2	
Ethanol	—CH ₃	420	0	0	1	25.58
	—CH ₂ —	270	0	0	1	
	—OH	210	500	20,000	1	

3.2.4 Preparation of Silica Sol

Tetraethyl orthosilicate (TEOS), supplied by Aldrich, a precursor for silica particles was used as an inorganic filler in the MMMs. TEOS was preferred because of its controllable reaction rate and ease of processability [120-121]. Silica sol was prepared by using the sol-gel technique since this method provides homogeneity and more controllability [156-157]. The reaction conditions took place at a moderate temperature and ambient pressure, and the concentrations of both organic and inorganic precursors were easy to operate. The inorganic medium was distributed at the molecular or nanometer scale in the membranes, and so the mixed matrixes formed were homogeneous. Mainly, this method employs metal-organic alkoxides, particularly for the synthesis of silica, as they can be shaped into an oxide network in an organic matrix. The reaction mechanism for sol-gel processing development of alkoxysilane can be presented in the following Eq. (3.1)-(3.4):



Complete sol-gel reaction:



Where, R refers to the alkyl group. Acid or base catalysts may be employed in the sol-gel process which can enhance the silicon reactivity. For gas separation through polymer/silica composites, if the membranes are prepared by the sol-gel process, then acid catalysts must be used [124-125]. Hydrochloric acid (HCl) was used in this study which was supplied by Merck.

In the fabrication of the composite membranes, proper control on the morphology to obtain homogeneity and to avoid phase separation is quite important. In this regard, 3-aminopropyltrimethoxysilane (APTMS) that acted as a coupling agent between the organic and inorganic mediums was used in this study, supplied by Aldrich. Yang et al. [126] prepared PMMA/silica nanocomposite membranes using (3-acryloxypropyl) methydimethoxysilane APMDMS and (3-acryloxypropyl)

trimethoxysilane APTMOS coupling agents. Modification of the silica surface by using APTMOS gave better results than APMDMOS. Nunes et al. [97] prepared polyetherimide (PEI) and silica composite membranes using 3-aminopropyltrimethoxysilane (AS) as a coupling agent. It was observed that the uniform dispersion in nano scale was possible using AS. The developed films showed homogeneity and enhanced thermal stability without any silica domains in the matrix as compared to the composites without AS.

Initially, a mixture of TEOS and ethanol was placed in a cold water bath to avoid the untimely hydrolysis. Subsequently, a mixture of water and HCl was then added dropwise to the former mixture under constant stirring. The molar ratio of this mixture (TEOS/ethanol/acid/water) was set to be 1/3.8/0.085/6.4 according to the standard recipe for silica-sol formation [107]. The mixture was then refluxed for 3 hours at 60°C. Surface modification with APTMOS was carried out by mixing it with ethanol in the ratio of 1:3.8. It was then added dropwise to the (TEOS/ethanol/acid/water) reaction mixture. The reaction mixture having the molar ratio of 0.1/1/7.6/0.085/6.4 was kept refluxing for another ½ hour at 60°C to obtain a clear and transparent silica-sol.

3.3 Membrane Development

Two different types of membranes were prepared in this work: asymmetric membranes and mixed matrix membranes. The scheme of the experimental procedures of the present work is shown in Figure 3.2 and elaborated in the next sections.

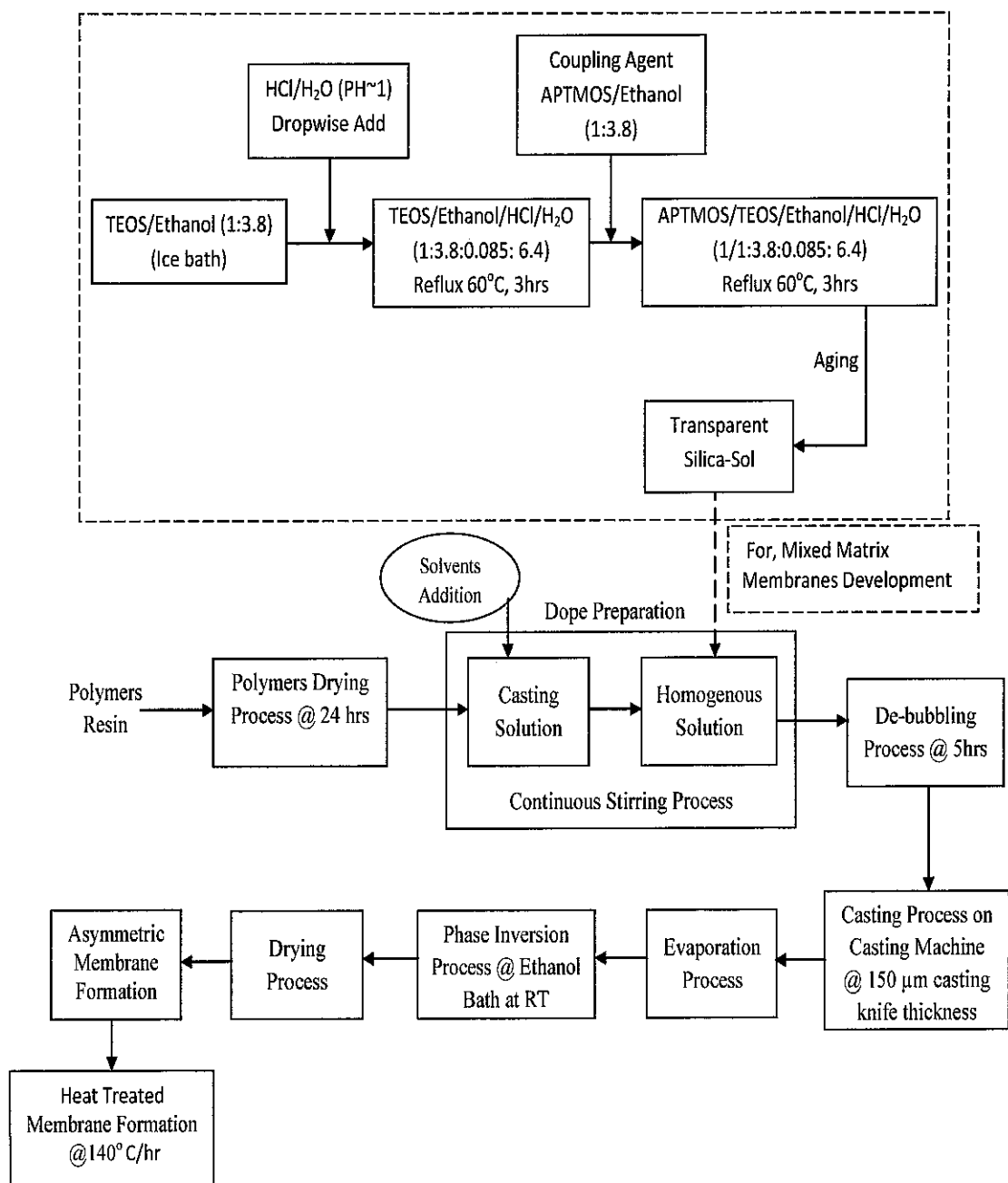


Figure 3.2 Flow diagram of asymmetric polymeric membranes and mixed matrix membranes development

3.3.1 Development of Asymmetric Polysulfone/Polyimide Membranes

To develop the membranes, the polymers PSF and PI were dried at 110°C for 24 hours prior to their use to remove moisture. The dried polymers were dissolved into

the solvents and stirred in 250 ml Duran® laboratory bottles till the polymers were dissolved completely. This mixture commonly referred as the casting solution was prepared by dissolving 15% (w/w) of polymer in the NMP and DCM solvents to develop membranes of different compositions.

The composition of NMP and DCM in the casting solution was varied in various compositions in order to understand the effect of the solvents on the morphology of the developed membranes. The various compositions of the polymeric blends and the solvents are shown in Table 3.4. The reaction mixture was stirred in a round bottom vessel at 35°C for 24 hours to ensure the complete dissolution of the polymers in order to produce a homogenous solution. The homogeneous casting solution was then subjected to an ultrasonic degasser, Model: Transsonic Digital S, Elma® for 5 hours to remove any bubbles from the agitation. This casting solution was then casted on a casting glass and the thickness of the membrane was adjusted to 150 µm using the casting knife on a flat plate membrane casting machine at ambient conditions. A stream of nitrogen gas was supplied above the casting solution for 15 seconds in a back and forth motion to promote evaporation. The casting solution on the glass plate was then immersed in a coagulant bath of ethanol at room temperature until the membrane was completely detached from the glass plate. The coagulant induced the precipitation of the membrane film through phase inversion technique. The developed membrane was then air dried for 12 hours followed by drying at room temperature for another 2 days to ensure the complete drying of the fabricated asymmetric membrane. A summarized flow diagram in Figure 3.2 shows the fabrication steps involved in the asymmetric membrane formation.

Table 3.4 Composition of the developed PSF/PI blended membranes

Solvent Compositions in Casting Solution	Polymer Blends	
	(PSF/PI)	
(NMP/DCM) (%)	PSF (%)	PI (%)
80/20	100	0
	95	5
	90	10
	85	15
	80	20
50/50	100	0
	95	5
	90	10
	85	15
	80	20
20/80	100	0
	95	5
	90	10
	85	15
	80	20

3.3.2 Development of Mixed Matrix Membranes

PSF/PI- silica mixed matrix membranes were prepared by the same method as in the case of the preparation of the asymmetric membranes, however, some additional steps were introduced. Before being utilised as fillers in the polymeric membranes, silica-sol was prepared by the steps followed in Section 3.2.4. It was then followed by the drop-wise addition of silica-sol in various fractions to the polymeric solution. The volume fraction, (ϕ_s), of silica in the polymer-silica membranes were calculated by

Eq.(3.5). The developed MMMs in various fractions along with their sample names and thicknesses are given in Table 3.5.

$$\phi_s = \frac{w_s / \rho_s}{w_s / \rho_s + w_p / \rho_p} \quad (3.5)$$

Where, W_s , W_p are silica and polymer weights while ρ_s, ρ_p are the density of the silica and polymer, respectively. The polymer/silica solution mixture was gently stirred in a round bottomed flask for 24 hours and 35°C followed by sonication in the Transsonic Digital S, Elma® for 2 hours. The clear solution was then casted on a levelled flat glass plate with a doctor's blade that was set at a gap opening of 150 μm . On the top of the casted solution, a nitrogen gas stream was sprayed for 15 seconds followed by coagulation in an ethanol medium. The detached developed membrane was then fan dried for 12 hours followed by drying at room temperature for 48 hours.

Table 3.5 PSF/PI-20%/silica mixed matrix membrane properties

Membrane samples	Silica weight fraction (wt %)	Membrane Thickness- (SEM) (μm)
S1	5	46 \pm 0.5
S2	10	52 \pm 0.7
S3	15	68 \pm 0.5
S4	20	82 \pm 0.4

3.4 Membrane Characterization Techniques

A number of different characterization techniques were performed for the evaluation of the physical and chemical properties of the developed membranes. Membrane morphology and silica-sol particle size were carried out by using the scanning electron microscope (SEM) and the transmission electron microscope (TEM). The thermal properties were evaluated by using differential scanning calorimetry (DSC) and thermogravimetric analysis (TGA). Spectral studies were performed by the

Fourier transform infrared spectroscopy (FTIR) while structural interactions among the organic and inorganic species were carried out by x-ray diffraction (XRD). The performance of the membranes was further carried out for their evaluation using a gas permeation unit.

3.4.1 Morphological Analysis

3.4.1.1 Scanning Electron Microscopy (SEM)

SEM can be used to directly detect morphological characteristics of membranes including some information about the interface between the polymeric asymmetric phases and the distribution of inorganic particles dispersed in the polymeric matrix. It forms magnified images at much higher magnification by using electrons instead of a conventional light microscope through light waves.

Random specimens from the developed membranes were carefully drawn to examine the morphology of the surfaces using a LEO 430VP SEM analyzer. A cross-section of the membranes was obtained by immersing the membrane samples in liquid nitrogen for at least 30 seconds which induced freeze fracturing. They were then gold sputter coated using the Polaron Range SC7640 in order to obtain a clear image of the membrane samples. The SEM images were then finally analysed by mounting the samples onto a circular stainless steel sample holder using conductive carbon tape.

3.4.1.2 Transmission Electron Microscopy (TEM)

TEM is a technique which is used for the identification of the internal structure of the solids by using high energy electrons at 100 keV generated by a tungsten filament that passes through the sample. Due to the electron flux which is generated as it leaves the thin specimen, a photographic representation of the image is recorded.

The morphology of the silica particles in the polymer matrix was examined by using the Carl Zeiss, Libra® 200FETEM. The membrane sample was diluted with

ethanol followed by dispersion in a digital ultrasonic cleaner (SS-8020) for 1 hour. It was then rested for ½ an hour in the test tube holder before a few drops were put on the copper grid. The grid was then allowed to dry for 24 hours followed by the direct observation of the prepared sample under TEM.

3.4.2 Thermal Analysis

3.4.2.1 Differential Scanning Calorimetry (DSC)

DSC is used for the measurement of heat flow and temperatures of various transitions that exist in a material as a function of temperature and time. It provides quantitative and qualitative information about the physical and chemical transformations that occur in a sample that involve an exothermic or endothermic process. It observes more subtle phase changes such as glass transition temperatures as the temperature of the amorphous solid is raised. Though DSC is used for a variety of materials, it is quite suitable for polymeric evaluations since it is sensitive to substances composed of large and extended molecular chains. Where other materials possess structural homogeneity among the molecules and possess relatively simple transition like melting and boiling points, polymers hold a variety of arrangements in their structures and heterogeneity among individual molecular units [158].

In order to determine the T_g of the blended and mixed matrix membranes, the samples were cut into small pieces, each weighing about 10 mg, in the aluminium pan. The thermal scans were carried from 50°C to 400°C with a heating rate of 10°C/min under a nitrogen atmosphere in a Perkin Elmer, DSC Pyris-1 calorimeter.

3.4.2.2 Thermogravimetric Analysis (TGA)

TGA is used to determine the amount and rate of change in the weight of a sample as a function of temperature or time under controlled conditions. These measurements are mainly employed to measure the thermal stability of a material and compositions of their products along with used precursors. It can particularly be studied for

polymeric materials of various types including thermoplastics, thermosets, composite films and the effect of additives like inorganic fillers on material properties. For an analysis of polymers, the sample can be heated from room temperature upto 1000°C in the presence of either oxidising gases like oxygen or a non-oxidising atmosphere like helium or nitrogen. Moreover, the analysis can be carried out under isothermal conditions or at dynamic heating rates. This technique can be useful for further determination of decomposition kinetics, volatile contents and compositional analysis of multi-component blended materials [159].

The TGA of the membranes were analyzed on the Perkin Elmer, TGA- 7 for evaluating their thermal stability. Samples weighing about 10-15mg were run from ambient to 900°C at varying heating rates of 5°C/min, 10°C/min and 15°C/min under nitrogen atmosphere at 20mL/min.

3.4.2.3 Heat Treatment

The heat-treatment protocol was carried out after the completion of drying procedure. The treated membranes were formed by treating the films in an oven, Model: Memmert UNE600; at 140°C for 1 hour. The treatment process was carried out in the presence of oxygen that was provided by the ventilated system of the oven by blowing air into the chamber. After the operation, the treated membranes were slowly cooled down to room temperature at the rate of 2°C/min. The films were then taken out from the oven and were analyzed for subsequent gas permeation evaluation.

3.4.3 Spectral Analysis

3.4.3.1 Fourier Transform Infrared Spectroscopy (FTIR)

Infrared Spectroscopy is used to identify the presence of functional groups and chemical bonds in the molecular configuration of a material. It is one of the methods of spectroscopic analysis and is used because of its advantages of high sensitivity, being mechanically simple as it has only one moving part, and it consumes less

analysis time in comparison to conventional infrared spectroscopy. In this case, an interferometer is used rather than a monochromator where the material to be tested is exposed to all infrared frequencies. The region of light used in infrared spectroscopy ranges from 4000cm^{-1} - 400cm^{-1} [160]. When light is absorbed by the organic molecule in this region, the infrared radiation is converted into vibrational, bending, stretching or rotational energy. There are two regions: (i) the fingerprint region corresponds to each individual molecule and provides unique identification while (ii) the functional group region is the same for molecules having the same functional group and thus have a similar reactivity.

A spectral analysis of the developed membranes was carried out on the FTIR, Perkin Elmer Spectrum One spectrometer. Potassium bromide (KBr) pellets were prepared by the hydraulic pressurizing of the powder followed by a thin coating of the pellet with the sample solution. The samples were then run under the transmittance mode in the wavelength range of 400 cm^{-1} to 4000 cm^{-1} .

3.4.3.2 X-Ray Diffraction (XRD)

XRD is used for determination of organic and inorganic crystallographic structures by monitoring the x-rays diffraction after their interaction with the sample. It can also provide useful information about the atomic arrangement of the polymers, thin films and nanoparticles [161]. The spectra plot between the scattering intensity (Cps) as a function of the diffraction angle (2θ) is shown in Figure 3.3. Crystalline and amorphous phases can be differentiated which corresponded to sharp and broadened peaks, respectively. The degree of crystallinity is achieved by determining the area under each peak. Though, the discrimination between the crystalline and amorphous scattering is difficult which indicates that the extent of crystallinity cannot be judged with very high accuracy. Moreover, the existence of small crystallites is difficult to evaluate since their scattering pattern resembles that of amorphous materials. However, these small crystallites effect to broaden the peaks and sometimes notify about the crystal size owing to the broadening of such peaks. From the figure, it is clear that the broadening band was formed with the amorphous scattering which implies a d-spacing distribution.

In this study, the Bruker A&S D8 advanced XRD diffractometer was used having a $\text{CuK}\alpha$ radiation source at 4kV and 30mA. The scanning speed was maintained at $1.2^\circ\text{C}/\text{min}$ over a diffraction angle range from $2-80^\circ$ for the analysis of the developed membranes.

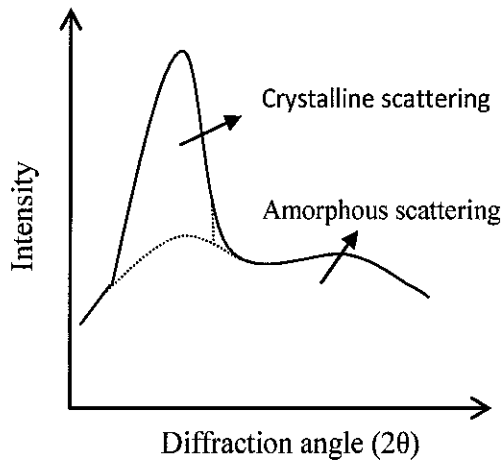


Figure 3.3 Typical Plot of the Intensity versus the Diffraction Angle

3.5 Kinetic analysis

The kinetics on the thermal degradation process was studied for a proper understanding of the degradation for the developed membranes using Friedman's model. The model used thermal degradation of the membrane samples using TGA at three heating rates of $5^\circ\text{C}/\text{min}$, $10^\circ\text{C}/\text{min}$ and $15^\circ\text{C}/\text{min}$.

If a solid to gas phase transformation during the degradation process is assumed, then the general reaction during the heat treatment can be represented in the following way, Eq.(3.6):



The fractional conversion α for the degradation process can be presented in the following way, (Eq.(3.7)), in terms of the weight changes during the thermal degradation.

$$\alpha = \frac{w_0 - w_t}{w_0 - w_f} \quad (3.7)$$

Where, w_0 is the initial weight of the dry sample, w_t is the actual mass of the sample at instant t and w_f is the final weight of the sample at the end of the TGA.

The isothermal degradation rate ($d\alpha/dt$) can be presented as a product of the rate constant $K(T)$ and a function of the conversion $f(\alpha)$ by the following Eq.(3.8) [162]:

$$\frac{d\alpha}{dt} = K(T)f(\alpha) \quad (3.8)$$

The reaction rate constant $K(T)$ is expressed by the Arrhenius Eq.(3.9) as:

$$K(T) = Ae^{-\frac{E}{RT}} \quad (3.9)$$

Where, A is the pre-exponential factor, E is the activation energy, R is the gas constant, T is the temperature for the decomposition.

Combining the Eq.(3.8) and Eq.(3.9) gives Eq.(3.10) [163],

$$\frac{d\alpha}{dt} = Ae^{-\frac{E}{RT}} f(\alpha) \quad (3.10)$$

Assuming β as the heating rate, Eq. (3.11)

$$\beta = dT/dt \quad (3.11)$$

Combining Eq.(3.10) and Eq. (3.11) gives Eq.(3.12),

$$\beta \frac{d\alpha}{dT} = Ae^{-\frac{E}{RT}} f(\alpha) \quad (3.12)$$

Taking the logarithm on both sides of Eq.(3.12), it takes the form of Eq.(3.13) written as [164]:

$$\ln\left(\beta \frac{d\alpha}{dT}\right) = \ln[Af(\alpha)] - \frac{E}{RT} \quad (3.13)$$

Therefore, a linear plot of the left hand side (L.H.S) against $1/T$ of the Friedman's model enabled to calculate the value of the activation energy (E) of the membrane samples from the slope of the straight line.

3.6 Mechanical analysis

Tensile analysis is a technique which is used to analyze the mechanical behavior of a material which involves the deformation of the material under the influence of an applied force until failure. The response of the force applied is recorded in a stress-strain curve also termed as a tensile test. The test estimates the quality of the material and its selection for a particular application. It is one of the best ways to evaluate mechanical properties and has been extensively used owing to its simple, robust and inexpensive parameters [165].

The tensile strength and related properties of the developed membranes were determined following ASTM D882-02 for thin films less than 0.1mm in thickness at $\sim 23^\circ\text{C}$. The dumb-bell sample specimen shown in Figure 3.4 had dimensions of 100mm x 9mm which was confirmed for 10 repetitions using the Fowler® digital micrometer before being tested on universal testing machine LR 5K Lloyd Instruments at a constant grip separation rate of 10mm/min. The tests were also

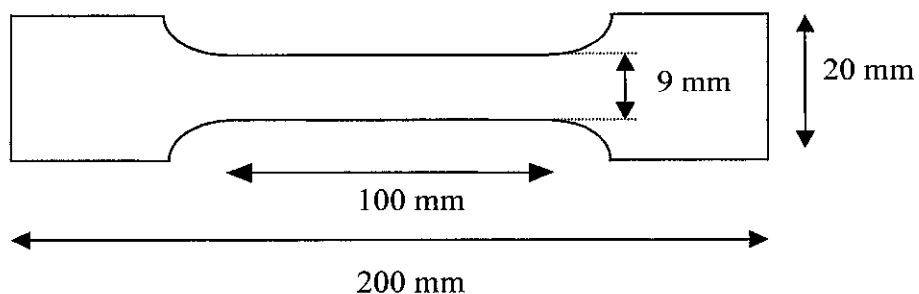


Figure 3.4 The dumbbell-shaped specimen for tensile testing

repeated for each membrane sample to provide the average tensile properties. The membrane specimen was placed between the two grips and clutched with one fixed to a stationary crosshead chamber while the other to a movable chamber. This assembly prevented the slippage of the specimen and uneven stress division. The change in length ($L-L_0$) of the specimen with respect to the original length (L_0) was recorded when the load (P) was applied to pull the sample in an opposite direction having an original cross-section area (A_0). The data from this elongation and the load measurements were used to calculate the engineering strain (ϵ) and stress (σ) which were determined using the following equations:

$$\epsilon = \frac{L-L_0}{L_0} \quad (3.14)$$

$$\sigma = \frac{P}{A_0} \quad (3.15)$$

$$\% \text{ strain at break} = 100 \quad (3.16)$$

From the plot of the stress-strain curve, the stress at break was reported as the tensile strength. The stress-strain curves were then used to further analyse the property of Young's modulus.

Young's modulus is defined as the index of stiffness of the material. It represents the stress generated in the limit of the small deformation produced in the material. This initial slope of the stress-strain curve is represented by the symbol E' . By definition, E' can be written as:

$$E' = \lim_{\sigma, \epsilon \rightarrow 0} \frac{d\sigma_0}{d\epsilon} \quad (3.17)$$

The E' value is calculated by a polynomial curve-fit to the power of 5, on the stress-strain data over the initial 1-2 % strain.

3.7 Gas Permeation Evaluation

The permeation experimentation for pure and mixed gases of CO_2 and CH_4 was conducted on a membrane gas permeation testing unit (Figure 3.5) with 2-10 bar feed

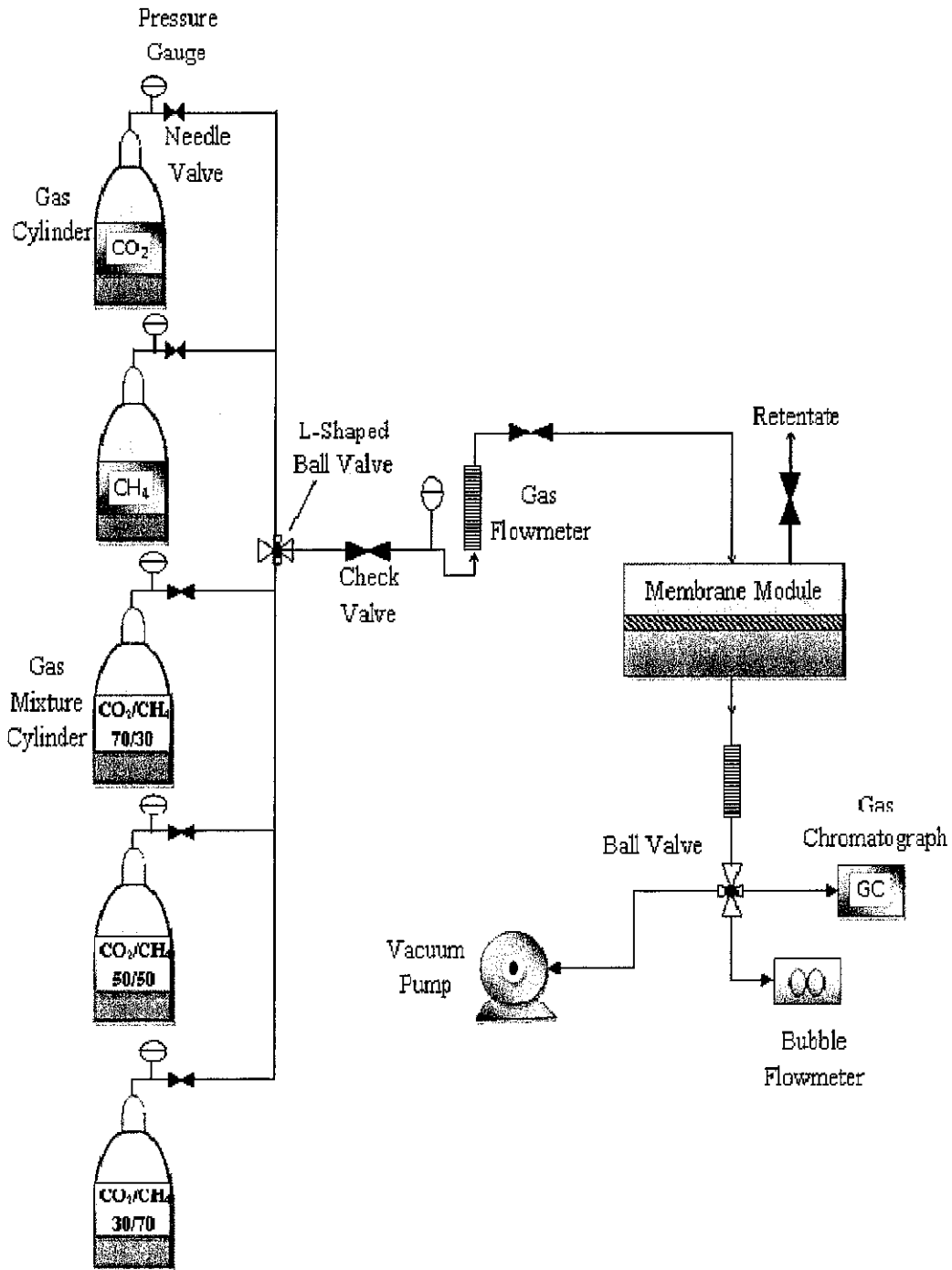


Figure 3.5 Schematic Illustration of the Membrane Gas Permeation Testing Unit

pressures for evaluating the performance of the developed membranes. Two pure gas cylinders of CO₂ and CH₄ and three mixed gas cylinders with compositions of 30/70%, 50/50% and 30/70% of CO₂/CH₄ were taken from MOX-Linde Gases Sdn. Bhd. for the pure and the mixed gas stream evaluations, respectively.

The test unit consisted of a stainless steel paired disk between which the membrane with an effective area of 14.54 cm² was placed. It was tightened by O-rings and flanges to eliminate the chances of gas leakage (Figure 3.6). Beneath the membrane sample was placed a polypropylene perforated circular sheet and a mesh for sample support. This dead-end membrane module allowed the feed gas streams to enter perpendicularly into the membrane sample. The assembly further consisted of pressure gauges; gas flowmeters, and Swagelok® fittings and valves were used in the assembly. The gas tests were dependent upon maintaining the feed side pressure while measuring the gas flux through the membrane of the known area. Before performing the test, the testing unit was completely vacuumed for ½ hour to remove the residual gases and impurities at a pressure of ≥ 0.1 bar. The permeation of the CO₂ and CH₄ gases through the permeate side was measured by using a bubble flowmeter. This flowmeter was used since it can measure low flowrates (i.e., less than 100 ml/min) more accurately than digital flowmeters. All the tests were performed at room temperature and were repeated at steady state conditions for accuracy purposes.

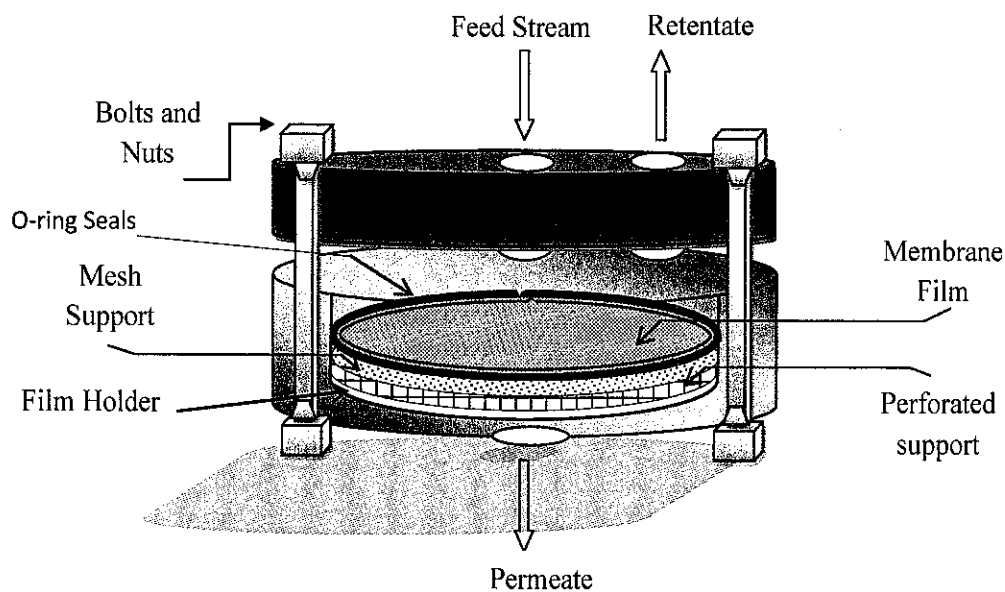
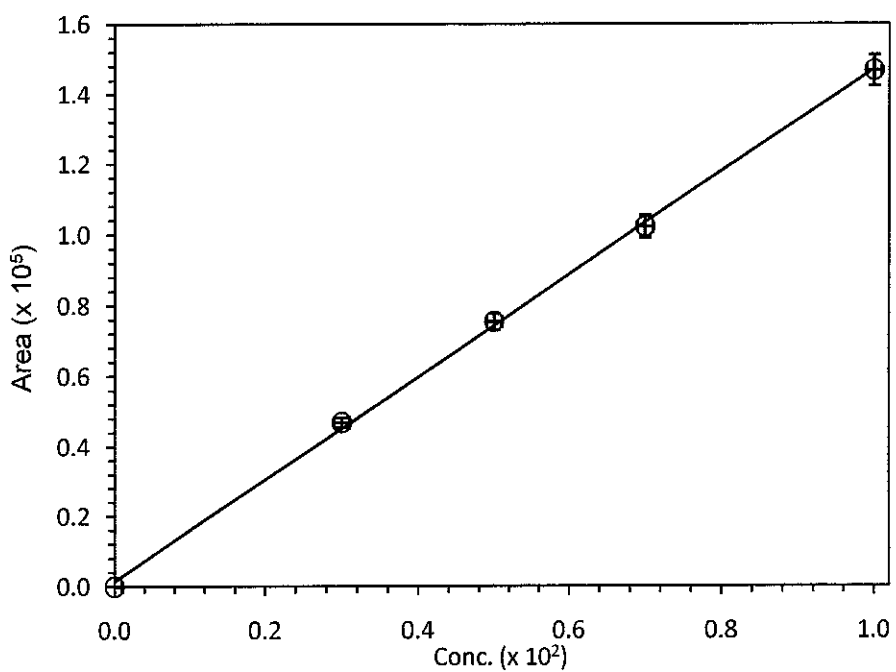
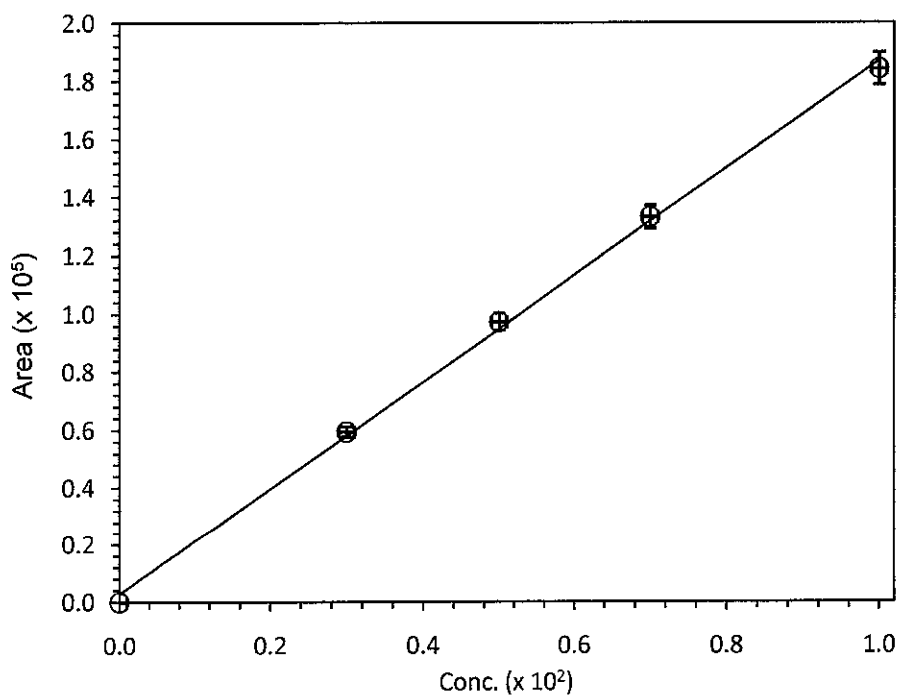


Figure 3.6 Schematic Illustration of the Membrane Module



(a)



(b)

Figure 3.7 Calibration curves of (a) CO₂ and (b) CH₄ respectively

The permeance of the CO₂ and CH₄ gases was calculated by the following equations:

$$\frac{P_{\text{CO}_2}}{l} = \frac{J_{\text{CO}_2}}{\Delta p_{\text{CO}_2}} ; \quad (3.18)$$

$$\frac{P_{\text{CH}_4}}{l} = \frac{J_{\text{CH}_4}}{\Delta p_{\text{CH}_4}} \quad (3.19)$$

Where, J is the flux of the CH₄ and CO₂ gases, Δp is the differential partial pressure of across the membrane for the gases and l denotes the thickness of the membrane.

For compositional analysis of the gas mixture, the samples were collected in sampling bags and were further examined under the Gas chromatograph (GC) (Shimadzu-2010) using a thermal conductivity detector (TCD) and nitrogen as the carrier gas. Prior to the sample evaluation, GC was standardized for pure CO₂ and CH₄ gases and their calibration curves are shown in Figure 3.7. The system was allowed to reach steady state conditions before the mixed gas evaluation and the stage-cut was maintained at 5%. Thus, the gas selectivity ($\alpha_{\text{CO}_2/\text{CH}_4}$) was calculated by taking the ratios of the CO₂ and CH₄ permeance [166].

$$\alpha_{\text{CO}_2/\text{CH}_4} = \frac{P_{\text{CO}_2} / l}{P_{\text{CH}_4} / l} \quad (3.20)$$

The details of all the gas permeation experiments performed on the polymeric membrane and MMMs are summarized in Table 3.6 and are further shown I Appendix C.

3.8 Modeling in MMMs

For the purpose of evaluating the gas permeance using the theoretical permeation models, experimental data is taken from CO₂ permeance in MMMs. The deviation obtained between the predicted and the experimental values were calculated using the percentage average absolute relative error (AARE %) as depicted by the following Eq. (3.21)-(3.22) :

Table 3.6 Design of experiments

Polymeric membranes blends (PSF/PI) wt. %	Solvent compositions (DCM/NMP) (vol. %)	Sample Examination	Gas analysis on membrane types	Feed pressures on each sample (bar)	No. of repeated test runs on each sample	Types of Gases
PSF	20/80, 50/50, 80/20	SEM, DSC, FTIR, TGA, Kinetic and Mechanical Analysis	Untreated Membranes & Heat treatment Membranes	2-10	2	Pure gases (CO ₂ , CH ₄)
PSF/PI-5%						
PSF/PI-10%						
PSF/PI-15%						
PSF/PI-20%						
Mixed Matrix Membranes (PSF/PI-20% + Silica wt. %)						
Silica contents	Solvent compositions (DCM/NMP) (vol. %)	Sample Examination	Gas analysis on membrane types	Feed pressures on each sample (bar)	No. of repeated test runs on each sample	Types of Gases
5 %	80/20	SEM, DSC, FTIR, XRD, TGA, Kinetic and Mechanical Analysis	Untreated Membranes & Heat treatment Membranes	2- 10	2	Pure gases (CO ₂ , CH ₄)
10%						
15%						
20%						
Mix Gas Analysis on best selected Membranes (Polymeric and Mixed Matrix membrane)						
Membranes samples	Solvent compositions (DCM/NMP) (vol. %)	Gas analysis on membrane type	Feed pressures (bar)	No. of repeated test runs on each sample	Types of Gases	
Polymer blends PSF/PI-20%	80/20	Heat treatment Membranes	2-10	2	Mix gases CO ₂ /CH ₄ (30/70%, 50/50% 30/70%)	
Mixed matrix membrane @ Silica 15 wt. %						

$$ARE_i = \left| \frac{P_i^{cal} - P_i^{exp}}{P_i^{exp}} \right| \quad (3.21)$$

$$AARE\% = \frac{100}{dp} \sum_{i=1}^{dp} ARE_i \quad (3.22)$$

Where, P_i^{cal} , P_i^{exp} are the relative permeance of CO₂ calculated theoretically and by experiment, respectively. While the subscript i is the data point index and dp indicates the total number of data points.

All the permeance calculations using the model equations and the corresponding shape factors are performed on MATLAB software, version 7.6.0.324.

CHAPTER 4

4. RESULTS AND DISCUSSION

4.1 Overview

This chapter is based upon all the experimental results carried out after the characterization and evaluation of the asymmetric polymeric and mixed matrix membranes. Section 4.2 discusses the characterization of the asymmetric membrane blends, solubility parameter and gas permeation evaluation. Section 4.4 is based upon the characterization and gas separation performance of the mixed matrix membranes. Section 4.5 deals with the various permeation models for the evaluation of the experimental results obtained with the MMMs.

4.2 Development of Asymmetric Membranes

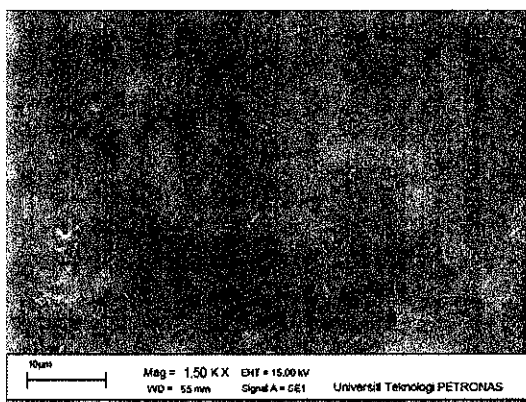
In the preparation of the asymmetric polymeric membranes, 25g of the total casting solution was prepared at various PSF/PI blend compositions for the selection of a suitable membrane blend for further processing in the MMMs. The morphologies of the membranes were analyzed using various characterization techniques.

4.2.1 Effect of Blends on Polymer Concentration

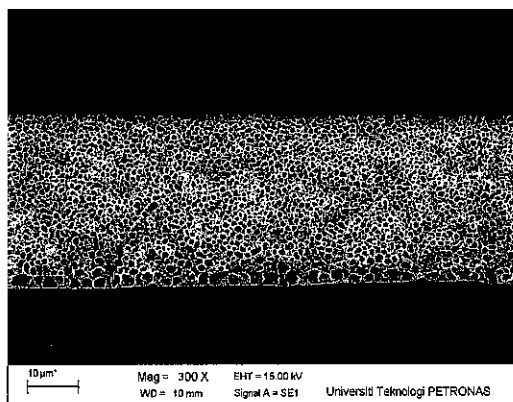
In the present investigation, asymmetric membranes were developed by phase inversion technique with different proportions of PI and PSF content in the system

shown in Table 3.4 for the 80/20 NMP/DCM ratio. The morphology of the surface and cross sections of pure PSF were compared with the blended membranes as shown in Figure 4.1. From the microstructures of the pure and blended asymmetric membranes it is apparent that the surfaces were reasonably homogeneous indicating miscibility between the two glassy polymers. The polymeric blends apparently showed no phase separation. The cross-sectional views of the membranes showed the presence of fairly dense skins and micro porous sub-layers in the structures and hence by definition, it could be described as an asymmetric membrane [45]. The development of the skin layer can be related to the proper control of dry and wet processes during the fabrication of a membrane. The observed microvoids in the membrane were produced by the removal of the non-solvent during the wet phase separation.

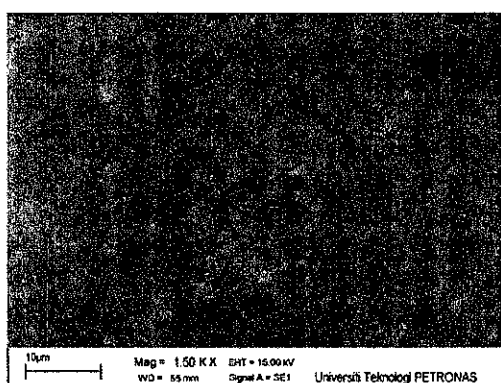
In the liquid phase, the coagulation process was quite fast at the surface of the membrane. This resulted in the rapid gelling of the polymeric molecules onto the surface, which formed a thin skin layer. NMP was used along with DCM in the ratio of 4:1 to control the rate of the solvent evaporation. The formation of a thin layer was evident within 30 seconds of the evaporation, demonstrating that the top layer of the film was subjected to the minimum nucleation rate. During the immersion step of the film in alcohol, the top skin acted as a barrier against the diffusion of the non-solvent for affecting the substructure. Once formed, the skin layer continued to increase in area until the diffusion of the ethanol (non-solvent) from the sub-layer of the membrane and through the skin layer was completely stopped. For the flat sheet membranes, an evaporation time of 10–15 seconds was considered to be suitable for the development of a defect-free top skin layer [167]. Therefore, in this study, an evaporation time of 15 seconds was maintained prior to the wet phase inversion process.



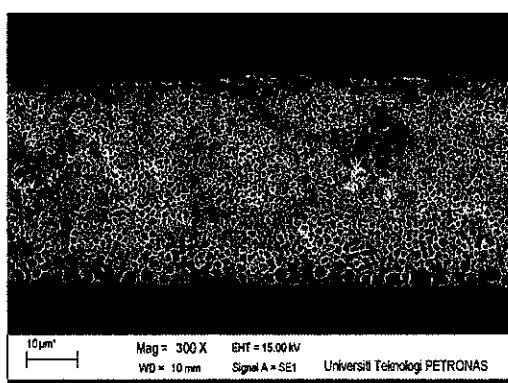
(a)



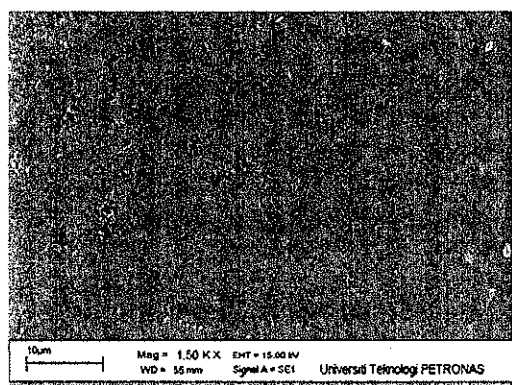
(d)



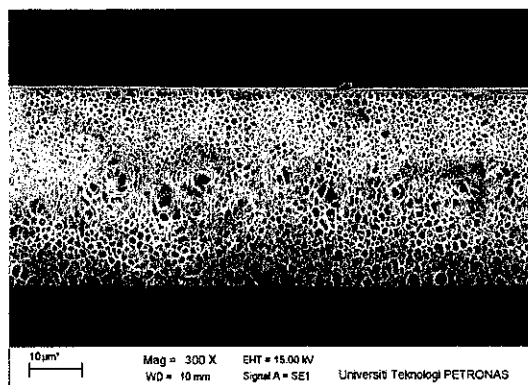
(b)



(e)



(c)



(f)

Figure 4.1 SEM images of the membranes surfaces (a) Pure PSF, (b) PSF/PI-10% and (c) PSF/PI-20%, and cross-sections (d) PSF, (e) PSF/PI-10% and (f) PSF/PI-20%

Relatively thinner skin layers with thick sub-porous structures were observed for the membrane under the experimental conditions. Thin skin layers with dense porous supports at the bottom have been observed to be quite suitable for gas separation applications. Microstructures of the developed membranes revealed sponge-like structures rather than finger-like macrovoids in the sub-porous layer; this indicates the absence of defects and pinholes at the membrane surfaces [45].

4.2.2 Glass Transition Temperature

The glass transition temperatures T_g 's for the developed membranes were measured by differential scanning calorimetry (DSC) analysis. The T_g values from the thermograms of PSF/PI membranes blends are shown in Figure 4.2. The miscibility of the polymers in the molecular level was confirmed since all the compositions exhibited a distinct single T_g value. Also, for these PSF/PI blends of various compositions, no phase separation was observed which is also consistent with past studies [168].

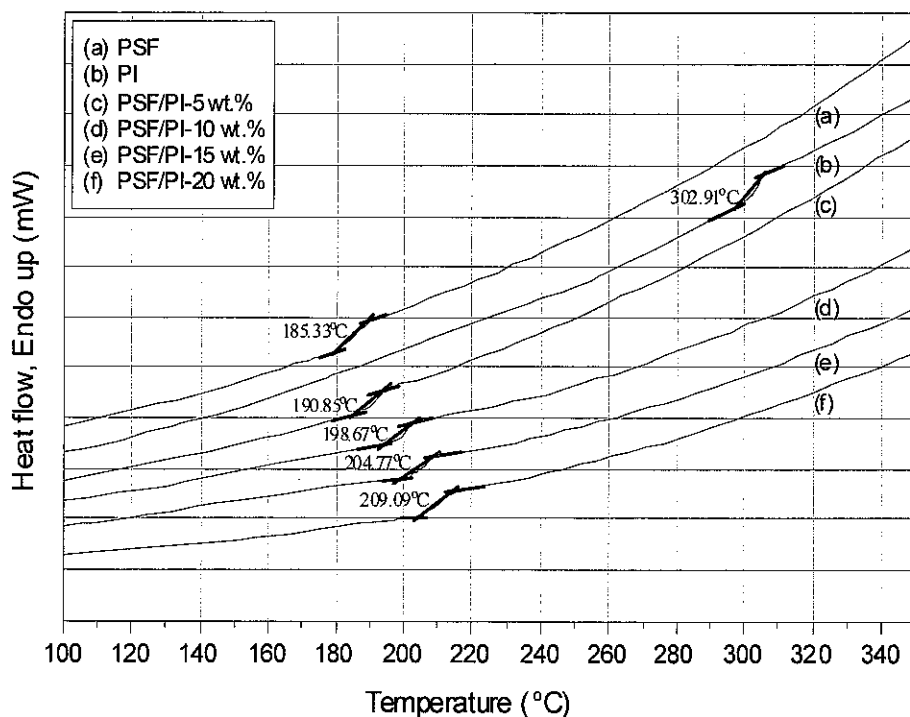


Figure 4.2 DSC thermograms of the membrane blends

The T_g of the samples for the pure and blended membranes were taken as the mid-point of the heat flow versus the temperature curve. Pure PSF and PI thermograms were found to be at their characteristic T_g values of 185.3°C and 302.9°C. While for the membrane blends, it was observed that with the increase in PI content, the T_g of the polymeric blend increased. A similar rise in T_g values was observed by Bos et.al in the polymeric blends with the increase in PI contents in another type of polyimide-P84 [36].

The T_g miscibility among the polymeric blends were further judged by using Fox equation (series model) or Wood's equation (parallel model) or Pochan's equation (logarithmic model) shown by the Eqs.(4.1)-(4.3) respectively [169]. The Figure 4.3 shows experimental T_g values together with the estimated T_g the models.

$$T_{g_b}^{-1} = w_1 T_{g_1}^{-1} + w_2 T_{g_2}^{-1} \quad (4.1)$$

$$T_{g_b} = w_1 T_{g_1} + w_2 T_{g_2} \quad (4.2)$$

$$\ln T_{g_b} = w_1 \ln T_{g_1} + w_2 \ln T_{g_2} \quad (4.3)$$

Where T_{g_b} , T_{g_1} and T_{g_2} indicate the glass transition temperatures of polymeric blends and individual polymers while w_1 and w_2 are the mass fractions of the corresponding polymer 1 and polymer 2 in the blend respectively.

The parallel model gave the closest fit to the empirical T_g value amongst the three models in this case. These three models are idealized equations and exist between the energetic (interactions) and entropic (free volume) terms. A positive deviation i.e higher T_g values indicates the existence of interactions while negative deviation i.e lower T_g values suggest changes in the free volume. It is observed that deviation from theoretical results is a common phenomenon observed for majority of polymer blends that reflects specific interactions between the components [170]. The empirical value exhibited a convex curve while the models showed a concave curve or a straight line. This discrepancy might be related to the non-consideration of the interactions

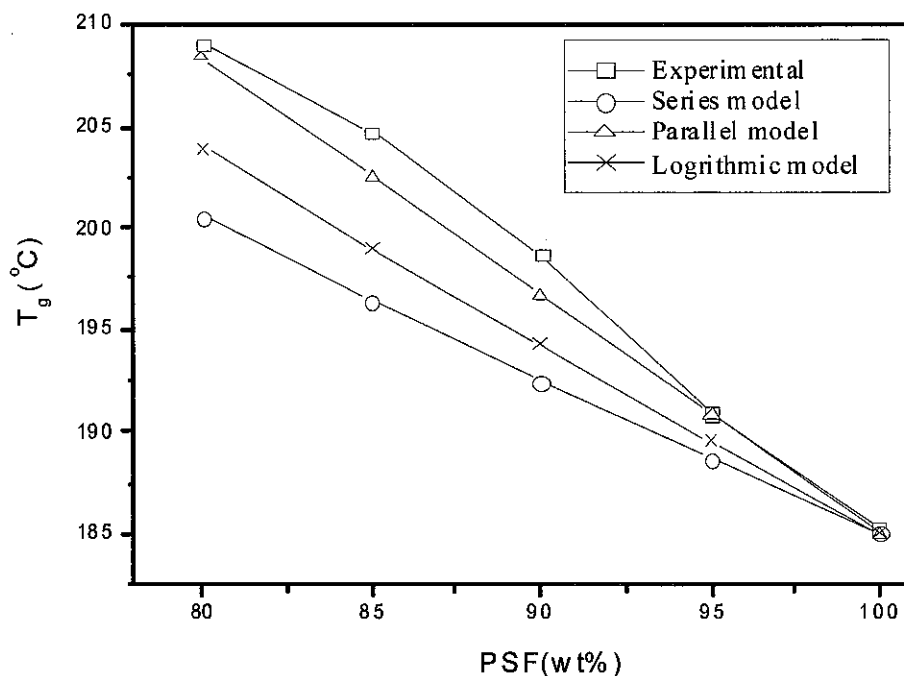


Figure 4.3 Comparison of glass transition temperature of the PSF/PI blended with theoretical models

between the two polymers in the models. A convex curve for the T_g profile has been reported in literature also for a binary polymer blend system with strongly interacting components [171].

4.2.3 Spectral Analysis

The FTIR spectra of the PSF, PI and PSF/PI-20% blended asymmetric membranes are shown in Figure 4.4. For PSF, symmetric and asymmetric vibrations associated with S=O were found at wave numbers of 1150 cm^{-1} and 1308 cm^{-1} , respectively. A C-SO₂-C asymmetric stretching vibration appeared at 1322 cm^{-1} . The band between 1587 cm^{-1} to 1489 cm^{-1} represents the region for benzene ring stretching. An asymmetric C-O stretching vibration appeared at 1244 cm^{-1} and 1014 cm^{-1} . The symmetric deformation associated with the CH₃-C-CH₃ group was found in the region of 1364 cm^{-1} and 1410 cm^{-1} . Similarly, in the case of the PI spectra, the symmetric and

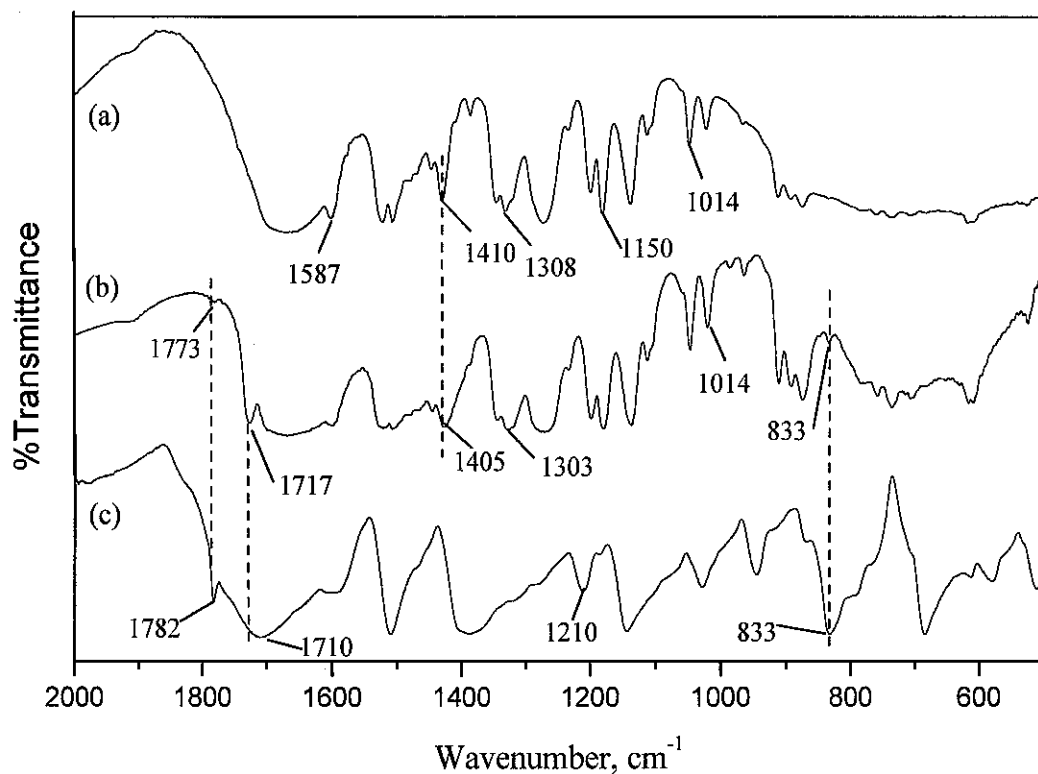


Figure 4.4 Comparative FTIR spectra of the PSF, PI and PSF/PI-20% membranes

asymmetric stretching of the C=O group was observed at 1710 cm^{-1} and 1782 cm^{-1} while the benzophenone carbonyl band was noticed at 1608 cm^{-1} . The peak related to C=C stretching of the aromatic ring was observed at 1510 cm^{-1} . A C-N-C axial vibration was observed in the region of 1210 cm^{-1} - 1389 cm^{-1} while a transverse stretching vibration was found at 1028 cm^{-1} . The band observed at 1144 cm^{-1} is ascribed to the presence of C_6H_4 . The peak due to the aromatic ring bending vibration was observed at 833 cm^{-1} . The stretching vibration due to the C-C=O bond occurred at 684 cm^{-1} . These observations are in good agreement with previous studies [172-174].

In comparison to pure polymers, various spectral shifts of the blended PSF/PI-20% membrane in terms of wave number were observed. For the symmetric and asymmetric carbonyl group for the PI spectral shift was observed from 1710 cm^{-1} to 1717 cm^{-1} and 1782 cm^{-1} to 1773 cm^{-1} and for the C-N-C axial vibration the shift was

observed from 1210 to 1206 while the peak at 1389 cm^{-1} remained unchanged. Spectral shifts were observed for the benzene ring of PSF (from 1587 cm^{-1} to 1584 cm^{-1} and from 1488 cm^{-1} to 1493 cm^{-1}), for the respective symmetric and asymmetric vibrations of S=O (from 1150 cm^{-1} to 1151 cm^{-1} and from 1308 cm^{-1} to 1303 cm^{-1}), for the asymmetric vibrations of C-O (from 1244 cm^{-1} to 1247 cm^{-1}) and for the symmetric vibrations of the $\text{CH}_3\text{-C-CH}_3$ group deformation (from 1410 cm^{-1} to 1405 cm^{-1}). The summarized form of the different shifts in the FTIR spectra are presented in Table 4.1 and supports the development of the interactions among the polymers which indicates their miscibility in the form of blended membranes [175].

Table 4.1 Summary of the FTIR Spectral Assignments

Spectral assignment	PSF Wave Number, cm^{-1}	Membrane blend Wave Number, cm^{-1}
C_6H_6 ring stretch	1488-1587	1493-1584
$\text{CH}_3\text{-C-CH}_3$ symmetric stretch	1410,1364	1405, 1364
C-O asymmetric stretch	1244, 1014	1247, 1014
S=O symmetric stretch	1308, 1150	1303, 1151
C -SO ₂ - C asymmetric stretch	1322	1322
Spectral assignment	PI Wave Number, cm^{-1}	Membrane blend Wave Number, cm^{-1}
C=O symmetric & asymmetric stretch	1710, 1782	1717, 1773
C - N-C axial stretch & transverse stretch	1210-1389	1206-1389
C=C stretch	1510	1510
C_6H_6 ring bend	833	833

On the basis of spectral interactions among the polymers, a model is proposed which is shown in Figure 4.5. It indicates the possible polymers interactions and its dissolution with the solvent that formed the π and hydrogen bonds. The repeating unit of PSF indicates its presence in excess as compared to PI and the arrows indicate the probable locations for bond formation. PI chains are likely to be sandwiched between the PSF chains and the phenyl rings of the polymeric units can be attached with each other by a π - π interaction. During the fabrication process the low boiling solvent,

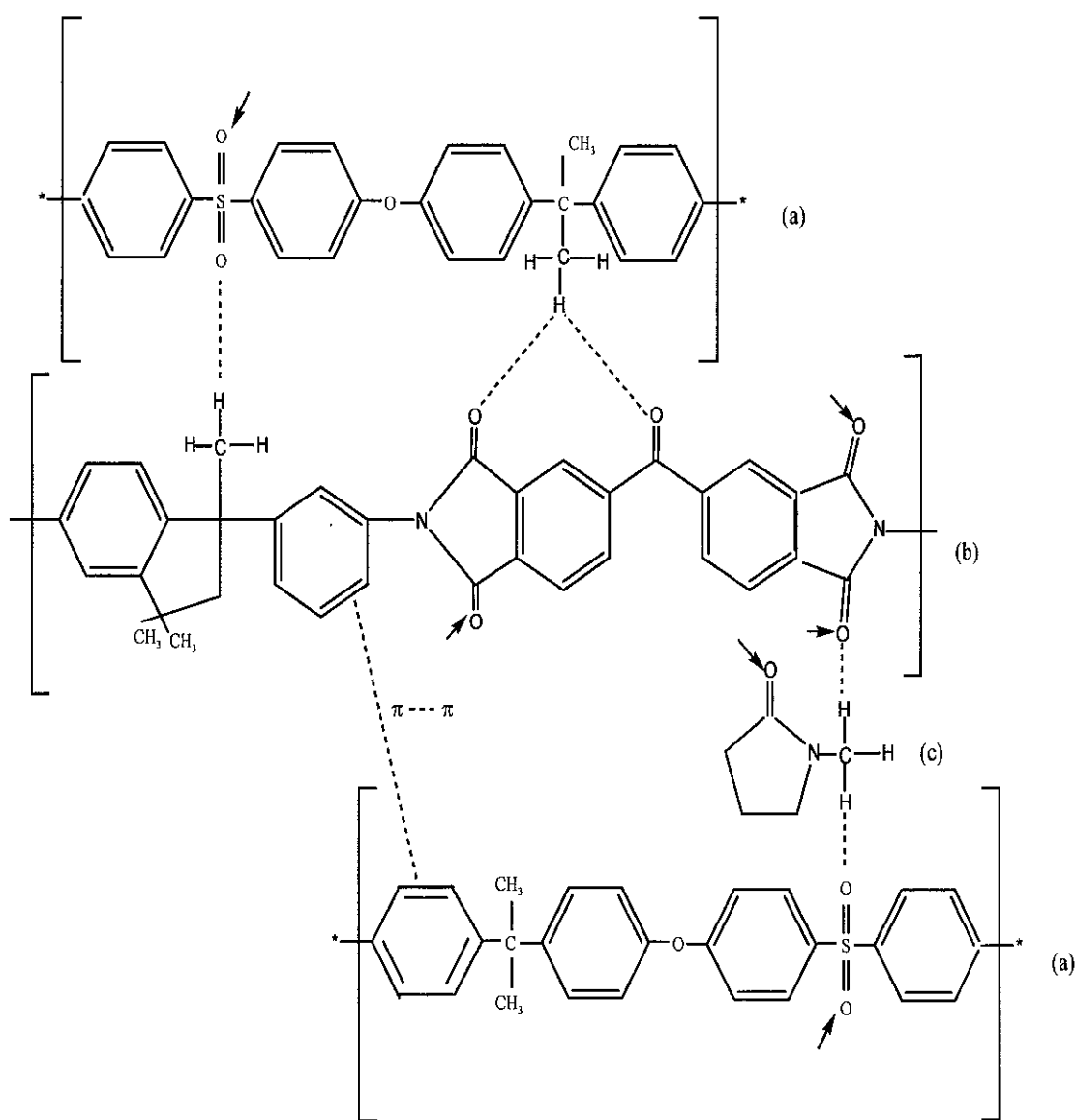


Figure 4.5 Structures of (a) PSF, Udel® P-1800, (b) PI, Matrimid® 5218 (c) NMP and the possible interactions among the polymer species indicated by arrows and dotted lines

DCM, resulted in the development of a diffused skin layer by using the rapid solvent evaporation, and NMP controlled the rate of the solvent evaporation.

4.3 Mechanical Analysis

The properties of the asymmetric membrane films were further evaluated on the basis of mechanical analysis, and the representative stress-strain curves of the developed membranes are shown in Figure 4.6. Young's modulus, tensile strength and strain at break obtained from the stress-strain plots are summarised in Table 4.2. Though the morphologies of the developed membranes remained almost the same at various concentrations of the polymers, the different samples showed different behavior in their properties at varying percentages of the polymers used. The stress- strain curve indicates that after the initial strain intervals, the membrane samples started to deviate from the linear relationship and reached a new equilibrium state after undergoing an intermolecular rearrangement in their structure.

It is observed that the strain at break and tensile strength gradually increased with the addition of PI contents in the PSF membranes. In comparison to the pure PSF membrane, PSF/PI-20% showed higher brittle characteristics and fractures at $28.55 \pm 0.73\%$ strain so the maximum tensile strength was 28.12 ± 2.0 MPa and 0.978 ± 0.29 GPa Young's modulus. It is because PSF possesses polar SO_2 group and rigid aromatic rings in its backbone structure with intrinsic values of Young's modulus and a tensile strength of 70.3 MPa and 2.48 GPa [176]. On the other hand, PI exceeded the intrinsic tensile properties of PSF having 85.5 MPa and 2.9 GPa, respectively, thus indicating the increased rigidity of the membrane blends [177]. The results, thus, obtained by the asymmetric polymeric membranes shows a similar behaviour as reported by Linares and Acosta on a PSF/PI dense membrane system [175]. Their results showed improved brittle characteristics and fractures to break at 63.22 MPa as the maximum tensile strength and Young's modulus of 2.39 GPa as compared to pure polymers.

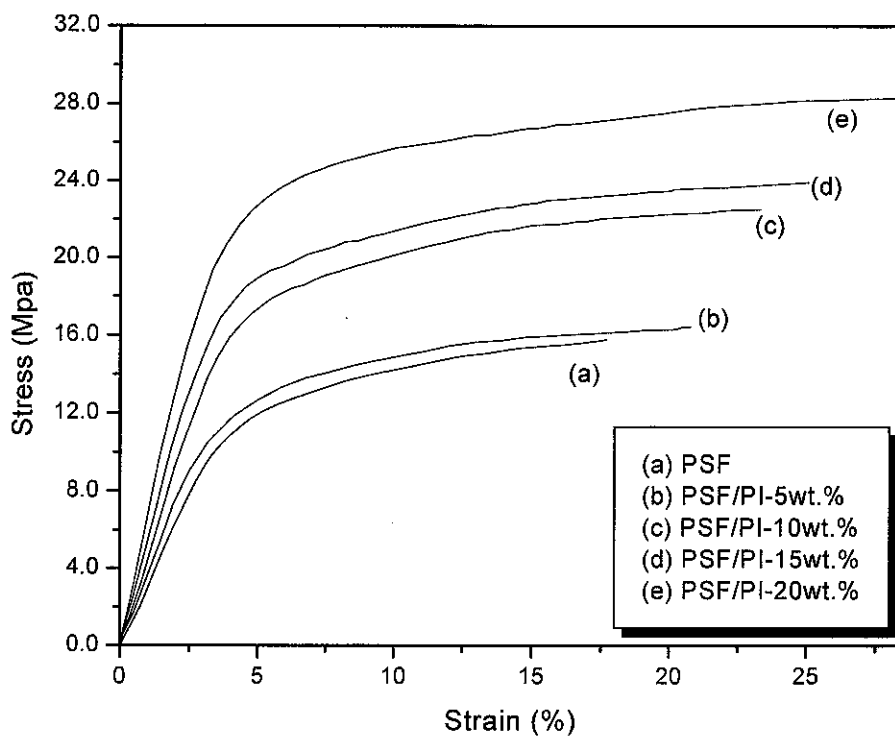


Figure 4.6 Representative stress-strain curves of the developed membranes at various polymer concentrations

Table 4.2 Mechanical properties of the developed PSF/PI membranes

PSF	PSF/PI-5wt.%	PSF/PI-10wt.%	PSF/PI-15wt.%	PSF/PI-20wt.%
Young's Modulus (GPa)				
0.570±0.40	0.597±0.31	0.802±0.15	0.885±0.22	0.978±0.29
Tensile Strength (MPa)				
15.87±1.6	16.15±2.3	22.54±3.1	23.95±1.8	28.12±2.0
Strain at Break (%)				
17.68±0.61	20.76±0.8	23.31±0.55	25.09±0.42	28.55±0.73

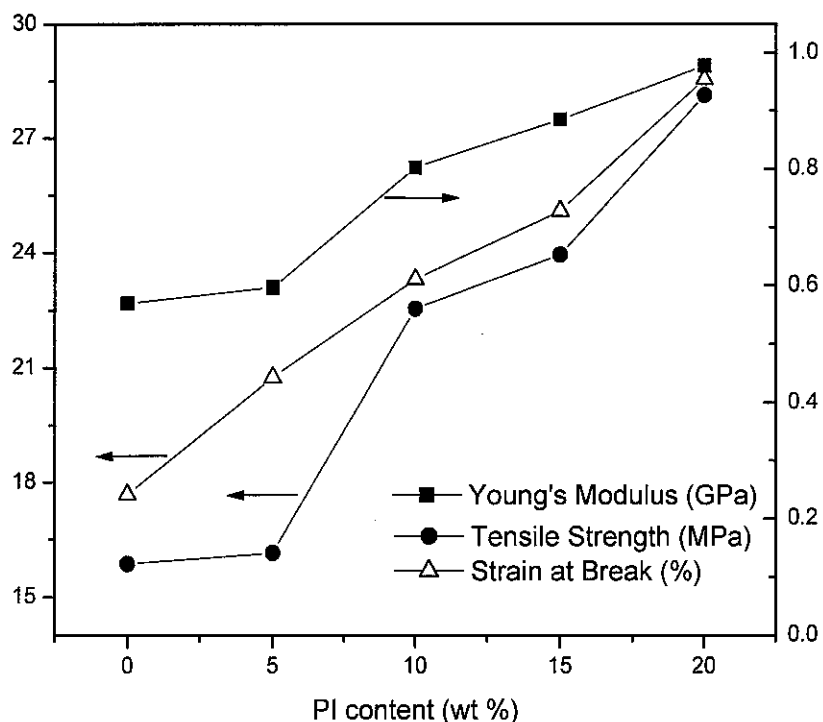


Figure 4.7 Young's modulus, Tensile strength and Strain at break for membrane blends as a function of the PI content

The plot of Young's modulus, tensile strength and strain at break as a function of the PI contents is shown in Figure 4.7. The increasing trend of Young's modulus and the tensile strength was observed with the increase in the PI content that indicates a strong interfacial interaction between the membrane blends. A rise of 72% and 77% in Young's modulus and the tensile strength were observed, respectively with the addition at 20 wt% PI, as compared to the pure PSF membrane. While the strain at break increased almost linearly with the increase in the PI contents and increased up to 62% at 20 wt% PI. This linear increase reflected a more elastic characteristic of the membrane blend with respect to the plain PSF membrane and indicates a stronger chain entanglement in the films thus leading to a longer elongation.

4.4 Gas Permeation Analysis

The permeation properties of the CO₂ and CH₄ gases enabled the development of the correlation with the membrane structures against various pressures. Figure 4.8 shows that the compositions of the membranes significantly affected the permeation

behaviour of both the gases. The trend of the gases shows that the permeance decreased slightly with the increase in the operating pressure indicating the absence of plasticization in the membrane matrix. In the presence of plasticization, especially for CO₂, the membranes show high values of permeance just after achieving the lowest value at high pressures, which indicates swelling of the membrane [32]. Here, in the figure, the CO₂ permeance decreased from 33.7±0.1 to 29.6±0.3 GPU with an increase in the pressure from 2 to 10 bar for pure PSF. It was observed that with the increase in the PI content in the PSF membrane, the permeance of the CO₂ increased gradually as compared to the slightly improved CH₄ gas molecules. So, the PSF/PI-20% membrane exhibited the maximum CO₂ permeance of 39.3±0.2 GPU that decreased to 35.0±0.3 GPU at 10 bar pressure (Figure 4.8). The high permeance of the CO₂ for the membranes with an increasing PI content was attributed towards the soaring affinity for the CO₂ in the membrane matrix. This is because CO₂ possess a linear structure with a relatively smaller kinetic diameter of 3.3°A as compared to the slower moving saturated CH₄ molecules with a kinetic diameter of 3.8°A and a tetrahedral structure. This high CO₂ permeance might be related to the increased

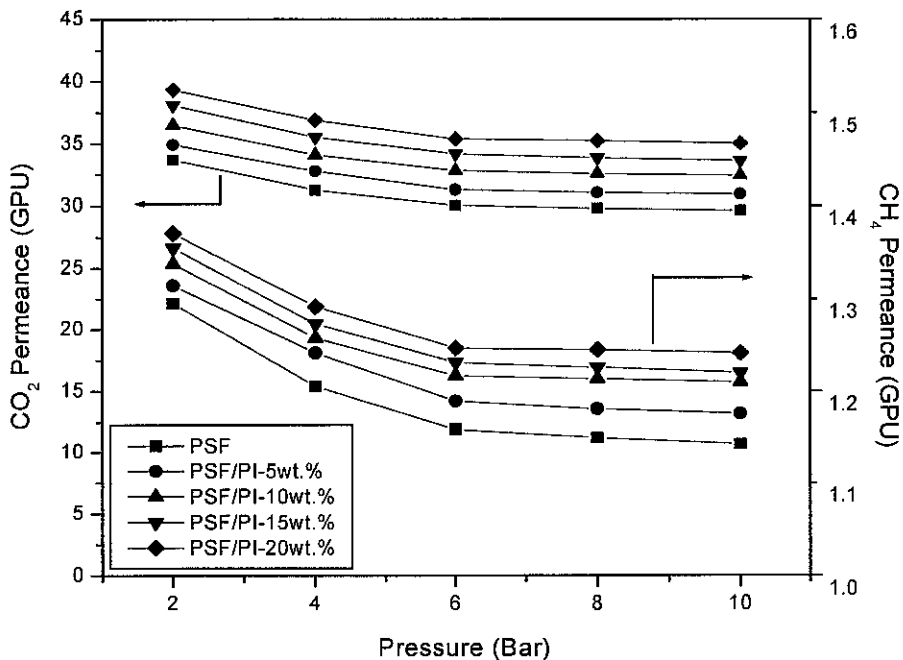


Figure 4.8 Permeance of CO₂ and CH₄ for the different membranes at various feed pressures

solubility of CO₂ as compared to CH₄. For high pressure natural gas streams above 10 bar, the CO₂ permeance would be quite momentous. So in such conditions, prevention must be considered for methane loss in excess. Though, in this study, this phase is beyond the scope.

The permeation behaviour of the gases was further evaluated by subjecting the membranes to a heat treatment at 140°C for 1 hour to minimize the chances of the membrane swelling at higher feed pressures. It was found that the permeance of the gases decreased slightly as compared with the untreated membranes (Figure 4.9). The ideal selectivity of CO₂/CH₄ for the untreated and treated membranes at various feed pressures has been shown in Figure 4.10. For all the membrane compositions, selectivity decreased with the increase in the feed pressure up to 10 bar under the experimental conditions. For the untreated membranes, the PSF/PI 20% blended membrane showed the maximum selectivity ($\alpha = 28.69 \pm 0.1 - 28.22 \pm 0.5$ from 2 to 10 bar pressure, respectively) compared to other membrane blends. The decreasing trends of selectivity with increasing feed pressures have also been reported by other workers [178-180]. It was found for the heat treated membranes that though the

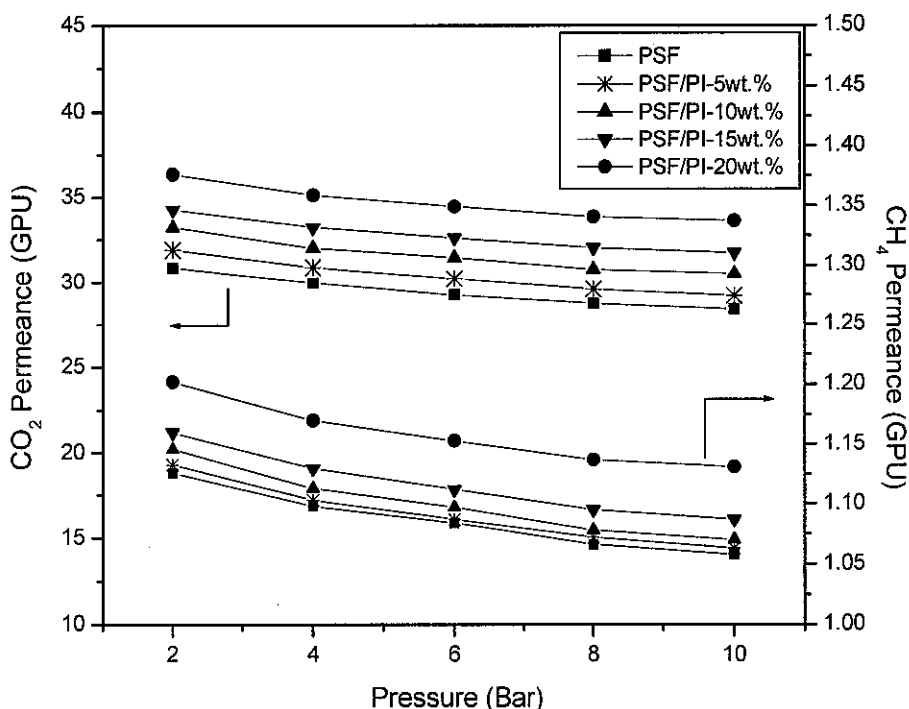


Figure 4.9 Effect of the heat treatment at 140°C on the permeance of CO₂ and CH₄ for different membranes at various feed pressures

permeance slightly decreased, the ideal selectivity increased for each membrane composition as compared to the untreated membranes (Figure 4.10). So for the treated membranes, the maximum selectivity of the PSF/PI-20% blended membrane increased to 30.24 ± 0.5 – 29.70 ± 0.7 followed by PSF/PI-15% ($\alpha = 29.54 \pm 0.5$ – 29.20 ± 0.2), PSF/PI-10% ($\alpha = 28.98 \pm 0.15$ – 28.49 ± 0.7), PSF/PI-5% ($\alpha = 28.16 \pm 0.3$ – 27.47 ± 0.3) and PSF ($\alpha = 27.43 \pm 0.20$ – 26.84 ± 0.4). This blending technique improved chemical and mechanical properties of the polymeric membrane blends resulting in improved intrinsic selectivity as compared to the pure PSF membrane.

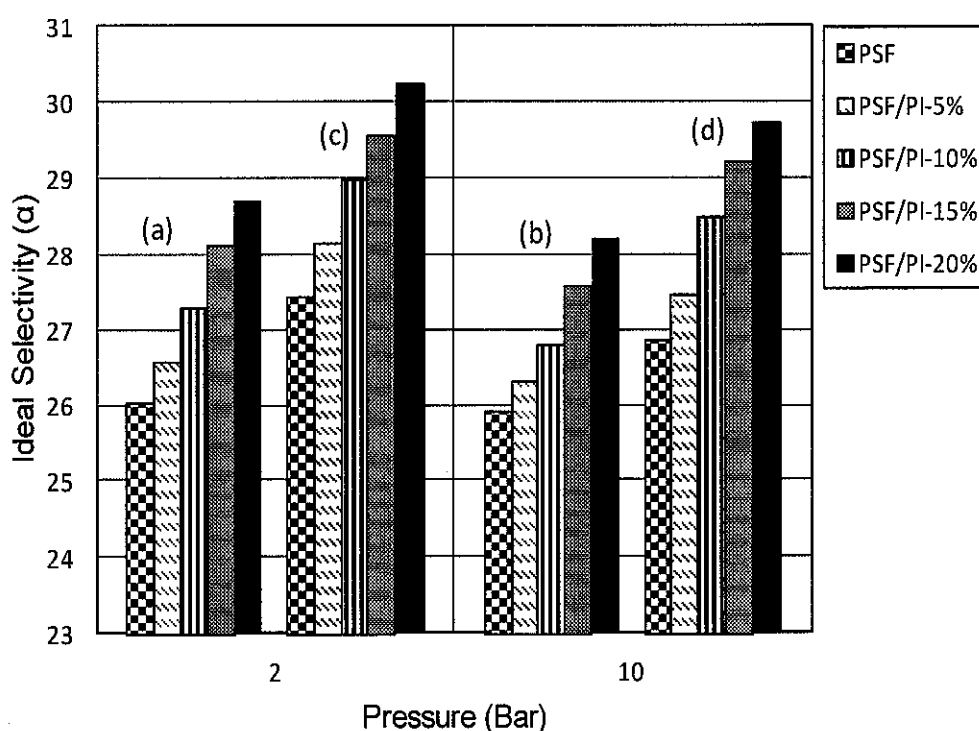


Figure 4.10 Comparison of the ideal selectivity of CO₂/CH₄ at various feed pressures: untreated (a),(b) and heat treated (c),(d)

4.5 Effect of Solvent Compositions on the Solubility Parameter

In the present study, various morphological asymmetric membranes were prepared with various compositions of PSF/PI blends and solvents as shown in Table 3.4. The suitable choice of solvents and non-solvents holds the key role in the optimization of developed membranes. The surface and cross-sectional views of the development of the asymmetric membranes of the PSF/PI blends are shown in Figure 4.11 and

Figure 4.12 respectively. The structures showed the homogenous surfaces of the pure and blended asymmetric membranes at higher magnification indicating miscibility between the two glassy polymers. The PSF, PSF/PI-10% membranes showed dead end pores of different sizes but these kinds of pores were not seen in PSF/PI-20% thus making them more resilient to harsh conditions.

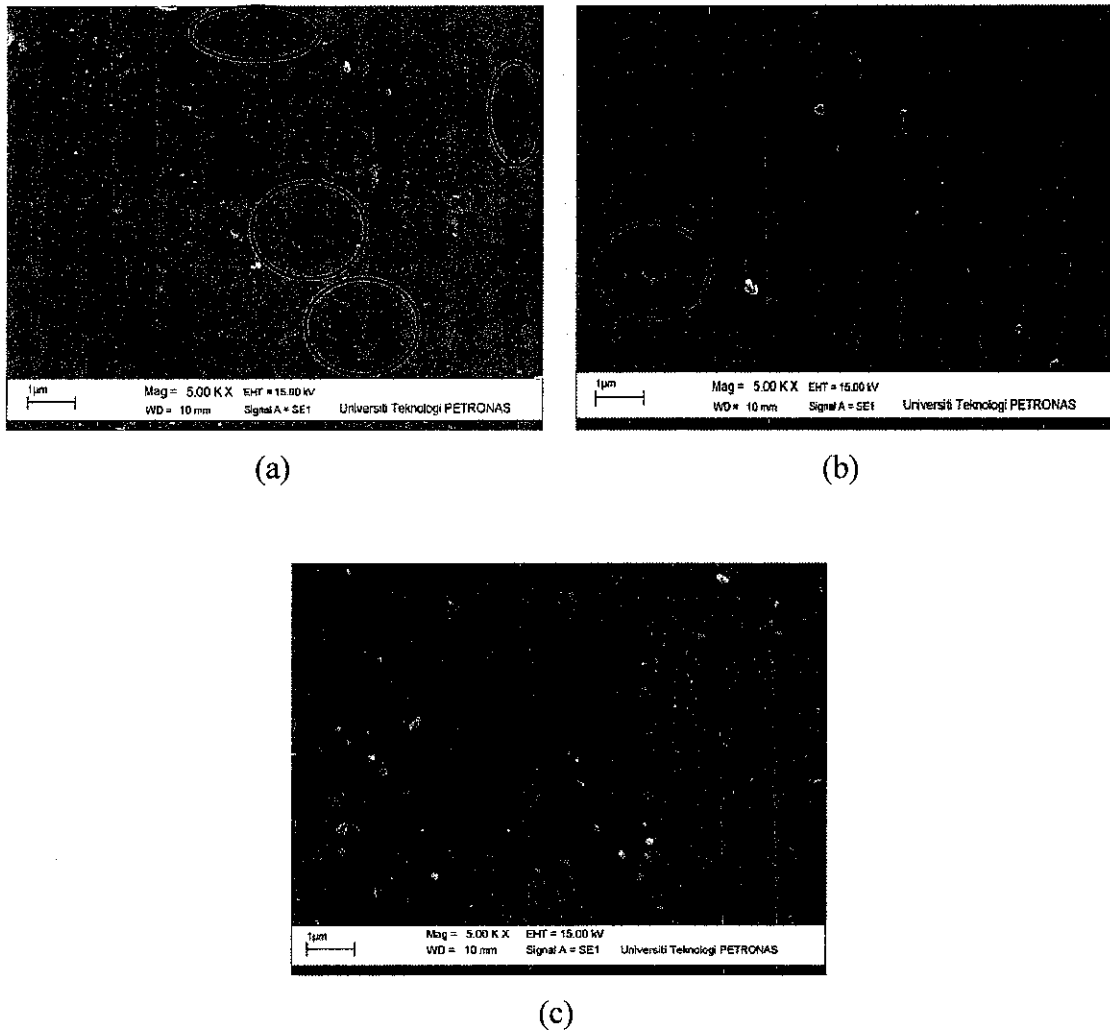


Figure 4.11 SEM images of the membranes surfaces (a) PSF, (b) PSF/PI-10% and (c) PSF/PI-20%

The cross-sectional views of the developed membranes showed a top skin layer supported by closed-cell sub-layers in the structures. However, different solvent compositions and polymeric blends produced different morphologies of the membranes in terms of skin and sub-porous layers. The miscibility among the solvent

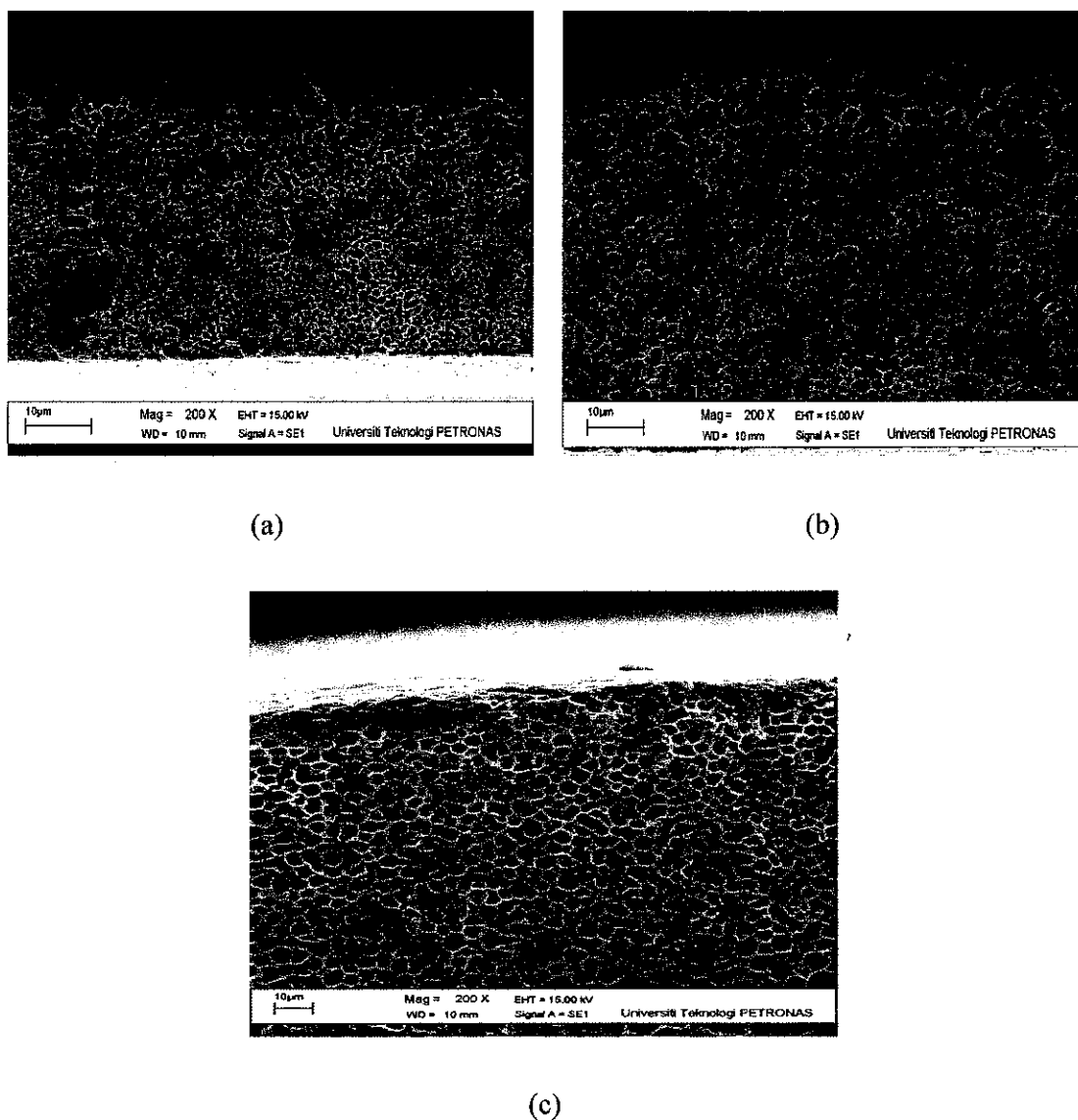


Figure 4.12 SEM images of the PSF/PI-20% membrane cross-sections with the NMP/DCM solvent mixtures (a) 80/20, (b) 50/50 and (c) 20/80

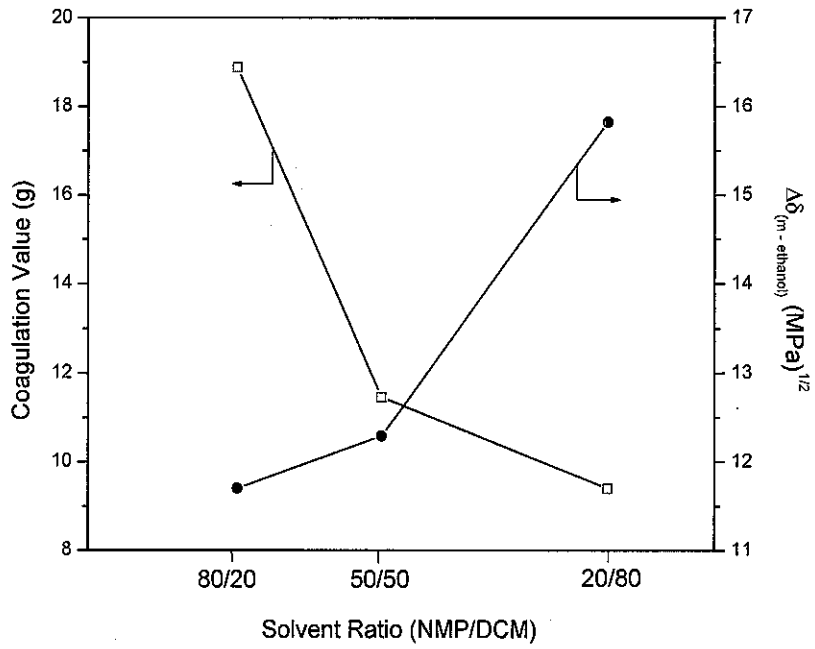
and non-solvent constituents has been addressed to evaluate the mechanism of the membrane morphology. The affinity of the PSF/PI and NMP/DCM (solvents) and ethanol (non-solvent) was examined on the basis of the solubility parameter difference approach. Three different compositions of NMP/DCM solvent mixtures 80/20, 50/50 and 20/80 (also shown in Table 3.4) were used in the membrane formation which affected the solubility parameter of the casting solution.

Table 4.3 shows the solubility parameter for each solvent mixture. It was found that the solubility parameter of the NMP/DCM solvent mixture composition with 20/80 was greater than 50/50 and 80/20. The table further indicates that each solvent mixture had a dissimilar solubility parameter difference, i.e., for ethanol [$\Delta\delta_{\text{mix}} - \Delta\delta_{\text{ethanol}}$] and polymeric membranes [$\Delta\delta_{\text{mix}} - \Delta\delta_{\text{polymer}}$]. It showed that for NMP/DCM solvent mixtures, the solubility parameter difference to ethanol as a coagulant [$\Delta\delta_{\text{mix}} - \Delta\delta_{\text{ethanol}}$] and polymeric membrane [$\Delta\delta_{\text{mix}} - \Delta\delta_{\text{polymer}}$] was in the order of $80/20 < 50/50 < 20/80$. There was a decrease in the solubility parameter difference as the PI contents in the PSF composition were increased for each of the NMP/DCM mixtures. So as the $\Delta\delta$ (m-polymer) value decreased, the time required to remove the solvent from the developed membranes increased. It resulted in delayed demixing, as the casted layer on the glass plate was immersed in the ethanol bath [181-182]. Porous sub-structures with a thin skin layer were supposed to appear more in the case of NMP/DCM (80/20) than with (50/50) and (20/80) [46]. It was observed from the SEM images (Figure 4.12) that in comparison to NMP/DCM (50/50) and (20/80), the membranes prepared with NMP/DCM (80/20) had a thin skin structure with a small size of pores in their sub-structure with a few eddies seen at the bottom part of the cross-section. This indicates that the low boiling DCM solvent in the least solvent composition of NMP/DCM (80/20) helped in reducing the skin structure while NMP controlling the rate of evaporation caused delayed demixing.

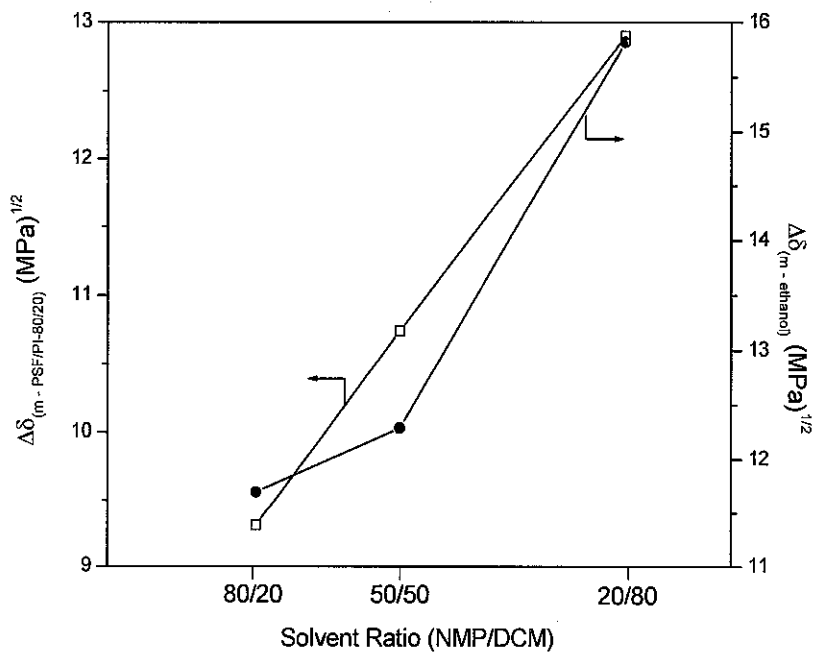
For further investigations of the various compositions of the solvent effects used on the rate of demixing, the coagulation value and the solubility parameter difference with respect to non-solvent (ethanol) was plotted in Figure 4.13(i). The graph shows that among the various compositions of the NMP/DCM solvent mixtures, the (80/20) composition showed the smallest [$\Delta\delta_{\text{mix}} - \Delta\delta_{\text{ethanol}}$] value that corresponded to the highest coagulation value in contrast to (50/50) and (20/80). The lower coagulation value indicates that once the casting layer of the membrane was immersed in the ethanol bath, it took less time for demixing and more bigger porous membranes sub-structure were created from NMP/DCM (20/80) [49] which was observed in the SEM images as shown in Figure 4.12. Figure 4.13(ii) indicated that for the PSF/PI-20% membranes, the solubility parameter difference was the minimum for the solvent mixture of NMP/DCM (80/20) whereas NMP/DCM (20/80) showed the maximum.

Table 4.3 Solubility Parameter Differences among the coagulant, solvents and polymers

Components	Solubility parameter (MPa) ^{1/2}				Solubility Parameter Difference	
	δ_d	δ_p	δ_h	δ_{mix}	With Coagulant [$\Delta\delta_{mix} - \Delta\delta_{ethanol}$]	
For Solvent Mixtures						
NMP/DCM(80/20)	16.36	12.45	7.72	21.96	11.70	
NMP/DCM(50/50)	16.97	13.98	6.33	22.88	12.29	
NMP/DCM(20/80)	17.71	15.99	4.74	24.33	15.82	
For Polymer Mixtures					With Solvent Mixture [$\Delta\delta_{mix} - \Delta\delta_{polymer}$]	
	δ_d	δ_p	δ_h	δ_{mix}	NMP/DCM (80/20)	NMP/DCM (80/20)
PSF/PI(100/0)	18.18	1.66	6.77	19.47	10.98	13.48
PSF/PI (95/5)	18.01	2.06	6.77	19.35	10.56	14.08
PSF/PI (90/10)	17.84	2.46	6.77	19.23	10.14	13.68
PSF/PI (85/15)	17.67	2.86	6.77	19.13	9.73	13.29
PSF/PI (80/20)	17.49	3.26	6.77	19.03	9.31	12.90



(i)



(ii)

Figure 4.13 Solubility parameter difference of the solvent mixtures with ethanol for the PSF/PI-80/20% blended membrane against (i) Coagulation value and (ii) solubility parameter difference of the solvent mixtures with the PSF/PI-80/20% membrane

4.6 Gas Permeation Evaluation at Varying Solvent Compositions

The developed asymmetric blended membranes at various solvent compositions were evaluated on the basis of gas separation characteristics. It was determined by the permeance of the CO₂ and CH₄ gases and their selectivities against the various feed pressures. Figure 4.14 shows that for the developed PSF/PI-20% membranes at varying solvent compositions, a significant difference is observed in their permeation behaviour for both of the gases. It is observed that the permeance of CO₂ and CH₄ increased with the decrease of the DCM composition in the NMP/DCM solvent composition. The increase in the permeance for all the membranes on the basis of the NMP/DCM solvent composition was in the order of 20/80 < 50/50 < 80/20.

The permeance value decreased from 39.34 GPU to 35.03 GPU with an increase in the pressure from 2 to 10 bar for the solvent composition of NMP/DCM (80/20) followed by (50/50) from 30.46 GPU to 24.92 GPU and (20/80) from 25.30 GPU to 20.03 GPU (Figure 4.14). It was further seen that with the increase in the pressure for both of the gases, the permeance value decreased showing the absence of membrane swelling at higher pressures [12]. This indicates that the developed membranes are

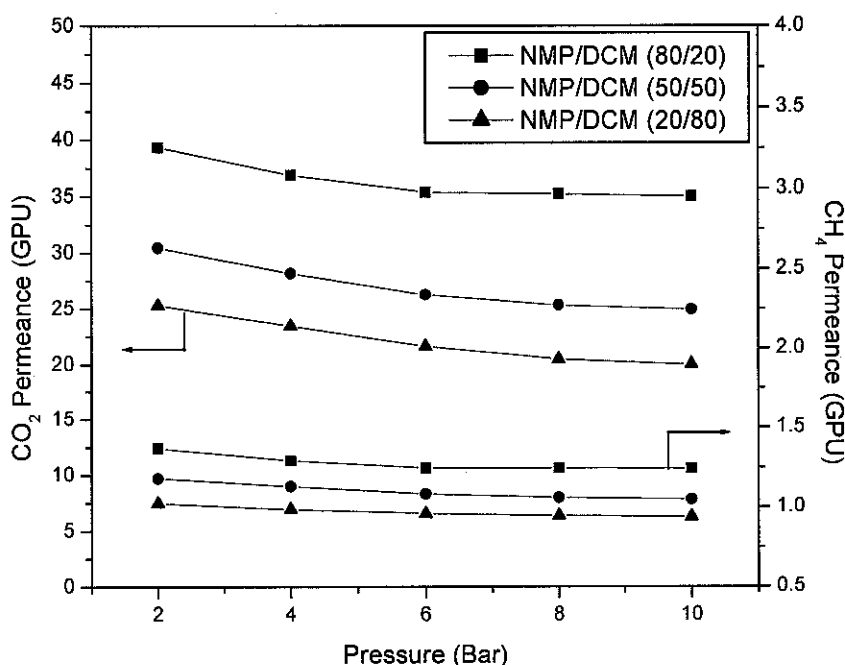


Figure 4.14 Permeance of CO₂ and CH₄ for the PSF/PI-20% blended membranes prepared by different solvent compositions at various feed pressures

resistant to harsh conditions. The permeation behaviour of the gases was further evaluated by the SEM images (Figure 4.12). The sub-porous layer of the membrane prepared solvent composition of NMP/DCM (80/20) and (50/50) looked similar but the former appeared with a thin top selective skin layer as compared to the thick top skins of NMP/DCM (50/50) and (20/80). This characteristic also explains the difference in the permeance of the gases in the membranes. The CO₂ and CH₄ permeation for the PSF/PI-20% membranes for each of the three compositions showed the maximum value in the comparison of the other PSF and PSF/PI membrane blends (Figure 4.14). It is observed that as the PI contents in the PSF membrane was increased, the CO₂ permeance improved significantly in comparison to the improvement in the CH₄ gas permeance (Figure 4.15). The membranes prepared from NMP/DCM (20/80) exhibited the lowest CO₂ and CH₄ gas permeance values in 50/50 and 80/20.

The Figure 4.15 still indicates that PSF/PI-20% (having the maximum addition of PI contents) exhibited the maximum permeance as compared to the other PSF/PI compositions prepared with NMP/DCM (20/80). It showed that the PSF/PI-20%

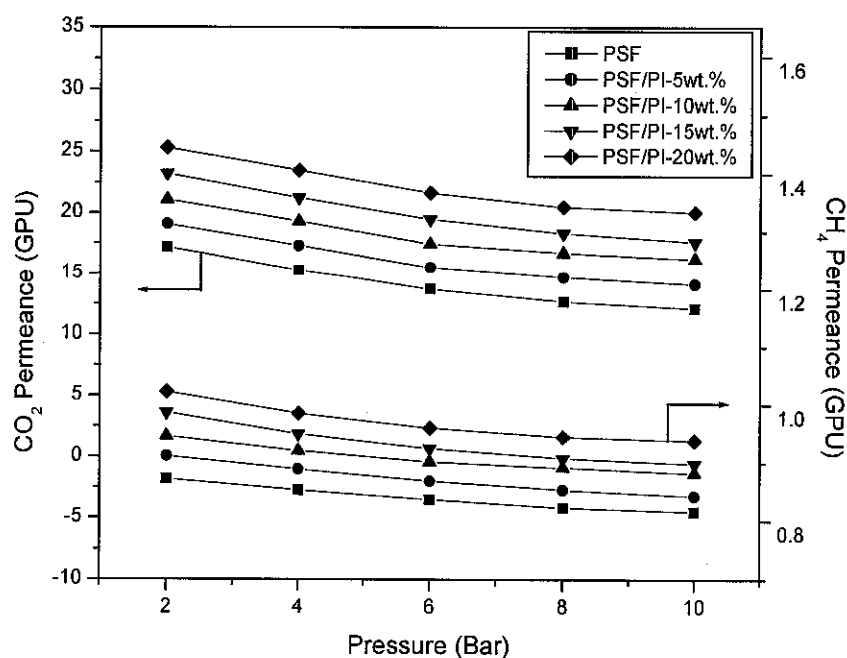


Figure 4.15 Effect of the PSF/PI membrane blends on the permeance of CO₂ and CH₄ at various feed pressures for the NMP/DCM (20/80) composition

membrane exhibited the maximum permeance of 25.30 GPU at 2 bar pressure that decreased to 20.03 GPU at 10 bar pressure. This increased CO₂ permeance with the increasing PI contents in the PSF/PI membrane blends was due to the increased CO₂ solubility as compared to the CH₄ molecules.

The ideal selectivity ($\alpha_{\text{CO}_2/\text{CH}_4}$) graph for all the developed membranes with various NMP/DCM solvent compositions against various feed pressures have been shown in Figure 4.16. It is observed that the selectivity values decreased as the pressure increased from 2 bar to 10 bar under the running conditions. For NMP/DCM (80/20), the PSF/PI 20% blended membrane showed the highest selectivity from 2 to 10 bar pressure, respectively ($\alpha_{\text{CO}_2/\text{CH}_4} = 28.70-28.22$) in comparison to the other membranes prepared from the NMP/DCM (50/50) and NMP/DCM (20/80) compositions. This declining trend of selectivity against an increasing pressure has also been observed earlier [178, 180, 183]. It is further noticed that the percentage

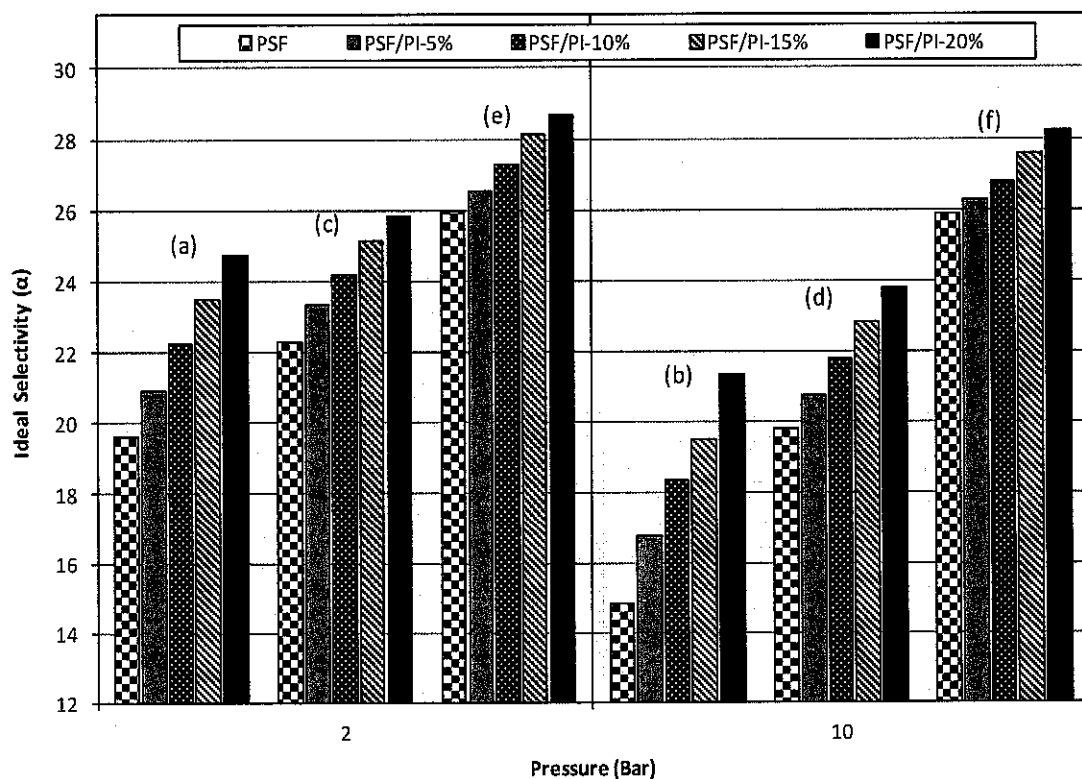


Figure 4.16 Comparison of the ideal selectivity of CO₂/CH₄ for the NMP/DCM solvent composition of (20/80):(a),(b); (50/50):(c),(d) and (80/20):(e),(f)

decrease in the selectivity value for the solvent mixture of NMP/DCM (80/20) from 2 to 10 bar pressure was found to be the minimum, i.e., 1.67 as compared to 7.88 for NMP/DCM (50/50) and 13.70 for NMP/DCM (20/80). This indicates that the membranes prepared by using the solvent compositions of NMP/DCM (80/20) showed better performance at higher pressures without losing much selectivity. The effect of polymer blending along with varying the solvent mixture composition proved to be a useful technique that provides deep inside to the improved chemical and thermal stability for the polymeric membranes.

4.7 Kinetic Analysis

Thermogravimetric analysis, TG study on membrane samples was carried out at three different heating rates. They were intentionally kept at relatively higher values

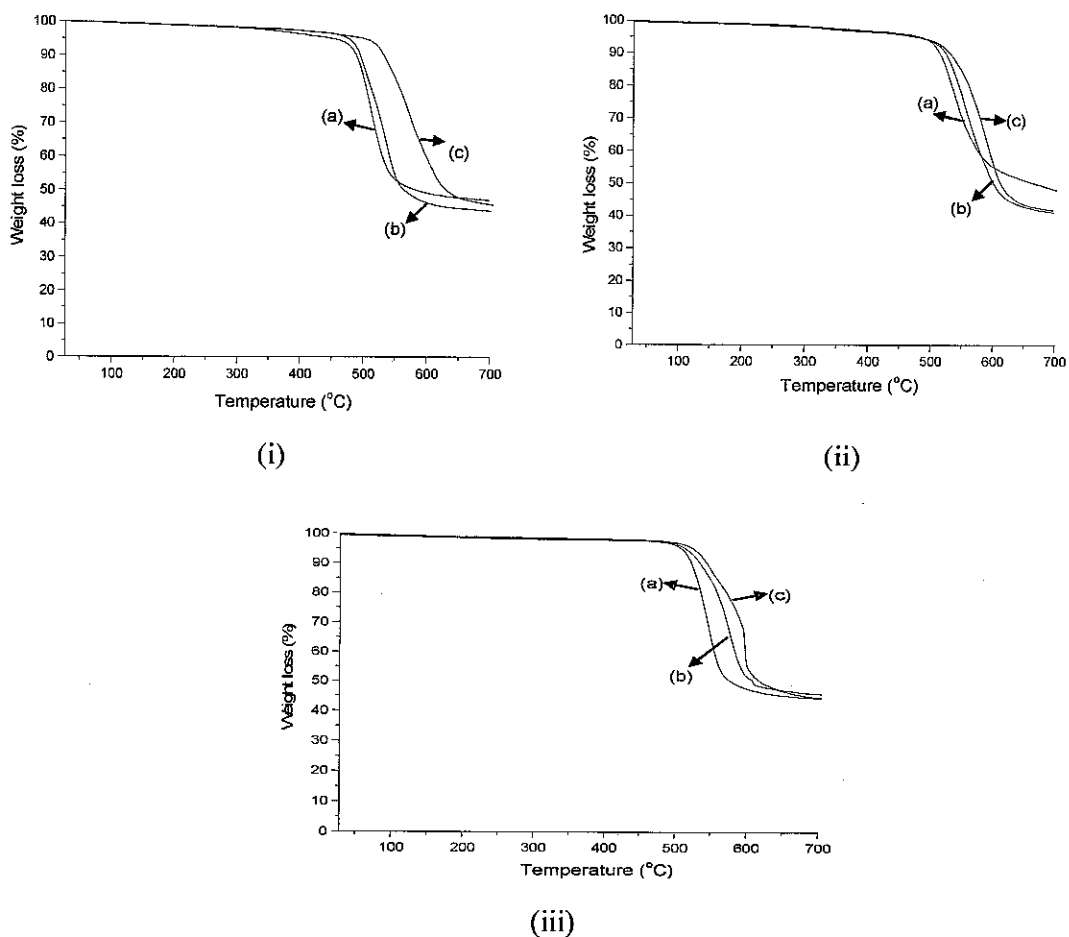


Figure 4.17 TG curves of (i) PSF, (ii) PSF/PI-10%, and (iii) PSF/PI-20% with heating rates for each at (a) 5, (b) 10, and (c) 15 °C/min

of 5, 10 and 15°C/min to gather insight into the degradation process under practical simulated conditions [184]. Only one range of thermal degradation temperatures was observed for all of the compositions; this supported the proper miscibility of the phases. A few typical TG traces for the thermal degradation of the polymeric membranes are presented in Figure 4.18.

The values for the degradation onset temperature and the maximum degradation temperatures for all of the compositions at different heating rates are reported in Table 4.4. It can be seen that with the increase in PI content in the composition, the peak temperature for the degradation increased from 510°C to 600°C (Figure 4.18). This increase in the peak temperature could have been related to the effect of the heat

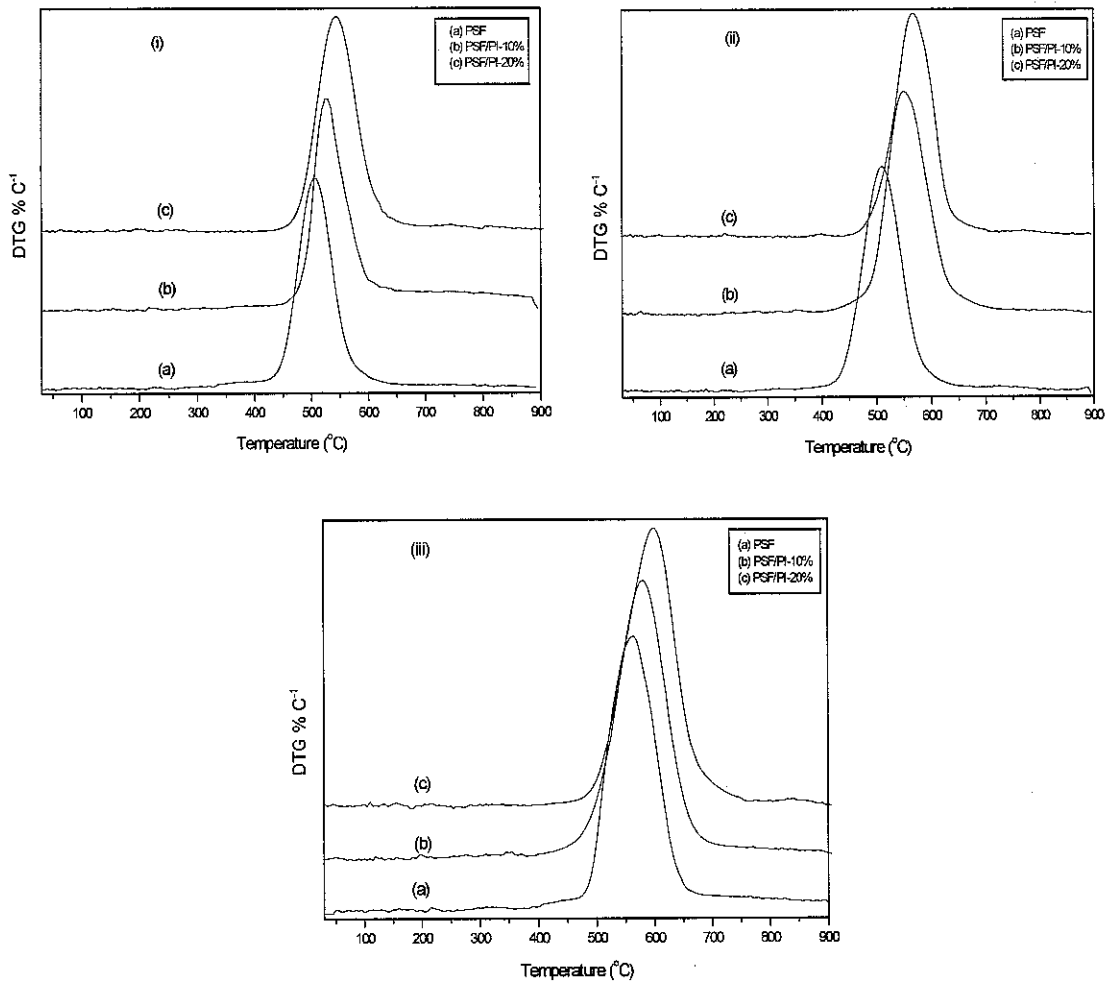


Figure 4.18 Derivative TG curves of PSF, PSF/PI-10%, and PSF/PI-20% at (i) 5, (ii) 10, and (iii) 15°C heating rates

Table 4.4 Dynamic TG Data and the E Values of Various PSF/PI Blends

Membrane	Heating Rate, $\beta = dT/dt$ (°C/min)	Degradation Onset Temperature (°C)	Maximum Degradation Temperature, T (°C)	Activation Energy, (E) KJ/mole
PSF	5	485	510	206.18
	10	497	533	
	15	526	567	
PSF/PI-5%	5	498	520	211.46
	10	509	537	
	15	534	572	
PSF/PI-10%	5	511	537	225.30
	10	528	557	
	15	545	583	
PSF/PI-15%	5	522	544	237.57
	10	537	560	
	15	556	585	
PSF/PI-20%	5	535	549	253.17
	10	548	568	
	15	567	600	

transfer in the material [185]. It might have been correlated to the enhanced blending of the polymers with the increase in the PI content, which resulted in the improvement in the thermal stability [186-187]. The presence of a single decomposition peak could have been related to the homogeneity of the membrane samples.

The kinetics on the thermal degradation was carried out by using Friedman's model on the membrane samples to calculate the activation energies from the Eq(3.13). A plot of the left hand side (L.H.S) of the equation against $1/T$ enabled the evaluation of the value of the activation energy (E) from the slope. Linearized plots thus obtained have been presented in Figure 4.19 and the activation energies for the different compositions have been presented in Table 4.4. From the results, it is evident that with the increase in the PI content in the PSF matrix, the activation energy for the degradation of the polymer membrane increased significantly. A similar finding was observed by Tiptipakorn et al. [188] who found that by increasing the PI contents in

base polymer significantly improved the activation energies of the polymer blends that were calculated from all the three different approaches; Kissinger-method, Flynn-Wall-Ozawa method and Coats-Redfern method. This indicated improvement in the thermal stability for the polymeric blends. A similar increase in activation energies is observed in this study by using Friedman method.

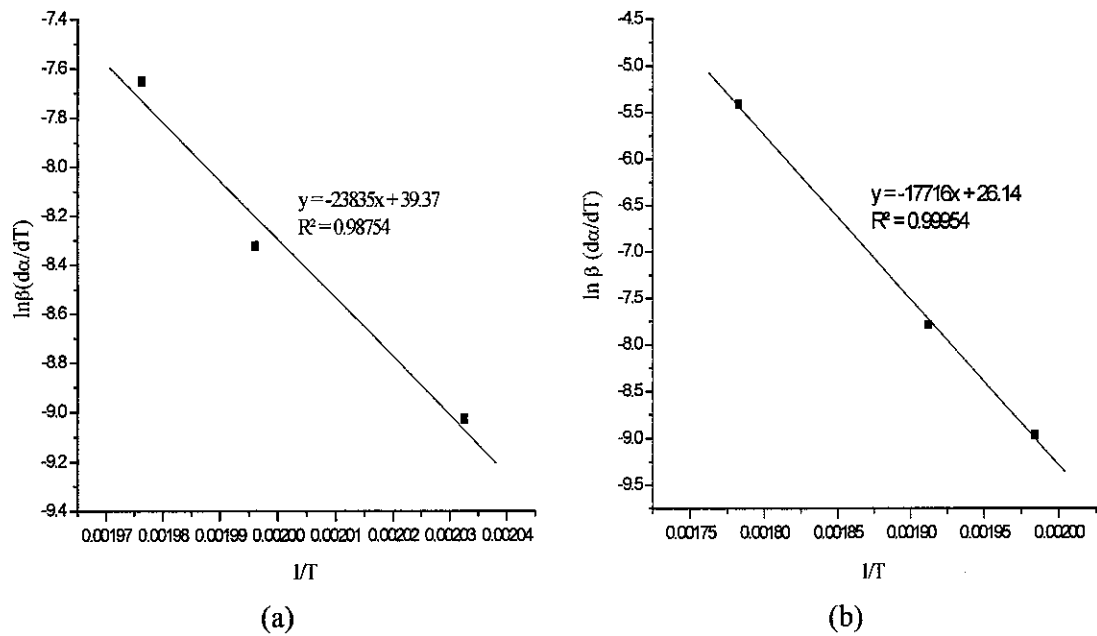


Figure 4.19 Linear Plots of $\ln \beta (d\alpha/dt)$ versus $1/T$ (a) PSF/PI-10% and (b) PSF/PI-20% at the same α values (0.01)

4.8 Development of Mixed Matrix Membranes

In the present investigation, MMM's were developed by incorporating various proportions of silica contents within the polymer matrix in the presence of a coupling agent. The morphology of the MMMs was studied in comparison to the pure polymeric membranes by using SEM. Table 3.5 shows the incorporation of the various compositions of silica contents in the PSF/PI-20% membrane. From the microstructures, it is observed that the surfaces are homogeneous which indicates good compatibility between the two glassy polymers (Figure 4.20(a)). It is noted that

with the addition of the silica contents up to 15.2 wt% in the S3 membrane, the particles were dispersed homogeneously in the polymer matrix (Figure 4.20(b)-(c)). However, the increase in the silica contents up to 20.1wt% in the S4 membrane caused the particles to coalesce, forming large aggregates in the matrix as shown in Figure 4.20(d)). Due to these aggregates, the surface of the S4 membrane did not show homogeneity in comparison to the other surfaces. Previous studies suggested the presence of a hydrogen bond interaction of the phenyl oxygen of PSF with surface silanol groups of the MCM-41 silica [189]. It is, therefore, possible here of having the same hydrogen bonding that provided good wetting properties among the two components of the MMM's.

The cross-sections of the developed membranes (Figure 4.21(a)-(d)) showed

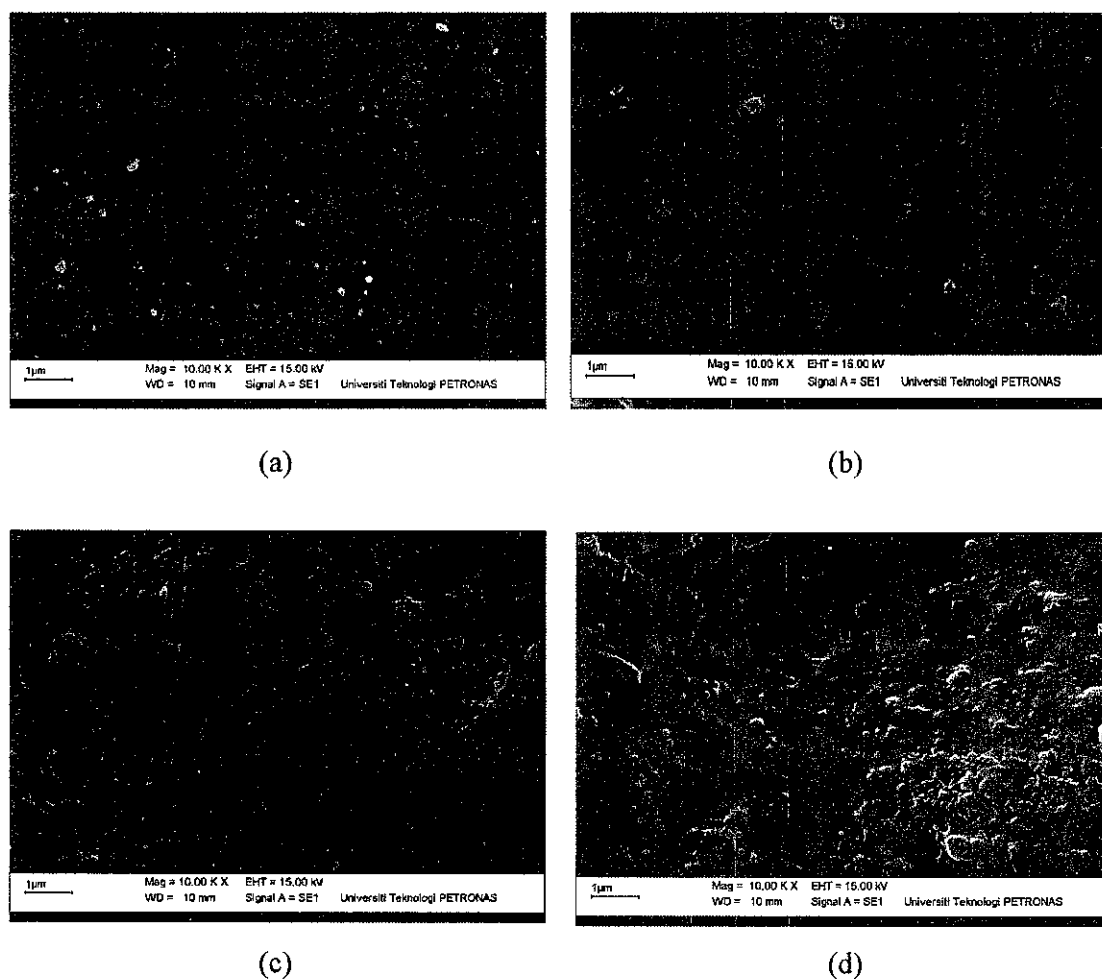
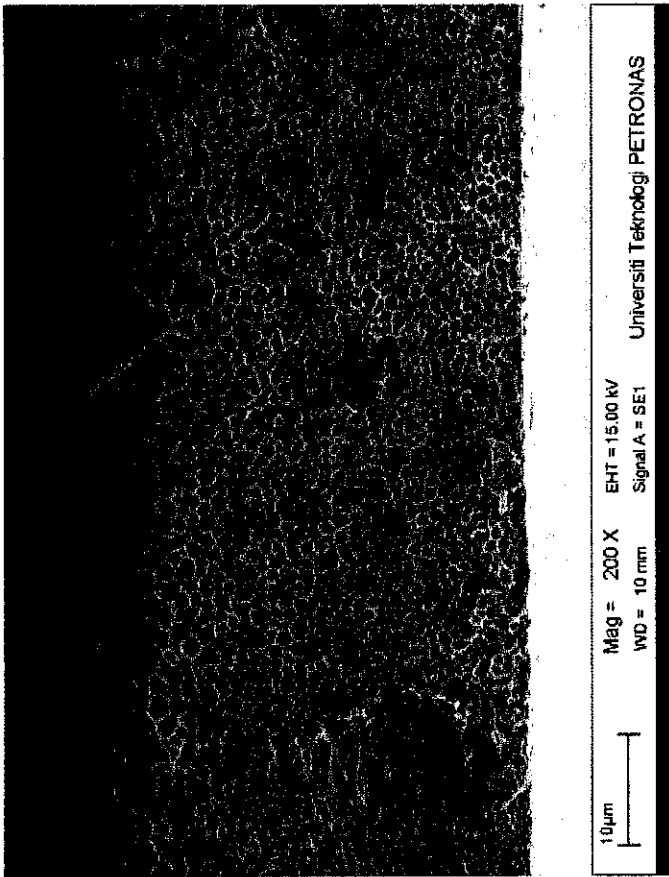
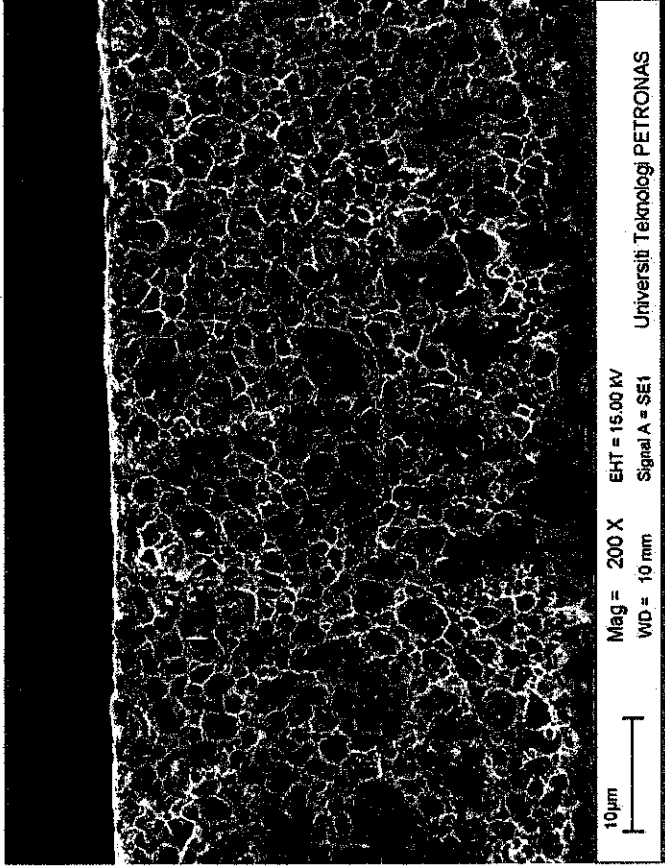


Figure 4.20 SEM images of the PSF/PI-20% membrane surfaces with silica contents (a) 0% (b) S1 (c) S3 and (d) S4



(a)



(b)

Figure 4.21 SEM images of the PSF/PI-20% membrane cross-sections with silica contents (a) 0% , (b) S1 at low magnification 200X; scale 1µm, and (c) S3, (d) S4 at high magnification 1000X; scale 1µm

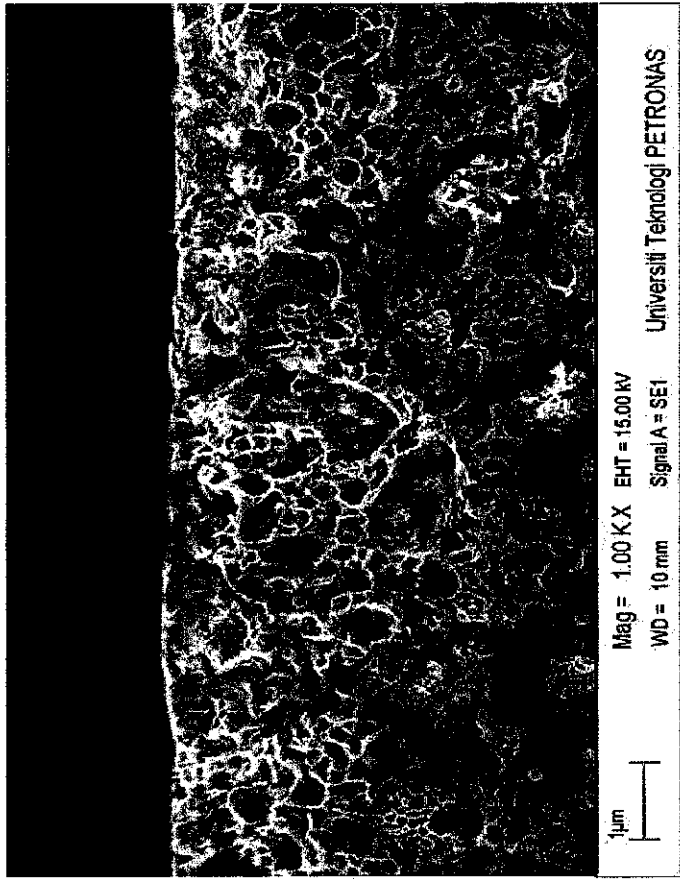
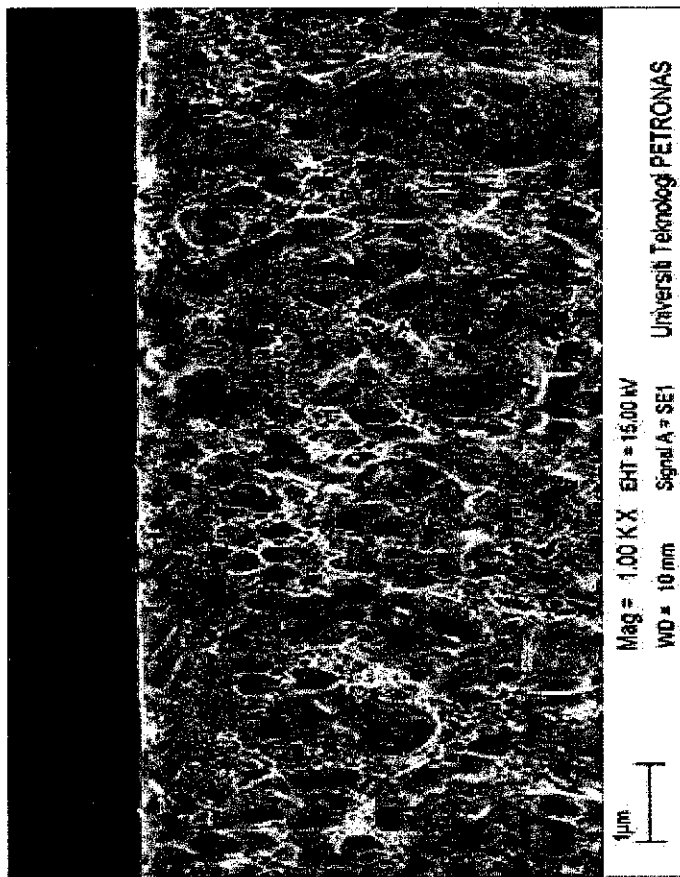


Figure 4.21 SEM images of the PSF/PI-20% membrane cross-sections with silica contents (a) 0%, (b) S1 at low magnification 200X; scale 1 μm , and (c) S3, (d) S4 at high magnification 1000X; scale 1 μm (contd.)

reasonably dense skins and sub-porous layers in their structures and hence, by definition it is expressed as an asymmetric membrane [45]. As discussed previously in Section 4.2.1, the skin layer formation during the membrane development largely depends upon on the appropriate control of the dry/wet processes. The formation of the skin layer is caused during the coagulation in the phase inversion process which causes a sudden gelling of the polymer molecules forming a skin layer. The skin thickness grows until the non-solvent diffusion from the membrane's bottom layer is stopped [190]. As also mentioned earlier, in the dry process, the evaporation time of 15 seconds was maintained to obtain a defect free thin skin layer [167]. The thin skin layer with a sub-porous layer as a mechanical support was reported to be quite suitable for the gas separation processes [191-192]. Hence, thinner skin layer MMMs were prepared with thick sub-porous structures under the experimental conditions with the NMP/DCM (80/20) solvent composition. This is consistent with the study Section 4.5, where the NMP/DCM solvent composition provided the thin skin thickness and porous sub-structure as compared to NMP/DCM (50/50) and (20/80). The MMMs prepared here also showed sponge-like structures rather than finger-like macrovoids in the porous sub-layer consistent with the previous approach. These microstructures indicate the deficiency of the defects at the membrane surfaces.

With the addition of the filler contents in the S1 to S3 membrane samples, the cross-sections showed uniform dispersion in the polymer matrix (Figure 4.21(b), (c)). This was due to the addition of the coupling agent which caused a strong adhesion between the two phases and is consistent with the past studies [97, 193]. The size of these nanoparticles was approximately ≤ 100 nm, thus forming a new hybrid structure with the silica inter-perpetrating in the polymeric network. However, with the increase in the silica loading up to 20.1wt% in the S4 membrane, the distribution is no longer uniform and the silica particles formed small isolated domains as shown in Figure 4.21(d). The structure showed unselective voids around the particle that suggested a poor wetting ability with the polymer matrix [194]. The distribution of the particles in the cross-section of the membranes was more evident with the SEM mapping that showed homogenous dispersion and silica clusters in the matrix (Figure 4.22).

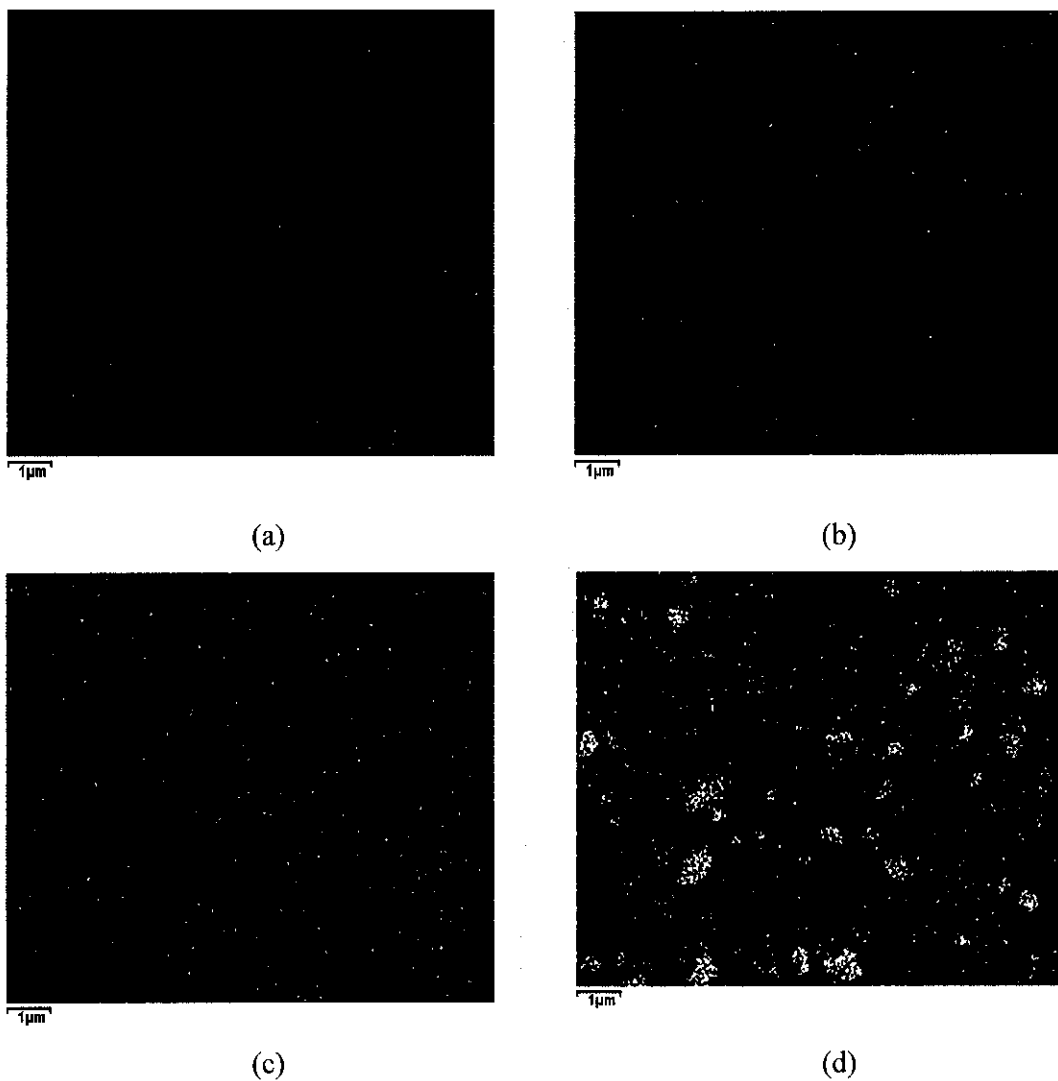


Figure 4.22 PSF/PI-20% having silica nanoparticles at the scale 1 μ m (a) S1, (b) S2, (c) S3 and (d) S4

The silica particles were further evaluated by using TEM in the PSF/PI-20% membrane and the image obtained is shown in Figure 4.23. After their incorporation, the TEM image showed the structure of the particles with sizes in a range of 15nm-100nm and the inter-particle spacing measured about 10nm-30nm which is in agreement with SEM (Figure 4.21 (c)).

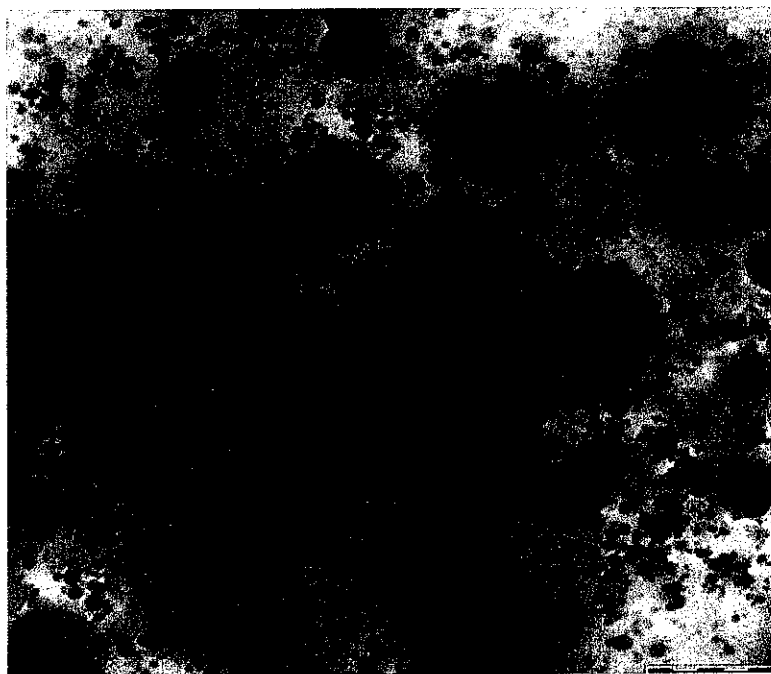


Figure 4.23 TEM image of the silica particles in the PSF/PI-20% blends

4.8.1 Spectral Analysis

The structural characterization of the MMMs is shown in Figure 4.24. The spectrums show a comparison and the possible interactions among the components of the MMMs. In spectra (a), the absorption band related to Si-O-Si symmetric stretching occurred at 804 cm^{-1} , which indicates the completion of the sol-gel process [117]. Intensive asymmetric stretching and bending peaks are observed at 1081 cm^{-1} and 465 cm^{-1} respectively [116]. Due to water absorption by silica structures, bending and stretching vibrations of the silanol (Si-OH) peaks occurred at 1634 cm^{-1} and 3462 cm^{-1} respectively [117]. By addition of 20 wt% silica contents in the S4 membrane (spectra (b)), a strong silica peak at 1081 cm^{-1} grew in intensity due to the Si-O-Si asymmetric stretching. A slight decrease in the intensity at 1717 cm^{-1} and 1773 cm^{-1} is observed in comparison to spectra (c), which indicates reduction in the imide rings of PI. Spectra (b) showed a peak shift to 855 cm^{-1} from 804 cm^{-1} (spectra (a)) and 833 cm^{-1} (spectra (c)), indicating the silica interaction with the polymeric matrix. Compared to spectra (c), the symmetric stretching of the S=O group of PSF shifted to 1157 cm^{-1} in spectra (b) (also see Figure 4.4). The results can be inferred that the occurrence of these

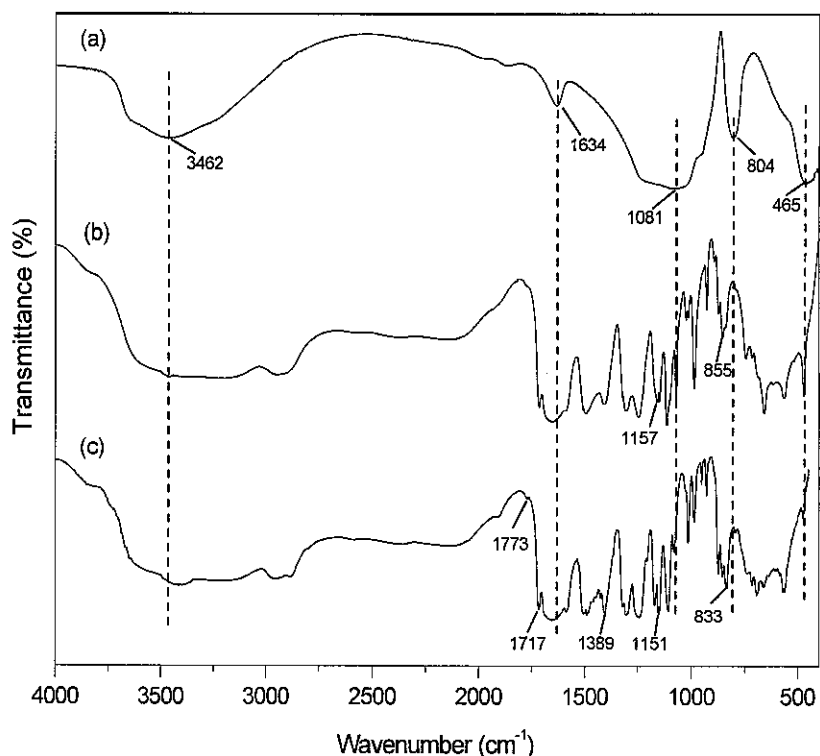


Figure 4.24 FTIR spectra of (a) silica (b) MMMs and (c) PSF/PI-20%

spectral changes in the MMMs indicates the presence of a strong interaction between the two phases at the molecular level.

On the basis of spectral interactions in MMMs, a model is proposed shown in Figure 4.25 which shows the possible interaction of PSF with APTMOS, silica particles and PI through hydrogen bonding and π - π interactions. The hydrogen bonding resulted from the interaction of sulfone and the ether groups of PSF with the hydrogen atom of the amine group that resided on APTMOS. In addition, the carbonyl groups of PI interacted with the amine group of APTMOS through the formation of a hydrogen bond. The π - π interactions emerged from the aromatic moieties of PSF and PI. The repeating unit of PSF indicates its presence in excess as compared to PI and the arrows suggests the probable sites for bond formation. The detailed description of the interactions in the prepared membranes has been explained in the FTIR spectral analysis section.

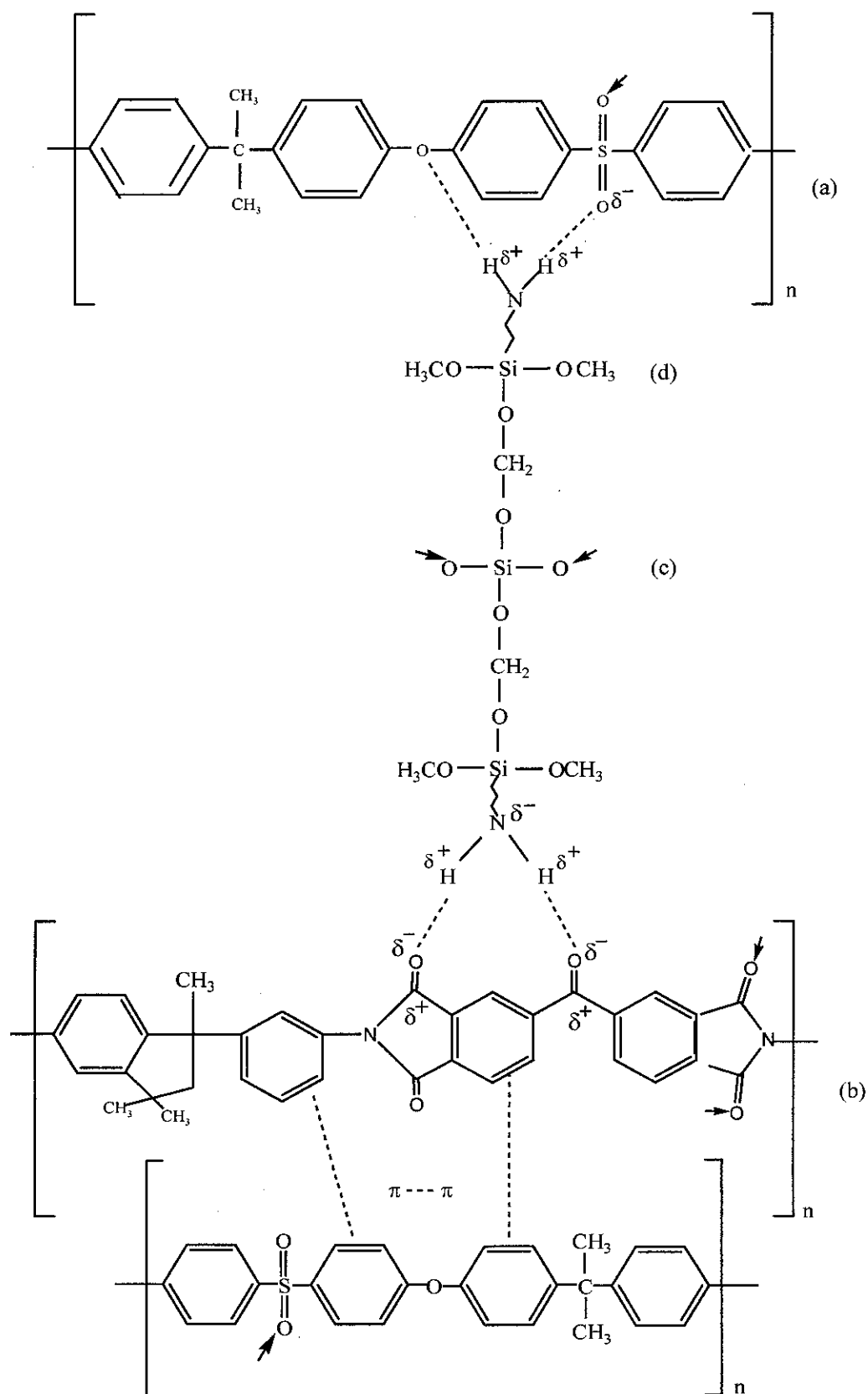


Figure 4.25 Structures of (a) PSF,Udel® P-1800, (b) PI,Matrimid® 5218 and (c) silica particles obtained from TEOS (d) APTMOS with their possible interactions

4.8.2 Glass Transition Temperature

The DSC analysis was carried out at a heating rate of 10°C/min in order to observe the effect of the silica contents on the PSF/PI blended membrane. In the previous Section 4.2.2, T_g for the PSF/PI blends using DSC confirmed their miscible nature [168]. It is observed that with the addition of the silica contents in the PSF/PI-20% membrane blend, a distinct T_g value was recorded for each MMMs. Furthermore, with the increase in the silica contents, T_g increased gradually as shown in Figure 4.26 and Table 4.5. This indicates strong interaction exist between the silica particles and the polymer matrix. An increase in T_g values with the silica contents have been also reported in the past [195]. A T_g rise of 4.2°C is observed with the silica loadings of 5.2 wt% in the S1 membrane sample that increased up to 25°C with the maximum silica loading of 20.1 wt% in the S4 membrane.

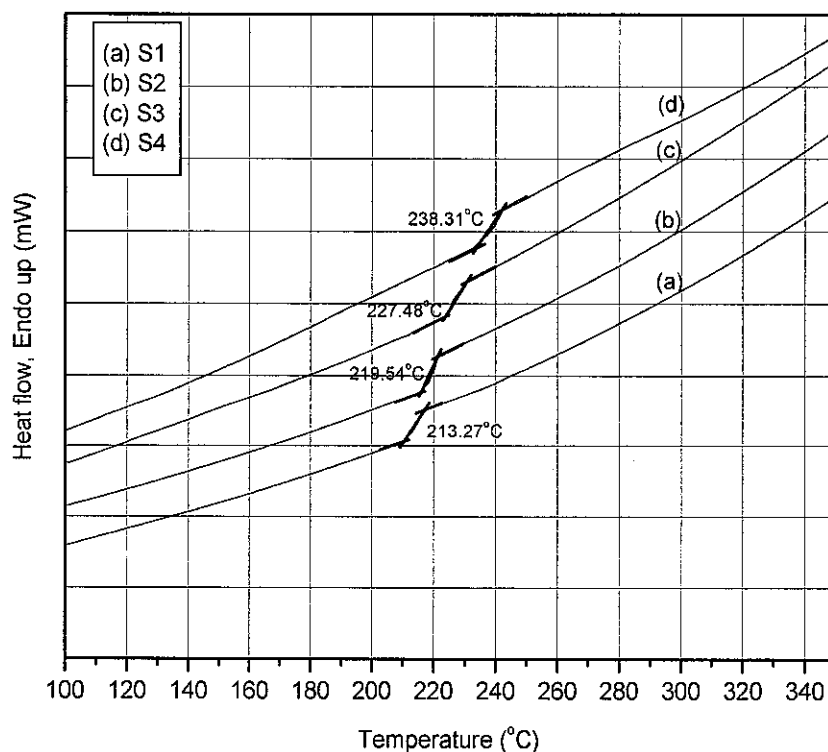


Figure 4.26 DSC thermograms of the PSF/PI-20% membranes at various silica loadings

Table 4.5 Membrane samples at various weight fractions and glass transition temperatures of PSF/PI-20%+Silica MMMs

Membrane samples [PSF/PI-20%+silica(S)]	Weight fraction of silica (wt %)	Glass transition, T_g (°C)
S1	5.2	213.3
S2	10.1	219.5
S3	15.2	227.5
S4	20.1	238.3

4.8.3 XRD Analysis

The microstructure of the hybrid membranes were further analyzed by using XRD at varying silica contents. XRD diffractograms of the developed membranes were recorded and compared as shown in Figure 4.27. A summary of the XRD analysis patterns for the pure blended and silica embedded MMMs are tabulated in Table 4.6. The intersegmental distance or d-spacing for the pure and blended membranes showed almost the same value at the location of $2\theta \sim 21.8^\circ$. With the increase in silica contents in the membrane blend, the d-spacing gradually decreased with the decrease in the peak intensity, $2\theta \sim 23.35^\circ$. This reduction in d-spacing restricted the polymer chain mobility due to the addition of inorganic fillers. The decrease in the peak intensity indicates that part of the orderly packed polymeric structures were destroyed due to which the intensity of the characteristic peak was reduced [98, 115]. With the increase in the filler contents in the matrix, the full-width at half the maximum (FWHM) value increased gradually which corresponded to a decrease in the intensity with the broadened peak. The relative increase in the FWHM value of the hybrid membranes from those of the pure and blended membranes indicates that some interactions were formed between the silica particles and the matrix which resulted in perturbation of the long-ranged spacing between the polymeric chains [196].

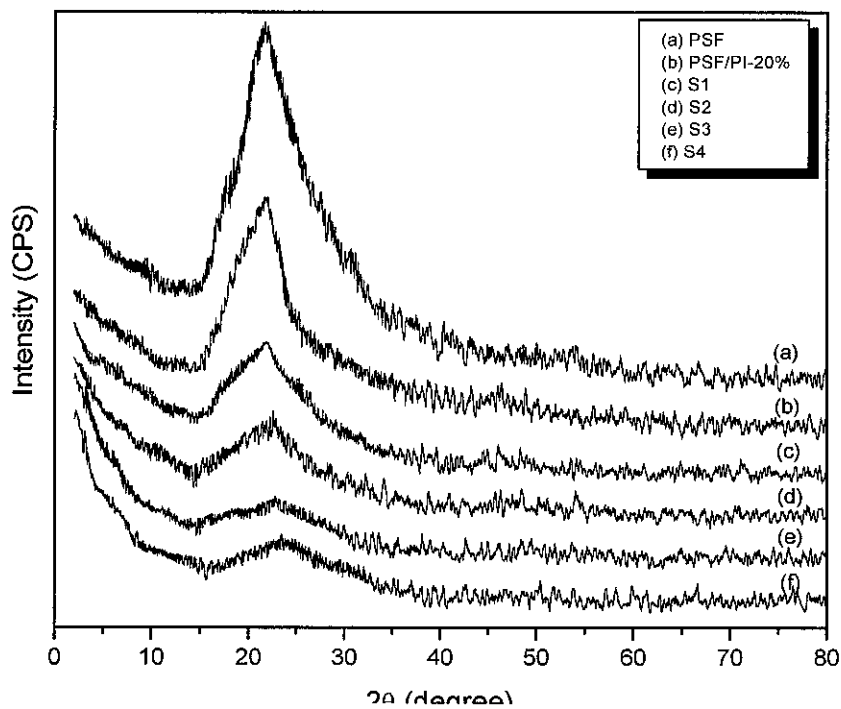


Figure 4.27 XRD analysis for the PSF/PI+ silica mixed matrix membranes

Table 4.6 XRD results of developed membranes

XRD	2θ	d-Space (°A)	FWHM
PSF	21.80	4.06	7.13
PSF/PI20%	21.81	4.07	7.24
S1	22.34	3.98	7.58
S2	22.71	3.91	8.01
S3	23.04	3.86	8.22
S4	23.35	3.82	8.64

4.9 Gas Permeation in the Mixed Matrix Membranes

Gas permeation studies were carried out on the developed membranes for both the pure and mixed gases of CH₄ and CO₂, in order to evaluate their performances. It was carried out by determining the permeance and selectivity of the gases against 2-10 bar feed pressures. Figure 4.28 shows that the MMMs depicted different permeation behaviour with the addition of silica contents. The permeance and the selectivity of the gases were measured according to the respective Eqs.(3.18)-(3.20).

In the previous section, 4.4 , an enhanced gas permeance was noticed in PSF/PI-20% (39.3±0.2 GPU) as compared to the pure PSF (33.7±0.1 GPU). The high permeance of CO₂ for the membranes with an increasing PI content was due to the soaring affinity for CO₂ in the membrane matrix. It was due to the fact that the CO₂ acquired a non-polar linear structure with a relatively smaller kinetic diameter of 3.3°A as compared to the slow moving CH₄ molecule, having a kinetic diameter of 3.8°A and a tetrahedral structure. With the addition of the silica contents from 5 to 20 wt. % in the S1 to S4 membrane samples (Figure 4.28), the CO₂ permeance increased

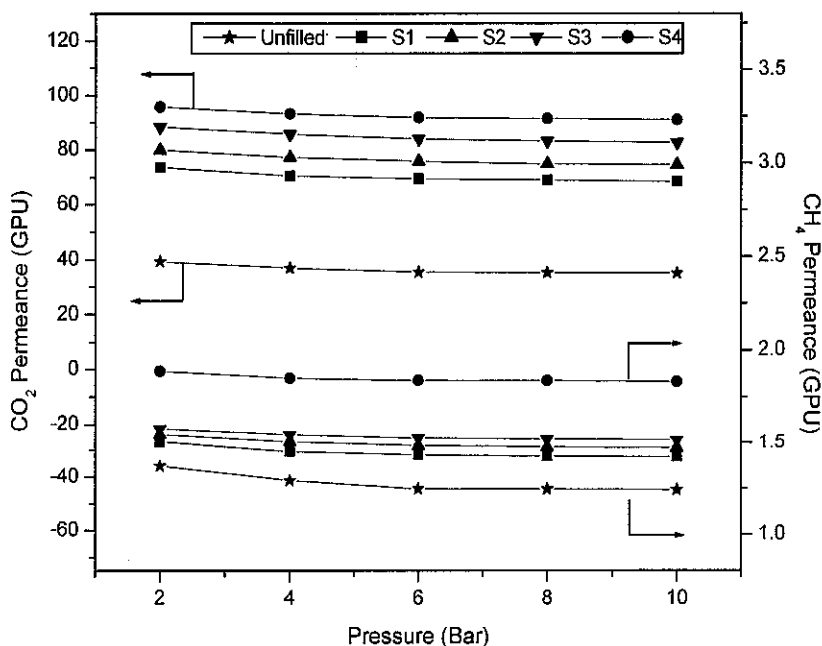


Figure 4.28 Permeance of the pure CO₂ and CH₄ gases for the PSF/PI-20% membrane at different silica compositions against feed pressures

from 73.7 ± 0.2 GPU (87%) to 95.7 ± 0.4 GPU (143%), respectively at the 2 bar feed pressure compared to the unfilled membranes. Similarly, for the slow moving CH_4 gas, the permeance increased with the increase in the silica contents. It was noticed that this increase in permeance was due to the fact that the silica particles caused a disruption in the polymer chain packing. Due to this disorder in the matrix, the growth in the free volume resulted in the MMMs which caused an enhanced gas permeance [197]. In relation with the SEM images (Figure 4.21 (b)-(d)), it is observed that with the highest silica loading of 20 wt.% in the S4 membrane, agglomeration of the silica particles took place. It might be possible that by moving from the lower to the higher silica contents in the S1 to S4 membrane samples, voids within the particles or at the interface may have increased thereby causing the enhanced permeance. Hence, the hypothesis of the porous silica particles is helpful [198]. Moreover, the skin thickness in Figure 4.21 is about $0.1 \mu\text{m}$ at various silica loadings which did not show much variation. This suggests that the thickness has a negligible effect on the gas permeance for the developed membranes. Figure 4.28 shows that the permeance trend decreased with the increase in the pressure from 2 to 10 bar. It indicates the absence

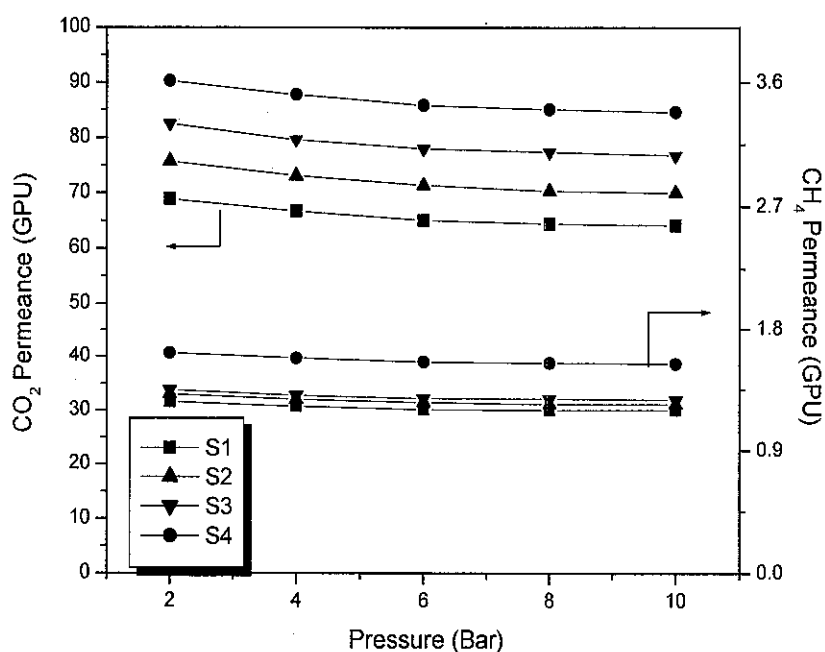


Figure 4.29 Effect of the heat treatment at 140°C on the permeance of the pure CO_2 and CH_4 gases for the PSF/PI-20% membrane at different silica compositions against feed pressures

of plasticization in the membrane matrix. In the presence of plasticization, especially for CO₂, membranes, high permeance values are shown just after achieving the lowest value at high pressures, which indicates swelling of the membranes [32]. In order to further eliminate chances of plasticization in the membranes, a heat treatment was conducted at 140°C for 1 hour. Figure 4.29 shows a decrease in the permeance for both gases which could be a consequence of reducing the interphase between the two components. Earlier studies showed that treated membranes for PSF systems were stable in a range of 100°C-140°C [24]. Treatment at higher temperatures ($\geq T_g$) destroyed the polymeric chain forming ordered chain segments. While mild treated conditions of 100°C still allowed the permeation rate to increase at a higher pressure. Restriction in the polymer chain mobility is observed; this hampered the gas transport owing to the subsequent heat treatment that helped in stabilizing the membranes. Thus, the heat treatment provided reorientation in the polymer chain for better packing and, thereby, reduced the chances of plasticization [30]. Hence, compared to untreated membranes, treated membranes showed a decrease in their permeance as

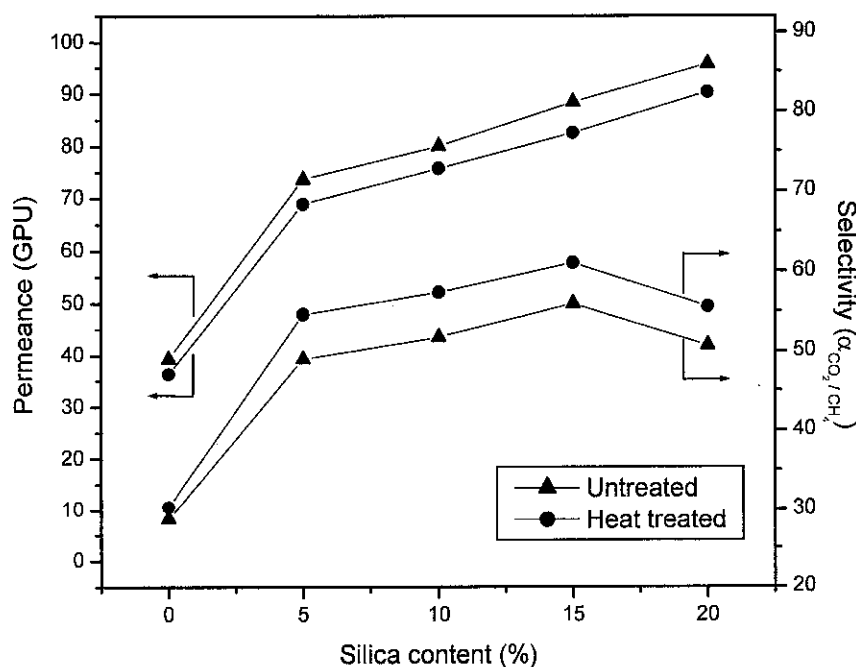


Figure 4.30 Permeance and selectivity of the pure CO₂ gas test for the PSF/PI-20% membrane at 2 bar pressure against various silica contents.

shown in Figure 4.30. Figure 4.31 shows the ideal selectivity ($\alpha_{\text{CO}_2/\text{CH}_4}$) for the untreated and treated membranes at 2-10 bar feed pressure. It is observed that all the membrane compositions showed reduction in the selectivity values with the increase in the feed pressure up to 10 bar. The maximum selectivity was achieved for the S3 membrane sample ($\alpha_{\text{CO}_2/\text{CH}_4} = 55.95 \pm 0.3 - 54.5 \pm 0.5$ from 2 to 10 bar pressure, respectively) compared to other untreated hybrid membranes. With the highest silica loading of 20.1 wt.% in the S4 matrix, despite the increase in permeance, the selectivity value decreased. This was attributed to the presence of small domains which are formed at this highest loading (Fig.3 (d)). The presence of these domains created a discontinuous path for the gas permeance through the filler rather than the continuous path of the polymeric system [194]. This condition enhanced the gas permeance through the inorganic filler for the S4 membrane sample and so the hypothesis of the above mentioned porous silica was reinstated. Hence, for the untreated membrane, the selectivity fell to $\alpha_{\text{CO}_2/\text{CH}_4} = 50.7 \pm 0.1 - 49.6 \pm 0.2$ from 2 to 10 bar pressure, respectively. It was found that for the treated membranes, though the permeance decreased slightly, the ideal selectivity value increased for each membrane as compared to the untreated membranes (Figure 4.30 and Figure 4.31). So for the treated membranes, the maximum ideal selectivity for the S3 membranes increased to $\alpha_{\text{CO}_2/\text{CH}_4} = 61.0 \pm 0.3 - 60.2 \pm 0.4$ from 2 to 10 bar feed pressure, respectively (Figure 4.31). Whereas, the S1 membrane sample showed the least selectivity value ($\alpha_{\text{CO}_2/\text{CH}_4} = 54.6 \pm 0.5 - 53.5 \pm 0.3$).

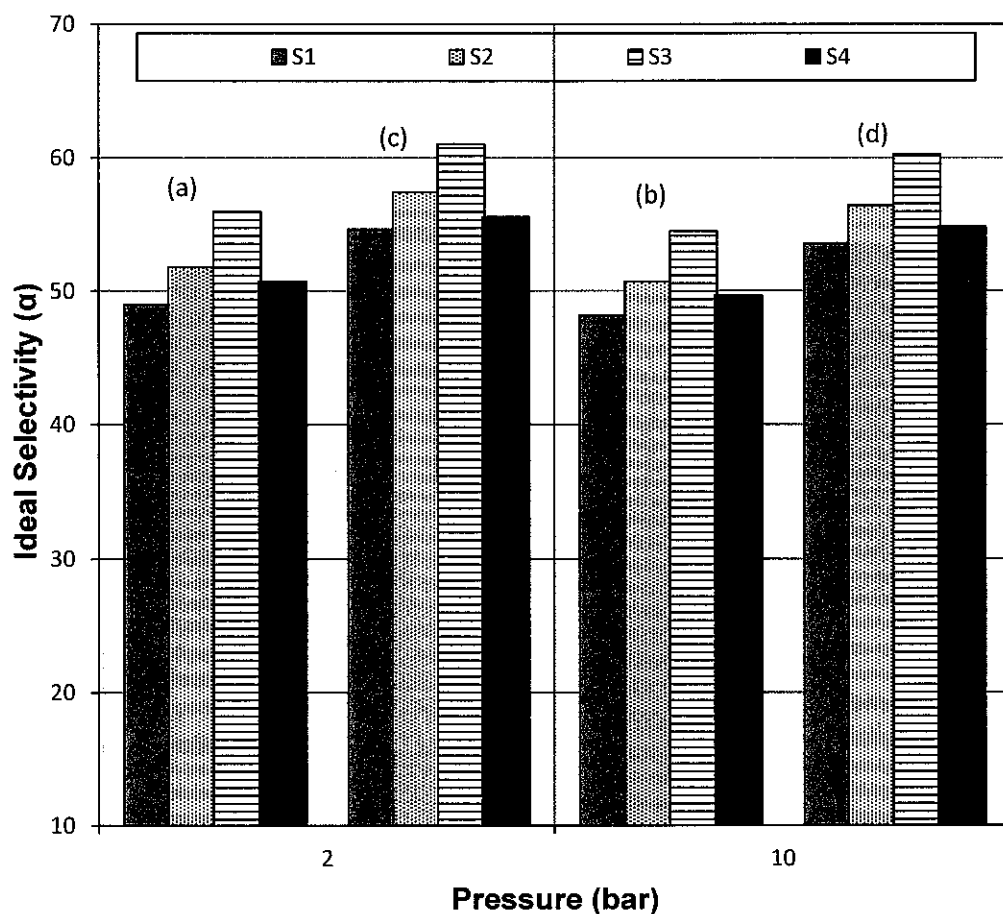


Figure 4.31 Comparison of the Ideal selectivity of CO_2/CH_4 at various feed pressures without heat treatment: (a), (b) and with heat treated: (c), (d)

4.10 Kinetic Analysis on the MMMs

Following the thermogravimetric analysis for the polymeric membranes in Section 4.7, the blends at various silica loadings for the best selected PSF/PI-20 membrane are shown in Figure 4.32. The analysis was carried out at the heating rates of 5, 10, 15°C/min for the kinetic evaluation. The thermograms of each membrane showed that there no weight loss occurred below 150°C, which indicates the complete removal of the solvents from the developed membranes. It is observed that the thermal stability of

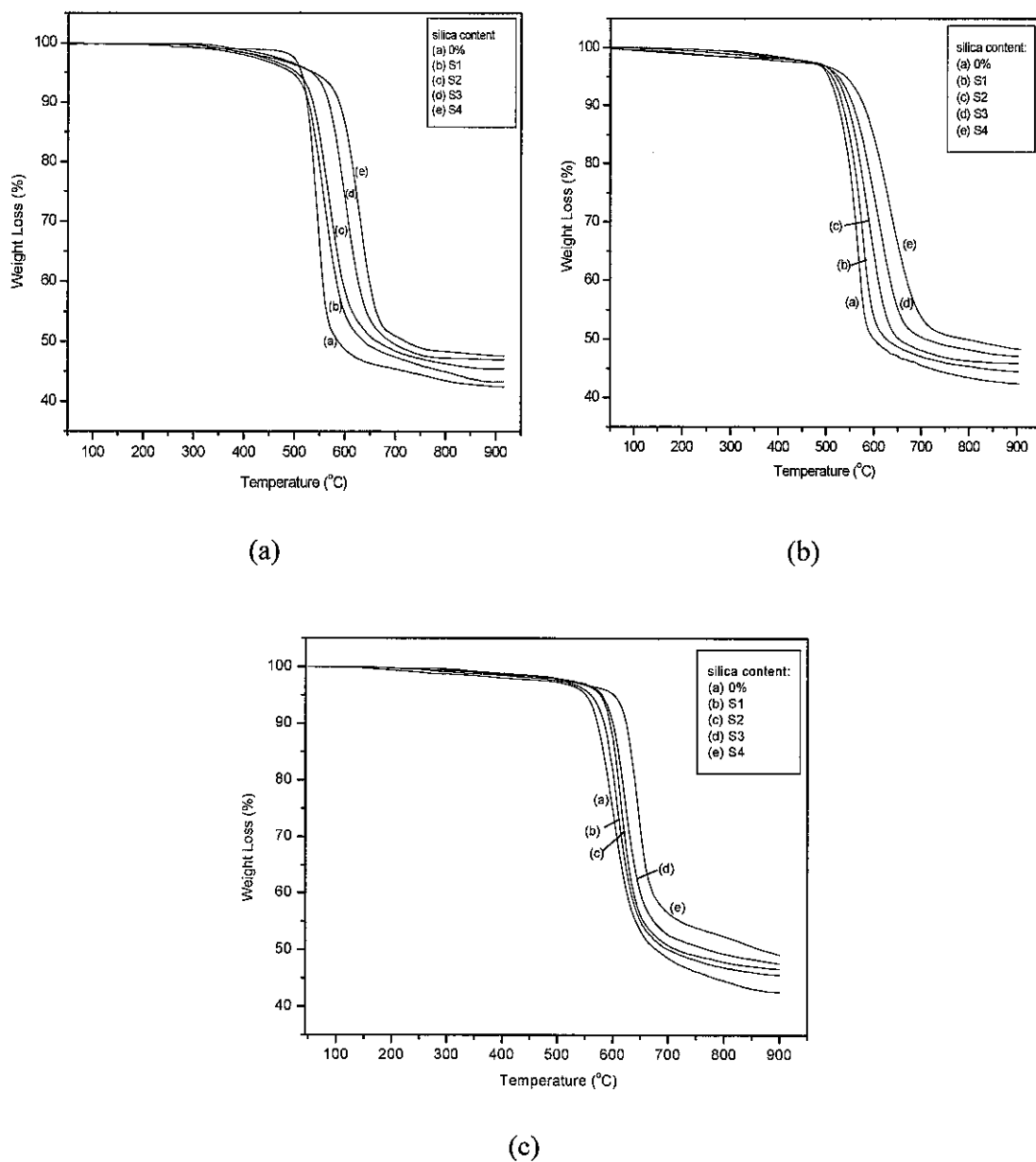


Figure 4.32 TGA isotherms of the PSF/PI-20% blended membrane with silica contents at (a) 5°C/min, (b) 10°C/min and (c) 15°C/min

the membranes increased gradually with the increase in the silica contents in the matrix [199]. The rise in the weight residues above 700°C suggests the successful incorporation of the silica contents that ultimately enhanced the thermal stability of

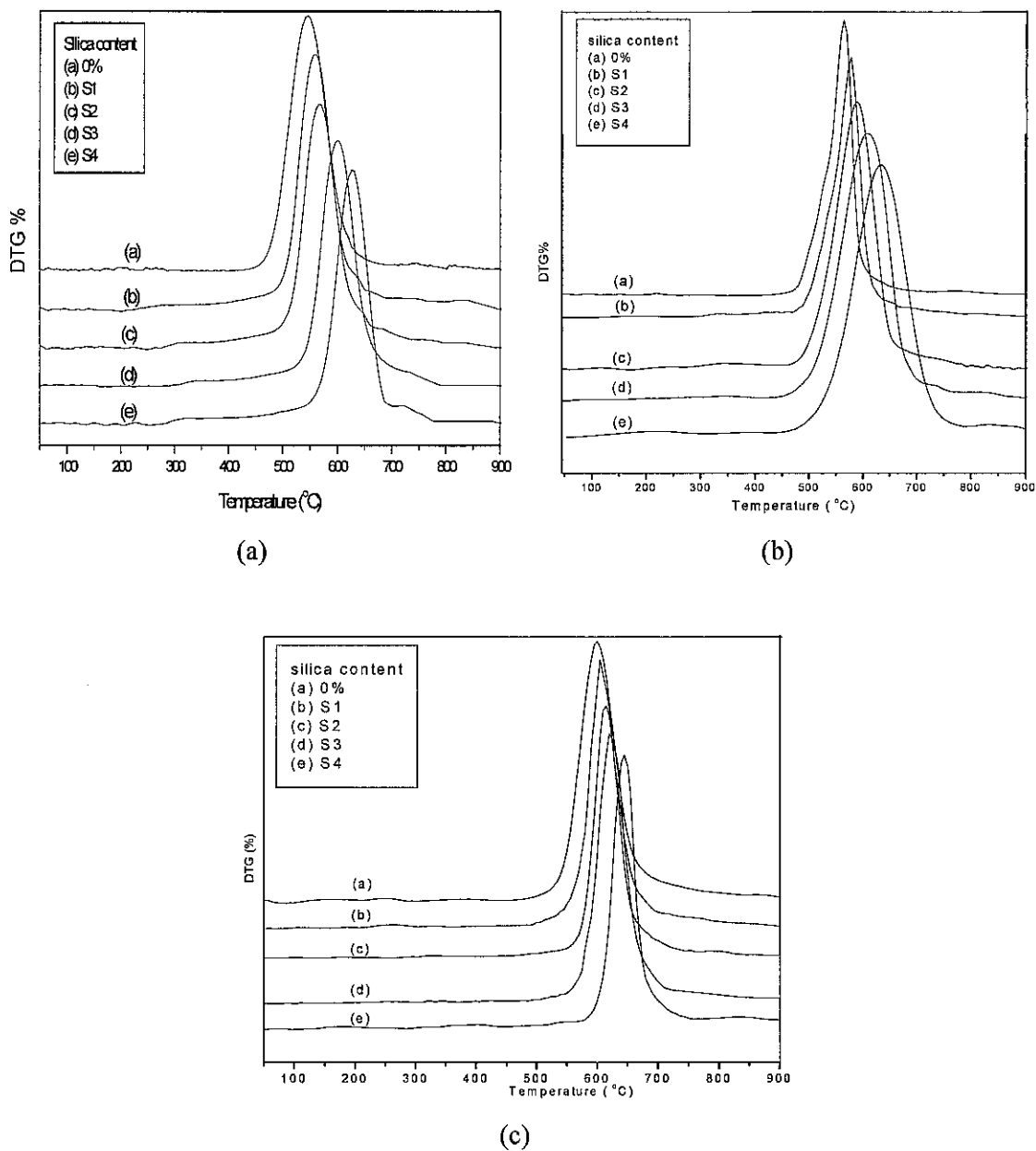


Figure 4.33 DTG curves of the PSF/PI-20% blended membrane with silica contents at (a) 5°C/min, (b) 10°C/min and (c) 15°C/min

the hybrid membranes (Table 4.7). The increase in the thermal stability is quite evident from Figure 4.33 that shows the maximum peak value of the thermal degradation for the membranes. It was obtained by taking the derivatives of the change in the consecutive weights to the heating rate and then plotting it against the temperature. Improvement in the thermal stability occurred due to their strong

interaction among the organic materials and inorganic fillers that formed a chemical bonded network structure in the mixed matrixes [200]. In addition, the presence of the silica at the nanometer scale greatly improved the thermal properties of the membranes. Similar results were observed by Shang et al. They also found improvement in the thermal stability and hence, the thermal decomposition temperature with the addition of the silica contents upto 30 wt.% in the PI membranes. This improvement was in relation with the distinct T_g values which also showed an increment with the increase of the silica contents in the PI/SiO₂ membranes.

Applying the kinetic of thermal decomposition, similar to the discussion made in the previous Section. The activation energy, E values were obtained by using Eq.(3.13) at various silica loadings in the MMMs (Table 4.7). From Figure 4.34, the E value was calculated from the slopes of the straight line obtained from the plots between $\ln \beta (d\alpha / dT)$ versus $1/T$. It is observed that the activation energy increased gradually with the increase in the silica content in the MMMs. This occurred due to the enhanced degree of the stability after the incorporation of the silica contents.

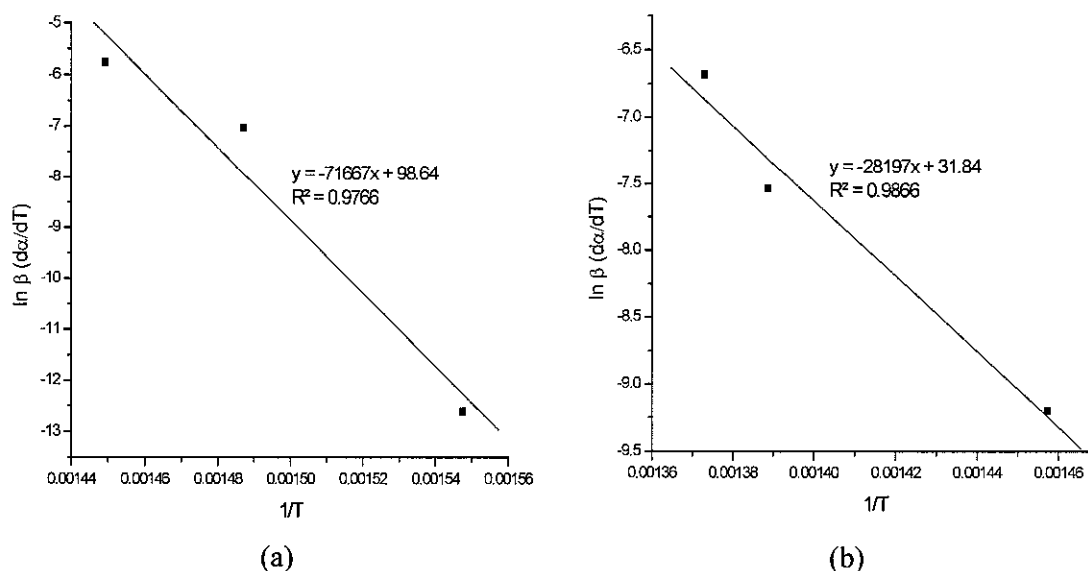


Figure 4.34 Linear Plots of $\ln \beta (d\alpha/dt)$ versus $1/T$ (a) S1 (b) S4 at same α values (0.004)

Table 4.7 Dynamic TG data and E values of various MMMs

Membrane	Heating Rate, $\beta = dT/dt$ (°C/min)	Degradation Onset Temperature (°C)	Maximum Degradation Temperature, T (°C)	Activation Energy, (E) KJ/mole
S1	5	539.0	557.0	260.24
	10	550.4	577.2	
	15	583.4	605.1	
S2	5	545.1	569.0	271.39
	10	555.0	587.3	
	15	597.8	613.7	
S3	5	570.0	598.0	296.50
	10	577.3	608.2	
	15	602.2	621.1	
S4	5	598.0	629.0	310.66
	10	601.7	633.9	
	15	626.1	643.7	

4.11 Mechanical Analysis on the MMMs

The MMMs at various silica loadings were further examined mechanically using a universal testing machine. The typical tensile stress–strain curves for the investigated MMMs system are shown in Figure 4.35. Their corresponding results in terms of Young’s modulus, tensile strength and percentage strain are summarized in Table 4.8. In the stress-strain curves, it is observed that with the increase in the silica contents (as indicated by the curves (b), (c), (d) and (e)), the extent of the plastic flow decreased in

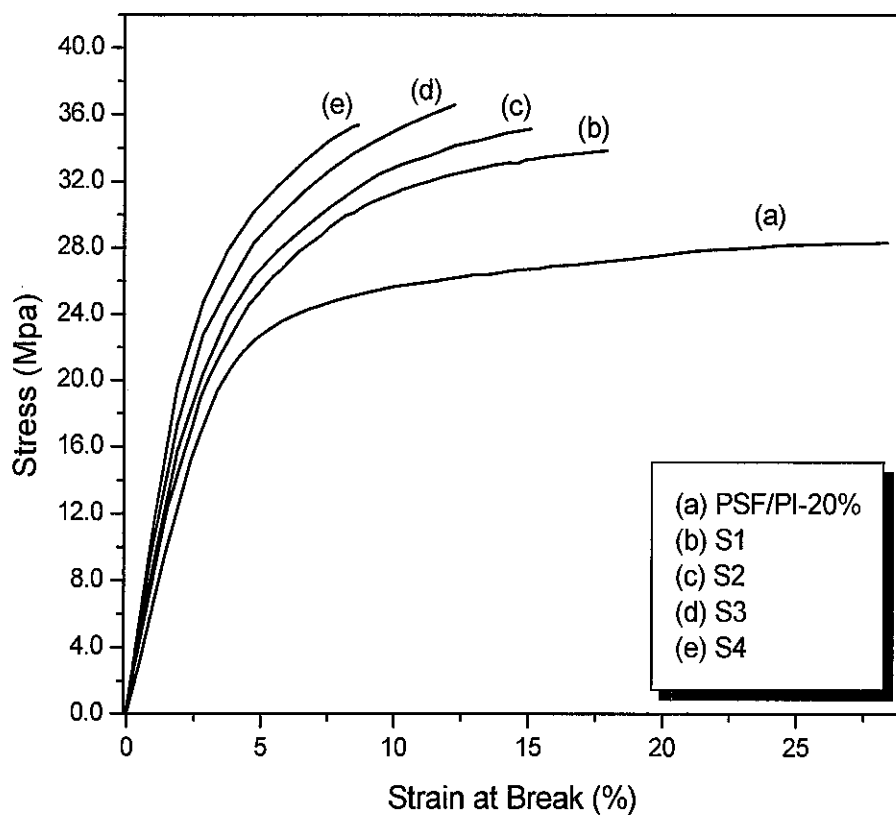


Figure 4.35 Stress-Strain curve of the mixed matrix membranes at different silica loadings

Table 4.8 Effect of the silica loading on the mechanical properties of the mixed matrix membranes

Sample	SiO ₂ content (wt %)	Young's Modulus (GPa)	Tensile Strength (MPa)	Strain at Break (%)
S1	5.2	1.00±0.35	33.86±2.2	17.90±0.88
S2	10.1	1.11±0.47	35.12±3.4	15.08±0.45
S3	15.2	1.25±0.18	36.57±1.1	12.25±0.67
S4	20.1	1.29±0.24	35.37±1.9	8.66±0.75

the MMMs as compared to the polymeric film (curve (a)) and hence, the gradual rupture took place at lower strains.

The properties derived from the stress-strain curves are further elaborated in Figure 4.36 and Figure 4.37. The plot indicates that Young's modulus showed a gradual increase in the mixed matrix films with the increase in the silica contents. It is noticed that with 5 to 15 wt.% silica contents, Young's modulus increased almost linearly. After this, the increment no longer followed an upward linear trend and deviated from this upward linear trend showing almost a constant trend upto 20 wt.%. The percentage difference in this increasing trend between 5 to 15 wt.% silica contents was found to be 11% and 12.6% which reduced to 4% as the silica content was increased from 15 to 20 wt.%. A total rise of 31.9% was found in Young's modulus with the increase in the silica contents up to 20 wt.% as compared to the PSF/PI-20% polymeric membrane blend. This trend indicates that up to 15 wt.% silica contents, the films exhibited uniform dispersion within the matrix and the silica domains were absent in the membranes. However, too high a silica content (20 wt.%)

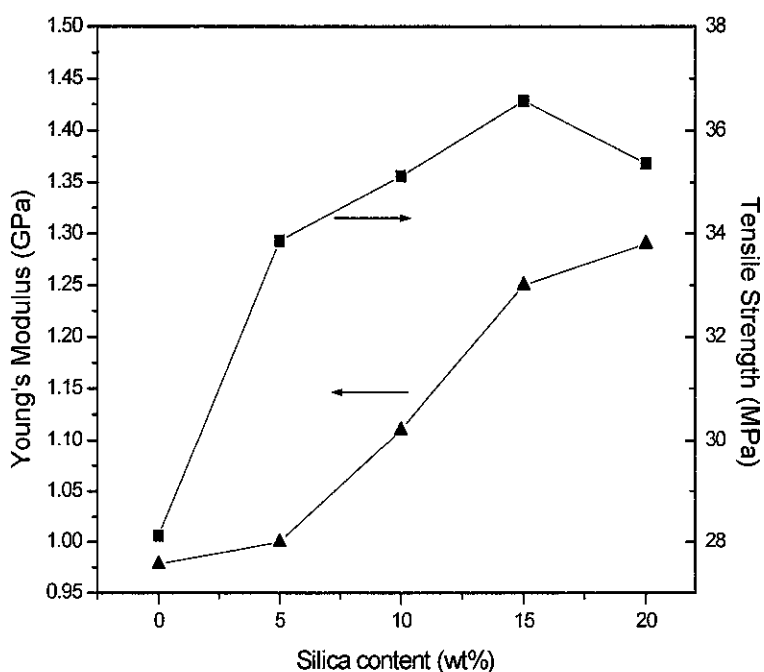


Figure 4.36 Young's Modulus and the Tensile Strength of the MMMs at various silica loadings

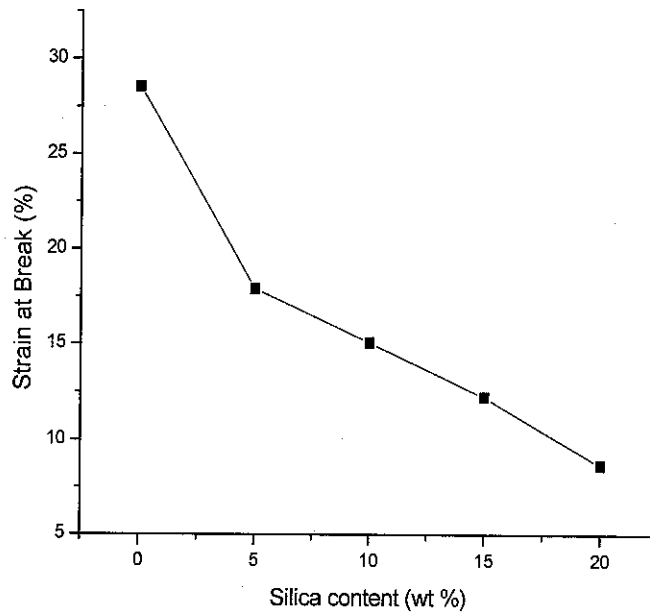


Figure 4.37 Strain at the Break property of the MMMs at various silica loadings

caused dispersion problems of the doping silica within the polymeric matrix and showed a decreasing behaviour due to the agglomeration of the fillers in the film. This caused a decrease in the tensile strength after attaining the highest values till 15 wt.% silica contents. Also, the presence of the coupling agent played an important role in increasing the interfacial adhesion between the polymeric matrix and the inorganic silica particles by reducing the particle size which enabled a strong cross-linking network between the two species. It was more visible in the SEM surfaces and the cross-sectional images (Figure 4.20 and Figure 4.21), where fine interconnected phase morphologies are observed with as high as 15 wt.% as compared to 20 wt% silica contents. The tensile strength showed a gradual improvement upto 15 wt.% and was increased by 30.1%. A gradual rise of about 3.7% and 4.1% is observed as the silica content was increased from 5 to 15% silica content while a decrease of 3.3% is noted as the silica content was increased from 15 to 20 wt.%.

On the other hand, the strain at the break property gradually decreased with the increase in the silica content as shown in Figure 4.37. It indicates that although the

polymeric matrix exhibited strong adhesion with the silica particles, the interconnected silica network hindered the plastic flow of the polymeric phase and hence, the fracture occurred before a large deformation could take place. It is observed that with the increase in the silica content upto 20 wt.% , an overall decrease of 69.7% in the strain at the break property is noted.

A similar trend of Young's modulus, tensile strength and strain at the break were observed in the past studies. Musto et al. [201] studied the effects of nano silica particles in polyimide membranes using TEOS as the silica precursor. It was observed that Young's modulus and the tensile strength increased with the increase in the silica content. The tensile strength increased upto 20 wt.% silica content and then decreased on further increasing the filler loadings. The elongation at the break showed a decreasing trend with the increase in the silica content. It was found that the use of the coupling agent caused a strong adhesion between the two phases and the mechanical properties were greatly enhanced over the absence of the coupling agent. It was further noticed that the use of the coupling agent reduced the particle size of the fillers to a range between 40-100 nm as compared to 1-2 μm for a non-compatibilized system. A similar finding was reported by Chen and Iroh [202] which observed an improvement in the polyimide/silica composite membranes by using a coupling agent. The modulus and ultimate tensile strength increased and the elongation at the break decreased with the increase in the silica contents. It was inferred that the presence of the chemical bonding between the groups in the presence of the coupling agent formed a strong interfacial interaction and improved the mechanical strength of the developed membranes.

It is concluded from the previous studies that the use of the coupling agent reduced the particle size of the silica particles and greatly improved the mechanical properties of the developed membranes. Moreover, the strong interfacial adhesion was obtained between the two phases that largely affected the properties of the membranes. However, a higher silica loading (20 wt.%) caused a decrease in the tensile properties and thus, the optimized loadings at 15 wt.% was favourable for further utilization in mixed matrix systems.

4.12 Mixed Gas Analysis

The purity of the CO₂/CH₄ gas mixtures for each composition i.e., 70%/30%, 50%/50% and 30%/70% were tested on GC prior to the membrane sample testing. The spectrums obtained from GC for various gas compositions are shown in Figure 4.38 and Appendix D.

It is observed from the spectrums that the characteristic peaks of CH₄ and CO₂ were reached at a specific retention time of 2.4±0.005 and 2.7±0.010 minutes. While the peak height and the corresponding area showed variation with the change in the CO₂/CH₄ composition. Eventually, the gas performance of the best selected S3 membranes from the heat treatment was evaluated from all the gas mixtures. Table 4.9 lists the selectivity data for the gas mixtures at 10 bar feed pressure that was initially obtained from the gas mixture compositions examined under GC, shown in Figure 4.39, Figure 4.40 and Appendix D.

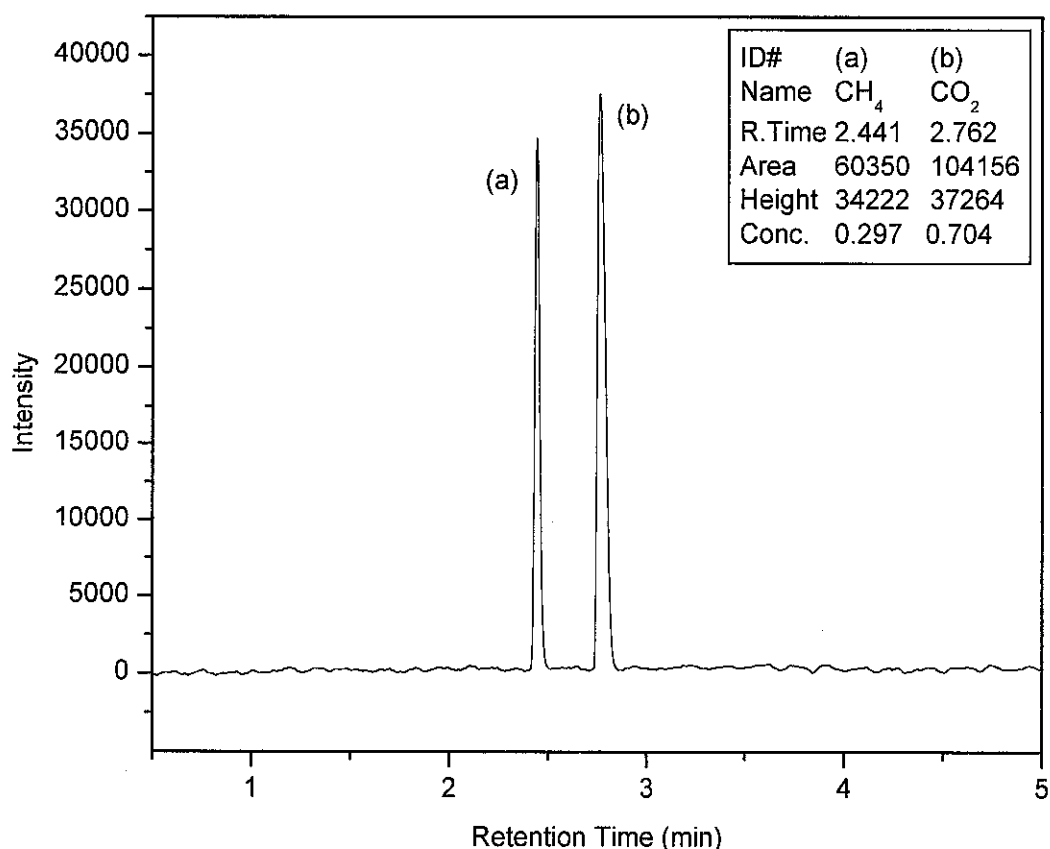


Figure 4.38 Spectrums of Standard CO₂/CH₄ mixtures composition (70%/30%) obtained from gas chromatograph

Table 4.9 Pure and mixed gas selectivity results for PSF/PI-20% and PSF/PI-20% + silica mixed matrix membrane

Membranes	Ideal selectivity $\alpha(\text{CO}_2/\text{CH}_4)$	Mixed gas selectivity		
		(30/70)	(50/50)	(70/30)
PSF/PI-20%	29.7±0.65	29.3±0.3	29.9±0.6	29.8±0.1
PSF/PI-20%+S3	60.2±0.43	60.1±0.3	60.0±0.07	60.8±0.01

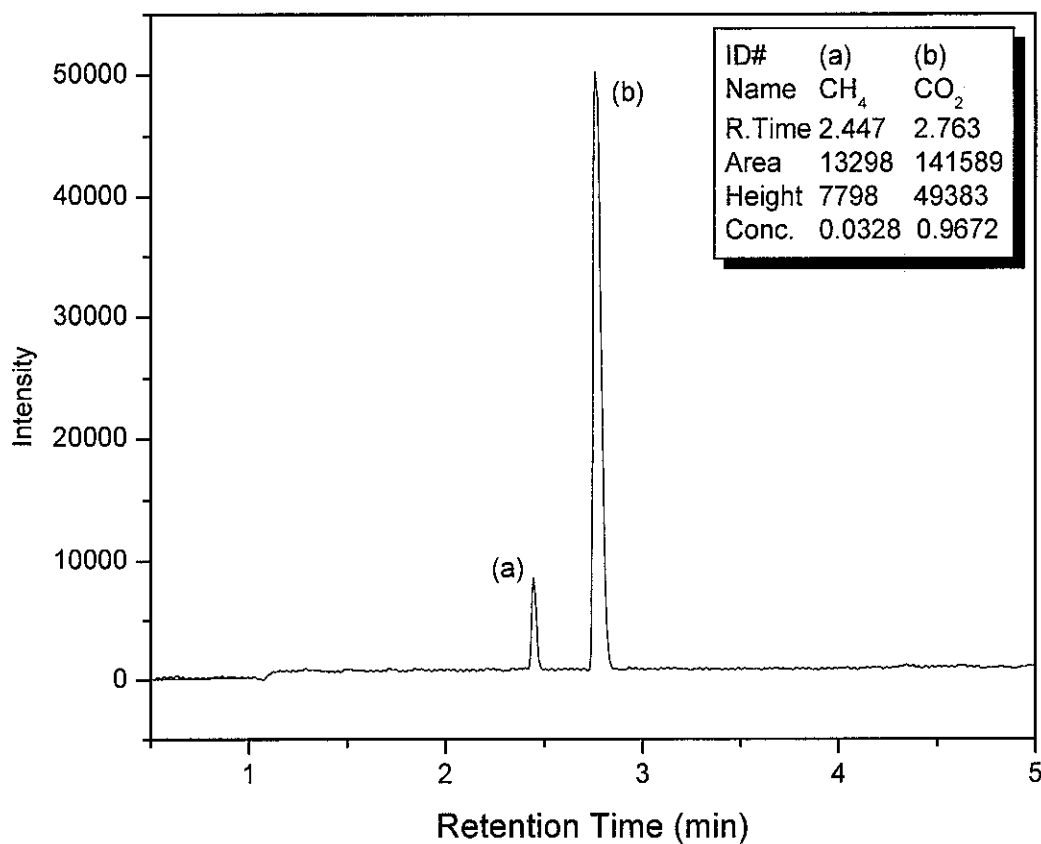


Figure 4.39 CO₂/CH₄ gas mixture composition obtained at 30%/70% CO₂/CH₄ feed mixtures for PSF/PI-20% membrane

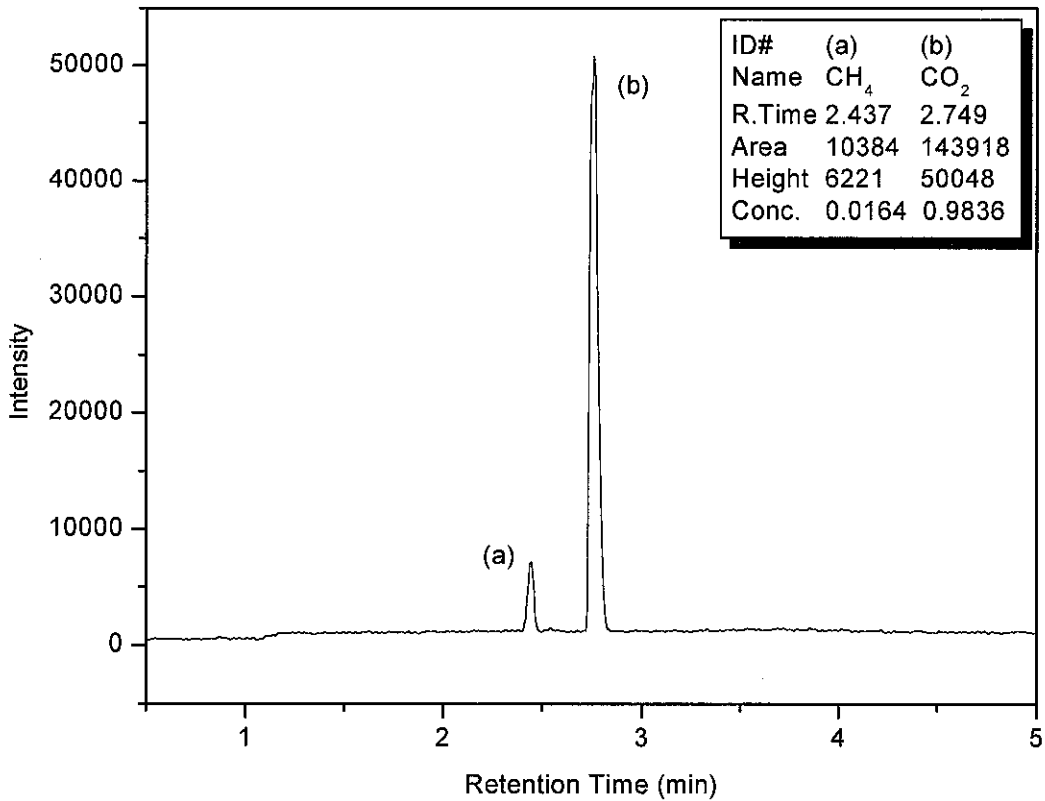


Figure 4.40 CO₂/CH₄ gas mixture the composition obtained at 50%/50% CO₂/CH₄ feed mixtures for the PSF/PI-20%+S3 membrane

The mixed gas selectivity of the developed membranes shows that the values are quite close to the ideal selectivity. It indicates that plasticization in the membranes did not exist, since at higher pressures of 10 bar, the membrane performance showed consistency with that of pure gases [30]. Hillock et al. [135] found that for PDMC/SSZ-13 hybrid membranes, higher selectivity was achieved for 10%/90% CO₂/CH₄ gas mixtures than the ideal selectivity from pure gases. It happened due to the absence of plasticization which occurred because the CO₂ permeance outperformed the CH₄ bulkier molecule. Thus, it effectively slowed the CH₄ transport through the matrix. Li et al. [137] also found no difference in the CO₂/CH₄ selectivity for the ideal and mixed gases (47/53%) for the PES-zeolite AgA blends that showed resistance to plasticization in the mixed matrix membranes. Experimental results for the mixed gas in Table 4.9 showed good agreement with the reported literature of having a negligible effect on selectivity for pure and CO₂/CH₄ mixed gases.

4.13 Effect of Particle Geometry on Permeance in MMMs through Modeling Approach

For the purpose of evaluating the gas permeance using the theoretical models, the experimental data taken from CO₂ permeance in the PSF/PI-20%-silica MMMs was considered and the data is shown in Table 4.10. The pure CO₂ permeance data were obtained for the intrinsic silica membrane from previous literature taken at 25°C bar and is also mentioned in Table 4.10. For modeling purposes, it was assumed that the silica intrinsic permeation value remains the same throughout the pressure range between 2-10 bar.

Table 4.10 Experimental CO₂ Permeation data for the PSF/PI-20%- SiO₂ membranes at 2 bar feed pressure

Membranes	P _{CO2} (GPU)	Ref.
PSF	33.7	This study
PSF/PI-20%	39.3	
S1	73.7	
S2	80.0	
S3	88.4	
S4	95.7	
Pure SiO ₂	680.6	[203]

The comparison between the used models and the experimental data plotted between the relative permeance of the CO₂ against the volume fraction of the silica particles (\square) is shown in Figure 4.41.

A comparative summary of the deviations between the models is listed in Table 4.11. The results show that the Lewis-Nielsen model provided the least deviation from

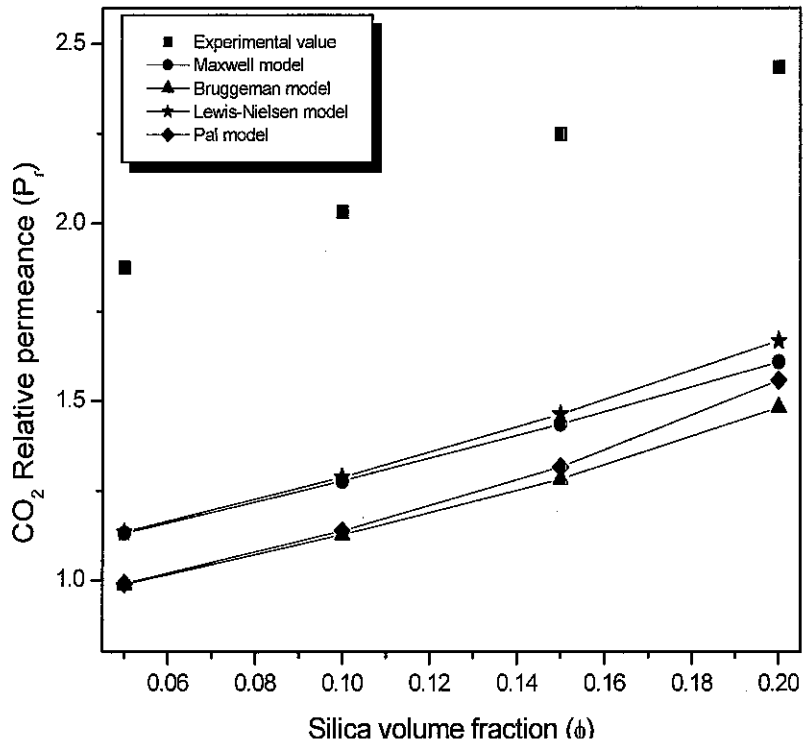


Figure 4.41 Overall comparison of theoretical models with experimental data for CO₂ relative permeance plotted against the volume fraction of the silica particles

Table 4.11 Variation of the theoretical models from the experimental data for relative permeability of CO₂ at 2 bar feed pressure

Theoretical models	Percentage average absolute relative error (AARE %)
Maxwell model	36.69
Bruggeman model	43.46
Lewis-Nielsen model	35.61
Pal model	42.14

the experimental data. The order of the deviation based on the AARE% is found in the increasing order as Lewis-Nielsen model < Maxwell model < Pal model < Bruggeman model. Nevertheless, significant deviations were observed between the calculated data from the theoretical models and the published experimental results which trigger a need for an improved model. Thus, the analysis on the range of the results obtained from the theoretical models seems to point towards the importance of particle morphology factors that need to be considered as well.

Observation from the SEM cross-sectional view of the MMMs as shown in Figure 4.42 indicates that the fillers are prolate ellipsoids instead of spherical as assumed in the theoretical models. In order to account for the shape factor, Lewis-Nielson and MWS models were used for the follow-up calculations.

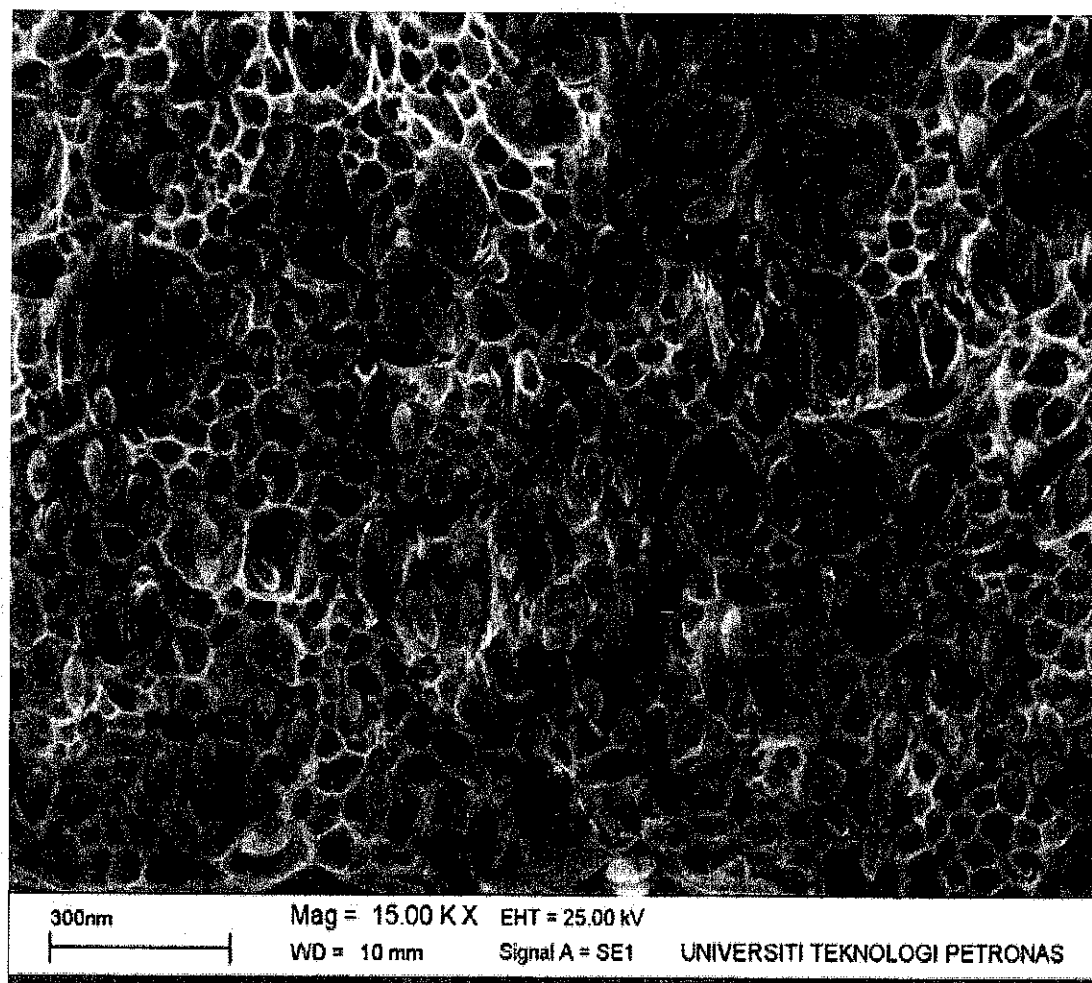


Figure 4.42 Cross-sectional image of the MMMs with a 15% silica loading at a magnification of 15KX; scale 300nm

In the Lewis-Nielson model, the ϕ_m is sensitive to particle size distribution, particle shape and aggregation. In practice, this parameter is very difficult to determine directly. However, an indirect method could be adopted through the fitting and optimization of the values of the parameters against experimental data to minimize the predicted errors from the models. Note that when the volume fraction of the fillers approaches unity i.e., $\phi_m \rightarrow 1$, the model reduces to the Maxwell model (Eq.(2.16). For the MWS model (Eq.(2.21), the shape factor (n) is directly used in the model. For prolates in which the applied pressure gradient is along the particle longest axis, the shape factor is within the range of $0 \leq n \leq 1/3$ [152]. The fitting and optimization procedures conducted on the Lewis-Nielson and MWS model against the experimental data produced results on the optimization curve of ϕ_m and n values as shown in Figure 4.43 (a) and (b).

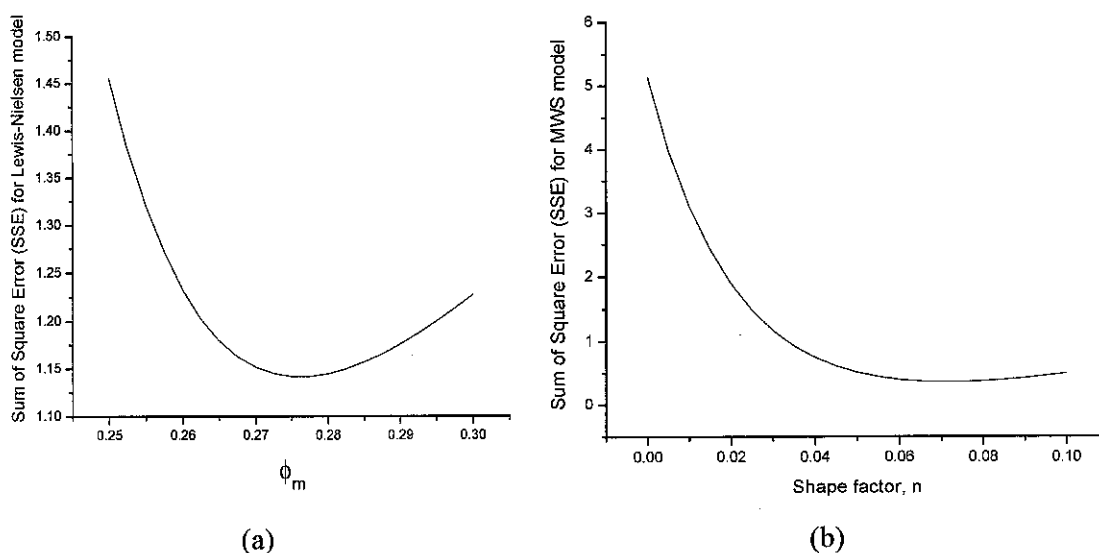
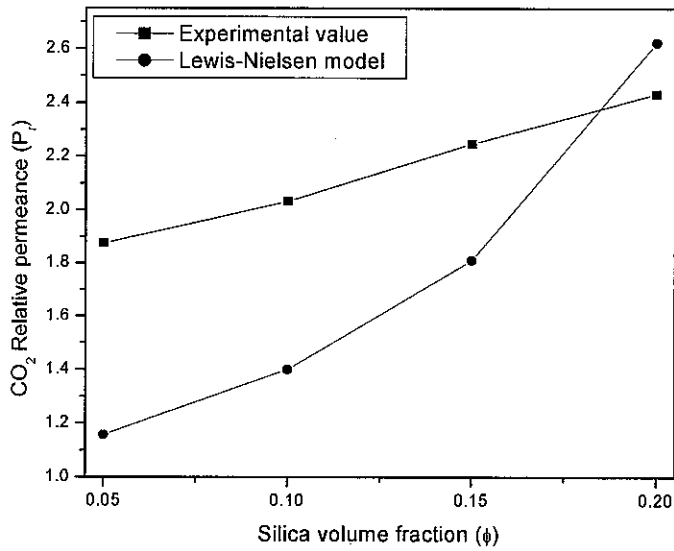


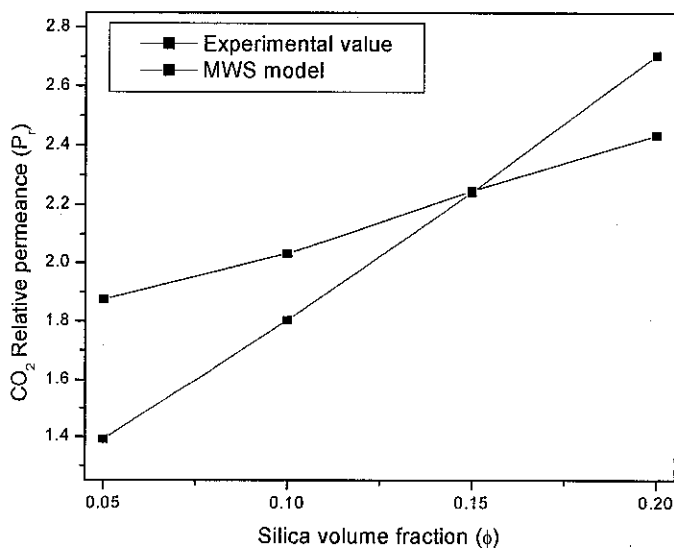
Figure 4.43 Optimization curves for (a) Lewis-Nielson model and (b) MWS model

From the optimized curves, the value for ϕ_m and n are found to be 0.276 and 0.07, respectively. Using these optimized values, the calculations on the CO₂ relative permeance with respect to the silica loading were repeated for the two models and compared against the experimental data. The results shown in Figure 4.44 represent better agreement between the calculated values from the two models and the

experimental data. The deviations, AARE%, from the experimental value was then calculated and is shown in Table 4.12 which indicates that the MWS model produced a better prediction. This analysis shows that the factors ϕ_m and n could be used to improve the model prediction if their optimized values are known. Nevertheless, one



(a)



(b)

Figure 4.44 Optimized comparative predictions of (a) Lewis-Nielsen model and (b) MWS model against the experimental data for the CO₂ relative permeance at 2 bar feed pressure

could argue that the outcome was expected given that the parameters used in the models were determined from the fitting exercise conducted on the experimental data. The question which will be addressed later is on how to acquire the parameters without performing the fitting exercise against the experimental data.

A direct comparison between the MWS and Lewis-Nielsen models shows that not only could the MWS model produce better predictions with respect to the experimental data, the model also allowed for the shape factor (n) to be directly incorporated in its equation thus leading to an easier application. The shape factor could be easily estimated from the SEM cross-sectional image if available. As a result, it is more logical in pursuing the improvement through this model. An important factor that needs to be realized is that in the original MWS model, the shape factor (n) solely represents the shape of the particle. However, the permeance is also affected by other morphological factors of the membrane such as particle distribution and aggregation which are a function of particle loading. Considering if all these factors could be lumped into the shape factor to form a new parameter that could represent the overall morphology, the application of the model could be made much easier and practical. This new parameter is introduced in this study as the fitted shape factor (n_f). Though a single optimized n_f value in the MWS model improved the overall prediction, the prediction accuracy could be further improved if the shape factor n_f value is fitted at a specific filler loading since the morphology is a function of the filler loading. Thus, if n_f at a specific filler loading is known, the prediction of permeance at any operating pressure could be accurately determined as n_f is independent of the operating pressure. To illustrate this, Table 4.12 shows the values of n_f fitted with the experimental data at various particle loadings but maintained at 2 bar operating pressure. The value varied as a function of the particle loading and it increased with the increase in the particle loading. This increasing trend was expected because as the loading increases, the overall morphological effects will move from the prolate towards the spherical shape effects ($n \rightarrow 0.33$) as the particles' distance is squeezed under the higher loading. Figure 4.45 (a)-(e) shows the plots on the changes in the relative permeance of CO_2 against the silica loading at pressures ranging from 2 to 10 bar, respectively. It shows the comparison of the MWS model prediction from the experimental value using the shape factor n_f of the particles from Table 4.12. Note

Table 4.12 Comparative Lewis-Nielsen and MWS model deviations along with the fitted shape factor value at the various filler loading in the MMMs at 2 bar feed pressure

silica loading, vol.%	Lewis-Nielsen model ($\phi_m = 0.276$)	MWS model ($n=0.07$)	Fitted shape factor, n_f
	AARE%		
5	20.29	6.54	0
10			0.04
15			0.07
20			0.1

that the set of predicted values obtained from the improved models were compared with the experimental results. The AARE% values calculated for the improved MWS model are found to be within the range of 1.12 to 2.17 at feed pressures varying from 2-10 bar. The results from the AARE% calculations as shown in Figure 4.45, clearly indicates significant reduction in the error between the predicted value from the theoretical model and the experimental results.

Thus, a comparison between the deviations from the Maxwell model (Table 4.11), MWS model for the constant value of n (Table 4.12) and the MWS model at fitted n_f values (Table 4.12 and Figure 4.45) show that the AARE% value shifted from 36.69 to 6.54 and to 1.12, respectively at 2 bar feed pressure. This was due to the fact that the fillers exhibited a prolate geometry that caused the addition of the n factor which showed variation with the particle loading and affected the predication of the relative permeance for the Maxwell model.

Further evaluation was conducted on the shape factor effect, where a cross-sectional SEM image was taken on the MMMs shown in Figure 4.42. The shape factor along the pressure gradient in the z -direction (n_z) corresponding to the prolates geometry was calculated based on the SEM images. A total of 10 randomly selected particles at various locations in the cross-sectional SEM image were used for

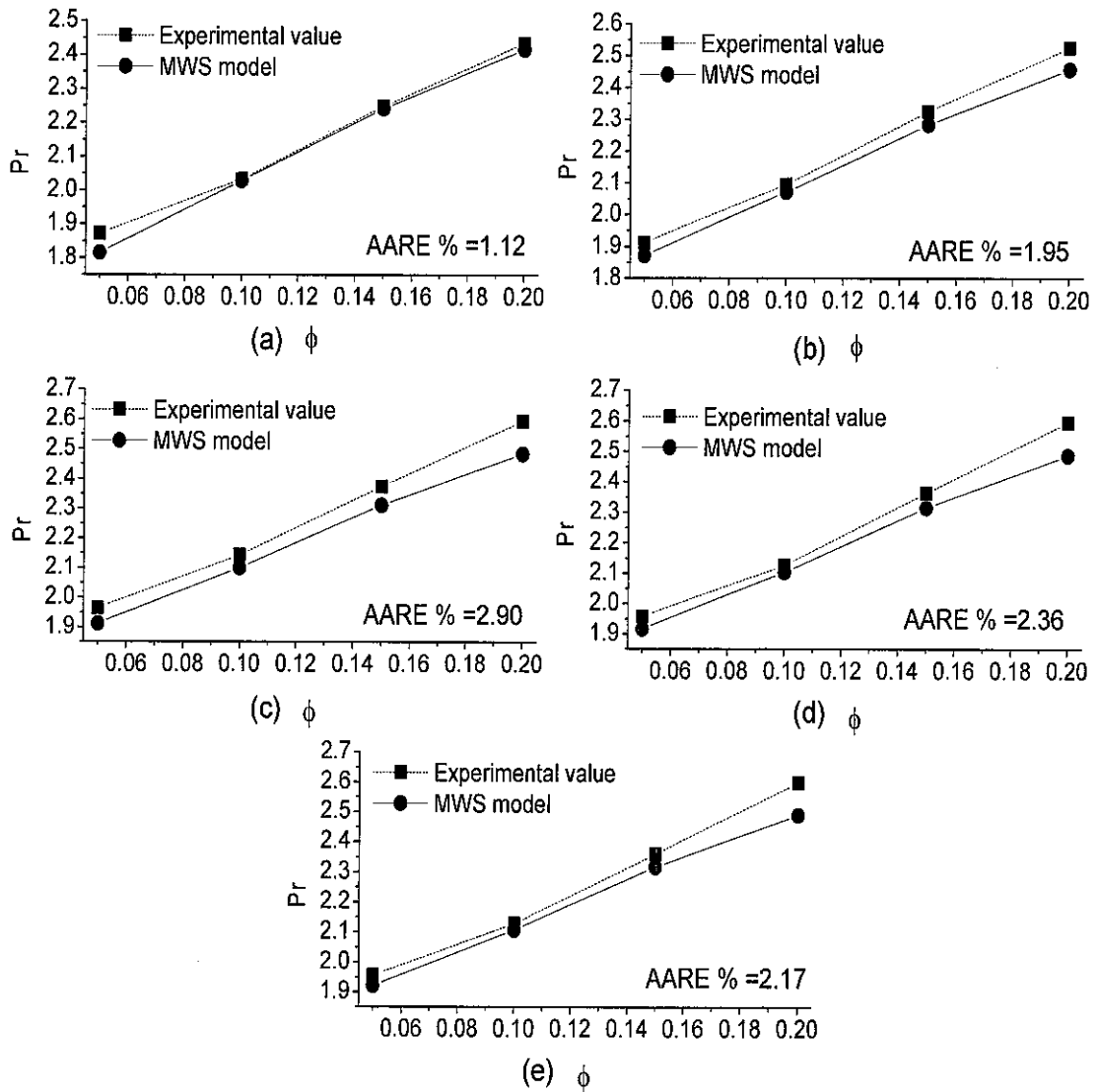


Figure 4.45 Comparison of the MWS model prediction versus the experimental data in terms of the relative permeance (P_r) for CO_2 at pressures: (a) 2 bar (b) 4 bar (c) 6 bar (d) 8 bar and (e) 10 bar for the different values of ϕ and n

determining their n_z values. The overall n_z was then taken from the average n_z values for the selected particles. The calculated n_z value was then compared with the shape factor n_f obtained from the fitting of the improved MWS model with the experimental data for the predicted relative permeance.

The results are summarised in Table 4.13 with n_z at 0.102 ± 0.01 showing a minimum AARE% deviation of 15.08 for the MWS model at 2 bar feed pressure. Although using the above technique for determining the shape factor (n_z) gave an AAR% deviation of about twice that compared to the experimentally fitted one (Table 4.12) and the best optimized values of 6.54 for n at 0.07. Still it is still much better as compared to the Maxwell model (AARE% 36.69, Table 4.11). The value n_z at 0.102 ± 0.01 accounted only for the effects related to the sphericity of the particles; however, n_f at 0.07 gave potentially the best prediction where the particle shape, distribution and aggregation factors were lumped. Though this n_z value was slightly higher than the n_f value of 0.1 (20 vol.%, Table 4.12), they could be said to be comparable. Thus, the measured shape factor from the SEM image (n_z) could still be used as the upper limit for n_f .

Table 4.13 MWS model deviations from the experimental permeation values determined from the SEM image and the estimated shape factor values at the various feed pressures

Feed Pressure (bar)	Using MWS model	
	At, $n_z = 0.102 \pm 0.01$	At, estimated Shape factor, n_e
	AARE %	
2	15.08	6.01
4	16.66	7.23
6	18.01	8.39
8	17.63	7.92
10	17.56	7.78

Another observation made in the study was on the relationship between n_f (Table 4.12) against each fraction of the silica loadings. Figure 4.46 shows the plot from the results where an almost linear relationship (where $R^2 \sim 1$) was observed between the two parameters. If the linear relationship could be assumedly generalized, then

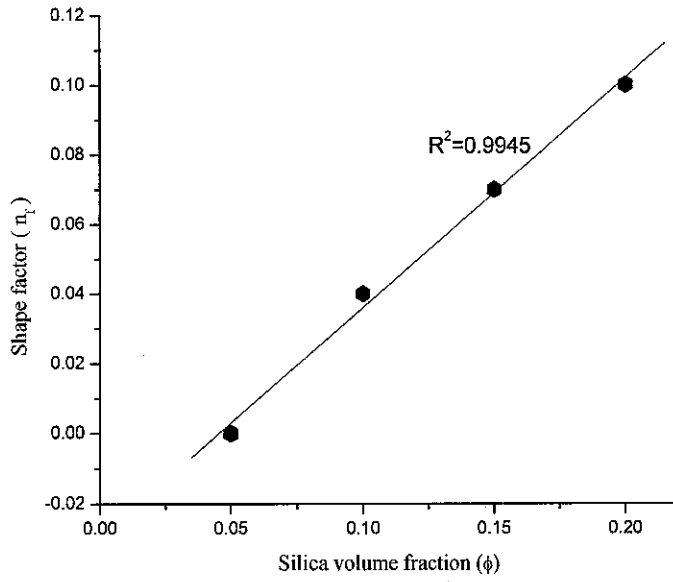


Figure 4.46 Graphs of the shape factor, n_f at various silica loadings (\square)

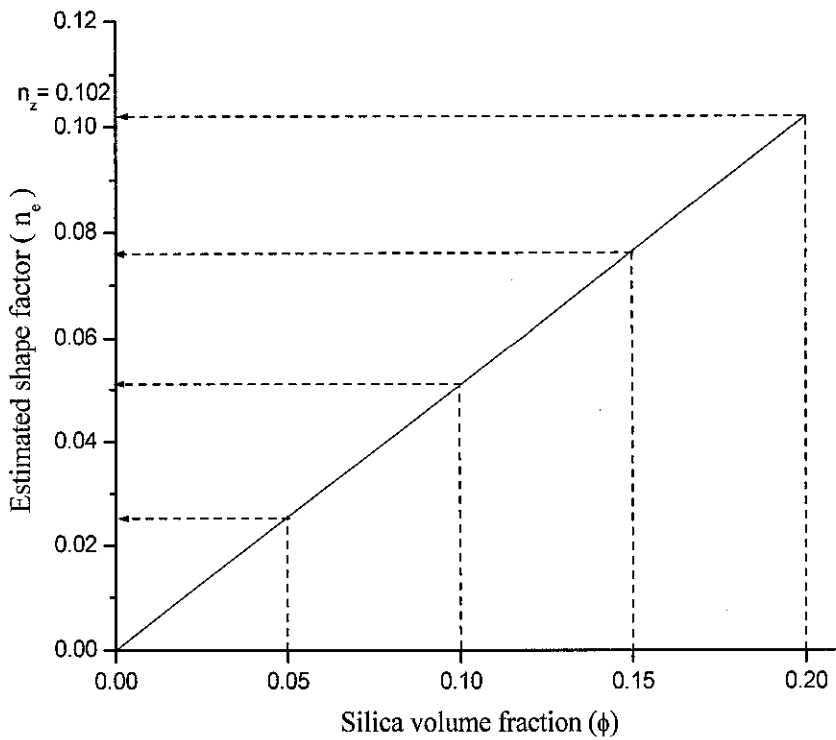


Figure 4.47 Estimated shape factor (n_e) values at various silica loadings with the maximum values of n_z

only two data points would be sufficient enough to estimate the n_f values for the different silica loadings. To differentiate between the n_f to the estimated value of n_e , the symbol is denoted by n_e . The simplest estimation of the shape factor (n_e) could easily be performed by taking the two points to be at (i) zero loading ($n_e = 0$) and (ii) maximum filler loading ($n_e = n_z$). Thus the n_e can be shown as follows:

$$n_e = f(\phi_f, \phi_m, n_z) \quad (4.4)$$

$$\text{Then } n_e = \frac{n_z}{\phi_m} \times \phi_f \quad (4.5)$$

So if, $\phi = \phi_m$, n_e is reduced to n_z . Hence, any points in between can be directly obtained from the above Eq.(4.5). This equation represents the straight line that connects the two points. Figure 4.47 demonstrates the application of the above approach.

Table 4.13 shows results on the calculated CO₂ permeance obtained by taking the estimated shape factor value (n_e) from Figure 4.47 and comparing it with the results obtained by taking the shape factor (n_z) determined from the SEM image. The results indicate that the generalization between two data points with n_z value serving as an upper limit, effectively reduced the AARE% deviations of n_e values and predicts closer to the experimental data. Though the n_e values were still higher than the n_f values; however, this approach is still useful for estimation of the true CO₂ permeance and design purposes.

From the MWS model (Eq. 2.21), the modified MWS model takes the form of the Eq.(4.6):

$$P = P_m \left\{ \frac{n_e P_f + (1 - n) P_m + (1 - n_e) \phi_f (P_f - P_m)}{n_e P_f + (1 - n_e) P_m - n_e \phi_f (P_f - P_m)} \right\} \quad (4.6)$$

So the modified MWS model can be applied to estimate the permeance of the mixed matrixes exhibiting the shape factor of prolate geometry at any pressure of feed gas streams.

CHAPTER 5

5. CONCLUSIONS AND RECOMMENDATIONS

5.1 Conclusions

Asymmetric flat sheet PSF/PI membranes were prepared by phase inversion technique and it was found that the developed membranes exhibited homogeneous and uniform membrane blends. The homogeneity in the membranes was confirmed by the DSC analysis that showed a single T_g for each membrane blends which indicated miscibility among the PSF/PI polymers. The kinetic analysis and mechanical properties performed on the developed membranes showed that the activation energies and tensile properties both increased with the increase in the PI contents and PSF/PI-20% showed maximum improvement. Heat treatment was carried out for stabilizing the membranes and it was observed that the membranes showed decrease in permeance. However, the ideal selectivity increased in comparison to the untreated membranes, giving higher selectivity for the PSF/PI-20% membrane from 30.24 ± 0.5 – 29.70 ± 0.7 at 2-10 bar feed pressure, respectively.

The effects of the solvents composition on the developed membranes showed that by increasing the DCM composition in the NMP/DCM solvent mixtures, the skin thickness increased in the order of: $80/20 < 50/50 < 20/80$. The solubility parameter difference between the solvent mixtures to the polymers and non-solvent showed the similar order. CO_2/CH_4 gas separation analysis showed that the permeance value decreased with the increase in operating pressures depicting the absence of membrane swelling at higher pressures. It was found that for the solvent composition NMP/DCM (80/20), PSF/PI-20% membrane showed the highest selectivity of 28.70-28.22 from 2 to 10 bar pressure respectively as compared to NMP/DCM (50/50) and NMP/DCM (20/80) membranes.

The MMMs prepared by incorporating nano porous silica obtained from TEOS at various loadings of 5-20 wt.% in the PSF/PI-20% blended membrane showed distinct T_g . A T_g rise of 4.2°C was observed with the 5 wt.% silica content that increased to 25°C at the maximum level of silica loading of 20 wt.%. The surface morphology of the MMMs showed homogenous distribution of the silica particles; however, agglomerated silica domains were formed at 20 wt.% silica loading which were absent in lower silica loadings. The XRD spectra showed that the d-spacing gradually decreased with the increase in the silica content and so the peak intensity decreased, i.e., 20~23.35° for PSF/PI-20%. Kinetic analysis showed that the degradation temperature and the activation energy increased with the increase in the silica content in the MMMs and 20 wt% silica contents showed the maximum degradation and activation energy values. The Young's modulus and the tensile strength increased considerably with 15 wt.% silica content. Gas performance of the membranes showed that with the 15wt.% of silica content, maximum ideal selectivity value was achieved for heat treated membranes; $\alpha_{CO_2/CH_4} = 61.0 \pm 0.3 - 60.2 \pm 0.1$ from 2 to 10 bar feed pressure respectively. The results from mixed gas analysis performed from various CO₂/CH₄ gas mixtures of 30/70%, 50/50% and 70/30% compositions showed that the mixed gas selectivities were closer to the ideal selectivity.

The results obtained from various gas permeation models indicated that MWS model showed least AARE% deviation from 1.12-2.90 for 2-10 bar, respectively.

5.2 Recommendations

Based on the present study, some recommendations for the extension as future work may be carried out for providing more insight into the developed membranes. The suggestions are as follows:

The present study was based upon the fabrication of polymeric blends of asymmetric membranes followed by mixed matrix membranes using silica as the inorganic filler. Following the recipes with polymeric blends, dense mixed matrix membranes and hollow fibre membranes using silica as the inorganic filler can be

compared. This will yield more information on various characterization affects and on the gas performance results.

Another future extension in the present work can be made by studying the effects of temperature variations on the CO₂/CH₄ gas performance, for both gases, as single and mixed gas feed streams. Running the gas permeation experiments at varying process temperature protocols will provide more information on the stability of the developed membranes. Moreover, studies on higher feed gas pressures will give more elaborative pictures of the developed membranes, and the effects of plasticization can be extensively studied at elevated pressures. However, this will require fabrication of another gas permeation unit design that allows for the gas testing at aggressive feed streams.

The reported work on modeling was carried out on mixed matrix membranes that were used extensively for dense membranes. Efforts were put into the present study by using existing gas permeation models for asymmetric membranes. New gas permeation models in light of asymmetric membranes seems to be one of the major future scopes to put effort on separately for gas prediction with the experimental data.

Other parametric future studies on fabrication of asymmetric polymeric membranes that may give more inside information on the membranes' mechanism that involves the effects of the casting rate, coagulation bath composition and humidity effects during membrane development.

REFERENCES

- [1] M. Kelkar, *Natural gas production engineering*: PennWell, 2008.
- [2] B. Petroleum, "BP statistical review of world energy," 2011.
- [3] K. G. Ooi, *Historical dictionary of Malaysia*: Scarecrow Press, 2009.
- [4] F. Orecchini and V. Naso, *Energy Systems in the Era of Energy Vectors: A Key to Define, Analyze and Design Energy Systems Beyond Fossil Fuels*: Springer, 2011.
- [5] S. P. Nunes and K. V. Peinemann, *Membrane Technology: In the Chemical Industry*: John Wiley & Sons, 2007.
- [6] R. L. Nersesian, *Energy for the 21st century: a comprehensive guide to conventional and alternative sources*: M E SHARPE INC, 2010.
- [7] E. I. Administration, "Natural gas: Issues and trends 1998," 1999.
- [8] S. A. Rackley, *Carbon capture and storage*: Butterworth-Heinemann/Elsevier, 2009.
- [9] G. Sartori and D. W. Savage, "Sterically hindered amines for carbon dioxide removal from gases," *Industrial & Engineering Chemistry Fundamentals*, vol. 22, pp. 239-249, 1983/05/01 1983.
- [10] R. T. Yang, *Adsorbents: fundamentals and applications*: Wiley-Interscience, 2003.
- [11] S.-L. Wee, C.-T. Tye, and S. Bhatia, "Membrane separation process—Pervaporation through zeolite membrane," *Sep. Purif. Technol.*, vol. 63, pp. 500-516, 2008.
- [12] J. D. Wind, D. R. Paul, and W. J. Koros, "Natural gas permeation in polyimide membranes," *J. Membr. Sci.*, vol. 228, pp. 227-236, 2004.
- [13] D. R. Paul, *Polymeric gas separation membranes*: CRC Press, 1994.
- [14] B. Van der Bruggen, "Chemical modification of polyethersulfone nanofiltration membranes: A review," *J. Appl. Polym. Sci.*, vol. 114, pp. 630-642, 2009.

- [15] Z. Wang, T. Chen, and J. Xu, "Gas Transport Properties of Novel Cardio Poly(aryl ether ketone)s with Pendant Alkyl Groups," *Macromolecules*, vol. 33, pp. 5672-5679, 2000/07/01 2000.
- [16] I. Pinnau, "Membrane Preparation," in *Encyclopedia of separation science*, I. D. Wilson, *et al.*, Eds., ed: Academic Press, 2000, pp. 1755-1764.
- [17] H. Strathmann, "Synthetic Membranes: Science, Engineering and Applications," in *Synthetic membranes and their preparation*, H. K. L. P.M. Bungay, M.N. de Pinto, Ed., ed Dordrecht, Holland: D. Reidel, 1986, pp. 1-37.
- [18] T.-S. Chung and X. Hu, "Effect of air-gap distance on the morphology and thermal properties of polyethersulfone hollow fibers," *J. Appl. Polym. Sci.*, vol. 66, pp. 1067-1077, 1997.
- [19] M. Wang, X. Zhu, and L. Zhang, "Hole structure and its formation in thin films of hydrolyzed poly(styrene maleic anhydride) alternating copolymers," *J. Appl. Polym. Sci.*, vol. 75, pp. 267-274, 2000.
- [20] A. F. Ismail and W. Lorna, "Penetrant-induced plasticization phenomenon in glassy polymers for gas separation membrane," *Sep. Purif. Technol.*, vol. 27, pp. 173-194, 2002.
- [21] R. Lloyd M, "Correlation of separation factor versus permeability for polymeric membranes," *J. Membr. Sci.*, vol. 62, pp. 165-185, 1991.
- [22] D. Q. Vu, "Formation and characterization of asymmetric carbon molecular sieve and mixed matrix membranes for natural gas purification," Ph.D. Dissertation, The University of Texas at Austin, 2001.
- [23] P. Bernardo, E. Drioli, and G. Golemme, "Membrane Gas Separation: A Review/State of the Art," *Industrial & Engineering Chemistry Research*, vol. 48, pp. 4638-4663, 2009/05/20 2009.
- [24] A. F. Ismail and W. Lorna, "Suppression of plasticization in polysulfone membranes for gas separations by heat-treatment technique," *Sep. Purif. Technol.*, vol. 30, pp. 37-46, 2003.
- [25] C. Zhou, T.-S. Chung, R. Wang, Y. Liu, and S. H. Goh, "The accelerated CO₂ plasticization of ultra-thin polyimide films and the effect of surface chemical cross-linking on plasticization and physical aging," *J. Membr. Sci.*, vol. 225, pp. 125-134, 2003.

- [26] C. L. Aitken, W. J. Koros, and D. R. Paul, "Gas transport properties of biphenol polysulfones," *Macromolecules*, vol. 25, pp. 3651-3658, 1992/07/01 1992.
- [27] A. Ghosh and S. Banerjee, "Thermal, mechanical, and dielectric properties of novel fluorinated copoly(imide siloxane)s," *J. Appl. Polym. Sci.*, vol. 109, pp. 2329-2340, 2008.
- [28] S. Mehdipour-Ataei and A. Amirshaghghi, "Novel thermally stable poly(ether imide ester)s from 2,6-bis (4-aminophenoxy) pyridine," *J. Appl. Polym. Sci.*, vol. 96, pp. 570-576, 2005.
- [29] A. Bos, I. G. M. Pünt, M. Wessling, and H. Strathmann, "CO₂-induced plasticization phenomena in glassy polymers," *J. Membr. Sci.*, vol. 155, pp. 67-78, 1999.
- [30] A. Bos, I. G. M. Pünt, M. Wessling, and H. Strathmann, "Plasticization-resistant glassy polyimide membranes for CO₂/CO₄ separations," *Sep. Purif. Technol.*, vol. 14, pp. 27-39, 1998.
- [31] M. Wessling, S. Schoeman, T. van der Boomgaard, and C. A. Smolders, "Plasticization of gas separation membranes," *Gas Separation & Purification*, vol. 5, pp. 222-228, 1991.
- [32] J. D. Wind, C. Staudt-Bickel, D. R. Paul, and W. J. Koros, "The Effects of Crosslinking Chemistry on CO₂ Plasticization of Polyimide Gas Separation Membranes," *Industrial & Engineering Chemistry Research*, vol. 41, pp. 6139-6148, 2002/11/01 2002.
- [33] J. S. Chiou, J. W. Barlow, and D. R. Paul, "Plasticization of glassy polymers by CO₂," *J. Appl. Polym. Sci.*, vol. 30, pp. 2633-2642, 1985.
- [34] D. T. Clausi and W. J. Koros, "Formation of defect-free polyimide hollow fiber membranes for gas separations," *J. Membr. Sci.*, vol. 167, pp. 79-89, 2000.
- [35] G. C. Kapantaidakis, G. H. Koops, and M. Wessling, "Preparation and characterization of gas separation hollow fiber membranes based on polyethersulfone-polyimide miscible blends," *Desalination*, vol. 145, pp. 353-357, 2002.

- [36] A. Bos, I. Pünt, H. Strathmann, and M. Wessling, "Suppression of gas separation membrane plasticization by homogeneous polymer blending," *AIChE J.*, vol. 47, pp. 1088-1093, 2001.
- [37] G. C. Kapantaidakis, S. P. Kaldis, X. S. Dabou, and G. P. Sakellaropoulos, "Gas permeation through PSF-PI miscible blend membranes," *J. Membr. Sci.*, vol. 110, pp. 239-247, 1996.
- [38] T. Graham, "On the law of the diffusion of gases," *J. Membr. Sci.*, vol. 100, pp. 17-21, 1995.
- [39] A. F. Ismail, R. Norida, W. A. W. A. Rahman, T. Matsuura, and S. A. Hashemifard, "Preparation and characterization of hyperthin-skinned and high performances asymmetric polyethersulfone membrane for gas separation," *Desalination*, vol. 273, pp. 93-104, 2011.
- [40] M. Mulder, *Basic principles of membrane technology*: Kluwer Academic, 1996.
- [41] L. K. WANG, J. P. Chen, Y. T. Hung, and N. K. Shamas, *Membrane and Desalination Technologies*: SPRINGER VERLAG NY, 2010.
- [42] J. C.-Y. Chen, "Evaluation of Polymeric Membranes for Gas Separation Processes: Poly(ether-b-amide) (PEBAXR2533) Block Copolymer," MSc Thesis, University of Waterloo, Ontario, Canada, 2002.
- [43] K. Scott and R. Hughes, *Industrial membrane separation technology*: Blackie Academic & Professional, 1996.
- [44] T.-S. Chung and Z.-L. Xu, "Asymmetric hollow fiber membranes prepared from miscible polybenzimidazole and polyetherimide blends," *J. Membr. Sci.*, vol. 147, pp. 35-47, 1998.
- [45] M. A. Aroon, A. F. Ismail, M. M. Montazer-Rahmati, and T. Matsuura, "Morphology and permeation properties of polysulfone membranes for gas separation: Effects of non-solvent additives and co-solvent," *Sep. Purif. Technol.*, vol. 72, pp. 194-202, 2010.
- [46] A. F. Ismail and P. Y. Lai, "Effects of phase inversion and rheological factors on formation of defect-free and ultrathin-skinned asymmetric polysulfone membranes for gas separation," *Sep. Purif. Technol.*, vol. 33, pp. 127-143, 2003.
- [47] D. M. Ruthven, *Encyclopedia of separation technology*: Wiley, 1997.

- [48] R. W. Baker, *Membrane separation systems: recent developments and future directions*: Noyes Data Corp., 1991.
- [49] D. Wang, K. Li, and W. K. Teo, "Relationship between mass ratio of nonsolvent-additive to solvent in membrane casting solution and its coagulation value," *J. Membr. Sci.*, vol. 98, pp. 233-240, 1995.
- [50] R. W. Baker, *Membrane technology and applications*: J. Wiley, 2004.
- [51] W. J. Koros and I. Pinnau, "Membrane formation for gas separation processes", Polymeric Gas Separation Membranes," in *Polymeric gas separation membranes*, D. R. Paul, Ed., ed: CRC Press, 1994.
- [52] P. S. T. Machado, A. C. Habert, and C. P. Borges, "Membrane formation mechanism based on precipitation kinetics and membrane morphology: flat and hollow fiber polysulfone membranes," *J. Membr. Sci.*, vol. 155, pp. 171-183, 1999.
- [53] I. Pinnau, "Skin formation of integral-asymmetric gas separation membranes made by dry/wet phase inversion," PhD Dissertation, The University of Texas Austin, 1991.
- [54] H. Strathmann, "Membrane separation processes," *J. Membr. Sci.*, vol. 9, pp. 121-189, 1981.
- [55] C. Gong, R. Guan, Y.-C. Shu, F.-S. Chuang, and W.-C. Tsen, "Effect of sulfonic group on solubility parameters and solubility behavior of poly(2,6-dimethyl-1,4-phenylene oxide)," *Polym. Adv. Technol.*, vol. 18, pp. 44-49, 2007.
- [56] C. M. Hansen, *Hansen solubility parameters: a user's handbook*: CRC Press, 2000.
- [57] D. W. Krevelen, *Properties of polymers: their correlation with chemical structure, their numerical estimation and prediction from additive group contributions*: Elsevier, 1990.
- [58] D. W. Krevelen and K. te Nijenhuis, *Properties of polymers: their correlation with chemical structure; their numerical estimation and prediction from additive group contributions*: Elsevier, 2009.
- [59] A. F. M. Barton, *CRC handbook of solubility parameters and other cohesion parameters*. Boca Raton, Florida: CRC Press, Inc., 1985.

- [60] J. Ren, T.-S. Chung, D. Li, R. Wang, and Y. Liu, "Development of asymmetric 6FDA-2,6 DAT hollow fiber membranes for CO₂/CH₄ separation: 1. The influence of dope composition and rheology on membrane morphology and separation performance," *J. Membr. Sci.*, vol. 207, pp. 227-240, 2002.
- [61] C. A. Scholes, S. E. Kentish, and G. W. Stevens, "Carbon dioxide separation through polymeric membrane system for flue gas applications," *Recent Patent Chem. Eng.*, vol. 1, pp. 52-66, 2008.
- [62] WSW Ho and K. Sirkar, *Gas permeation in: Membrane handbook*. New York: Van Nostrand Reinhold, 1992.
- [63] H. Czichos, T. Saito, and L. Smith, *Springer Handbook of Materials Measurement Methods*: Springer, 2006.
- [64] D. R. Paul and W. J. Koros, "Effect of partially immobilizing sorption on permeability and the diffusion time lag," *Journal of Polymer Science: Polymer Physics Edition*, vol. 14, pp. 675-685, 1976.
- [65] D. Q. Vu, "Formation and characterization of asymmetric carbon molecular sieve and mixed-matrix membranes for natural gas purification," Ph.D. Ph.D., The University of Texas at Austin, 2001.
- [66] J. N. Barsema, G. C. Kapantaidakis, N. F. A. van der Vegt, G. H. Koops, and M. Wessling, "Preparation and characterization of highly selective dense and hollow fiber asymmetric membranes based on BTDA-TDI/MDI copolyimide," *J. Membr. Sci.*, vol. 216, pp. 195-205, 2003.
- [67] W. S. W. Ho and K. K. Sirkar, *Membrane handbook*: Chapman & Hall, 1992.
- [68] S. Loab and S. Sourirajan, "Asymmetric Membrane Formation," U.S. Patent 3,133,132 Patent, 1964.
- [69] L. M. Robeson, "Correlation of separation factor versus permeability for polymeric membranes," *J. Membr. Sci.*, vol. 62, pp. 165-185, 1991.
- [70] C. Staudt-Bickel and W. J. Koros, "Improvement of CO₂/CH₄ separation characteristics of polyimides by chemical crosslinking," *J. Membr. Sci.*, vol. 155, pp. 145-154, 1999.
- [71] M. Wessling, M. Lidon Lopez, and H. Strathmann, "Accelerated plasticization of thin-film composite membranes used in gas separation," *Sep. Purif. Technol.*, vol. 24, pp. 223-233, 2001.

- [72] W. J. Koros, G. K. Fleming, S. M. Jordan, T. H. Kim, and H. H. Hoehn, "Polymeric membrane materials for solution-diffusion based permeation separations," *Prog. Polym. Sci.*, vol. 13, pp. 339-401, 1988.
- [73] A. G. Wonders and D. R. Paul, "Effect of CO₂ exposure history on sorption and transport in polycarbonate," *J. Membr. Sci.*, vol. 5, pp. 63-75, 1979.
- [74] C. Zhou, T.-S. Chung, R. Wang, Y. Liu, and S. H. Goh, "The accelerated CO₂ plasticization of ultra-thin polyimide films and the effect of surface chemical cross-linking on plasticization and physical aging," *J. Membr. Sci.*, vol. 225, pp. 125-134, 2003.
- [75] J. J. Krol, M. Boerrigter, and G. H. Koops, "Polyimide hollow fiber gas separation membranes: preparation and the suppression of plasticization in propane/propylene environments," *J. Membr. Sci.*, vol. 184, pp. 275-286, 2001.
- [76] A. L. Khan, X. Li, and I. F. J. Vankelecom, "SPEEK/Matrimid blend membranes for CO₂ separation," *J. Membr. Sci.*, vol. 380, pp. 55-62, 2011.
- [77] X. Duthie, S. Kentish, C. Powell, K. Nagai, G. Qiao, and G. Stevens, "Operating temperature effects on the plasticization of polyimide gas separation membranes," *J. Membr. Sci.*, vol. 294, pp. 40-49, 2007.
- [78] E. S. Sanders, "Penetrant-induced plasticization and gas permeation in glassy polymers," *J. Membr. Sci.*, vol. 37, pp. 63-80, 1988.
- [79] A. Bos, "High Pressure CO₂/CH₄ separation with glassy polymer membranes," PhD Thesis, University of Twente, 1996.
- [80] S. S. Hosseini and T. S. Chung, "Carbon membranes from blends of PBI and polyimides for N₂/CH₄ and CO₂/CH₄ separation and hydrogen purification," *J. Membr. Sci.*, vol. 328, pp. 174-185, 2009.
- [81] A. F. Ismail, R. A. Rahim, and W. A. W. A. Rahman, "Characterization of polyethersulfone/Matrimid® 5218 miscible blend mixed matrix membranes for O₂/N₂ gas separation," *Sep. Purif. Technol.*, vol. 63, pp. 200-206, 2008.
- [82] H. May-Britt, "Membranes in Gas Separation," in *Handbook of Membrane Separations*, ed: CRC Press, 2008, pp. 65-106.
- [83] A. Yamasaki, R. K. Tyagi, A. E. Fouda, T. Matsuura, and K. Jonasson, "Effect of gelation conditions on gas separation performance for asymmetric polysulfone membranes," *J. Membr. Sci.*, vol. 123, pp. 89-94, 1997.

- [84] H.-J. Kim and S.-I. Hong, "The transport properties of CO₂ and CH₄ for trimethylsilylated polysulfone membrane," *Korean J. Chem. Eng.*, vol. 14, pp. 382-389, 1997.
- [85] H.-J. Kim and S.-I. Hong, "The sorption and permeation of CO₂ and CH₄ for dimethylated polysulfone membrane," *Korean J. Chem. Eng.*, vol. 14, pp. 168-174, 1997.
- [86] H. Kawakami, M. Mikawa, and S. Nagaoka, "Gas Transport Properties of Asymmetric Polyimide Membrane with an Ultrathin Surface Skin Layer," *Macromolecules*, vol. 31, pp. 6636-6638, 1998/09/01 1998.
- [87] J. M. A. Tan and T. Matsuura, "Effect of nonsolvent additive on the surface morphology and the gas separation performance of poly(2,6-dimethyl-1,4-phenylene)oxide membranes," *J. Membr. Sci.*, vol. 160, pp. 7-16, 1999.
- [88] J. Zhang, J. Lu, W. Liu, and Q. Xue, "Separation of CO₂ and CH₄ through two types of polyimide membrane," *Thin Solid Films*, vol. 340, pp. 106-109, 1999.
- [89] W.-J. Lee, D.-S. Kim, and J.-H. Kim, "Preparation and gas separation properties of asymmetric polysulfone membranes by a dual bath method," *Korean J. Chem. Eng.*, vol. 17, pp. 143-148, 2000.
- [90] J. C. Jansen, M. Macchione, and E. Drioli, "High flux asymmetric gas separation membranes of modified poly(ether ether ketone) prepared by the dry phase inversion technique," *J. Membr. Sci.*, vol. 255, pp. 167-180, 2005.
- [91] A. Sannomiya, S. Nagaoka, Y. Suzuki, M. Iwaki, and H. Kawakami, "Gas diffusion and solubility in He⁺-irradiated asymmetric polyimide membranes," *Polymer*, vol. 47, pp. 6585-6591, 2006.
- [92] A. Torres-Trueba, F. A. Ruiz-Treviño, G. Luna-Bárceñas, and C. H. Ortiz-Estrada, "Formation of integrally skinned asymmetric polysulfone gas separation membranes by supercritical CO₂," *J. Membr. Sci.*, vol. 320, pp. 431-435, 2008.
- [93] M. Iqbal, Z. Man, H. Mukhtar, and B. K. Dutta, "Solvent effect on morphology and CO₂/CH₄ separation performance of asymmetric polycarbonate membranes," *J. Membr. Sci.*, vol. 318, pp. 167-175, 2008.
- [94] T. Tezuka, T. Kobayashi, D. Muraoka, S. Nagaoka, Y. Suzuki, and H. Kawakami, "Gas transport properties of asymmetric polyimide membranes

- prepared by plasma-based ion implantation," *Polym. Adv. Technol.*, vol. 20, pp. 987-992, 2009.
- [95] F. Peng, L. Lu, H. Sun, Y. Wang, J. Liu, and Z. Jiang, "Hybrid organic-inorganic membrane: solving the tradeoff between permeability and selectivity," *Chem. Mater.*, vol. 17, pp. 6790-6796, 2005.
- [96] S. C. George and S. Thomas, "Transport phenomena through polymeric systems," *Prog. Polym. Sci.*, vol. 26, pp. 985-1017, 2001.
- [97] S. P. Nunes, K. V. Peinemann, K. Ohlrogge, A. Alpers, M. Keller, and A. T. N. Pires, "Membranes of poly(ether imide) and nanodispersed silica," *J. Membr. Sci.*, vol. 157, pp. 219-226, 1999.
- [98] C. Joly, S. Goizet, J. C. Schrotter, J. Sanchez, and M. Escoubes, "Sol-gel polyimide-silica composite membrane: gas transport properties," *J. Membr. Sci.*, vol. 130, pp. 63-74, 1997.
- [99] T. C. Merkel, Z. He, I. Pinnau, B. D. Freeman, P. Meakin, and A. J. Hill, "Effect of Nanoparticles on Gas Sorption and Transport in Poly(1-trimethylsilyl-1-propyne)," *Macromolecules*, vol. 36, pp. 6844-6855, 2003/09/01 2003.
- [100] T. S. Chung, L. Y. Jiang, Y. Li, and S. Kulprathipanja, "Mixed matrix membranes (MMMs) comprising organic polymers with dispersed inorganic fillers for gas separation," *Prog. Polym. Sci.*, vol. 32, pp. 483-507, 2007.
- [101] T. M. Gür, "Permselectivity of zeolite filled polysulfone gas separation membranes," *J. Membr. Sci.*, vol. 93, pp. 283-289, 1994.
- [102] R. Mahajan, C. M. Zimmerman, and W. J. Koros, "Fundamental and practical aspects of mixed matrix gas separation membranes," *ACS symposium Series No. 733*, pp. 277-286, 1999.
- [103] I. F. J. Vankelecom, E. Merckx, M. Luts, and J. B. Uytterhoeven, "Incorporation of Zeolites in Polyimide Membranes," *The Journal of Physical Chemistry*, vol. 99, pp. 13187-13192, 1995/08/01 1995.
- [104] I. F. J. Vankelecom, S. Van den broeck, E. Merckx, H. Geerts, P. Grobet, and J. B. Uytterhoeven, "Silylation To Improve Incorporation of Zeolites in Polyimide Films," *The Journal of Physical Chemistry*, vol. 100, pp. 3753-3758, 1996/01/01 1996.

- [105] D. Q. Vu, W. J. Koros, and S. J. Miller, "Mixed matrix membranes using carbon molecular sieves: I. Preparation and experimental results," *J. Membr. Sci.*, vol. 211, pp. 311-334, 2003.
- [106] H. Cong, M. Radosz, B. F. Towler, and Y. Shen, "Polymer-inorganic nanocomposite membranes for gas separation," *Sep. Purif. Technol.*, vol. 55, pp. 281-291, 2007.
- [107] R. M. de Vos, W. F. Maier, and H. Verweij, "Hydrophobic silica membranes for gas separation," *J. Membr. Sci.*, vol. 158, pp. 277-288, 1999.
- [108] Y.-L. Liu, C.-Y. Hsu, and K.-Y. Hsu, "Poly(methylmethacrylate)-silica nanocomposites films from surface-functionalized silica nanoparticles," *Polymer*, vol. 46, pp. 1851-1856, 2005.
- [109] S. R. Corrie, G. A. Lawrie, and M. Trau, "Quantitative Analysis and Characterization of Biofunctionalized Fluorescent Silica Particles," *Langmuir*, vol. 22, pp. 2731-2737, 2006/03/01 2006.
- [110] L. Sartore, M. Penco, F. Bignotti, I. Peroni, M. H. Gil, M. A. Ramos, and A. D'Amore, "Grafting of selected presynthesized macromonomers onto various dispersions of silica particles," *J. Appl. Polym. Sci.*, vol. 85, pp. 1287-1296, 2002.
- [111] Y.-S. Kim, K. Kusakabe, S. Morooka, and S.-M. Yang, "Preparation of Microporous Silica Membranes for Gas Separation," *Korean J. Chem. Eng.*, vol. 18, pp. 106-112, 2001.
- [112] Z. He, I. Pinnau, and A. Morisato, "Nanostructured poly(4-methyl-2-pentyne)/silica hybrid membranes for gas separation," *Desalination*, vol. 146, pp. 11-15, 2002.
- [113] Y.-W. Wang and W.-C. Chen, "Synthesis, properties, and anti-reflective applications of new colorless polyimide-inorganic hybrid optical materials," *Compos. Sci. Technol.*, vol. 70, pp. 769-775, 2010.
- [114] C. J. Cornelius and E. Marand, "Hybrid silica-polyimide composite membranes: gas transport properties," *J. Membr. Sci.*, vol. 202, pp. 97-118, 2002.
- [115] M. Sadeghi, G. Khanbabaei, A. H. S. Dehaghani, M. Sadeghi, M. A. Aravand, M. Akbarzade, and S. Khatti, "Gas permeation properties of ethylene vinyl

- acetate–silica nanocomposite membranes," *J. Membr. Sci.*, vol. 322, pp. 423-428, 2008.
- [116] K. Kusakabe, K. Ichiki, J.-i. Hayashi, H. Maeda, and S. Morooka, "Preparation and characterization of silica–polyimide composite membranes coated on porous tubes for CO₂ separation," *J. Membr. Sci.*, vol. 115, pp. 65-75, 1996.
- [117] M. Sadeghi, M. A. Semsarzadeh, and H. Moadel, "Enhancement of the gas separation properties of polybenzimidazole (PBI) membrane by incorporation of silica nano particles," *J. Membr. Sci.*, vol. 331, pp. 21-30, 2009.
- [118] M. Sadeghi, M. A. Semsarzadeh, M. Barikani, and M. Pourafshari Chenar, "Gas separation properties of polyether-based polyurethane–silica nanocomposite membranes," *J. Membr. Sci.*, vol. 376, pp. 188-195, 2011.
- [119] J. H. Kim and Y. M. Lee, "Gas permeation properties of poly(amide-6-b-ethylene oxide)–silica hybrid membranes," *J. Membr. Sci.*, vol. 193, pp. 209-225, 2001.
- [120] B. N. Nair, W. J. Elferink, K. Keizer, and H. Verweij, "Sol–Gel Synthesis and Characterization of Microporous Silica Membranes I: SAXS Study on the Growth of Polymeric Structures," *J. Colloid Interface Sci.*, vol. 178, pp. 565-570, 1996.
- [121] C. R. Silva and C. Airoidi, "Acid and Base Catalysts in the Hybrid Silica Sol–Gel Process," *J. Colloid Interface Sci.*, vol. 195, pp. 381-387, 1997.
- [122] W. Kim, S. Chung, S. B. Park, S. C. Lee, C. Kim, and D. D. Sung, "Sol-Gel Method for the Matrix of Chloride-Selective Membranes Doped with Tridodecylmethylammonium Chloride," *Anal. Chem.*, vol. 69, pp. 95-98, 1997.
- [123] Y. Xia, Z. Liangyinga, and W. Sasa, "Pore size and pore-size distribution control of porous silica," *Sens. Actuators, B*, vol. 25, pp. 347-352, 1995.
- [124] Y.-C. Chou, Y.-Y. Wang, and T. E. Hsieh, "Transparent photo-curable copolyacrylate/silica nanocomposites prepared by sol-gel process," *J. Appl. Polym. Sci.*, vol. 105, pp. 2073-2082, 2007.
- [125] P. Hajji, L. David, J. F. Gerard, J. P. Pascault, and G. Vigier, "Synthesis, structure, and morphology of polymer–silica hybrid nanocomposites based on

- hydroxyethyl methacrylate," *J. Polym. Sci., Part B: Polym. Phys.*, vol. 37, pp. 3172-3187, 1999.
- [126] F. Yang and G. L. Nelson, "PMMA/silica nanocomposite studies: Synthesis and properties," *J. Appl. Polym. Sci.*, vol. 91, pp. 3844-3850, 2004.
- [127] C. J. Cornelius and E. Marand, "Hybrid inorganic–organic materials based on a 6FDA–6FpDA–DABA polyimide and silica: physical characterization studies," *Polymer*, vol. 43, pp. 2385-2400, 2002.
- [128] T. Suzuki and Y. Yamada, "Physical and Gas Transport Properties of Novel Hyperbranched Polyimide – Silica Hybrid Membranes," *Polym. Bull.*, vol. 53, pp. 139-146, 2005.
- [129] C. Hibshman, C. J. Cornelius, and E. Marand, "The gas separation effects of annealing polyimide–organosilicate hybrid membranes," *J. Membr. Sci.*, vol. 211, pp. 25-40, 2003.
- [130] X. Hu, H. Cong, Y. Shen, and M. Radosz, "Nanocomposite Membranes for CO₂ Separations: □ Silica/Brominated Poly(phenylene oxide)," *Industrial & Engineering Chemistry Research*, vol. 46, pp. 1547-1551, 2007/02/01 2007.
- [131] M. F. A. Wahab, A. F. Ismail, and S. J. Shilton, "Studies on gas permeation performance of asymmetric polysulfone hollow fiber mixed matrix membranes using nanosized fumed silica as fillers," *Sep. Purif. Technol.*, vol. 86, pp. 41-48, 2012.
- [132] S. Kim, L. Chen, J. K. Johnson, and E. Marand, "Polysulfone and functionalized carbon nanotube mixed matrix membranes for gas separation: Theory and experiment," *J. Membr. Sci.*, vol. 294, pp. 147-158, 2007.
- [133] T.-S. Chung, S. S. Chan, R. Wang, Z. Lu, and C. He, "Characterization of permeability and sorption in Matrimid/C60 mixed matrix membranes," *J. Membr. Sci.*, vol. 211, pp. 91-99, 2003.
- [134] Y. Li, H.-M. Guan, T.-S. Chung, and S. Kulprathipanja, "Effects of novel silane modification of zeolite surface on polymer chain rigidification and partial pore blockage in polyethersulfone (PES)–zeolite A mixed matrix membranes," *J. Membr. Sci.*, vol. 275, pp. 17-28, 2006.
- [135] A. M. W. Hillock, S. J. Miller, and W. J. Koros, "Crosslinked mixed matrix membranes for the purification of natural gas: Effects of sieve surface modification," *J. Membr. Sci.*, vol. 314, pp. 193-199, 2008.

- [136] H. H. Yong, H. C. Park, Y. S. Kang, J. Won, and W. N. Kim, "Zeolite-filled polyimide membrane containing 2,4,6-triaminopyrimidine," *J. Membr. Sci.*, vol. 188, pp. 151-163, 2001.
- [137] Y. Li, T.-S. Chung, and S. Kulprathipanja, "Novel Ag⁺-zeolite/polymer mixed matrix membranes with a high CO₂/CH₄ selectivity," *AIChE J.*, vol. 53, pp. 610-616, 2007.
- [138] S. Husain and W. J. Koros, "Mixed matrix hollow fiber membranes made with modified HSSZ-13 zeolite in polyetherimide polymer matrix for gas separation," *J. Membr. Sci.*, vol. 288, pp. 195-207, 2007.
- [139] P. Yang, G. Wang, X. Xia, Y. Takezawa, H. Wang, S. Yamada, Q. Du, and W. Zhong, "Preparation and thermo-mechanical properties of heat-resistant epoxy/silica hybrid materials," *Polym. Eng. Sci.*, vol. 48, pp. 1214-1221, 2008.
- [140] X. Y. Shang, Z. K. Zhu, J. Yin, and X. D. Ma, "Compatibility of Soluble Polyimide/Silica Hybrids Induced by a Coupling Agent," *Chem. Mater.*, vol. 14, pp. 71-77, 2002.
- [141] S. P. Nunes, K. V. Peinemann, K. Ohlrogge, A. Alpers, M. Keller, and A. T. N. Pires, "Membranes of poly(ether imide) and nanodispersed silica," *J. Membr. Sci.*, vol. 157, pp. 219-226, 1999.
- [142] Y. H. Hu, C. Y. Chen, and C. C. Wang, "Viscoelastic properties and thermal degradation kinetics of silica/PMMA nanocomposites," *Polym. Degrad. Stab.*, vol. 84, pp. 545-553, 2004.
- [143] G. A. Wang, C. C. Wang, and C. Y. Chen, "The disorderly exfoliated LDHs/PMMA nanocomposites synthesized by in situ bulk polymerization: The effects of LDH-U on thermal and mechanical properties," *Polym. Degrad. Stab.*, vol. 91, pp. 2443-2450, 2006.
- [144] G. L. Jadav and P. S. Singh, "Synthesis of novel silica-polyamide nanocomposite membrane with enhanced properties," *J. Membr. Sci.*, vol. 328, pp. 257-267, 2009.
- [145] Y. Sun, Z. Zhang, K. S. Moon, and C. P. Wong, "Glass transition and relaxation behavior of epoxy nanocomposites," *J. Polym. Sci., Part B: Polym. Phys.*, vol. 42, pp. 3849-3858, 2004.

- [146] X.-G. Li and M.-R. Huang, "Thermal degradation of bisphenol A polysulfone by high-resolution thermogravimetry," *React. Funct. Polym.*, vol. 42, pp. 59-64, 1999.
- [147] B. Zornoza, S. Irusta, C. Tellez, and J. Coronas, "Mesoporous Silica Sphere-Polysulfone Mixed Matrix Membranes for Gas Separation," *Langmuir*, vol. 25, pp. 5903-5909, 2009.
- [148] S. A. Hashemifard, A. F. Ismail, and T. Matsuura, "Prediction of gas permeability in mixed matrix membranes using theoretical models," *J. Membr. Sci.*, vol. 347, pp. 53-61, 2010.
- [149] P. Rajinder, "Permeation models for mixed matrix membranes," *J. Colloid Interface Sci.*, vol. 317, pp. 191-198, 2008.
- [150] P. Rajinder, "On the Lewis–Nielsen model for thermal/electrical conductivity of composites," *Composites Part A: Applied Science and Manufacturing*, vol. 39, pp. 718-726, 2008.
- [151] L. E. Nielsen, "Thermal conductivity of particulate-filled polymers," *J. Appl. Polym. Sci.*, vol. 17, pp. 3819-3820, 1973.
- [152] R. H. B. Bouma, A. Checchetti, G. Chidichimo, and E. Drioli, "Permeation through a heterogeneous membrane: the effect of the dispersed phase," *J. Membr. Sci.*, vol. 128, pp. 141-149, 1997.
- [153] H. S. Göktürk, T. J. Fiske, and D. M. Kalyon, "Effects of particle shape and size distributions on the electrical and magnetic properties of nickel/polyethylene composites," *J. Appl. Polym. Sci.*, vol. 50, pp. 1891-1901, 1993.
- [154] E. Rudnik and Z. Dobkowski, "Investigations and molecular modeling of some thermophysical properties of polysulfones," *J. Therm. Anal. Calorim.*, vol. 45, pp. 1153-1158, 1995.
- [155] D. Q. Vu, W. J. Koros, and S. J. Miller, "High Pressure CO₂/CH₄ Separation Using Carbon Molecular Sieve Hollow Fiber Membranes," *Industrial & Engineering Chemistry Research*, vol. 41, pp. 367-380, 2002/02/01 2001.
- [156] H. Kim, J. Han, K. Chun, Y. Shul, and Y. Joe, "Synthesis of organic-inorganic composite membrane by sol-gel process," *Korean J. Chem. Eng.*, vol. 12, pp. 405-409, 1995.

- [157] H.-S. Roh, J.-S. Chang, and S.-E. Park, "Synthesis of mesoporous silica in acidic condition by solvent evaporation method," *Korean J. Chem. Eng.*, vol. 16, pp. 331-337, 1999.
- [158] B. H. Stuart, *Polymer analysis*: J. Wiley, 2002.
- [159] M. J. Forrest, *Analysis of thermoset materials, precursors and products*: Rapra Technology Limited, 2003.
- [160] Y. C. Ning and R. R. Ernst, *Structural identification of organic compounds with spectroscopic techniques*: Wiley-VCH, 2005.
- [161] C. R. Brundle, C. A. Evans, and S. Wilson, *Encyclopedia of materials characterization: surfaces, interfaces, thin films*: Butterworth-Heinemann, 1992.
- [162] J. Park, S. Oh, H. Lee, H. Kim, and K. Yoo, "Kinetic analysis of thermal decomposition of polymer using a dynamic model," *Korean J. Chem. Eng.*, vol. 17, pp. 489-496, 2000/09/01 2000.
- [163] S. Maitra, N. Bandyopadhyay, S. Das, A. J. Pal, and J. Pramanik, "Non-Isothermal Decomposition Kinetics of Alkaline Earth Metal Carbonates," *J. Am. Ceram. Soc.*, vol. 90, pp. 1299-1303, 2007.
- [164] A. O. Aboyade, T. J. Hugo, M. Carrier, E. L. Meyer, R. Stahl, J. H. Knoetze, and J. F. Görgens, "Non-isothermal kinetic analysis of the devolatilization of corn cobs and sugar cane bagasse in an inert atmosphere," *Thermochim. Acta*, vol. 517, pp. 81-89, 2011.
- [165] L. H. Sperling, *Introduction to physical polymer science*: Wiley-Interscience, 2006.
- [166] J. Asad, "Membranes for solubility-based gas separation applications," *Chem. Eng. J.*, vol. 112, pp. 219-226, 2005.
- [167] S. C. Pesek and W. J. Koros, "Aqueous quenched asymmetric polysulfone membranes prepared by dry/wet phase separation," *J. Membr. Sci.*, vol. 81, pp. 71-88, 1993.
- [168] B. Krause, K. Diekmann, N. F. A. van der Vegt, and M. Wessling, "Open Nanoporous Morphologies from Polymeric Blends by Carbon Dioxide Foaming," *Macromolecules*, vol. 35, pp. 1738-1745, 2002/02/01 2002.

- [169] D. Walsh and S. Rostami, "The miscibility of high polymers: The role of specific interactions Key Polymers Properties and Performance." vol. 70, ed: Springer Berlin / Heidelberg, 1985, pp. 119-169.
- [170] S. S. Hosseini, M. M. Teoh, and T. S. Chung, "Hydrogen separation and purification in membranes of miscible polymer blends with interpenetration networks," *Polymer*, vol. 49, pp. 1594-1603, 2008.
- [171] J. Prinios and C. Panayiotou, "Glass transition temperature in hydrogen-bonded polymer mixtures," *Polymer*, vol. 36, pp. 1223-1227, 1995.
- [172] S. Sridhar, R. S. Veerapur, M. B. Patil, K. B. Gudasi, and T. M. Aminabhavi, "Matrimid polyimide membranes for the separation of carbon dioxide from methane," *J. Appl. Polym. Sci.*, vol. 106, pp. 1585-1594, 2007.
- [173] R. Raslan and A. W. Mohammad, "Polysulfone/pluronic F127 blend ultrafiltration membranes: Preparation and characterizations," *J. Appl. Sci.*, vol. 10, pp. 2628–2632, 2010.
- [174] L. Y. Jiang, T. S. Chung, and S. Kulprathipanja, "An investigation to revitalize the separation performance of hollow fibers with a thin mixed matrix composite skin for gas separation," *J. Membr. Sci.*, vol. 276, pp. 113-125, 2006.
- [175] A. Linares and J. L. Acosta, "Structural characterization of polymer blends based on polysulfones," *J. Appl. Polym. Sci.*, vol. 92, pp. 3030-3039, 2004.
- [176] *Material Data Center Datasheets of Udel® P-1800 Polysulfone*. Available: www.materialdatacenter.com/ms/en/Udel/Solvay/Udel%C2%AE+P-1800/7b32bd68/2290
- [177] *Huntsman Matrimid 5218 Resin*. Available: www.lindberg-lund.fi/files/Tekniske%20datablad/VAN-5218-TD.pdf
- [178] K. Haraya, K. Obata, N. Itoh, Y. Shndo, T. Hakuta, and H. Yoshitome, "Gas permeation and separation by an asymmetric polyimide hollow fiber membrane," *J. Membr. Sci.*, vol. 41, pp. 23-35, 1989.
- [179] W. J. Koros, A. H. Chan, and D. R. Paul, "Sorption and transport of various gases in polycarbonate," *J. Membr. Sci.*, vol. 2, pp. 165-190, 1977.
- [180] W. J. Koros, R. T. Chern, V. Stannett, and H. B. Hopfenberg, "A model for permeation of mixed gases and vapors in glassy polymers," *Journal of Polymer Science: Polymer Physics Edition*, vol. 19, pp. 1513-1530, 1981.

- [181] J. Barzin and B. Sadatnia, "Correlation between macrovoid formation and the ternary phase diagram for polyethersulfone membranes prepared from two nearly similar solvents," *J. Membr. Sci.*, vol. 325, pp. 92-97, 2008.
- [182] C. A. Smolders, A. J. Reuvers, R. M. Boom, and I. M. Wienk, "Microstructures in phase-inversion membranes. Part 1. Formation of macrovoids," *J. Membr. Sci.*, vol. 73, pp. 259-275, 1992.
- [183] W. R. Vieth, J. M. Howell, and J. H. Hsieh, "Dual sorption theory," *J. Membr. Sci.*, vol. 1, pp. 177-220, 1976.
- [184] C. A. Gracia-Fernández, S. Gómez-Barreiro, S. Ruíz-Salvador, and R. Blaine, "Study of the degradation of a thermoset system using TGA and modulated TGA," *Prog. Org. Coat.*, vol. 54, pp. 332-336, 2005.
- [185] S. Völker and T. Rieckmann, "Thermokinetic investigation of cellulose pyrolysis — impact of initial and final mass on kinetic results," *J. Anal. Appl. Pyrolysis*, vol. 62, pp. 165-177, 2002.
- [186] C. Xiao, L. Weng, and L. Zhang, "Improvement of physical properties of crosslinked alginate and carboxymethyl konjac glucomannan blend films," *J. Appl. Polym. Sci.*, vol. 84, pp. 2554-2560, 2002.
- [187] T. Muraki, M. Ueta, E. Ihara, and K. Inoue, "Enhancement of thermal stability of polystyrene and poly(methyl methacrylate) by cyclotriphosphazene derivatives," *Polym. Degrad. Stab.*, vol. 84, pp. 87-93, 2004.
- [188] S. Tiptipakorn, S. Damrongsakkul, S. Ando, K. Hemvichian, and S. Rimdusit, "Thermal degradation behaviors of polybenzoxazine and silicon-containing polyimide blends," *Polym. Degrad. Stab.*, vol. 92, pp. 1265-1278, 2007.
- [189] B. D. Reid, F. A. Ruiz-Trevino, I. H. Musselman, K. J. Balkus, and J. P. Ferraris, "Gas Permeability Properties of Polysulfone Membranes Containing the Mesoporous Molecular Sieve MCM-41," *Chem. Mater.*, vol. 13, pp. 2366-2373, 2001/07/01 2001.
- [190] N. Leblanc, D. Le Cerf, C. Chappey, D. Langevin, M. Métayer, and G. Muller, "Influence of solvent and non-solvent on polyimide asymmetric membranes formation in relation to gas permeation," *Sep. Purif. Technol.*, vol. 22-23, pp. 277-285, 2001.
- [191] I. D. Sharpe, A. F. Ismail, and S. J. Shilton, "A study of extrusion shear and forced convection residence time in the spinning of polysulfone hollow fiber

- membranes for gas separation," *Sep. Purif. Technol.*, vol. 17, pp. 101-109, 1999.
- [192] S. J. Shilton, A. F. Ismail, P. J. Gough, I. R. Dunkin, and S. L. Gallivan, "Molecular orientation and the performance of synthetic polymeric membranes for gas separation," *Polymer*, vol. 38, pp. 2215-2220, 1997.
- [193] A. Romero, M. Parentis, A. Habert, and E. Gonzo, "Synthesis of polyetherimide/silica hybrid membranes by the sol-gel process: influence of the reaction conditions on the membrane properties," *Journal of Materials Science*, vol. 46, pp. 4701-4709, 2011.
- [194] S. Kim, E. Marand, J. Ida, and V. V. Guliyants, "Polysulfone and Mesoporous Molecular Sieve MCM-48 Mixed Matrix Membranes for Gas Separation," *Chem. Mater.*, vol. 18, pp. 1149-1155, 2006/03/01 2006.
- [195] M. S. Boroglu, I. Boz, and M. A. Gurkaynak, "Structural characterization of silica modified polyimide membranes," *Polym. Adv. Technol.*, vol. 17, pp. 6-11, 2006.
- [196] S. Wen, C. Gong, W.-C. Tsen, Y.-C. Shu, and F.-C. Tsai, "Sulfonated poly(ether sulfone)/silica composite membranes for direct methanol fuel cells," *J. Appl. Polym. Sci.*, vol. 116, pp. 1491-1498, 2010.
- [197] M. Moaddeb and W. J. Koros, "Gas transport properties of thin polymeric membranes in the presence of silicon dioxide particles," *J. Membr. Sci.*, vol. 125, pp. 143-163, 1997.
- [198] C. Joly, M. Smaïhi, L. Porcar, and R. D. Noble, "Polyimide-Silica Composite Materials: How Does Silica Influence Their Microstructure and Gas Permeation Properties?," *Chem. Mater.*, vol. 11, pp. 2331-2338, 1999/09/01 1999.
- [199] Y. Chujo, "Organic-inorganic hybrid materials," *Curr. Opin. Solid State Mater. Sci.*, vol. 1, pp. 806-811, 1996.
- [200] F. Al-Sagheer, A. A. M. Ali, S. Muslim, and Z. Ahmad, "Thermal and mechanical properties of chemically bonded aramid-silica nano-composites," *Science and Technology of Advanced Materials*, vol. 7, pp. 111-118, 2006.
- [201] P. Musto, G. Ragosta, G. Scarinzi, and L. Mascia, "Polyimide-silica nanocomposites: spectroscopic, morphological and mechanical investigations," *Polymer*, vol. 45, pp. 1697-1706, 2004.

- [202] Y. Chen and J. O. Iroh, "Synthesis and Characterization of Polyimide/Silica Hybrid Composites," *Chem. Mater.*, vol. 11, pp. 1218-1222, 1999/05/01 1999.
- [203] R. M. de Vos and H. Verweij, "Improved performance of silica membranes for gas separation," *J. Membr. Sci.*, vol. 143, pp. 37-51, 1998.

PUBLICATION LIST

International Journals:

1. Sikander Rafiq, Zakaria Man, Abdulhalim Maulud, Nawshad Muhammad and Saikat Maitra, "Separation of CO₂ from CH₄ using Polysulfone/Polyimide Silica Nanocomposite Membranes" Separation and Purification Technology- Elsevier, Vol. 92 (2012) pp. 162-172. (Impact Factor: 2.921)
2. Sikander Rafiq, Zakaria Man, Abdulhalim Maulud, Nawshad Muhammad and Saikat Maitra, "Preparation and Characterization of Blended Composite Membranes" Journal of Advanced Materials Research Journal- TransTech Publications (TTS), Vols. 488-489 (2012) pp. 506-510. (Scopus Indexed)
3. Sikander Rafiq, Zakaria Man, Saikat Maitra, Nawshad Muhammad and Farooq Ahmad, "Kinetics of Thermal Degradation of PSF/PI Blended Polymeric Membranes", Journal of Applied Polymer Science - Wiley, Vol. 123 (2012) pp. 3755-3763. (Impact Factor : 1.24)
4. Sikander Rafiq, Zakaria Man, Abdulhalim Maulud, Nawshad Muhammad and Saikat Maitra, "Effect of Varying Solvents Compositions on Morphology and Gas Permeation properties on Membranes Blends for CO₂ Separation from Natural gas", Journal of Membrane Science Vol. 378(2011) pp.444-452 (Impact Factor : 3.850)
5. Sikander Rafiq, Zakaria Man, Saikat Maitra, Farooq Ahmad, Nawshad Muhammad, "Preparation of Asymmetric PSF/PI blended Membranes for CO₂ Separation", Korean Journal of Chemical Engineering, SpringerLink. Vol. 28 (2011) pp. 2050-2056. (Impact Factor: 0.991)
6. S. Rafiq, Z. Man, F. Ahmad, S. Maitra, "Silica-Polymer Nanocomposite Membranes for Gas Separation – a Review, Part I", Interceram. Vol.59 (2010) pp. 341-349. (Scopus Indexed).

7. S. Rafiq, Z. Man, F. Ahmad, S. Maitra, "Silica-Polymer Nanocomposite Membranes for Gas Separation – a Review, Part II", *Interceram*. Vol. 60 (2011) 8-13.(Scopus Indexed).

Local Journal:

Sikander Rafiq, Farooq Ahmad, Zaka Man, H. Mukhtar, Azmi Shariff, Saikat Maitra, "Separation of Carbon Dioxide from Natural Gas through Silica-Polymer Mixed Matrix Membranes", *Intoceram*, 45 (2009) 85.

Patent and Copyright Filed:

Zakaria Man, Sikander Rafiq, Abdulhalim Maulud, "Separation of CO₂ from CH₄ using Polysulfone/Polyimide Silica Nanocomposite Membranes for Natural Gas Purification" (PI2012700952).

International Journal (under review):

Sikander Rafiq, Abdulhalim Maulud, Zakaria Man, M.I. Abdul Mutalib and Nawshad Muhammad, "Investigation of Particle Geometry Effects on Permeance of Mixed Matrix Membranes for Gas Separation through Modeling Approach" *Separation and Purification Technology- Elsevier*. (Impact Factor: 2.921)

Conferences Presentations

1. 2nd International Conference on Process Engineering and Advance Material, ESTCON 2012, held in Kuala Lumpur Convention Centre, Malaysia. A Presentation on "Comparative Study on Theoretical Models for Evaluating Permeation of Mixed Matrix Membranes for Gas Separation".
2. 2nd International Conference on Key Engineering Materials (ICKEM) 2012, held in Singapore. A Presentation on "Preparation and Characterization of Blended Composite Membranes".
3. 5th International Conference of Chemistry and Environment, 2011 held in Port Dickson-Malaysia. A Presentation on "Effect of Solvents on Morphology and Permeation Characterization of PSF/PI Blended Membranes for CO₂ Separation from Natural gas."

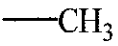
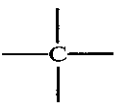
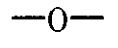
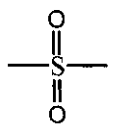
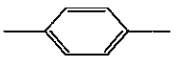
4. Asia Nano Camp (ANC) 2010 held at University of Malaya in Kuala Lumpur-Malaysia. A presentation on “Development of Mixed Matrix membranes for CO₂ separation from Natural Gas”.
5. XXVI EMS Summer School 2009 on Membrane Technology for CO₂ separation held in Geesthacht- Germany. A Poster Presentation on “Separation of Carbon Dioxide from Natural Gas through PSF-PI Blended Membranes”.

APPENDIX A

(Calculations of Solubility Parameter)

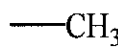
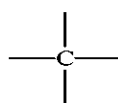
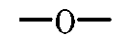
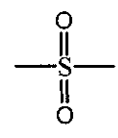

A.1 Example Calculations of Solubility Parameter

Table A.1 Group contribution of PSF functional group

Functional group	F_{di} ($J^{1/2} \cdot cm^{3/2} \cdot mol^{-1}$)	F_{pi} ($J^{1/2} \cdot cm^{3/2} \cdot mol^{-1}$)	F_{hi} ($J \cdot mol^{-1}$)	Frequency
	420	0	0	2
	-70	0	0	1
	100	401	3000	1
	591	0	13490	1
	1270	110	0	4

From Table A.1, the total group contribution component of PSF can be calculated as in the following Table A.2

Table A.2 Total group contribution of PSF structure

Functional group	F_{di} ($J^{1/2} \cdot cm^{3/2} \cdot mol^{-1}$)	F_{pi}^2 ($J^{1/2} \cdot cm^{3/2} \cdot mol^{-1}$)	F_{hi} ($J \cdot mol^{-1}$)
	840	0	0
	-70	0	0
	100	160801	3000
	591	0	13490
	5080	193600	0
Total	6541	354401	16490

The solubility parameter component of PSF is then determined from Van-Kravelen and Hoftyzer's method by using the following equations:

$$\delta_d = \frac{\sum F_{di}}{V}; \delta_p = \frac{\sqrt{\sum F_{pi}^2}}{V}; \delta_h = \frac{\sqrt{\sum E_{hi}}}{V}$$

The molar volume, V is determined from molecular weight, M of PSF (442.5g/mol) and ρ (1.2 g/cm³), calculated as:

$$V = \frac{M}{\rho} = \frac{442.5}{1.23} = 359.77 \text{ cm}^3 / \text{mole}$$

Thus solubility parameter of PSF is calculated as:

$$\delta_d = \frac{\sum F_{di}}{V} = \frac{6541}{359.77} = 18.18(\text{MPa})^{1/2}$$

$$\delta_p = \frac{\sqrt{\sum F_{pi}^2}}{V} = \frac{\sqrt{354401}}{359.77} = 1.65(\text{MPa})^{1/2}$$

$$\delta_h = \frac{\sqrt{\sum E_{hi}}}{V} = \frac{\sqrt{16490}}{359.77} = 6.77(\text{MPa})^{1/2}$$

Thus the overall solubility parameter of PSF is calculated as:

$$\begin{aligned} \delta &= \sqrt{\delta_d^2 + \delta_p^2 + \delta_h^2} \\ &= \sqrt{18.18^2 + 1.658^2 + 6.77^2} \\ &= 19.47(\text{MPa})^{1/2} \end{aligned}$$

Similarly as an example of solvent NMP, the overall solubility parameter can be calculated as:

Table A.3 Group contribution of PSF functional group

Functional group	F_{di} ($J^{1/2} \cdot cm^{3/2} \cdot mol^{-1}$)	F_{pi} ($J^{1/2} \cdot cm^{3/2} \cdot mol^{-1}$)	F_{hi} ($J \cdot mol^{-1}$)	Frequency
$\diagup C=O$	290	770	2000	1
$—CH_2—$	270	0	0	3
$—CH_3$	420	0	0	1
Tertiary amine	20	800	5000	1

From Table A.2, the total group contribution component of PSF can be calculated as in the following Table A.4

Table A.4 Total group contribution of PSF structure

Functional group	F_{di} ($J^{1/2} \cdot cm^{3/2} \cdot mol^{-1}$)	F_{pi}^2 ($J^{1/2} \cdot cm^{3/2} \cdot mol^{-1}$)	F_{hi} ($J \cdot mol^{-1}$)
$\diagup C=O$	290	592900	2000
$—CH_2—$	810	0	0
$—CH_3$	420	0	0
Tertiary amine	20	64000	5000
Total	1540	1232900	7000

The molar volume, V of NMP is calculated to be:

$$V = \frac{M}{\rho} = \frac{99.13}{1.03} = 96.24 \text{ cm}^3 / \text{mole}$$

Thus solubility parameter of PSF is calculated as:

$$\delta_d = \frac{\sum F_{di}}{V} = \frac{1540}{96.24} = 16 (\text{MPa})^{1/2}$$

$$\delta_p = \frac{\sqrt{\sum F_{pi}^2}}{V} = \frac{\sqrt{1232900}}{96.24} = 11.53(\text{MPa})^{1/2}$$

$$\delta_h = \sqrt{\frac{\sum E_{hi}}{V}} = \sqrt{\frac{7000}{96.24}} = 8.52(\text{MPa})^{1/2}$$

Thus the overall solubility parameter of PSF is calculated as:

$$\delta = \sqrt{\delta_d^2 + \delta_p^2 + \delta_h^2}$$

$$= \sqrt{16^2 + 11.53^2 + 8.52^2}$$

$$= 21.47(\text{MPa})^{1/2}$$

APPENDIX B

(Membrane Thickness and Density)

B.1 Membrane Thickness and Density

Membrane thickness is measured from twelve various points by using micrometer screw gauge. For each membrane, the area for measuring the thickness was kept constant ($L \times W = 144 \text{ cm}^2$).

The densities of the membranes were then measured by using the buoyancy measurement approach in which the membrane sample was weighted in the air followed by weighing after being immersed in water at 25°C . Volumes of the membrane sample were obtained from the weight difference divided by the density of water. Eventually, dividing the membrane sample weight in air from its volume, the density of the membrane sample was obtained.

Table B.1 Thickness and Density of Membranes

Solvent		Polymer Blends		Membrane Thickness-(SEM)	Membrane Density
Compositions in Casting Solution (NMP/DCM) (%)	PSF (%)	PI (%)	(μm)	(g/cm^3)	
80/20	100	0	40 ± 0.8	1.152	
	95	5	40 ± 0.5	1.153	
	90	10	36 ± 0.6	1.149	
	85	15	41 ± 0.7	1.154	
	80	20	36 ± 0.5	1.148	
50/50	100	0	75 ± 0.6	1.180	
	95	5	73 ± 0.5	1.179	
	90	10	80 ± 0.5	1.182	
	85	15	83 ± 0.6	1.184	
	80	20	80 ± 0.8	1.183	
20/80	100	0	136 ± 0.7	1.226	
	95	5	135 ± 0.6	1.225	
	90	10	139 ± 0.8	1.228	
	85	15	138 ± 0.8	1.227	
	80	20	133 ± 0.9	1.225	

APPENDIX C

(Results and Calculations of Some Gas Permeation Data Records)

C.1 Example Calculations of the Gas Permeance and the CO₂/CH₄ Ideal Selectivity

The permeance of the CO₂ and CH₄ gases was determined by passing the gas at a certain volumetric flow rate through the membrane. It was then followed by measuring the time taken to flow the gas in the bubble soap flowmeter. All of the experiments were carried out at 25°C, by varying the upstream feed gas from 2-10 barg under steady state conditions.

An example calculation is shown below for the PSF membrane having an effective area of 14.52 cm². The time taken to flow a 2.0 cm³ of CO₂ was 24.59 seconds at 2 bar feed pressure. The CO₂ permeance was determined as follows:

Step1: CO₂ volumetric flow rate, Q :

$$\begin{aligned} Q &= \frac{\Delta V}{\Delta t} \\ &= \frac{2.0}{24.58} = 8.13 \times 10^{-2} \text{ cm}^3/\text{s} \end{aligned}$$

Step2: The Q is then corrected to standard temperature and pressure (STP). So Q_{STP} is:

$$\begin{aligned} Q_{\text{STP}} &= \frac{T_{\text{STP}}}{T_{25^\circ\text{C}}} \times Q \\ Q_{\text{STP}} &= \frac{273\text{K}}{298\text{K}} \times 8.13 \times 10^{-2} \text{ cm}^3/\text{s} \\ &= 7.45 \times 10^{-2} \text{ cm}^3 (\text{STP})/\text{s} \end{aligned}$$

Step 3: The CO₂ flux J, is then calculated as:

$$\begin{aligned} J &= \frac{Q_{\text{STP}}}{A} \\ &= \frac{7.45 \times 10^{-2}}{14.52} \\ &= 5.131 \times 10^{-3} \text{ cm}^3 (\text{STP})/\text{cm}^2 \cdot \text{s} \end{aligned}$$

Step 4: The CO₂ permeance, $\frac{P}{l}$ is then calculated by using the following formula:

$$\begin{aligned} \frac{P}{l} &= \frac{J}{\Delta p} \\ &= \frac{5.131 \times 10^{-3} \frac{\text{cm}^3(\text{STP})}{\text{cm}^2 \cdot \text{s}}}{2 \text{ bar} \times 76 \frac{\text{cmHg}}{\text{bar}}} \\ &= 33.76 \times 10^{-6} \frac{\text{cm}^3(\text{STP})}{\text{cm}^2 \cdot \text{cmHg} \cdot \text{s}} \\ &= 33.76 \text{ GPU (Gas Permeation Unit)} \end{aligned}$$

Similarly, the CH₄ permeance was calculated by following the same steps. Under the same experimental conditions, the permeance of the CH₄ at 1.288 GPU was obtained. So CO₂/CH₄ ideal selectivity, $\alpha_{\text{CO}_2/\text{CH}_4}$ is calculated by taking the ratios permeance of CO₂ over CH₄:

$$\begin{aligned} \alpha_{\text{CO}_2/\text{CH}_4} &= \frac{(P/l)_{\text{CO}_2}}{(P/l)_{\text{CH}_4}} \\ &= \frac{33.76}{1.288} = 26.21 \end{aligned}$$

C.2 Example Calculations for CO₂/CH₄ Mixed Gas Permeance and Selectivity

For mixed CO₂/CH₄ gas analysis, Steps 1-4 from Appendix C.1 are carried out to obtain the total permeance of gas mixtures followed by the compositional analysis under GC.

As an example, the permeation evaluation through a PSF/PI-20% membrane with 30%/70% CO₂/CH₄ mixtures was calculated at 10 bar feed pressure from the total

permeance, $(P/l)_{\text{Mix}}$ 34.45 GPU obtained in step 4. The permeate gas mixture was then tested under GC to obtain compositions of CO_2 and CH_4 gases as 3.28% and 96.72%, respectively. The CO_2 and CH_4 permeance is then calculated as:

$$\begin{aligned}(P/l)_{\text{CO}_2} &= 96.72\% \times (P/l)_{\text{Mix}} \\ &= (0.9672) \times 34.45 \\ &= 33.32 \text{ GPU}\end{aligned}$$

Similarly, $(P/l)_{\text{CH}_4} = 1.13 \text{ GPU}$

So, the selectivity of the gas mixture is calculated by the following formula:

$$\begin{aligned}\alpha_{\text{CO}_2/\text{CH}_4} &= \frac{(P/l)_{\text{CO}_2}}{(P/l)_{\text{CH}_4}} \\ &= \frac{33.32}{1.13} = 29.5\end{aligned}$$

Table C.1 Gas permeation results from PSF membranes

Membranes	Runs	P (bar)	t_{CO_2} (s)	t_{CH_4} (s)	V (cm ³)	(P/) CO_2 (GPU)	(P/) CH_4 (GPU)	Selectivity CO_2/CH_4
M1	1		24.59	644.50	2.0	33.76	1.29	26.21
	2	2	24.69	637.61	2.0	33.62	1.30	25.82
	Average		24.64	641.06	2.0	33.69	1.30	26.02
	Std. Dev.		0.07	4.87	0.0	0.10	0.01	0.27
M2	1		13.26	346.46	2.0	31.29	1.20	26.12
	2	4	13.28	342.48	2.0	31.26	1.21	25.80
	Average		13.27	344.47	2.0	31.28	1.21	25.96
	Std. Dev.		0.01	2.81	0.0	0.02	0.01	0.23
M3	1		9.22	232.42	2.0	30.00	1.19	25.20
	2	6	9.19	245.10	2.0	30.10	1.13	26.66
	Average		9.21	238.76	2.0	30.05	1.16	25.93
	Std. Dev.		0.01	4.49	0.0	0.04	0.02	0.52
M4	1		6.91	180.94	2.0	30.05	1.15	26.19
	2	8	7.02	180.00	2.0	29.56	1.15	25.64
	Average		6.96	180.47	2.0	29.80	1.15	25.92
	Std. Dev.		0.08	0.66	0.0	0.34	0.00	0.39
M5	1		5.64	147.64	2.0	29.41	1.12	26.16
	2	10	5.57	142.89	2.0	29.82	1.16	25.66
	Average		5.61	145.26	2.0	29.62	1.14	25.91
	Std. Dev.		0.05	3.36	0.0	0.29	0.03	0.35

Table C.2 Gas permeation results from PSF/PI-20% membranes

Membranes	Runs	P (bar)	t_{CO_2} (s)	t_{CH_4} (s)	V (cm ³)	(P/I)CO ₂ (GPU)	(P/I)CH ₄ (GPU)	Selectivity CO ₂ /CH ₄
M1	1		21.04	602.06	2.0	39.45	1.38	28.61
	2		21.17	609.07	2.0	39.22	1.36	28.78
	Average	2	21.11	605.57	2.0	39.34	1.37	28.69
	Std. Dev.		0.09	4.96	0.0	0.16	0.01	0.12
M2	1		11.17	326.05	2.0	37.14	1.27	29.17
	2		11.32	316.62	2.0	36.67	1.31	27.97
	Average	4	11.25	321.33	2.0	36.91	1.29	28.57
	Std. Dev.		0.10	6.67	0.0	0.34	0.03	0.85
M3	1		7.74	219.31	2.0	35.75	1.26	28.34
	2		7.89	224.61	2.0	35.05	1.23	28.45
	Average	6	7.82	221.96	2.0	35.40	1.25	28.39
	Std. Dev.		0.11	3.75	0.0	0.49	0.02	0.08
M4	1		5.92	165.25	2.0	35.04	1.26	27.90
	2		5.86	168.19	2.0	35.42	1.23	28.71
	Average	8	5.89	166.72	2.0	35.23	1.24	28.30
	Std. Dev.		0.04	2.08	0.0	0.27	0.02	0.57
M5	1		4.77	136.12	2.0	34.83	1.22	28.56
	2		4.71	131.36	2.0	35.22	1.26	27.87
	Average	10	4.74	133.74	2.0	35.03	1.24	28.22
	Std. Dev.		0.04	3.37	0.0	0.27	0.03	0.49

Table C.3 Gas permeation results from PSF membranes after heat treatment

Membranes	Runs	P (bar)	t_{CO_2} (s)	t_{CH_4} (s)	V (cm ³)	(P/I) CO ₂ (GPU)	(P/I) CH ₄ (GPU)	Selectivity CO ₂ /CH ₄
M1	1		26.79	730.46	2.0	30.99	1.14	27.27
	2		26.98	744.55	2.0	30.77	1.12	27.60
	Average	2	26.88	737.50	2.0	30.88	1.13	27.43
	Std. Dev.		0.13	9.96	0.0	0.15	0.02	0.23
M2	1		13.64	385.52	2.0	30.42	1.08	28.23
	2	4	14.07	370.61	2.0	29.50	1.12	26.34
	Average		13.86	378.06	2.0	29.96	1.10	27.29
	Std. Dev.		0.30	10.54	0.0	0.65	0.03	1.34
M3	1		9.53	254.67	2.0	29.04	1.09	26.73
	2	6	9.40	255.99	2.0	29.45	1.08	27.25
	Average		9.46	255.33	2.0	29.25	1.08	26.99
	Std. Dev.		0.09	0.93	0.0	0.29	0.00	0.37
M4	1		7.10	197.60	2.0	29.20	1.05	27.79
	2	8	7.34	191.81	2.0	28.26	1.08	26.12
	Average		7.22	194.71	2.0	28.73	1.07	26.96
	Std. Dev.		0.17	4.09	0.0	0.66	0.02	1.18
M5	1		5.86	155.51	2.0	28.35	1.07	26.55
	2	10	5.83	158.28	2.0	28.46	1.05	27.13
	Average		5.85	156.89	2.0	28.41	1.06	26.84
	Std. Dev.		0.02	1.96	0.0	0.08	0.01	0.41

Table C.4 Gas permeation results from PSF/PI-20% membranes after heat treatment

Membranes	Runs	P (bar)	t_{CO_2} (s)	t_{CH_4} (s)	V (cm ³)	(P/I) CO ₂ (GPU)	(P/I) CH ₄ (GPU)	Selectivity CO ₂ /CH ₄
M1	1		22.90	696.78	2.0	36.25	1.19	30.42
	2		22.79	684.96	2.0	36.42	1.21	30.05
	Average	2	22.85	690.87	2.0	36.34	1.20	30.24
	Std. Dev.		0.08	8.36	0.0	0.12	0.01	0.26
M2	1		11.87	358.87	2.0	34.98	1.16	30.24
	2	4	11.78	350.58	2.0	35.24	1.18	29.76
	Average		11.82	354.73	2.0	35.11	1.17	30.00
	Std. Dev.		0.06	5.87	0.0	0.19	0.02	0.34
M3	1		7.97	241.51	2.0	34.71	1.15	30.29
	2	6	8.10	238.55	2.0	34.16	1.16	29.45
	Average		8.04	240.03	2.0	34.44	1.15	29.87
	Std. Dev.		0.09	2.09	0.0	0.39	0.01	0.60
M4	1		6.16	185.34	2.0	33.67	1.12	30.07
	2	8	6.11	179.69	2.0	33.99	1.16	29.43
	Average		6.13	182.51	2.0	33.83	1.14	29.75
	Std. Dev.		0.04	3.99	0.0	0.23	0.03	0.45
M5	1		4.92	143.63	2.0	33.73	1.15	29.18
	2	10	4.96	149.99	2.0	33.46	1.11	30.23
	Average		4.94	146.81	2.0	33.60	1.13	29.71
	Std. Dev.		0.03	4.50	0.0	0.19	0.03	0.74

Table C.5 Gas permeation results from mixed matrix membranes at 5 wt.% silica content

Membranes	Runs	P (bar)	t_{CO_2} (s)	t_{CH_4} (s)	V (cm ³)	(P/I) CO ₂ (GPU)	(P/I) CH ₄ (GPU)	Selectivity CO ₂ /CH ₄
M1	1		11.25	554.41	2.0	73.82	1.50	49.30
	2		11.30	549.78	2.0	73.49	1.51	48.67
	Average	2	11.27	552.10	2.0	73.65	1.50	48.98
	Std. Dev.		0.04	3.28	0.0	0.24	0.01	0.45
M2	1		5.90	288.42	2.0	70.36	1.44	48.89
	2		5.86	283.72	2.0	70.86	1.46	48.44
	Average	4	5.88	286.07	2.0	70.61	1.45	48.67
	Std. Dev.		0.03	3.32	0.0	0.36	0.02	0.32
M3	1		3.97	194.18	2.0	69.75	1.42	48.94
	2		3.99	191.84	2.0	69.35	1.44	48.08
	Average	6	3.98	193.01	2.0	69.55	1.43	48.51
	Std. Dev.		0.01	0.83	0.0	0.14	0.01	0.31
M4	1		2.99	147.56	2.0	69.30	1.41	49.27
	2		3.02	143.73	2.0	68.66	1.44	47.55
	Average	8	3.01	145.64	2.0	68.98	1.43	48.41
	Std. Dev.		0.02	2.71	0.0	0.45	0.03	1.22
M5	1		2.42	117.89	2.0	68.67	1.41	48.76
	2		2.43	115.46	2.0	68.38	1.44	47.55
	Average	10	2.42	116.68	2.0	68.53	1.42	48.16
	Std. Dev.		0.01	1.72	0.0	0.20	0.02	0.85

Table C.6 Gas permeation results from mixed matrix membranes at 10 wt.% silica content

Membranes	Runs	P (bar)	t_{CO_2} (s)	t_{CH_4} (s)	V (cm ³)	(P/I) CO ₂ (GPU)	(P/I) CH ₄ (GPU)	Selectivity CO ₂ /CH ₄
M1	1		10.35	539.34	2.0	80.21	1.54	52.11
	2		10.42	535.94	2.0	79.68	1.55	51.44
	Average	2	10.38	537.64	2.0	79.95	1.54	51.78
	Std. Dev.		0.05	2.41	0.0	0.37	0.01	0.47
M2	1		5.38	278.02	2.0	77.17	1.49	51.69
	2		5.36	273.98	2.0	77.48	1.52	51.14
	Average	4	5.37	276.00	2.0	77.33	1.50	51.42
	Std. Dev.		0.02	2.86	0.0	0.22	0.02	0.39
M3	1		3.64	186.82	2.0	75.95	1.48	51.27
	2		3.65	186.47	2.0	75.80	1.48	51.08
	Average	6	3.65	186.65	2.0	75.87	1.48	51.18
	Std. Dev.		0.01	0.25	0.0	0.10	0.00	0.14
M4	1		2.76	141.32	2.0	75.11	1.47	51.14
	2		2.78	140.33	2.0	74.72	1.48	50.52
	Average	8	2.77	140.82	2.0	74.92	1.47	50.83
	Std. Dev.		0.01	0.70	0.0	0.28	0.01	0.44
M5	1		2.23	114.21	2.0	74.51	1.45	51.26
	2		2.23	111.66	2.0	74.60	1.49	50.17
	Average	10	2.23	112.93	2.0	74.56	1.47	50.71
	Std. Dev.		0.00	1.81	0.0	0.06	0.02	0.77

Table C.7 Gas permeation results from mixed matrix membranes at 15 wt.% silica content

Membranes	Runs	P (bar)	t_{CO_2} (s)	t_{CH_4} (s)	V (cm ³)	(P/I) CO ₂ (GPU)	(P/I) CH ₄ (GPU)	Selectivity CO ₂ /CH ₄
M1	1		9.37	526.24	2.0	88.59	1.58	56.15
	2		9.41	524.72	2.0	88.21	1.58	55.75
	Average	2	9.39	525.48	2.0	88.40	1.58	55.95
	Std. Dev.		0.03	1.07	0.0	0.26	0.00	0.28
M2	1		4.84	267.57	2.0	85.73	1.55	55.26
	2		4.83	269.71	2.0	85.89	1.54	55.81
	Average	4	4.84	268.64	2.0	85.81	1.55	55.54
	Std. Dev.		0.01	1.51	0.0	0.11	0.01	0.39
M3	1		3.30	180.78	2.0	83.89	1.53	54.80
	2		3.29	182.17	2.0	84.17	1.52	55.41
	Average	6	3.29	181.48	2.0	84.03	1.52	55.11
	Std. Dev.		0.01	0.99	0.0	0.20	0.01	0.43
M4	1		2.50	137.93	2.0	82.95	1.50	55.13
	2		2.48	135.12	2.0	83.56	1.54	54.40
	Average	8	2.49	136.52	2.0	83.25	1.52	54.77
	Std. Dev.		0.01	1.99	0.0	0.44	0.02	0.51
M5	1		2.00	109.77	2.0	82.94	1.51	54.83
	2		2.01	109.08	2.0	82.42	1.52	54.15
	Average	10	2.01	109.43	2.0	82.68	1.52	54.49
	Std. Dev.		0.01	0.49	0.0	0.37	0.01	0.48

Table C.8 Gas permeation results from mixed matrix membranes at 20 wt.% silica content

Membranes	Runs	P (bar)	t_{CO_2} (s)	t_{CH_4} (s)	V (cm ³)	(P/I) CO ₂ (GPU)	(P/I) CH ₄ (GPU)	Selectivity CO ₂ /CH ₄
M1	1		8.65	438.70	2.0	96.02	1.89	50.74
	2	2	8.70	440.64	2.0	95.42	1.88	50.65
	Average		8.67	439.67	2.0	95.72	1.89	50.69
	Std. Dev.		0.04	1.38	0.0	0.43	0.01	0.07
M2	1		4.45	221.60	2.0	93.31	1.87	49.82
	2	4	4.46	226.57	2.0	93.07	1.83	50.80
	Average		4.45	224.09	2.0	93.19	1.85	50.31
	Std. Dev.		0.01	3.52	0.0	0.17	0.03	0.70
M3	1		3.01	149.12	2.0	92.03	1.86	49.59
	2	6	3.02	151.88	2.0	91.59	1.82	50.27
	Average		3.01	150.50	2.0	91.81	1.84	49.93
	Std. Dev.		0.01	1.95	0.0	0.31	0.02	0.48
M4	1		2.27	112.68	2.0	91.24	1.84	49.54
	2	8	2.27	113.23	2.0	91.60	1.83	49.97
	Average		2.27	112.95	2.0	91.42	1.84	49.75
	Std. Dev.		0.01	0.39	0.0	0.25	0.01	0.31
M5	1		1.83	90.91	2.0	90.91	1.83	49.78
	2	10	1.82	90.24	2.0	91.10	1.84	49.51
	Average		1.82	90.57	2.0	91.01	1.83	49.64
	Std. Dev.		0.00	0.48	0.0	0.14	0.01	0.19

Table C.9 Gas permeation results from mixed matrix membranes at 5 wt.% silica content after heat treatment

Membranes	Runs	P (bar)	t_{CO_2} (s)	t_{CH_4} (s)	V (cm ³)	(P/I) CO ₂ (GPU)	(P/I) CH ₄ (GPU)	Selectivity CO ₂ /CH ₄
M1	1		12.00	659.40	2.0	69.19	1.26	54.95
	2		12.09	656.47	2.0	68.68	1.26	54.31
	Average	2	12.04	657.94	2.0	68.93	1.26	54.63
	Std. Dev.		0.06	2.07	0.0	0.36	0.00	0.46
M2	1		6.23	339.31	2.0	66.62	1.22	54.46
	2		6.21	336.37	2.0	66.81	1.23	54.14
	Average	4	6.22	337.84	2.0	66.72	1.23	54.30
	Std. Dev.		0.01	2.08	0.0	0.13	0.01	0.23
M3	1		4.28	233.10	2.0	64.63	1.19	54.45
	2		4.23	226.82	2.0	65.44	1.22	53.64
	Average	6	4.26	229.96	2.0	65.03	1.20	54.04
	Std. Dev.		0.04	4.44	0.0	0.57	0.02	0.57
M4	1		3.23	175.06	2.0	64.29	1.19	54.23
	2		3.21	171.10	2.0	64.59	1.21	53.24
	Average	8	3.22	173.08	2.0	64.44	1.20	53.74
	Std. Dev.		0.01	2.80	0.0	0.21	0.02	0.70
M5	1		2.59	138.28	2.0	64.08	1.20	53.37
	2		2.59	138.94	2.0	64.22	1.20	53.74
	Average	10	2.59	138.61	2.0	64.15	1.20	53.55
	Std. Dev.		0.00	0.47	0.0	0.10	0.00	0.27

Table C.10 Gas permeation results from mixed matrix membranes at 10 wt.% silica content after heat treatment

Membranes	Runs	P (bar)	t_{CO_2} (s)	t_{CH_4} (s)	V (cm ³)	(P/I) CO ₂ (GPU)	(P/I) CH ₄ (GPU)	Selectivity CO ₂ /CH ₄
M1	1		10.98	628.68	2.0	75.61	1.32	57.26
	2	2	10.94	629.39	2.0	75.85	1.32	57.51
	Average		10.96	629.04	2.0	75.73	1.32	57.38
	Std. Dev.		0.03	0.50	0.0	0.17	0.00	0.18
M2	1		5.70	326.37	2.0	72.85	1.27	57.28
	2	4	5.66	322.18	2.0	73.34	1.29	56.92
	Average		5.68	324.27	2.0	73.09	1.28	57.10
	Std. Dev.		0.03	2.97	0.0	0.34	0.01	0.26
M3	1		3.89	219.25	2.0	71.21	1.26	56.42
	2	6	3.87	220.70	2.0	71.53	1.25	57.05
	Average		3.88	219.98	2.0	71.37	1.26	56.74
	Std. Dev.		0.01	1.02	0.0	0.23	0.01	0.44
M4	1		2.96	168.48	2.0	70.06	1.23	56.88
	2	8	2.94	165.11	2.0	70.60	1.26	56.16
	Average		2.95	166.79	2.0	70.33	1.24	56.52
	Std. Dev.		0.02	2.38	0.0	0.38	0.02	0.50
M5	1		2.38	133.60	2.0	69.81	1.24	56.17
	2	10	2.36	133.86	2.0	70.25	1.24	56.63
	Average		2.37	133.73	2.0	70.03	1.24	56.40
	Std. Dev.		0.01	0.19	0.0	0.31	0.00	0.33

Table C.11 Gas permeation results from mixed matrix membranes at 15 wt.% silica content after heat treatment

Membranes	Runs	P (bar)	t_{CO_2} (s)	t_{CH_4} (s)	V (cm ³)	(P/I) CO ₂ (GPU)	(P/I) CH ₄ (GPU)	Selectivity CO ₂ /CH ₄
M1	1		10.03	614.38	2.0	82.74	1.35	61.23
	2		10.08	613.43	2.0	82.33	1.35	60.83
	Average	2	10.06	613.91	2.0	82.53	1.35	61.03
	Std. Dev.		0.04	0.67	0.0	0.29	0.00	0.28
M2	1		5.20	319.75	2.0	79.75	1.30	61.43
	2		5.22	314.46	2.0	79.45	1.32	60.19
	Average	4	5.21	317.10	2.0	79.60	1.31	60.81
	Std. Dev.		0.01	3.74	0.0	0.21	0.02	0.88
M3	1		3.56	216.02	2.0	77.63	1.28	60.60
	2		3.53	213.69	2.0	78.32	1.30	60.48
	Average	6	3.55	214.85	2.0	77.97	1.29	60.54
	Std. Dev.		0.02	1.65	0.0	0.49	0.01	0.09
M4	1		2.68	162.84	2.0	77.50	1.27	60.81
	2		2.69	161.01	2.0	77.29	1.29	59.96
	Average	8	2.68	161.93	2.0	77.39	1.28	60.38
	Std. Dev.		0.01	1.30	0.0	0.15	0.01	0.60
M5	1		2.17	129.95	2.0	76.55	1.28	59.92
	2		2.16	130.51	2.0	77.00	1.27	60.52
	Average	10	2.16	130.23	2.0	76.78	1.27	60.22
	Std. Dev.		0.01	0.39	0.0	0.31	0.00	0.43

Table C.12 Gas permeation results from mixed matrix membranes at 20 wt.% silica content after heat treatment

Membranes	Runs	P (bar)	t_{CO_2} (s)	t_{CH_4} (s)	V (cm ³)	(P/I) CO ₂ (GPU)	(P/I) CH ₄ (GPU)	Selectivity CO ₂ /CH ₄
M1	1		9.21	508.78	2.0	90.13	1.63	55.24
	2		9.17	511.82	2.0	90.50	1.62	55.79
	Average	2	9.19	510.30	2.0	90.31	1.63	55.52
	Std. Dev.		0.03	2.14	0.0	0.26	0.01	0.39
M2	1		4.73	263.66	2.0	87.85	1.57	55.80
	2		4.74	259.91	2.0	87.62	1.60	54.87
	Average	4	4.73	261.79	2.0	87.73	1.59	55.33
	Std. Dev.		0.01	2.65	0.0	0.16	0.02	0.66
M3	1		3.22	178.21	2.0	85.97	1.55	55.36
	2		3.23	177.50	2.0	85.68	1.56	54.96
	Average	6	3.22	177.85	2.0	85.82	1.56	55.16
	Std. Dev.		0.01	0.50	0.0	0.20	0.00	0.28
M4	1		2.44	134.36	2.0	85.20	1.54	55.15
	2		2.44	133.40	2.0	85.03	1.56	54.66
	Average	8	2.44	133.88	2.0	85.12	1.55	54.91
	Std. Dev.		0.00	0.68	0.0	0.12	0.01	0.35
M5	1		1.96	108.09	2.0	84.89	1.54	55.26
	2		1.97	107.05	2.0	84.31	1.55	54.36
	Average	10	1.96	107.57	2.0	84.60	1.54	54.81
	Std. Dev.		0.01	0.74	0.0	0.41	0.01	0.64

Table C.13 Gas permeation results for the mixed gas analysis for heat treated membranes at 10bar feed pressure

Membranes	Runs	t_{Mix} (s)	V (cm ³)	(P/I) _{Mix} (GPU)	(P/I) CO ₂ (GPU)	(P/I) CH ₄ (GPU)	Selectivity CO ₂ /CH ₄
PSF/PI-20% Gas Mixture (30/70)	1	4.98	2.0	34.45	33.32	1.13	29.50
	2	5.01	2.0	34.25	33.11	1.14	29.12
	Average	5.00	2.0	34.35	33.22	1.13	29.31
	Std. Dev.	0.02	0.0	0.14	0.15	0.01	0.27
PSF/PI-20% Gas Mixture (70/30)	1	4.93	2.0	34.79	33.66	1.13	29.81
	2	4.99	2.0	34.42	33.30	1.11	29.89
	Average	4.96	2.0	34.60	33.48	1.12	29.85
	Std. Dev.	0.04	0.0	0.27	0.26	0.01	0.1
PSF/PI-20% + Silica (15 wt. %)	1	2.18	2.0	77.60	76.33	1.27	60.00
	2	2.15	2.0	78.51	77.22	1.29	59.91
	Average	2.16	2.0	78.06	76.78	1.28	59.96
	Std. Dev.	0.02	0.0	0.64	0.63	0.01	0.07
PSF/PI-20% + Silica (15 wt. %)	1	2.17	2.0	77.95	76.68	1.26	60.73
	2	2.16	2.0	78.25	76.98	1.26	60.86
	Average	2.16	2.0	78.10	76.83	1.26	60.79
	Std. Dev.	0.01	0.0	0.21	0.21	0.00	0.09

APPENDIX D

(Graphs For Various Gas Mixture Compositions)

Figure D1. Gas mixture composition (CO₂/CH₄) 50%/50%

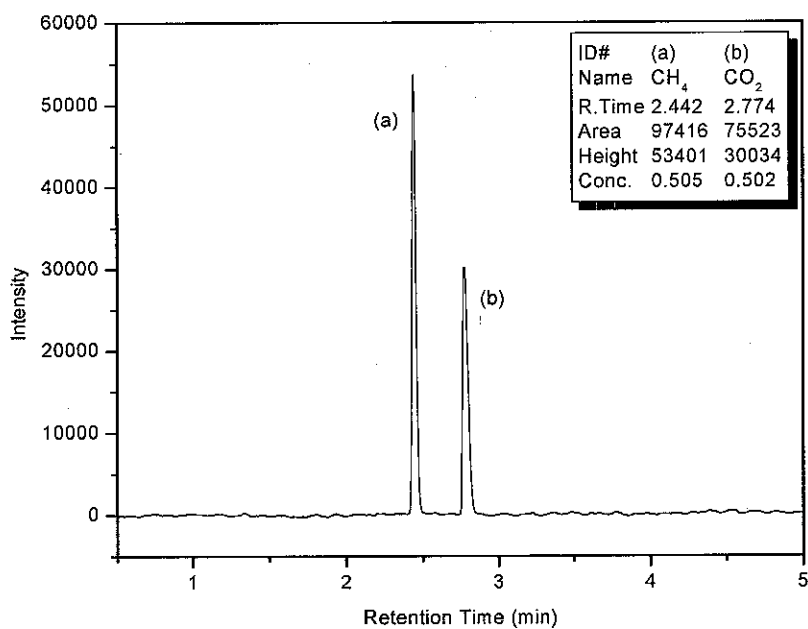


Figure D2. Gas mixture composition (CO₂/CH₄) 70%/30%

